THE UNIVERSITY OF CALGARY

Cellular and Network Substrates

of Neuronal Excitability in Relation to Epileptic Seizures

by

Houman Khosravani

A DISSERTATION

SUBMITTED TO THE FACULTY OF GRADUATE STUDIES

IN PARTIAL FULFILLMENT OF THE REQUIREMENTS FOR THE

DEGREE OF DOCTOR OF PHILOSOPHY

DEPARTMENT OF NEUROSCIENCE

CALGARY, ALBERTA

JULY, 2007

UNIVERSITY OF CALGARY

FACULTY OF GRADUATE STUDIES

The undersigned certify that they have read, and recommend to the Faculty of Graduate Studies for acceptance, a dissertation entitled "Cellular and Network Substrates of Neuronal Excitability in Relation to Epileptic Seizures" submitted by Houman Khosravani in partial fulfillment of the requirements for the degree of DOCTOR OF PHILOSOPHY.

Dr. Gerald W. Zamponi
Department of Neuroscience

Dr. Paolo Federico
Department of Neuroscience

Dr. Bin Hu
Department of Neuroscience

Dr. Wayne R. Giles
Internal-external,
Department of Cardiovascu-
lar & Respiratory Sciences

Dr. Raymond W. Turner
Department of Neuroscience

Dr. Robert O. Messing
External, Ernest Gallo Clinic
& Research Center, Univer-
sity of California, San Fran-
cisco

_____
Date

Abstract

Brain function is, in part, maintained by an appropriate balance between excitatory and inhibitory elements. In relation to excitability, factors such as the complement and distribution of ion channels, properties and composition of synaptic proteins, and dynamics affecting network synchrony all interact to modulate neuronal firing and network activity. In this dissertation, I present a series of three focused studies at the level of ion channels (T-type calcium channels), synaptic transmission (prion protein), and network activity (high frequency oscillations) that affect neuronal excitability. With regards to $Ca_v3.2$ T-type voltage-gated calcium channels, I demonstrate that novel missense mutations, as identified in patients with idiopathic generalized epilepsies, can result in alteration of channel biophysical properties. The majority of mutants altered gating properties consistent with greater channel activity. However, most of these biophysical alterations were not large in magnitude suggesting that the role of these channels in relation to other cellular processes may be affected. At the level of synapses, I describe a novel interaction/modulation of NMDA receptor currents by the endogenous prion protein (PrP). Using PrP-null mice, I show that loss of PrP results in enhanced synaptic NMDA currents with greater amplitude and prolonged deactivation kinetics. These changes do not seem to be related to developmental effects and possibly involve an NMDA receptor subunit switch to functional receptors containing NR2D. At the network level, I show that high frequency oscillations in field recordings *in vitro* and in the EEG from patients with epilepsy are localized to the seizure onset zone and increase over time during the immediate pre-seizure period. This knowledge can be used to better localized seizures for surgical resection, thereby improving seizure control in intractable patients. These three topics and their relevance to hyperexcitable states are discussed in the context of epileptiform seizure activity and neurological disease.

Dedication & Acknowledgements

To my wife Julia, son Lucas, and my parents for their immeasurable support throughout. Thank you.

Many thanks to Drs. Gerald Zamponi and Paolo Federico for being marvelous supervisors; I have learned a great deal from you and enjoyed academic freedom to explore exciting science and for that I am grateful. Your collective scientific perspective and support for me have greatly aided my understanding of science and life in general! To Drs. Bin Hu and Ray Turner for your tremendous support and for being an important part of my training. Also to Dr. Morley Hollenberg for your fantastic support of my combined MD/PhD training. Special thanks to Dr. Wayne Giles and Dr. Bob Messing (external examiners) for taking the time to be part of my training and for their insightful comments. Along with my supervisors, also thanks to Dr. Bill Stell (Neuroscience Graduate Coordinator) for supporting my untraditional path of combining basic and clinical research at the PhD level. Thanks also to Julie Boyd our Neuroscience programme secretary for all her hard work and support.

Special thanks to all members of the Zamponi lab, specially: Christophe "Kara" Altier, Chris Bladen, Lina Chen, Robyn Flynn and Michael Colicos, Jawed Hamid, Shahid Hameed, Mircea Iftinca, Jean Peloquin, Diego "VarelaL" Varela and Tamara Hermosilla, and Yunfeng Zheng. A very Special Thanks to Yunfeng for her hardwork as we ventured to conduct many novel and demanding experiments in the lab dealing with the "prion project" (Chapter 4). Also thanks to Michael Colicos for showing me the ways of primary culture neurons. Special mention to the following "blackops" members: Bruce "Agent B" McKay, Robi Butt, Matthew Churchward, Regan Taylor, Michael Molinoux, Hamish Mahaffey, Fernando Fernandez, Steven Peters, Jun Yan, and Scott Jarvis who was elemental to convincing me to come to the Zamponi Lab and U of Calgary for its great MD/PhD programme. Finally, HK acknowledges the metallic sounds of HellrazeR (DrZ, Kegger, and Pinnegar of Death) - Calgary's heaviest!

"The first step in applying the scientific method consists in being curious about the world..."

- Linus Pauling

This document was typeset, in accordance with the University of Calgary's dissertation style template provided in the form of a LaTeX 2$_\varepsilon$ TUTA class file (ucalgthes.cls, *www.ucalgary.ca/it*)

Acknowledgement of Scientific Contributions

Chapter 2 The author (Houman Khosravani) performed all of the molecular biology associated with the creation and verification of missense mutations in the $Ca_v3.2$ cDNA clone, electrophysiology of mutant channels, and associated analysis with the exception of the following contributions as gratefully acknowledged here: mutations in Section 2.3.2 were created by Mr. Chris Bladen with the author selecting the mutagenesis primers and involved in sequencing-based verification. Molecular biology associated with the creation and verification of mutations in Section 2.3.3 were performed by Mr. Chris Bladen and Dr. Diego Varela; Dr. Varela was also participated alongside the author in characterizing each of the electrophysiologically identified mutations. Identification of missense mutations in the epileptic population in Sections 2.3.2 and 2.3.3 was performed primarily by Ms. Sarah Heron with the aid of Ms. Tristiana Williams and Ms. Michelle Newman. These individuals are part of the research groupings of Drs. John Mulley (primary), Ingrid Schaffer, and Samuel Berkovic in Australia. Both rat and human $Ca_v3.2$ T-type calcium channel WT cDNA was provided by the laboratory of Dr. Terrance Snutch.

Chapter 3 All experimental design, data acquisition, and analysis were performed by the author. The technical assistance of Mr. Michael Rigby and the EEG technical team at Foothills Hospital is acknowledged. The raw Morlet wavelet-based spectrum analysis used in Section 3.4.1 was extensively modified from a Matlab script, originally used to process MRI images, as provided by Dr. Robert Pinnegar.

Chapter 4 The experimental design (the hypothesis of prion protein affecting glutamatergic synaptic transmission), electrophysiology, and imaging experiments and associated analysis were performed by the author. The following individual's contribution is gratefully acknowledged: Many of the electrophysiological experiments were performed alongside the author (in parallel) by Dr. Yunfeng Zhang. RT-PCR experiments were performed by Dr. Jawed Hamid. Western blot and immunostaining experiments were performed by Dr. Shahid Hameed with the author involved in image acquisition and analysis. TUNEL staining was performed by Dr. Shigeki Tsutsui. The ELISA experiment was performed by Dr. Christophe Altier. Dr. Lina Chen provided the majority of primary hippocampal cultures used in experiments.

Major Publications Arising from this Work

1. **Khosravani H.**, Zhang Y., Tsutsui S., Hameed S., Hamid J., Chen L., Altier C., Jirik FR., Functional modulation of NMDA receptor kinetics by endogenous prion protein. (2007) Manuscript in preparation.

2. **Khosravani H.**, Mehrotra N., Rigby M., Hader W.J., Pinnegar C.R., Pillay N., Wiebe S., Federico F. (2007) Spatial localization and time-dependant changes of high frequency oscillations in EEG of patients with temporal lobe epilepsy. *Epilepsia*. Submitted.

3. Peloquin J.B., **Khosravani H.**, Barr W., Bladen C., Evans R., Mezeyova J., Parker D., Snutch T.P., McRory J.E., Zamponi G.W. (2006) Functional analysis of $Ca_v3.2$ T-type calcium channel mutations linked to childhood absence epilepsy. *Epilepsia*, 47(3):655-8

4. **Khosravani H.**, Zamponi G.W. (2006) Voltage-gated calcium channels and idiopathic generalized epilepsies. *Physiological Reviews*, 86(3):941-66

5. Peloquin J.B., **Khosravani H.**, Barr W., Bladen C., Mezeyova J., Parker D.B., Snutch T.P., McRory J.E., Zamponi G.W. (2006) Functional effects of $Ca_v3.2$ T-type calcium channel mutations linked to Childhood Absence Epilepsy. *Epilepsia*, 47(3):655-8

6. **Khosravani H.**, Bladen C., Parker D.B., Snutch T.P., McRory J.E., Zamponi G.W. (2005) Functional effects of mutations in the $Ca_v3.2$ T-type calcium channel associated with idiopathic generalized epilepsy. *Annals of Neurology*, 57(5):745-9

7. **Khosravani H.**, Pinnegar R.C., Bardakjian B.L., Mitchell J.R., Federico P., Carlen P.L. (2005) Increased high frequency oscillations precede *in vitro* low Mg^{2+} seizures. *Epilepsia*, 46(8):1188-97

8. **Khosravani H.**, Altier C., Simms B., Hamming K.S., Snutch T.P., McRory J.E., Zamponi G.W. (2004) Gating effects of mutations in the $Ca_v3.2$ T-type calcium channel associated with Childhood Absence Epilepsy. *Journal of Biological Chemistry*, 279:9681-9684

Table of Contents

List of Tables

List of Figures

Chapter 1

General Introduction

1.1 Neuronal Excitability in the Normal and Epileptic Brain: A Preamble on Three Focused Studies at the Level of Channels, Receptors, and Networks

The human brain ranks amongst the most complex systems in the known universe. The brain is composed of neuronal, glial, and vascular-associated (endothelial) elements, and together these integrated components govern the system's overall function. There are approximately 10^{11} neurons in the human brain, much fewer than the number of glia and each neuron can make upwards of 10^3 synaptic connections [159]; upper estimates for the total number of synapses in the cerebral cortex range around 300 trillion [182]. The overarching functions of the brain encompass sensory information processing, information storage, decision making, and regulation of a wide range of bodily processes such as neuroendocrine control. The overall complexity of the brain is a manifestation of different levels of intricacy that start at the single neuron-level and extend to nonlinear aspects of network dynamics. Indeed, interconnections in the brain are numerous and each neuronal element, along with glial and vascular counterparts, play integrated roles in information processing. At the cell level, neurons exhibit much of the same cellular functions (e.g. gene regulation/expression, protein modification/trafficking, intra- and inter-cell signalling, etc.) as other cells in other organs. However, due to the strong influence of electrochemical activity, and the sheer number of interacting cells and modes of communication (chemical and electrical synapses, in addition to ephaptic interactions), each neuron can exhibit a wide range of behaviour. Moreover, the activity of sub-populations of neurons can influence the activity of larger neuronal networks and conversely the activity of the network can trigger radical and cell-type-specific changes in single cells and subpopulations thereof.

The behaviour of neurons is in large part governed by genetic and activity-dependent processes, which at the mechanistic level, act on proteins to alter factors such as: expression, trafficking, modulation via phosphorylation, allosteric effectors, in addition to properties such as voltage-dependence, and pH & temperature sensitivity. In particular, ion channels and synapse-associated ligand-gated channels are key proteins that govern neuronal firing and are central to the neuron's information processing ability. The mechanisms of neuronal firing are attributable to a diverse complement of ionic currents which, depending on cell-type and location in the brain, are modulated by and modulate, the action of synaptic proteins at pre- and post-synaptic terminals. As a crude categorization, neurons can be grouped by their morphology, neurotransmitter type, and/or location in particular neuronal circuits within anatomical structures. The transmitter can then subclassify neuronal type into excitatory vs. inhibitory. Thus, it can be inferred that proper brain function is dependent on the appropriate, yet dynamic, balance between excitatory and inhibitory neuronal networks. There are numerous instances where this balance can be compromised or exacerbated leading to pathological brain activity, as is the case in epilepsy, and perhaps other neurological disorders ranging from autism to Parkinson's, and even depression. As epilepsy is the context in which I will discuss modulators of neuronal excitability, I will focus on the three specific elements that have bearing on neuronal excitability at three levels: (1) ion channels, (2) synapses, and (3) networks (Fig. 1.1).

Neuronal firing, whether due to intrinsic membrane properties or due to synaptic inputs, is arguably the final readout of its computational/information processing. Firing patterns can vary between being regular (tonic), irregular, chaotic, and even stochastic. Often, a single neuron is capable of several modes of firing, and can undergo rapid switching between types on short time scales due to intrinsic membrane properties and/or network dynamics. Indeed, this is very common in neocortical neurons that seem to exhibit at least six different modes of firing. Moreover, some neurons may even be silent and only become active during particular (network) states of activity. Since firing is synonymous with spiking, attributes of action potentials can also be as variable as the neuronal cell types that generate them. Differently shaped spikes, spike latencies, and time courses of neurotransmitter release from terminals are all variables that can be cell-type specific and can be altered in pathological conditions. In response
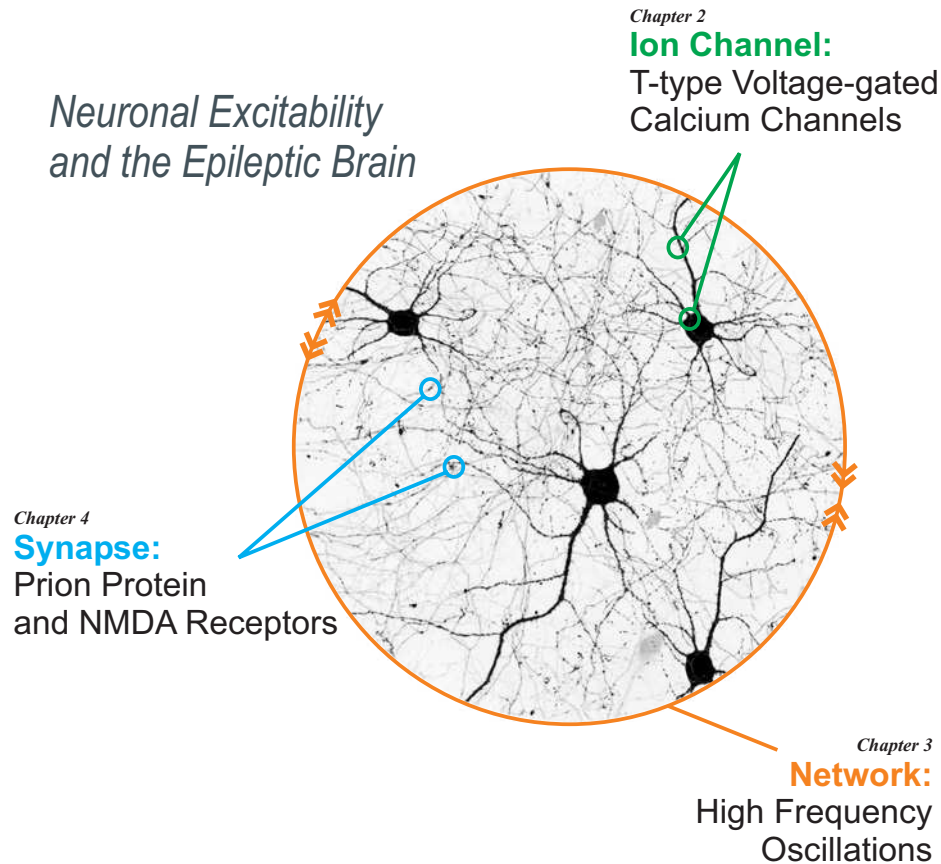
Figure 1.1: Dissertation at a glance showing the focus of each chapter: (Chapter 2) T-type calcium channels, (Chapter 3) High Frequency Oscillations, and (Chapter 4) Prion proteins and NMDA receptors. Each of these chapters focuses at a different level, from cellular proteins found on soma and dendrites (T-type channels), to synaptic proteins (prion protein and NMDA receptors), and up-scale to the level of network activity (High Frequency Oscillations, HFOs). In Chapter 2 I will explore the functional consequences of reported T-type $Ca_v3.2$ channel mutations associated with a form of generalized epilepsy (see seizure classification, section 1.2). In Chapter 3 I will investigate HFOs, a neuronal population phenomenon observed in EEG and its use for seizure localization and detection of pre-seizure changes. In the final Chapter 4, I report on a novel study, with serendipitous beginnings, showing that the endogenous cellular prion protein (PrP), a protein with ill-defined function, seems to have a protective role in modulating the activity of the NMDA receptor.

to synaptic inputs, even cells of the same type and localization can behave completely differently, and the converse is also true, where very different neurons can exhibit virtually identical firing patterns. This diversity in activity is believed to be governed by factors such as different complements of ion channels, receptors, location of synaptic inputs (i.e. morphology), and the prior state of activity of the neuron (computational history). However, as important as these factors are, they do not determine (in a pure deterministic sense) the output of the neuron per se. Rather, these factors can be considered as 'system parameters'. A subset of these parameters can be considered as state variables, which are elemental to governing the overall dynamics of the neuron. In other words, these state variables define the rules by which the neuron operates. A consequence of this is that different conductances can result in the same set of governing rules and therefore firing modes, and conversely, similar currents can results in different responses. Therefore, "the currents define what kind of dynamical system the neuron is" [159]. These notions extend beyond physiological functions and into disease states where neuronal dynamics can be altered by changes in one or more system variables. For example, alterations in protein function due to missense mutations can alter neuronal firing properties that can have consequences at the network level. Indeed, in the context of epilepsy there is precedence for this. Point mutations have been reported in a series of ion channels (including Na^+, K^+, and Ca^{+2} voltage-gated channels), in addition to ligand-gated channels such as $GABA_A$. When considering neuronal dynamics, it is helpful to consider the following categorization of variables, in particular relation to ionic currents [159]: (1) membrane potential, (2) excitation variables: e.g. Na^+ channel activation, in general, variables responsible for the upstroke of spikes, (3) recovery variables: e.g. Na^+ channel inactivation and activation of voltage-gated K^+ conductances responsible for repolarization, and finally (4) adaptation variables: transient or slow conductances such as Ca^{+2} activated currents; any such currents come into play during prolonged spiking activity. In-line with the notion of ionic channel alterations and their meaning as a system variable capable of altering firing dynamics, I investigated altered properties of one such ionic conductance (categorized under excitation variables), the $Ca_v3.2$ T-type calcium channel, and studied the effects of epilepsy-associated missense mutations on channel biophysical properties as reported in Chapter 2.

Highly interconnected neuronal networks in the brain are substrates in which brain function takes place. These networks, in their various anatomical structures, have the ability to oscillate and synchronize and often do so for a variety of purposes ranging from secretion of hormones, to pattern generation for fine motor control, and generation of sleep rhythms. In each instance, sub-populations of neurons in a larger network exhibit transient synchronization that define normal physiological brain rhythms. It should be noted that synchrony of neurons is brought on, mechanistically, predominantly by neurotransmission, but can include the action of electrotonic and ephaptic communication. The activity of individual neuronal elements can result in altered population (i.e. ensemble) activity. However, once again, complex and diverse network activity can be observed from a cluster of identical neurons that, due to synergistic interactions, at the 'network level' give it properties that go beyond the law of linear superposition (i.e. network behaviour can be more than the sum of its parts). Each parameter, both at the cell and network levels, is available for alteration under the disease condition, and once pathological processes have taken hold it is often difficult to dissociate causal relations between participating elements (e.g. a current dilemma in human epilepsy is whether mesial temporal lobe sclerosis is the cause or effect of seizure activity in that structure). This notion is complicated by the fact that neuronal properties can feedback to alter network dynamics, and vice versa. Moreover, activity at the network level can trigger alterations in gene expression that can affect parameters such as the firing properties and regulation of cellular homeostasis. I recently discovered a novel regulation of NMDA receptors by the endogenous cellular prion protein (PrP^C). This interaction was unmasked by using PrP-null mice, which seem to exhibit markedly enhanced NMDA receptor function with significant physiological consequences in relation to excitability and excitotoxicity (see Chapter 4 for more details).

In the context of altered network excitability, as it relates to epileptic activity, several network-level alterations have been widely studied. The hallmark of an epileptic network is the presence of sharpwaves or field spikes in extracellular recordings; these are referred to as interictal (i.e. between seizures) spikes. Underlying interictal spikes are synchronized bursts of activity from a local population of neurons in the vicinity of the recording electrode. Most brain structures do not exhibit this activity unless an epileptiform condition is present, although some

physiological sharpwave activity has been observed in the hippocampus of rodents. When it comes to ictal (i.e. seizure) genesis, not all brain regions have the same threshold. A large body of evidence supports the notion that the cerebral cortex and hippocampus are particularly seizure-prone areas, with the former being the more difficult to treat clinically (i.e. neocortical epilepsy, also see Section 1.2)

The intracellular correlate of interictal spikes is called the paroxysmal depolarizing shift (PDS), which represents a sustained depolarization that converts regular spiking neurons to burst-mode activity for the duration of the PDS. The PDS is believed to be caused by strong synaptic inputs resulting from synchronous firing of cells. It is postulated that this is due to alterations in the balance between inhibition and excitation (e.g. pathological GABAergic interneuron function in the hippocampus can result in abnormal synchronization in pyramidal neurons). However, such alterations can at times be nonintuitive, since there is a significant amount of evidence that exacerbated GABAergic activity can actually cause seizure activity [15]. In relation to PDS generation, recent evidence suggests that glutamate released by astrocytes and/or R-type calcium currents can also contribute to the prolonged transient depolarization that is the PDS [184]. An indicator for the presence of an epileptic condition relates to the frequency components observed within population field activity; given that sharpwaves can also have a physiological purpose. Studies have shown that oscillations in the range of 100-200 Hz can be present during both normal and epileptiform activity; this evidence includes recordings *in vitro*, *in vivo*, and in patients with epilepsy undergoing invasive EEG monitoring. However, oscillations greater than 200 Hz are believed to be exclusively pathophysiological. I will expand on this theme in my study of High Frequency Oscillations (HFOs) (see Chapter 3 for more details).

1.2 Seizures and the Route to Epilepsy

Imagine the brain as a large construction project where the neuronal elements are the workers and planners. The brain, like the construction site, is a rich and dynamic environment where many processes are occurring both simultaneously, cooperatively, and in some cases independently. Normally, the workers go about their assigned tasks to advance the project mostly

asynchronously, but at times they work in groups together on a common task. Now imagine a scenario where some of the workers begin to synchronously engage in a single task that serves no purpose for the overall function of the project. Rapidly, the sentiment spreads and now all of the workers are performing the same disruptive task - the rich and dynamic system is now periodic and dysfunctional. This is the essence of the transition to an epileptic seizure.

Epilepsy is a disorder of recurrent spontaneous seizures and is amongst the most common neurological conditions, accounting for 0.5% of the whole burden of diseases worldwide [194]. One in ten persons with a normal life span can expect to experience at least one seizure [109]. Epileptic seizures are characterized as abnormal hyperexcitable, hypersynchronous neuronal population activity and manifest themselves in different ways depending on their site of origin and subsequent spread [108]. The clinical diversity observed in epileptic seizure disorders is a reflection of the numerous cellular and network routes to seizure genesis. Seizures can originate in different brain regions that are responsible for motor, sensory, cognitive, and autonomic systems. The transition to seizure activity can be considered as a disruption of normal brain function. This transformation to pathological activity can be manifested by changes that occur at the level of single neurons (e.g., molecular alterations in ion channels, complements thereof, and regulatory proteins), local circuitry (e.g., alterations in cell-to-cell coupling via chemical and electrical synapses as well as ephaptic communication), or at the level of anatomically defined neuronal networks (e.g., structural changes and alteration between excitatory and inhibitory neuronal, interneuronal, and glial elements) [225].

The dynamics of how epileptogenesis arises from local neuronal populations or circuits and anatomically spreads to the point of becoming a clinically relevant seizure event is not known. This transition is putatively brought on by complex interactions between neuronal populations, both within and between local neuronal circuits. This may explain the observed diversity in the clinical manifestation of seizures between and within patients. Furthermore, neuronal systems are known to respond with sensitivity to slight stimuli and environmental changes, illustrating their nonlinear properties. Based on the characterized nonlinear properties of neuronal populations and the clinical presentation of epileptic phenomenon, epilepsy is regarded as a "dynamic disease", where a pathological loss of complexity in the brain gives rise

to abnormal hypersynchronous activity that underlies a seizure [207, 208]. This notion rests on experimentally confirmed observations that normal brain activity can be quantified (modeled) as a system with multiple (complex) states. In contrast, seizure activity corresponds to a model system with reduced complexity, and hence a reduced number of states; this change in state can be interpreted in terms of information loss [199]. Indeed, during most seizures, there is a loss of higher brain functions, such as memory formation, and in the case of complex seizures, consciousness is disrupted.
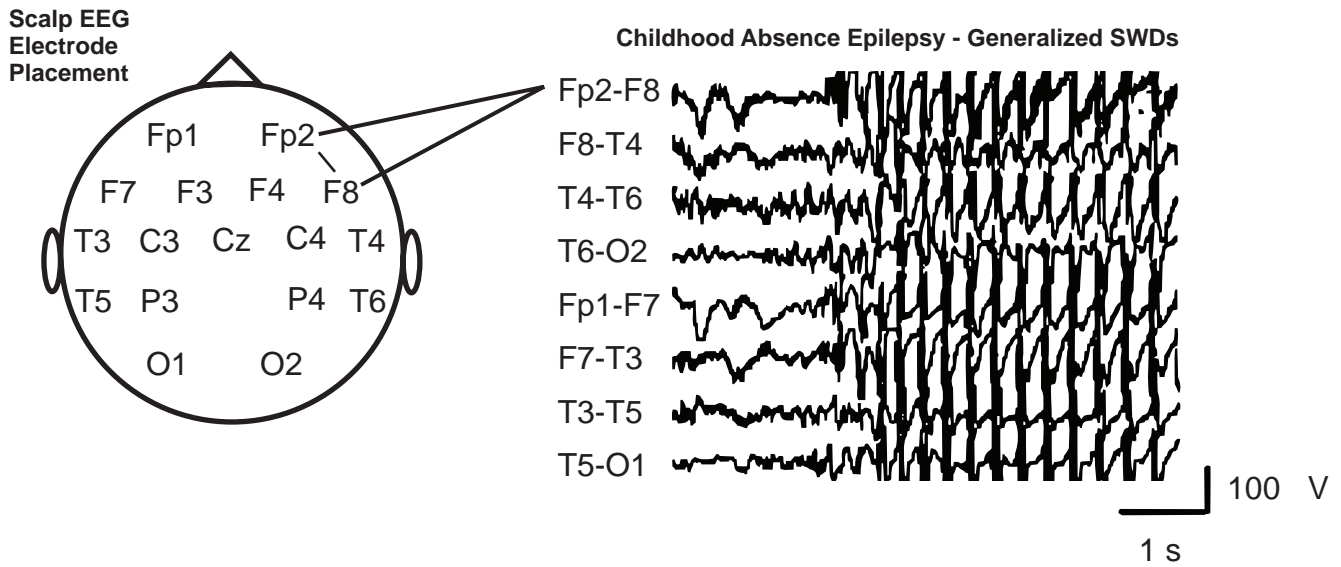
Figure 1.2: Spike-wave discharges in human absence epilepsy. Typical 3-4 Hz spike-wave discharges observed over the entire brain, a hallmark of generalized epilepsy. Electroencephalographic (EEG) recordings are presented for a selection of electrodes placed over the scalp covering the entire head. Placement of EEG electrodes is depicted on a head model. Voltage tracings are presented in a bi-polar manner with potentials, originally recorded in reference to a non-involved electrode, represented as a subtraction from two neighboring electrodes to produce a single tracing. Adapted from Ref. [385].

Table 1.1: Clinical attributes of Generalized Idiopathic Epilepsy. Generalized seizures show bilateral and synchronous onset observed in EEG recordings. Seizures in idiopathic generalized epilepsy are usually one of several types: generalized tonic-clonic, myoclonic, absence, or atypical absence. Idiopathic generalized epilepsy is a subtype of generalized epilepsy that has a genetic predisposition and includes the following epileptic disorders [3]

A - Childhood absence epilepsy
- Absence seizures manifest between ages of 4 to 8
- More common in females
- Respond well to antiepileptic drugs
B - Juvenile absence epilepsy
- Onset around puberty
- No sex predominance
- Atypical absence seizures
- Often have other seizure types (generalized tonic-clonic, myoclonic, and atonic seizures
- Patients may be intellectually impaired
C - Juvenile myoclonic epilepsy
- Seizure onset between ages of 8 to 18
- Have generalized tonic-clonic and myoclonic seizures
- Myoclonic seizures are characterized by sudden jerks of the neck, shoulders, and arms that may be repetitive without losing awareness
- Patients may exhibit photosensitivity
- Most common form of idiopathic generalized epilepsy
D - Generalized tonic-clonic seizures alone
− Seizures occur upon awakening
− Seizures can occur during sleep
− Time of seizure occurrence may not be linked to any external factors

Table 1.2: Other voltage- and ligand-gated ion channel genes carrying mutations that have been linked to idiopathic generalized epilepsies. *Abbreviations:* EA - episodic ataxia, BFNC - benign familial neonatal convulsions, CAE - childhood absence epilepsy, GEFS+ - generalized epilepsy with febrile seizures plus, SMEI - severe myoclonic epilepsy of infancy, BFNIS - benign familial neonatal and infantile seizures, JME - juvenile myoclonic epilepsy, FS - febrile seizures.

Gene	Channel or Subunit	Epilepsy Disorder	References
KCNA1	$K_v 1.1$	EA1	[35, 391]
KCNQ2	$K_v 7.2$	BFNC, myokymia	[85]
KCNQ3	$K_v 7.3$	BFNC	[50, 304]
CLCN2	CLC-2	CAE	[142]
SCN1A	$Na_v 1.1$	GEFS+, SMEI	[60, 112]
SCN2A	$Na_v 1.2$	GEFS+, BFNIS	[148, 326]
SCN1B	β_1	GEFS+	[357]
GABRA1	$GABA_A (\alpha_1)$	JME	[68]
GABRG2	$GABA_A (\gamma_2)$	GEFS+, FS, CAE	[12, 356]
GABRD	$GABA_A (\delta)$	GEFS+	[92]

1.2.1 Features of Idiopathic Generalized Epilepsy

From a clinical perspective, epilepsy can be classified into two broad categories [134]. First, focal (or partial) epileptic seizures arise from small localized brain regions (e.g. motor cortex). Partial epileptic seizures can also arise from focal brain lesions caused, for example, by traumatic brain injury [145]. Moreover, it is now known that certain focal epilepsies can have a genetic origin [347]. The second category comprises generalized epilepsies, where seizures are characterized by virtually simultaneous onset over both brain hemispheres as seen using scalp electroencephalography (EEG, see Fig. 1.2). The generalized epileptic syndromes can further be classified as either symptomatic or idiopathic. Symptomatic generalized epilepsy is thought to be caused by identifiable factors such as anoxia and infection, which can result in widespread brain damage. In contrast, idiopathic generalized epilepsies have no clear etiology and may be at least partly caused by defects at the genetic level [20, 247]. Data gathered from several cohort studies suggests that the frequency of idiopathic generalized epilepsies in the general epilepsy population is between 15-20% (reviewed in [160]). As outlined above, although epileptic disorders span a continuum of conditions, I focus here predominantly on

idiopathic generalized epilepsies in order to highlight recent developments implicating the involvement of voltage-gated calcium channels in this spectrum of epilepsy disorders. Absence-type epilepsies account for 3 to 4 percent of all seizure disorders [86]. As classified by the International League Against Epilepsy (ILAE) [3], typical absence seizures are a defining attribute of several of the idiopathic generalized epilepsies (Table 1.1). Seizures are characterized by a sudden impairment in consciousness, behavioural arrest, and may be accompanied by facial clonus, or other subtle physical manifestations. These seizures are generally short in duration (lasting typically less than 10 seconds) and terminate suddenly without any post-seizure alterations in behaviour. The electrographic hallmark of absence seizures are generalized spike-wave discharges (SWDs) that can be recorded using scalp EEG. These discharges typically arise synchronously over both brain hemispheres with a frequency of approximately 3-4 Hz and are maximal over frontal midline regions with minimal involvement of posterior brain regions [108, 153, 283]. In generalized epilepsy, SWDs are principally mediated by interactions between thalamic and cortical networks [20] and are known to involve the activity of voltage-gated calcium channels. It must be noted that although absence seizures are always associated with SWDs, the converse is not true as SWDs are observed in other forms of epilepsy [108]. This is a relevant point when considering subsequent discussion on models of spike-wave epilepsy.

Patients affected by idiopathic generalized epilepsy commonly present with their first seizure between the ages of six and sixteen [134], however adult onset has also been reported [220]. Patients with idiopathic epilepsy syndromes exhibit no underlying structural or brain lesions visible on MRI (magnetic resonance imaging) and are otherwise neurologically normal [134, 109]. In the case where absence seizures are the predominant epileptic seizure type [109], childhood absence epilepsy and juvenile absence epilepsy encompass the two main idiopathic epilepsy subtypes. Patients with childhood absence epilepsy are typically neurologically normal. On the other hand, juvenile absence epilepsy patients may have intellectual impairment and they have atypical absence seizures, characterized by a longer duration, less abrupt onset, loss of postural tone, and often the co-occurrence of other seizure types (Table 1.1). Two other idiopathic generalized epilepsy seizure types - juvenile myoclonic epilepsy and idiopathic generalized

epilepsy with tonic-clonic seizures alone [8] (Table 1.1) are recognized by the international classification [3]. Specific diagnosis of different idiopathic generalized epilepsy types occurs best when both clinical and EEG data are available. It is interesting to note that generalized tonic-clonic seizures in idiopathic generalized epilepsy usually occur after awakening, particularly from a brief period of sleep when preceded by sleep depravation. This relation is particularly clear in patients with juvenile myoclonic epilepsy and implicates the thalamocortical network, which is known to be involved in both sleep rhythm and SWD generation.

Of the absence-type idiopathic generalized epilepsy disorders, childhood absence epilepsy is perhaps the one that has been most extensively studied at the genetic level. Patients with childhood absence epilepsy can have a family history of epilepsy that is inherited in an autosomal dominant manner, with concordances of up to 85% reported in monozygotic twins [14]. However, genetic studies have also identified individuals with mutant genes who do not exhibit the epileptic phenotype [294]. Moreover, the precise identification of gene loci is complicated by the presence of a large number of genetic polymorphisms in the childhood absence epilepsy population [289]. Therefore, it is not entirely clear what the relative contributions of external or endogenous factors (such as involvement of multiple genes) are in bringing about the spectrum of epileptic seizure types observed in idiopathic generalized epilepsies. Nonetheless, there is substantial evidence implicating a genetic component in idiopathic generalized epilepsy, and in particular in absence-type seizure disorders [151]. Genetic association studies have identified mutations in a number of different types of voltage-gated channels and ligand-gated channels, including $GABA_A$ receptors, as well as voltage-dependent Na^+, K^+, and Cl^- channels, resulting in either a gain or loss of function [127, 246, 345] (see Table 1.2). In the context of idiopathic epilepsies, the two brain structures that have received the most attention are the neocortex and the thalamus. The normal connectivity of these two brain structures differs at the level of neuronal/interneuronal cell types and at the level of network organization. Interactions between the thalamus and neocortex bring about synchronized oscillations that, under normal conditions, serve physiological roles such as the generation of sleep spindles, which occur in early stages of sleep [321]. During spike-wave seizures, the normal function of this circuitry is somehow altered in a manner that results in the generation of SWDs. As such, voltage-gated

calcium channels have increasingly emerged as important players in the generation of SWDs in both humans and in experimental models of epilepsy.

In Chapter 2, I review the current state of knowledge concerning the role of these channels (i.e. T-types) in relation to idiopathic generalized epilepsy. Although there are several well documented mutations involving P/Q-type channels (reviewed in [176]), I will focus on the $Ca_v3.2$ T-type channel isoform and report on functional consequences of missense mutations as identified by three independent genetic linkage studies (see Chapter 2).

1.2.2 Epileptic Neuronal Networks and High Frequency Oscillations & Dynamics

The brain and its neuronal networks are a complex system. Since the 1960s a relatively new branch of science, nonlinear dynamical systems theory, has been used to describe complex biological and mainly physical systems. Nonlinear dynamical systems theory (i.e. chaos theory) is a mathematical framework where a system's behaviour is characterized in terms of state-variables. These variables are fundamental parameters that define the state(s) of the system at a given time (or point in space). The time-dependent change in state-variables is therefore a trajectory in a multidimensional space, the "state-space", where the trajectory completely describes the system over a period of time. Trajectories (system behaviours at different times) can then be explored mathematically to reveal subtleties such as stable, unstable, and metastable dynamical regimes. For example, the behaviour of a single neuron, over time, could be viewed as a continuous trajectory in a state-space with dimension equal to the number of variables required to describe its firing (e.g. ion channels, pumps/exchangers, synaptic inputs). The trajectory could be explored to reveal tonic, phasic, and variants of bursting behaviour. The problem that arises for biological systems is that it is difficult to determine the system's state-variables and furthermore to measure those variables with sufficient accuracy in order to reconstruct the state space. Nonetheless, significant progress has been made by selecting a few measurable parameters (i.e. observables) of the system and reconstructing a lower dimensional version of the actual state-space. This is equivalent to a projection (shadow) of the trajectory in the actual state-space, and fundamentals of the system's dynamical behaviour are retained and accessible for further analysis.

The following is a brief introduction to High Frequency Oscillations, which have been demonstrated to be surrogate markers of epileptogenicity in neuronal networks (see Chapter 3). Therefore, the temporal evolution of particular frequencies, specifically HFOs (in time and space), can be used as state-space markers of the system to further characterize local network dynamics in a seizure; the transition to seizure activity can also be represented by specific parameters (coordinates) in state-space.

Neuronal population activity recorded electrophysiologically in the range of 80 Hz and above is collectively referred to as High Frequency Oscillations (HFOs) [341]. Waveforms with spectral components in the HFO range have been recorded in the hippocampus and entorhinal cortex in both normal [42, 58, 383] and epileptic neuronal networks [118, 25, 24, 26, 27, 31]. HFOs are further classified into two frequency bands: ripple ($\approx$100-200 Hz) and fast ripple (FR, 200 Hz +) frequency bands. Cellular and network mechanisms underlying HFOs are believed to involve both excitatory and inhibitory synaptic transmission [215], in addition to electrotonic coupling [102]. These modalities of coupling allow for dynamic and transient changes in synchronization of sub-populations of neurons in larger networks. Recent evidence suggests gap-junctions located between axons of hippocampal pyramidal cells can underlie high frequency activity [339, 340, 338, 76].

Under non-epileptic conditions, ripples may play a role in memory consolidation, transferring information from the hippocampus to the neocortex [41, 300]. Ripples and FRs can coexist under epileptic conditions. They have been observed in in vivo recordings of seizure-like activity and in intracranial EEG recordings from hippocampal and entorhinal cortices of epileptic patients during video-EEG monitoring [25, 24]. Although HFOs in the ripple band are observed in both normal and epileptic states of brain activity, FRs occur predominantly in seizure foci [27, 31, 29, 315]. Therefore, observation of FRs may serve as "surrogate markers" for the presence of an underlying epileptic condition and may have implications for seizure initiation [340, 28]. Thus, identification and characterization of fast ripples, particularly during a pre-ictal period [199], may have clinical value. To date, there are few studies that have quantitatively analyzed how HFOs change over time from interictal to ictal activity [106, 187, 377]. To further investigate both spatial and temporal characteristics of HFOs, in relation to pre-seizure

changes, I engaged in a combined *in vitro* and patient-based study (see Chapter 3).

1.2.3   Overview of Experimental Data

This dissertation is comprised of three data chapters, each of which are reasonably independent from the other in their main contribution towards the topic of neuro-excitability in relation to seizure activity.

Hypotheses:

- Chapter 2 - *We hypothesize that missense mutations, identified in patients with idiopathic generalized epilepsy (IGE), can result in altered $Ca_v3.2$ T-type channel function.* In this chapter I report on the functional consequences of three different sets of mutations. Each set represents material from a different manuscript, and more importantly, corresponds to a series of mutations that were reported in separate genetic linkage studies in different populations of epileptic patients. I observed biophysical alterations for a subset of mutant channels, however the majority of $Ca_v3.2$ T-type channel mutations do not result in large biophysical effects.

- Chapter 3 - *We hypothesize that high Frequency Oscillations (HFOs): (a) display a spatial distribution that correlates with the sites of seizure onset. (b) HFOs undergo measurable and consistent changes during the immediate epoch leading up to seizures.* In this chapter, I utilize two different experimental modalities to test the localization, spatial distribution, and time-dependent changes of HFOs. Firstly, in an *in vitro* seizure model, I demonstrated that HFOs are generated locally and exhibit a sharp increase in power (>100 Hz) approximately 30 sec. prior to seizure-like events. Secondly, in a clinical setting, I investigated the intracranial EEG of seven patients with different classifications of epilepsy. I observed that HFOs localized to electrode contact where ictal onset was observed. Furthermore, the observed spatial distribution reflected the size of the underlying seizure generator; for example, HFOs were observed over several contacts when they were over an expansive brain lesion. I also observed that HFOs undergo a selective increase in high frequencies approximately 10 sec. prior to seizure onset.

- Chapter 4 -*We hypothesize that PrP-null mice exhibit altered synaptic physiology with specific alterations to glutamatergic synaptic transmission.* Using brain slices and a model of *in vitro* seizure activity, I demonstrated that PrP-null mice exhibited a lower threshold for activity both under physiological and epileptic conditions (zero Mg^{+2} model). Exploring miniature synaptic currents, I observed that PrP-null mice exhibit a slightly decreased GABAergic activity, but moreover, show greatly enhanced NMDA receptor activation. This was also confirmed via evoked responses using puffs of NMDA. The pattern of activation seems to be most consistent with an alteration in NR2 subtype composition; somehow the activity of NR2D is increased. There do not seem to be differences in transcription, trafficking, or expression of NR2D between WT and PrP-null mice in adults and P0 mice. Consistent with increased NMDA activity, I assayed excitotoxicity differences and observed that PrP-null mice show marked susceptibility to NMDA-mediated excitotoxicity. Taken together, these findings suggest a modulatory role (perhaps protective role) for the endogenous PrP^C protein in relation to the NMDA receptor.

Chapter 2

Functional Characterization of $Ca_v3.2$ T-type Voltage-gated Calcium Channel Mutations Associated with Idiopathic Generalized Epilepsies

2.1 Introduction: T-type Calcium Channels and Spike-wave Seizures

2.1.1 Subtypes and Physiological Roles of Voltage-gated Calcium Channels

Voltage-gated calcium channels are key mediators of calcium entry into neurons in response to membrane depolarization. Calcium influx via these channels mediates a number of essential neuronal responses, such as the activation of calcium-dependent enzymes, gene expression [95, 117, 327], the release of neurotransmitters from presynaptic sites [298, 311, 368], and the regulation of neuronal excitability [261]. The nervous system expresses a number of different calcium channels with unique cellular and subcellular distributions and specific physiological functions. They have been classified into two major categories [49]: low voltage-activated (LVA) calcium channels (i.e., T-type channels) and high voltage-activated (HVA) channels, although this classification should not be applied rigidly, as some of the HVA channel subtypes can, under certain circumstances, be activated at relatively negative voltages [379]. As outlined in greater detail below, LVA channels are activated by small depolarizations near typical neuronal resting membrane potentials and are key contributors to neuronal excitability. Their functional identification is aided by their sensitivities to blockers such as nickel ions [120, 192], mibefradil [224], and the scorpion venom derived peptide kurtoxin [59, 301], however, the above blockers cannot be considered as truly selective for T-type channels. HVA channels require larger membrane depolarizations to open and can be further subdivided, based on pharmacological and biophysical characteristics, into L-, N-, R-, P- and Q-types. L-type channels are slow to activate and inactivate with barium as the charge carrier, and are defined by their

sensitivities to dihydropyridine agonists and antagonists [120]. They are typically found on cell bodies where they participate, among other functions, in the activation of calcium dependent enzymes and in calcium dependent gene transcription events [11, 95, 362]. N-type channels produce inactivating currents that are selectively and potently inhibited by ω-conotoxins GVIA and MVIIA, two peptides isolated from fish hunting marine snails [2, 115, 255, 279]. P- and Q-type channels are identified by their differential sensitivities to the American funnel web spider toxin ω-agatoxin IVA [2], and like N-type channels, they are concentrated at presynaptic nerve terminals where they are linked to the release of neurotransmitters [366, 367]. In the context of neurotransmitter release, N-type and P/Q-type channels do not appear to be created equally, as N-type channels tend to support inhibitory neurotransmission, whereas the P/Q-type channels have more frequently been linked to the release of excitatory neurotransmitters but can also support inhibitory release [40, 43, 99, 193, 268]. R-type channels were originally termed as such because of their resistance to the above blockers [277]. These channels are rapidly inactivating and activate at somewhat more hyperpolarized potentials compared with the other HVA calcium channel subtypes [310]. They can potently, albeit not totally selectively, be inhibited by SNX-482, a peptide toxin isolated from tarantula venom [23, 249]. R-type channels are distributed in proximal dendrites and presynaptic nerve termini [348, 384, 388]. Their precise physiological function remains enigmatic, however, there is evidence that these channels underlie carbachol dependent plateau potentials in hippocampal CA1 neurons [184] and may mediate neurotransmitter release at select synapses [359].

2.1.2   Molecular Structure of Voltage-gated Calcium Channels and Ancillary Subunits

The principal pore forming subunit of both LVA and HVA calcium channels is the α_1-subunit which contains the key structural moieties that are required for a functional calcium channel, and which is the sole determinant of the calcium channel subtype. To date, nine different types of neuronal calcium channel α_1-subunits have been identified and shown to fall into three major classes - Ca_v1, Ca_v2, and Ca_v3 (Fig. 2.1). The Ca_v1 family encodes different isoforms of L-type channels [183, 229, 233, 336, 373]. Among the Ca_v2 family, alternate splice isoforms of $Ca_v2.1$ encode P- and Q-type channels [22], $Ca_v2.2$ represents N-type channels [104, 373],

and $Ca_v2.3$ corresponds to R-type channels [277, 312, 374] (for review, see [306]). Finally, the Ca_v3 family represents three different types of T-type channels (i.e., $Ca_v3.1$, $Ca_v3.2$, and $Ca_v3.3$) with distinct kinetic properties [51, 72, 179, 191, 228, 238, 239, 260]. These different types of calcium channel α_1-subunits support specific physiological functions, as evident from findings obtained from calcium channel knockout mice, and by studying genetic abnormalities in calcium channels in disease states (for review see [263]).

HVA calcium channels are heteromultimers that are formed through association of α_1-, β-, $\alpha_2 - \delta$-, and γ-subunits (Fig. 2.1). While calcium channel α_1-subunit is sufficient to form functional channels, the association of HVA channel α_1-subunits with ancillary β- [96], $\alpha_2 - \delta$- [9, 44, 181], and γ [18] subunits is known to result in altered functional properties and/or increased plasma membrane expression.

The $\alpha_2 - \delta$-subunit is translated as a single gene product, and then post translationally cleaved into a membrane spanning δ-peptide (27 kDa) and extracellular α_2-peptide (143 kDa) [81], which are subsequently re-linked via disulfide bonds. Expression studies have shown that the $\alpha_2 - \delta$-protein alters current kinetics and current densities when coexpressed with HVA α_1-subunits, although to different degrees with different channels [181, 382]. The $\alpha_2 - \delta$-subunit is the only known calcium channel ancillary subunit to interact with a clinically active drug compound, in that its association with gabapentin mediates analgesia [303]. To date four genes encoding four different $\alpha_2 - \delta$-proteins ($\alpha_2 - \delta_1$, $\alpha_2 - \delta_2$, $\alpha_2 - \delta_3$, $\alpha_2 - \delta_4$) have been identified, with several potential additional splice variants [180].

Four different types of β-subunits (β_1 through β_4), along with various splice variants (reviewed in [96, 281]) have been identified and characterized. Unlike $\alpha_2 - \delta$-proteins, β-subunits appear to be exclusively cytosolic in nature, with the exception of β_{2a}, which can become palmitoylated and thus membrane anchored [114, 273]. The β-subunit core resembles membrane-associated guanylate kinase homologs with conserved interacting SH3 and guanylate kinase (GK) domains [329]. Residues in the GK domain participate in the formation of a hydrophobic groove that is involved in the high affinity binding to a conserved region within the domain I-II linker region of HVA calcium channels, termed alpha interaction domain (AID) [55, 350]. Recently published crystal structure data have revealed that binding of the β-subunit

to the channel is critically dependent on a functional association of the SH3 and GK regions [55, 256, 350] which is stabilized by the beta interaction domain, a short amino acid stretch that was originally thought to directly interact with the calcium channel AID region [350]. The functional consequences of β-subunit coexpression include increased plasma membrane expression of the α_1-subunit [17, 57, 269], as well as altered channel kinetics [114, 382] (reviewed in [9]). Consistent with an important role in calcium channel function, knockout of individual β-subunit genes results in severe physiological consequences.

Eight different types of γ-subunits have been identified (γ_1 through γ_8) [9]. The γ-subunits are comprised of four transmembrane domains with intracellular N- and C-termini, but the mutual sites of interaction with the α_1-subunit remain unknown. While it has been observed that some of the γ-subunits have the propensity to alter the functional characteristics of HVA calcium channels [286] (reviewed in [18]), the precise action of these subunits on HVA calcium channels remains to be completely understood, and there is evidence that these subunits can interact with other membrane proteins such as AMPA receptors [52].

Considering the important roles of these subunits in regulating calcium channel function, it is not surprising that missense mutations have been discovered that result in their altered function with effects on calcium channel gating and targeting.

In contrast to HVA channels, LVAs seem to require only the α_1-subunit, however, this remains an area of controversy. While effects of ancillary subunit co-expression on T-type channel function have been reported in certain expression systems [98, 103, 152], antisense knockdown of calcium channel β-subunits in neurons does not appear to affect T-type channel function [185, 196]. Moreover, a biochemical association between T-type channel α_1- and ancillary subunits has not been demonstrated [103].

One may perhaps expect that naturally occurring mutations in calcium channel subunit genes may have the propensity to alter normal physiological responses in animals and humans. As I will outline below, this does indeed occur within the context of idiopathic generalized epilepsies. Although HVA channels, P/Q-type in particular, have been associated with several forms of generalized seizure conditions (several genetic animal models of absence epilepsy), a clear link to the typical form of this epileptic syndrome in patient populations remains unclear.

In contrast, several recent genetic linkage studies have brought LVA channels, $Ca_v3.2$ in particular, in to the limelight and I will discuss these channels in the context of both physiology and altered function in relation to idiopathic generalized epilepsy (see Sections 2.1.4, 2.1.6, and 2.1.8).
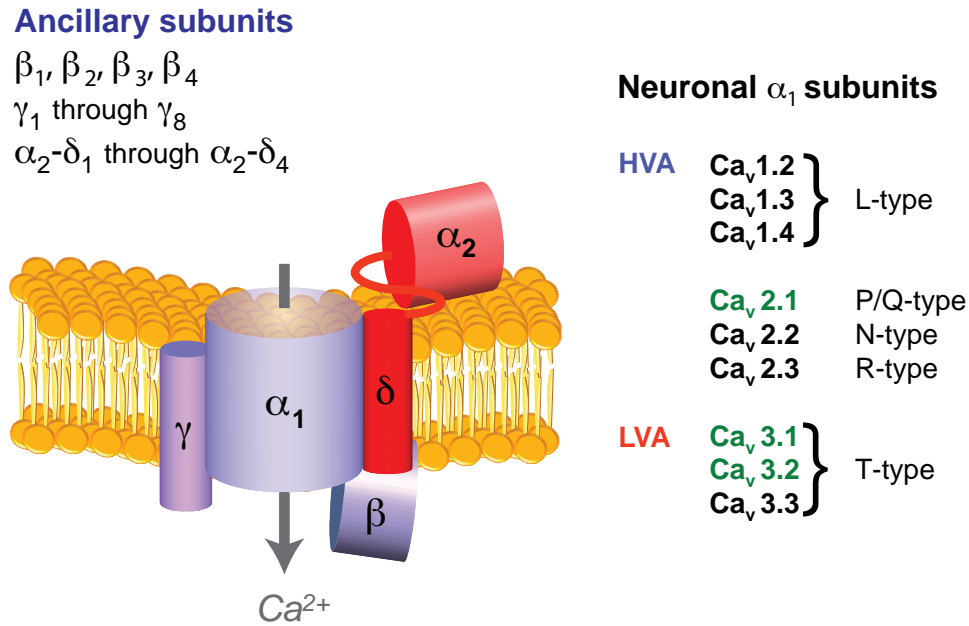
Figure 2.1: Subunit assembly and subtypes of voltage-gated calcium channels. Graphic representation of the high voltage-activated (HVA) calcium channel complex consisting of the main pore forming α_1 subunit plus ancillary, β, γ, and $\alpha_2 - \delta$ subunits. Low voltage activated calcium (LVA) channels may consist of only the α_1 subunit (not shown separately). Different neuronal α_1 subunits correspond to different calcium channel isoforms identified in native neurons; those highlighted in green exhibit missense mutations that have been associated with generalized absence seizures. Adapted from Ref. [176].

2.1.3 Structural Basis of Calcium Channel Function

To provide a context for the effects of mutations in calcium channel genes that have been linked to the etiologies of neurological disorders such as epilepsy, I will briefly touch on the structural determinants of calcium channel function. The α_1 subunits are comprised of four major transmembrane domains that are structurally homologous to those found voltage-gated sodium and potassium channels (reviewed in [47, 48], see Fig. 2.1). Each domain consists of six transmembrane helices, with intracellularly localized N- and C-termini. The fourth membrane

spanning alpha helix (S4 segment) contains positively charged arginine and lysine residues every three to four amino acids. Mutagenesis and crystallization studies involving potassium channels have confirmed early suggestions that this region forms the voltage sensor [46], a structural element that translocates within the membrane in response to changing membrane potential [100, 161, 206] and mediates channel opening. The reentrant p-loops between S5 and S6 segments are believed to line the pore of the channel to allow for the passage of permeant ions. The p-loops each contain a critical glutamic acid residue (4 in total) that together form a ring of negative charge and allow for selectivity of divalent cations over monovalent ions [107, 378, 381]. However, other amino acid residues in the outer vestibule of the pore are likely to contribute to ion permeation and selectivity [116, 291]. The α_1 subunits also contain the key structural elements that allow the channel to inactivate upon prolonged membrane depolarization. Voltage-dependent inactivation, a key feature that regulates availability of a calcium channel to open, is thought to involve a physical occlusion of the channel pore by a cytoplasmic gating particle. This inactivation gate appears to be formed at least in part by the cytoplasmic domain I-II linker region. However, other regions of the channel, in particular the S6 helices are also important (reviewed in [322]), perhaps by forming a docking site for the inactivation gate [323]. The C-terminus region of the α_1 subunit contains the key loci responsible for calcium dependent inactivation, a process that is observed only when calcium is used as the charge carrier. Originally thought to occur only with L-type channels, more recent evidence indicates that all types of high voltage activated channels are subject to this type of regulation by calcium ions. Mechanistically, this process involves a dynamic interaction of the calcium binding protein calmodulin with the C-terminus region of the α_1 subunit [189, 197, 262, 392].

The cytoplasmic linker regions of various types of calcium channel α_1 subunits form key interaction sites for regulatory proteins, and may be substrates for phosphorylation events. For example, the I-II linker regions of $Ca_v2.1$ and $Ca_v2.2$ subunits interact with G protein $G\beta_2$-subunits (for review see, [84, 97, 387]); the II-III linker regions of these two channels interact with a number of synaptic proteins (for review, see [48, 312]); the domain II-III linker region of $Ca_v3.2$ interacts with $G\beta_2$- subunits [376] and is a substrate for calmodulin dependent protein kinase phosphorylation [365]. These are but a few examples, as the list of calcium channel in-

teracting proteins is too extensive to comprehensively review here. Nonetheless, in the context of epilepsy-associated genetic mutations, it is important to consider that their physiological effects may manifest themselves by interfering with calcium channel regulatory mechanisms, without necessarily causing alterations in the biophysical properties of the channels per se.

2.1.4   T-type Channel Physiology

T-type channels mediate a spectrum of physiological roles including pace-maker activity and various forms of physiological and pathophysiological neuronal oscillations [122, 261]. Moreover, it was recently demonstrated that T-type channel activity can result in calcium induced calcium release in neurons of the paraventricular nucleus of the thalamus and other midline neurons associated with the thalamocortical system [282] (note that calcium induced calcium release is known to occur in thalamocortical neurons but it does not involve the action of T-type channels [37]). This novel role for T-type channels in the thalamocortical system putatively lends itself to numerous calcium-dependent signaling pathways that extend the role of these channels beyond their biophysical attributes and into complex processes such as synaptic plasticity [285].

T-type channels display several unique biophysical features compared with HVA channels. They activate and inactivate near the resting membrane potential of neurons ($\approx$ -60 mV), display more rapid inactivation kinetics, and deactivate more slowly to produce pronounced tail currents [39]. There is also an increased overlap in the voltage-dependences of activation and inactivation which gives rise to a phenomenon termed the "window current". At membrane voltages where the window current is operational, a small fraction of T-type channels never fully inactivates and can be rapidly recruited for calcium influx upon depolarization. Interactions between the window current and the K^+ leak current in thalamic (reticular and thalamocortical) and possibly cortical neurons can result in membrane bi-stability [73]. This T-type mediated potential can interact with other active currents (e.g. I_h) to modulate neuronal output between non-oscillatory and oscillatory modes that have different physiological correlates such as the slow ($<$1Hz) sleep rhythm [73, 155]. In response to a membrane hyperpolarization, a large fraction of T-type channels is recovered from the inactivated state, thus priming them

for opening events. The ensuing calcium entry is thought to mediate a low threshold calcium potential, a transient membrane depolarization that is sufficiently large to trigger a succession of sodium spikes [83, 186, 221, 296, 386]. This feature is commonly referred to as "rebound bursting" and has been shown to occur in various neuronal subtypes including thalamocortical relay neurons, thalamic reticular neurons [69, 89, 156, 205], and a subpopulation of neocortical cells [82].

2.1.5 T-type Calcium Channel Distribution

It is important to note that the precise biophysical characteristics of T-type calcium channels in relation to their physiological roles vary with Ca_v3 channel subtype, and can be dramatically affected by alternate splicing of a given T-type channel gene [248]. Their unique gating kinetics in addition to their specific regional distribution allows for these channels to be used by different neuronal subtypes to generate a variety of network dynamics. The exact distribution and protein expression levels of T-type calcium channels in the brain was not well understood until recently demonstrated by McKay and colleagues [226]. Most of the previous knowledge on T-type channel distributions was derived from in situ hybridization studies in rat brain slices [70, 169, 331]. While T-type channel mRNA and immunolabel have been detected across all brain regions including the cerebellum, I will focus predominantly on the major brain structures thought to be involved in spike-wave seizures (i.e., the thalamus and neocortex), and also include the hippocampus given that it is believed to be the brain structure with the lowest seizure threshold.

The hippocampus shows intense labeling for all T-type channel isoforms for both mRNA levels and protein expression. T-type isoforms are expressed at relatively high levels in the hippocampus [331]. Immunolabel was observed to exhibit a gradient of increasing staining intensity from the CA3 molecular layer towards CA1, with maximal intensity observed for subicular neurons [226]. A class of interneurons in the molecular layer of the dentate gyrus (DG) also exhibited intense immunolabel for all three T-type isoforms. Granule cells of the DG exhibited more intense $Ca_v3.2$ and $Ca_v3.3$ staining and much weaker staining for $Ca_v3.1$. Subcellular examination of immunolabel showed that $Ca_v3.1$ was expressed in somatic and

proximal dendritic regions. $Ca_v3.2$ labeling exhibited a more distal dendritic distribution although some somatic labeling was also observed. Interestingly, $Ca_v3.3$ distribution was robust and extended from the somatic region through to apical dendrites. Inhibitory interneurons were observed to be either positive or negative for different T-type isoforms, but most exhibited immunolabel for $Ca_v3.3$ channels.

The thalamus is perhaps the most studied structure in the context of T-type channel expression and function. Varying degrees of labeling for T-type channel isoforms was detected in the various thalamic nuclei. Most relevant to spike-wave seizures are the thalamic reticular neurons, thalamocortical relay neurons, and local GABAergic interneurons. Early in situ studies identified specific $Ca_v3.2$ and $Ca_v3.3$ staining in neurons within the nucleus reticulars (nRT) [331]. It should be noted, however, that it is not clear whether the presence of mRNA correlates well with protein expression levels in the plasma membrane, and what particular splice isoform of the channel may be present [131]. Indeed, immunolabeling identified $Ca_v3.2$ and $Ca_v3.1$ as the main T-type channel isoforms present in nRT cells, with a subset of neurons expressing lower levels of $Ca_v3.3$ [226]. Cells in the nRT are primarily GABAergic interneurons that play a key role in synchronizing thalamic outputs onto thalamocortical neurons that then project to the cortex [321]. Thalamocortical (relay) neurons exhibited broad immunolabel for all three isoforms with greater intensity for $Ca_v3.1$ and $Ca_v3.2$, with a lesser degree of labeling observed for $Ca_v3.3$ channels [226]. Low levels of immunolabel were observed for local circuit interneurons, although $Ca_v3.3$ staining was most intense for GABAergic neurons as identified by GAD (glutamate decarboxylase, catalyzes GABA synthesis from glutamate) staining [226].

Diffuse mRNA levels have been detected for $Ca_v3.1$ and $Ca_v3.3$ in most cortical areas [321]. Transcript levels of $Ca_v3.2$ in the cortex have been reported to occur at lower levels, except in layer V cortical pyramidal neurons [331]. When investigated by immunolabeling all layers of the cortex showed expression for all Ca_v3 isoforms but for each level there were some cells showing lack of staining for one type of isoform [226]. Cellular distribution localized $Ca_v3.1$ to soma and proximal dendrites, whereas $Ca_v3.2$ and $Ca_v3.3$ were observed at more distal processes, especially in layer V pyramidal neurons. Intriguingly, $Ca_v3.1$ somatic labeling was observed for some inhibitory (GAD positive) local interneurons. In addition to

the recent description of subcellular distribution of T-type channels, demonstrated using immunolabeling, a number of functional studies also exist that describe possible roles for varied T-type channel isoforms along the neuronal axis. Concordant evidence from numerous electrophysiological and functional imaging studies suggests that they are located both on and near the soma [165], and purportedly at more distal dendritic sites [158, 168, 170, 211, 221]. Moreover, a recent study using electrophysiological and pharmacological investigation of reticular cells in thalamic brain slices indicates the presence of a slowly inactivating T-type current in the proximal dendrites and a fast inactivating current at the soma [163]. Pharmacological manipulations have suggested that the fast inactivating current is likely to be carried by $Ca_v3.2$ channels, whereas the slow T-type current may be mediated by $Ca_v3.3$ channels. These results are generally consistent with findings from in situ hybridization and protein expression studies in reticular neurons [331, 226]. The subcellular distribution (e.g. soma vs. dendrites) is likely subject to further heterogeneity when considering the different T-type channel isoforms, splice variants, and developmental changes in the lifetime of the organism. For example, previous reports in reticular thalamic neurons have reported differences in the rates of inactivation of T-type currents in intact slices [87] (slow) as compared to acutely dissociated neurons [156] (fast).

2.1.6 T-type Channels, the Thalamocortical Network, and Spike-Wave Seizure Generation

The thalamocortical circuit is the primary link between peripheral sensory systems and the cerebral cortex. This circuitry is also one the most studied in the context of neurophysiological rhythm generation and encompasses structures responsible for the regulation of brain states such as arousal and slow-wave sleep - a hallmark thalamocortical oscillation [318]. From a simplistic anatomical perspective, this circuit consists of a network of reticular, thalamocortical (also referred to as relay), and neocortical neurons. Cortical neurons directly innervate reticular and thalamocortical neurons, whereas the reticular neurons provide GABAergic projections onto each other and onto thalamocortical neurons, which in turn, synapse onto neocortical neurons (Fig. 2.2). Indeed, although the thalamus receives many sensory inputs, the

primary source of excitatory synapses on to it come from the cortex [110, 111, 202, 203], which exemplifies the influence of neocortical activity on thalamic information processing. Both neocortical and thalamocortical cells have excitatory projections back onto reticular neurons, and the activity of the circuit is further regulated via thalamic (local-circuit) and neocortical interneurons [222, 299]. The intra-connectivity between reticular neurons is believed to be a form of lateral inhibition [346] and central to the role of this local network in modulating overall thalamic outputs to cortical areas during both physiological and seizure activity [123, 307].

Thalamic neuronal firing can be broadly categorized into tonic-mode and bust-mode firing. The latter involves the action of T-type calcium channels in the thalamocortical circuitry and is highlighted by their contribution to the propagation of thalamically generated spindles to the neocortex. Bursting in reticular neurons is mediated by low threshold calcium potentials [156] in response to corticofugal volleys from neocorticofugal inputs [66]. The bursts are preceded by prolonged hyperpolarizing potentials [318] that are triggered by the activity of G-protein coupled inward rectifier potassium channels [124], and lead to the activation of T-type currents in dendrites of reticular neurons [156]. Modeling studies have demonstrated a sensitive link between the compartmental distribution of T-type conductances and the ability of thalamocortical, and more so, reticular neurons to fire in burst mode [89]. Specifically, for a fixed burst threshold in a model of reticular neurons, GABAergic conductances are required to be relatively larger if the T-type current is localized to the soma vs. dendrites.

The low threshold calcium potential-induced bursts of action potentials occur in a subpopulation of reticular neurons and are manifested as tonic firing with burst-like modulation due to membrane bistability [123]. The GABAergic activity of reticular neurons (involving both $GABA_A$ and $GABA_B$) results in hyperpolarization and subsequent low threshold calcium potential-mediated rebound bursting in thalamocortical neurons, which faithfully track the bursts in the reticular network and manifest themselves as sleep spindles [318]. There is some evidence from *in vivo* studies that burst-mode firing in thalamic neurons can occur during wakefulness [135, 136], however this is not a common occurrence and this interpretation may be complicated by an intermediate state of brain activity such as drowsiness [317].

Absence-type seizures occur preferentially during drowsiness or slow-wave sleep, which

Thalamocortical Circuit
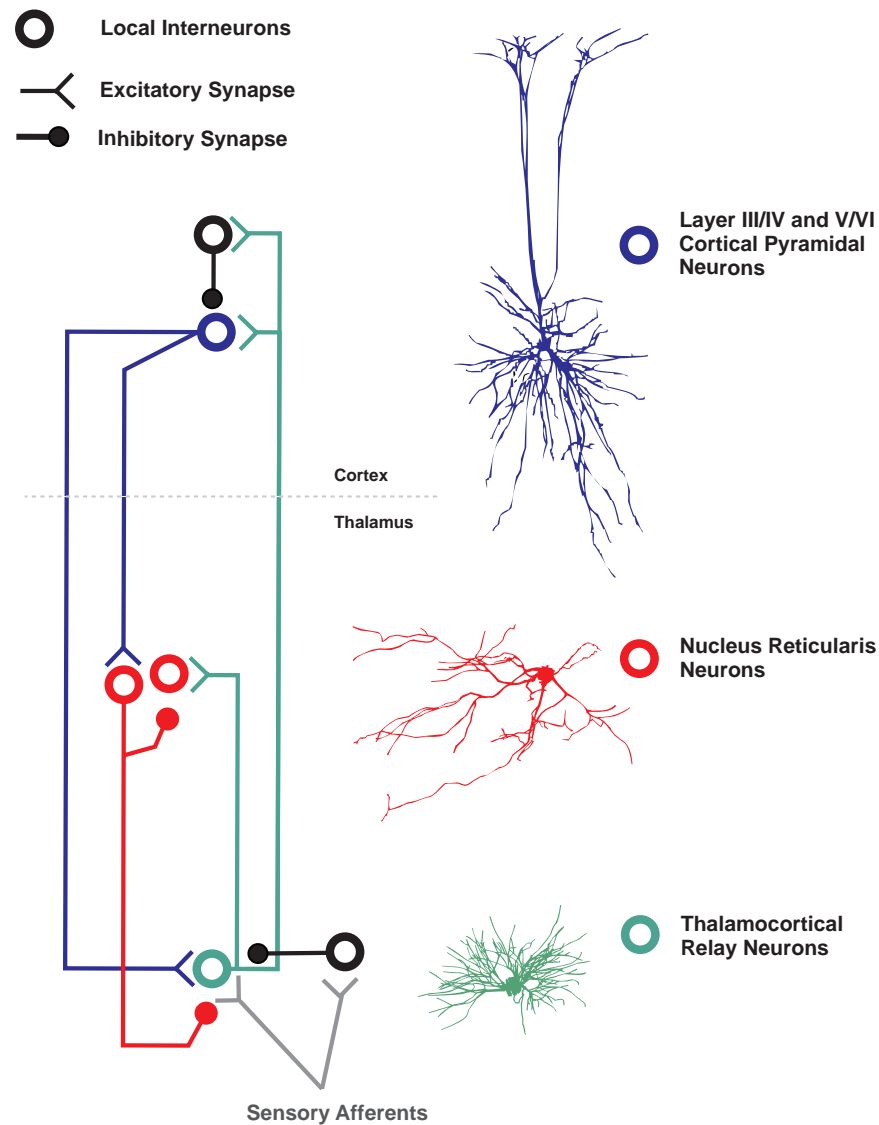
Figure 2.2: The simplified thalamocortical circuit involved in the generation of spike-wave discharges. Left: Neuronal circuitry implicated in the generation of spike-wave seizures. For simplicity, local-circuit interneurons in the thalamus and cortex are not illustrated. Neurons are indicated in form of color coded circles that correspond to neuronal phenotypes obtained from staining experiments in cats that were used in modeling studies [65, 87, 88]. Thalamic relay neurons (green) receive sensory inputs and project onto cortical pyramidal neurons in layers III/IV and V/VI in the cerebral cortex (blue). Sensory inputs can also project onto thalamic inhibitory interneurons (black - thalamus) that can in turn modulate the firing of relay neurons. Thalamocortical relay neurons can also synapse onto cortical inhibitory interneurons (black - cortex). Corticothalamic projections from Layer VI of the cortex can reciprocally synapse onto relay neurons in addition to neurons in the thalamic reticular nucleus (red). The GABAergic reticular neurons are highly interconnected both via chemical and electrical synapses and form a pacemaker sub-circuit within the thalamus. Both reticular and relay neurons express T-type calcium channels and can exhibit rebound bursts. Adapted from Ref. [176].

highlights the involvement of common synchronizing elements (such as the reticular network) underlying certain sleep and seizure states. However, unlike the state when sleep spindles are generated [124], the presence and interaction with the cortex is critical for the generation of SWDs [320]. During cortically generated SWDs the GABAergic reticular neurons faithfully follow the cortical bursting activity and are synchronized with the activity recorded in the cortex (Fig. 2.3). In contrast, thalamocortical neurons undergo a sustained hyperpolarization in response to phasic IPSPs, which are however incapable of recovering a sufficiently large fraction of T-type channels. Consequently, thalamocortical neurons do not exhibit rebound bursts during the epoch when SWDs are observed in the cortex [319] (Fig. 2.3). Reticular neurons are thus driven by the activity in the cortex, which leads to the inhibition of thalamocortical neurons, and prevents the feedback to cortical areas. Therefore, in one possible scenario, increased T-type channel (i.e., $Ca_v3.2$ and $Ca_v3.3$) activity could result in increased burst-mode firing in thalamic reticular neurons. The persistent activity of reticular neurons during SWDs causes increased membrane conductance in thalamocortical neurons in the form of steady inhibition, which may perhaps explain the unconsciousness during absence seizures caused by inhibition of synaptic transmission of signals from the outside world [318]. It should be noted that there are a large number of modeling studies in which underlying ionic currents and network dynamics are explored in the context of both physiological and epileptiform thalamocortical oscillations. Although review of these works is beyond the scope of this manuscript, a concise review by Destexhe and Sejnowski [90] is available.

The rhythmic activity that is observed in EEG recordings during an epileptic seizure is a reflection of cortical and thalamic network interactions. In a number rodent models of epilepsy, the frequencies of SWDs are typically faster than the 3-4 Hz observed with the common form of human absence seizures, which may hint at interspecies differences in these network interactions, or perhaps somewhat different pathways for seizure generation. Indeed, the frequency of SWDs in these rodent models is complicated by the notion that some of the observed thalamocortical oscillations may be part of normal physiological activity [264, 371]. Historically, there has been much debate with regards to the site of initiation for SWD-based seizures (reviewed in [230, 318]); specifically, the question pertaining to which structure, cortex vs. thalamus,
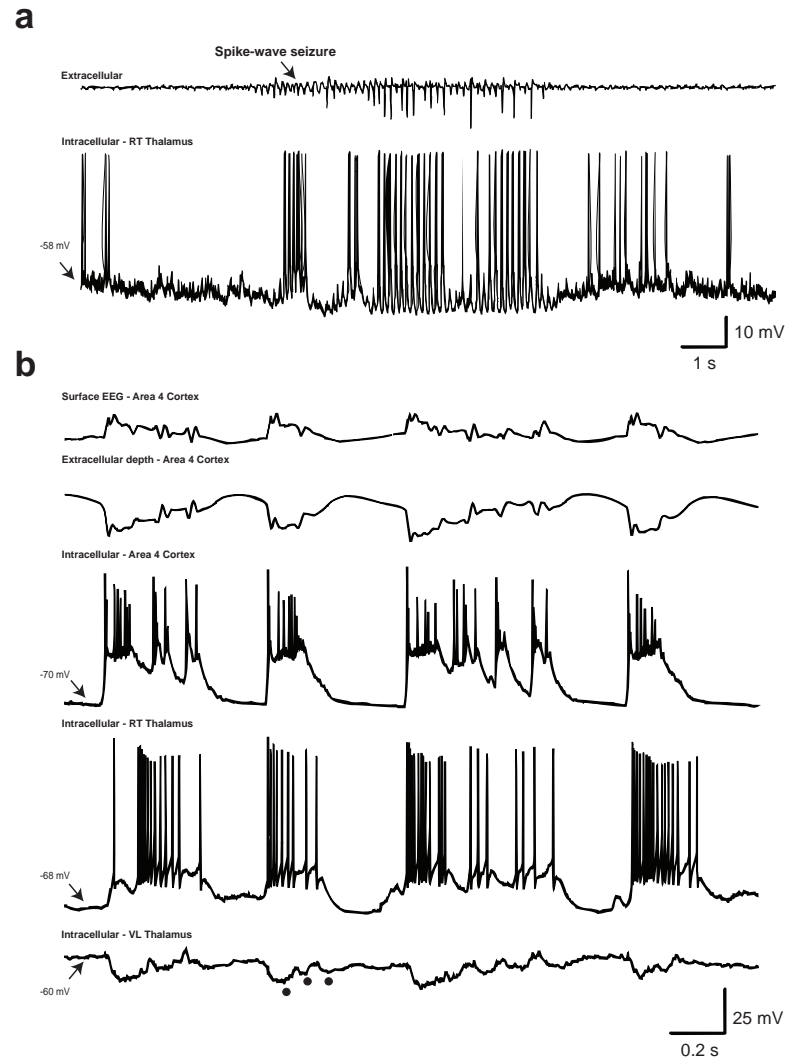
Figure 2.3: Firing patterns of thalamic and cortical elements in animal models of spike-wave seizures. **(A)** Simultaneous extracellular and intracellular recording of absence seizure activity in an adult Genetic Absence Epilepsy Rat from Strasbourg (GAERS). The intracellular recording is from a thalamic reticular neuron, which exhibits bursting activity in synchrony with spike-wave discharges recorded extracellularly. Adapted from Ref . [305]. **(B)** Simultaneous electroencephaolographic (EEG), extracellular field, and intracellular recordings of cortical and thalamic neurons during an epoch of spontaneous poly-spike-and-wave seizure activity in a cat under ketamine-xylazine anesthesia. Cortical and thalamocortical (in the ventrolateral nucleus, VL) recordings were obtained simultaneously and reticular neurons were recorded later and superimposed due to the repeatability of the oscillation. Cortical neurons exhibit bursting during each of the paroxysmal depolarizing shifts [225]. This activity is closely tracked by reticular neurons that exhibit T-type mediated bursting activity. The GABAergic influence of reticular neurons on thalamocortical cells can be seen by the series of inhibitory postsynaptic potentials (see dots), which result in tonic hyperpolarization of these neurons for the duration of the spike-wave activity. Similar observations have been reported during spike-wave seizures in the GAERS rat [265]. Whether thalamocortical neurons exhibit rebound spikes is a function of their membrane potential caused by inputs from reticular and cortical neurons. A large fraction of these cells however cannot fire, which is believed to result in disruption of information flow to the cortex resulting in the absence phenotype during seizures. Adapted from Refs. [318] and [319]. Adapted from Ref. [176].

is the key anatomical substrate for initiating SWDs. Initial evidence for the involvement of both structures came from human studies undergoing invasive intracranial EEG monitoring (reviewed in [19]), which is now deemed unethical for generalized forms of epilepsy due to a consensus that large networks in the brain are involved. However, a body of evidence from *in vivo* experiments in rats and cats suggests that the cortex may be the minimal substrate for generating spike-wave seizures (reviewed in [318]). Moreover, recent studies utilizing multi-site recordings in two accepted rat genetic models of absence epilepsy, the Genetic Absence Epilepsy Rat from Strasbourg (GAERS) and the Wistar Albino Glaxo rats, bred in Rijswijk (WAG/Rij), have suggested that neocortical cell firing temporally precedes (on the order of milliseconds) the activity in the thalamus [230, 264]. Taken together, these studies imply that complex interactions involving the entire thalamocortical network are necessary in generating rhythmic activity under both physiological and pathophysiological states, with T-type channels playing a key role in modulating the firing properties of neuronal elements.

2.1.7 Genetic Animal Models of Absence Epilepsy involving T-type Channels

Animal studies have provided insights as to whether T-type expression is altered via epileptic activity, or whether increased T-type expression is a requirement for the development of seizures. For example, the GAERS rat exhibits 7-11 Hz SWDs, usually after 30 days of life. In this rat model of absence epilepsy, an increase in T-type currents in reticular neurons has been reported after the second postnatal week [342]. This increase in T-type currents is putatively mediated by elevated $Ca_v3.2$ expression in reticular neurons, which as the animal develops to exhibit absence-like seizures, is also accompanied by elevated expression of $Ca_v3.1$ in relay neurons [330]. This suggests that an increase in T-type channel expression can precede the development of seizures, perhaps by altering network dynamics via mechanisms that affect potentiation. In support of this notion, a modeling study employing a strictly thalamic network has demonstrated differential effects on network activity in response to an augmented T-type conductance in reticular neurons [333]. Although rebound spiking number in individual reticular neurons was relatively unchanged, the increased T-type conductance resulted in increased network synchrony by introducing a phase-lag between reticular and thalamocorti-

cal firing. It should be noted that a similar effect on synchrony was observed for increased calcium-activated potassium conductance in the model. Nonetheless, a degree of caution is warranted when attempting to interpret these results in relation to *in vivo* recordings that take place in the context of larger and more complexly connected networks. Presently, a precise causal connection between increased T-type channel activity and subsequent development of seizures remains to be established. It is conceivable that developmental causes involving either modulation of the channels, their redistribution with other isoforms, and alternate splicing may be contributing factors. Indeed, such developmental effects occur in the heart where $Ca_v3.1$ and $Ca_v3.2$ undergo differential developmental expression [252]. Such alterations resulting in an epileptic phenotype represent gradual neurophysiological changes over time. In converse to these more slowly developing processes of epileptogenesis, it has been shown that even a single episode of status epilepticus[1] in rat hippocampal brain slices can result in a selective increase in T-type channel activity, indicating that epileptic seizures per se may have the propensity to rapidly alter T-type currents [325], thus potentially lowering the threshold for subsequent seizure events.

Recent *in vivo* studies involving T-type ($Ca_v3.1$) KO mice have provided additional insights into the role of T-type channels in the generation of SWDs and absence-like seizure episodes [177]. Ablation of the $Ca_v3.1$ gene in mice abolishes rebound spiking in dissociated adult thalamocortical neurons, but does not alter their ability to fire tonically. Deep thalamic recordings from $Ca_v3.1$ KO mice also revealed a lack of synchronized activity. *In vivo* recordings from the cortical surface in these mice demonstrated a resistance to baclofen induced 3-5 Hz SWDs that could be induced in control animals. This resistance could be due to a loss of rebound bursting in thalamocortical neurons, which are known to express high levels of $Ca_v3.1$ channels and to receive strong GABAergic inputs. Intriguingly, these mice are not resistant to SWDs induced by bicuculline, and tonic-clonic seizures were inducible in both KO and control animals with 4-aminopyridine injection. A possible explanation of why these mice experience bicuculline induced seizures may be due to cortical involvement. Indeed, previous work has shown that the isolated cortex is able to generate bicuculline-induced SWDs, suggesting that the cortex can act

---

[1]Recurrent seizures without resumption of baseline central nervous system function.

as the seizure generating zone [320]. An alternative explanation for lack of protection against seizures in some models versus others may involve the reticular neurons that are known to predominantly express $Ca_v3.2$ and $Ca_v3.3$ T-type channels rather than $Ca_v3.1$. Therefore, it is conceivable that other T-type calcium channel isoforms (for example $Ca_v3.2$) may be involved in the generation of hypersynchronous activity in some models of epilepsy without requiring the action of $Ca_v3.1$ channels in thalamocortical neurons. The findings obtained with $Ca_v3.1$ KO mice also indicate that full-blown convulsive seizures may recruit different mechanistic pathways. Moreover, consistent with the functional link between T-types and intra-thalamic rhythm generation, $Ca_v3.1$ KO mice show altered sleep architecture, with markedly diminished thalamic delta (1-4 Hz) waves and sleep spindles (7-14 Hz) [190]. Intriguingly, the slow (<1 Hz) rhythms, which can be sustained by the cortex remained relatively intact in KO animals. More recently, it has been demonstrated that a $Ca_v3.1$ knockout also rescues the epileptic phenotypes seen in a number of murine models of absence seizures, including $Ca_v2.1$ knockout mice, which display severe absence seizures [309]. Thalamocortical neurons isolated from $Ca_v2.1$ KO mice were shown to exhibit an approximate $\approx 50\%$ increase in T-type currents (predominantly due to Cav3.1). In contrast, $Ca_v2.1^{-/-}$ / $Ca_v3.1^{+/-}$ mice exhibited a 25% reduction in T-type currents, yet they continued to exhibit SWDs with no changes in seizure frequency or duration. Thalamic mRNA transcript levels for $Ca_v3.1$ were not different between $Ca_v2.1^{+/+}$ and $Ca_v2.1^{-/-}$ mice. These findings suggest that, under certain conditions, even reduced levels of T-type channel activity are capable of sustaining SWDs. Overall these results indicate that complete KO of $Ca_v3.1$ channels can play a protective role against SWDs in these genetic models of absence epilepsy, as well as in a subset of pharmacological seizure models (Fig. 2.4).

2.1.8 $Ca_v3.2$ T-type Channel Mutations in Epileptic Patients

Ion channel defects are considered to be one of the primary etiological causes of idiopathic generalized epilepsy [294]. The involvement of T-type channels has long been suspected due to their eminent presence in cortical and thalamic structures, and their established physiological role in modulating neuronal firing. Moreover, clinically active antiepileptic drugs have
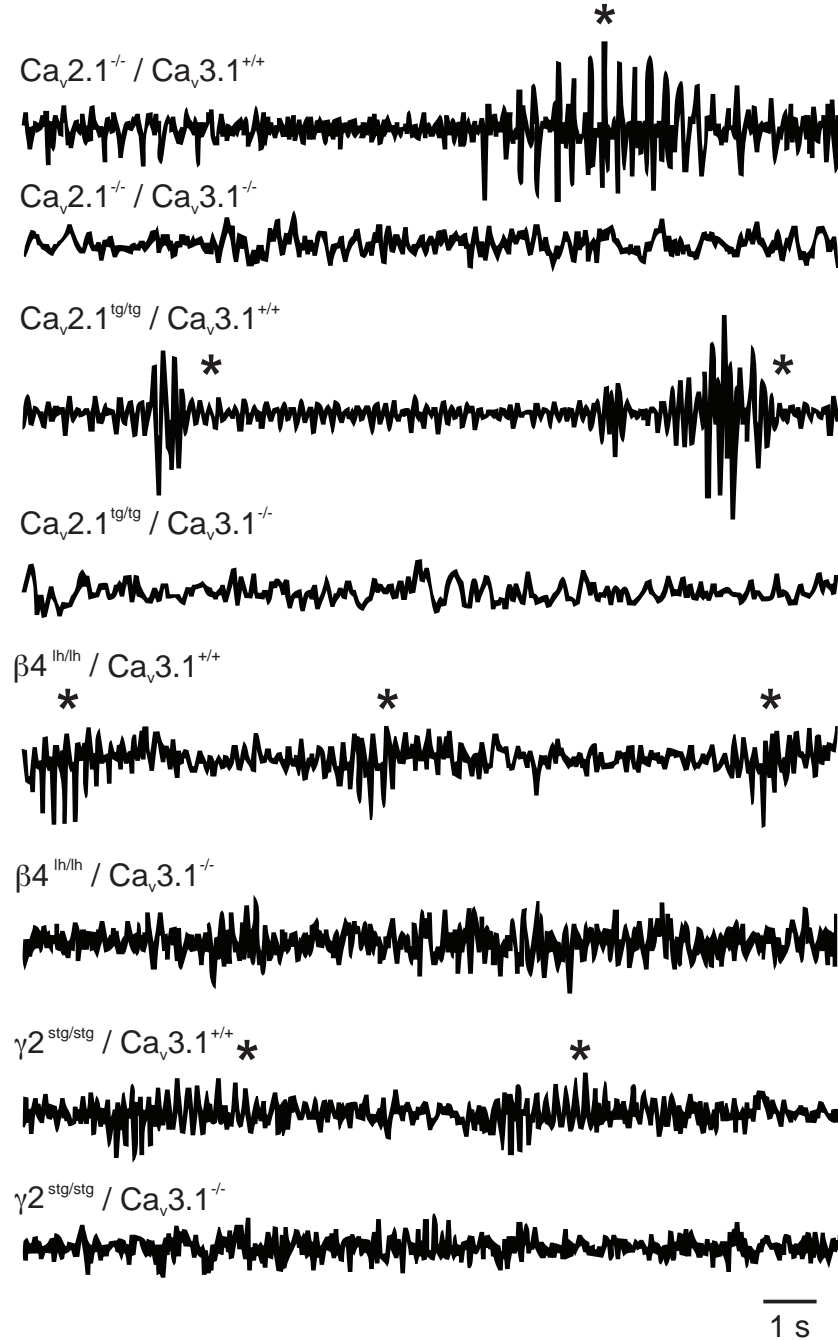
Figure 2.4: Ablation of $Ca_v3.1$ T-type calcium channels can rescue several genetic models (involving P/Q-type KO and HVA ancillary subunit mutations) of absence seizures from the epileptic phenotype. Electroencephalographic recording (15 s) from the cortex of $Ca_v2.1^{-/-}$, $Ca_v2.1^{tg/tg}$ (tottering), $\beta_4^{lh/lh}$ (lethargic), and $\gamma_2^{stg/stg}$ (stargazer) mice with or without the ablation of $Ca_v3.1$ channels, during spike-wave discharges corresponding to absence seizures (asterisks). In each genetic model, a complete ablation ($Ca_v3.1^{-/-}$) is required to rescue the animal from the epileptic phenotype. Adapted from Ref. [309]. Adapted from Ref. [176].

been associated with T-type calcium channel inhibition [129, 280, 320, 195]. However, although long suspected, a direct link involving T-type channels and the generalized spike-wave epilepsies in humans was only recently established. A number of missense mutations, twenty-six in total have recently been identified in the $Ca_v3.2$ calcium channel gene (CACNA1H) in patients diagnosed with idiopathic generalized epilepsy (Fig. 2.5). These mutations were identified from three separate genetic linkage studies and each study is complemented with one or more functional study [172, 173, 259, 355, 354]; indeed all of these mutations have been characterized in Dr. Zamponi's laboratory with the author (HK) participating as the primary in characterizing 19/26 mutations ([172, 173], in addition to 11 unpublished mutations shown in Section 2.3.3). In this chapter I will show results from biophysical characterization of the nineteen mutations. While the remaining seven mutations were characterized by our group in another study, they are not included as part of this dissertation (see Ref. [259]). Figure 2.5 illustrates the amino acid locations of all twenty-six mutations and also can be used as a guide to which results sections in this dissertation correspond to their biophysical characterization.

Before biophysical results are presented, let us discuss the details of the genetic linkage studies. The first genetic study involved 118 patients with childhood absence epilepsy (CAE, a subtype of IGEs, see Section 1.2 and Table 1.1) and reported missense mutations in 14 of these patients that were not present in 230 control individuals [54] (see Fig. 2.5). However, none of the affected individuals had a family history of epilepsy, but carriers inherited a mutant copy of the gene in a heterozygous manner from one parent. A large number of polymorphisms were also reported that were identified in both CAE and control groups. Of the identified 12 mutations only two were found in more than one affected individual. The second study investigated a heterogeneous population of patients with a spectrum of idiopathic generalized epilepsy disorders including: childhood absence epilepsy , juvenile myoclonic epilepsy, febrile seizures, and myoclonic astatic epilepsy [149] (see Table 1.1 for sub-classifications) and identified three additional missense mutations and one nonsense mutation that occurred in 9 out of 192 individuals [149] (see Fig. 2.5). Importantly, none of these new mutations segregated with a specific epileptic phenotype and their presence was not associated with a single subtype of idiopathic generalized epilepsy. Moreover, it is imperative to note that every single one

of the reported $Ca_v3.2$ mutations identified in Study 2 (Section 2.3.2) could also be found in seizure-free individuals. Also, non of these mutations were found in the Chinese Han population that was sequenced in Study 1 [54]. The third study is also be Heron and colleagues and was performed in collaboration with our group, where I investigated a subset of the identified mutations for biophysical changes; these results are presented in Section 2.3.3. In this study, 240 patients exhibiting the spectrum of IGEs in addition to one focal form of epilepsy (temporal lobe epilepsy), in addition to 95 control individuals were sequenced. The patient population was diverse including mostly Australian citizens (presumably of Caucasian descent) and citizens of Israeli and regional Asian-Pacific countries. Each patient was screened for CACNA1H variants (Exons 3-8 and 12-35 for 192 patients, exons 3-35 for 48 patients). Over 100 sequence variants were identified in patients and control populations. These included: 50 variants in the introns and 3' untranslated region, 30 synonymous coding variants, and 32 variants causing amino acid changes. Twenty of these amino acid changes have not been reported previously (i.e. by studies 1 and 2). Eleven of these mutations were selected for biophysical characterization. The variants selected for analysis fulfilled at least one of the following criteria: alteration of a conserved amino acid, partial segregation with affection status in a family, absence in controls, or location in a region of the protein of known functional significance (Table 2.1). I also chose to investigate R788C, which was found in unaffected control individuals, but co-occurred with epilepsy-associated mutations in three of the investigated patient's families. Similarly, R2005C is a polymorphism that occurs in both affected and control populations but does not co-occur with other mutants. Most importantly, three of the eleven mutations displayed full or partial segregation with the epileptic phenotype (A876T *full*, A1059S *partial*, and R1892H *full*). Only one of these segregating mutations was found in one control individual (A1059S). These mutations (Table 2.1) represent novel variants identified in the largest and most complete population study to-date.

Table 2.1: A listing of a subset of mutations identified in genetic linkage Study 3 by Heron and colleagues (unpublished results). In total 19 variants were identified of which 11 were selected for biophysical characterization (see Section 2.3.3). Note that several of the mutations segregate with the epileptic phenotype and were not found in control individuals (asterisk).

AA Change	Frequency	Evidence for Pathogenicity
R788C	3 families, polymorphism	Polymorphism, found also in unaffected patients
A876T*	1 family	Segregates with phenotype
G983S	1 family	AA highly conserved
A1059S	3 families, 1 control	Conserved and segregates with phenotype
E1170K	1 family	Non-conservative change in conserved AA
Q1264H	3 families	AA not conserved but change not seen in controls
T1606M	2 families	Non-conservative change in conserved AA
A1705T	3 families	Conserved AA
T1733A	1 family	AA conserved
R1892H*	1 family	Segregates with phenotype
R2005C	Polymorphism	Non-conservative change, AA conserved $Ca_v3.1/3.2$

2.2 Experimental Methods

2.2.1 Site-directed Mutagenesis

Site-directed mutagenesis was performed on the $Ca_v3.2$ calcium channel $\alpha 1$ subunit template for each of the mutations studied. In each case, slightly different strategies were used to make the three sets of mutations corresponding to the yellow, blue, and red color code in Fig. 2.5 (see inset, Biophysical studies); each color code corresponding to characterization results presented in Sections 2.3.1, 2.3.2, and 2.3.3 respectively.

Study 1 (F161L,E282K,C465S,V831M, and D1463N). Site-directed mutagenesis of the rat $Ca_v3.2$ calcium channel α_1 subunit (accession NM-153814) in pCDNA-3.1(Zeo) [228] was carried out using the Quick change mutagenesis kit (Stratagene) following the manufacturer's instructions. For each of the five mutations, the entire $Ca_v3.2$-pCDNA-3 plasmid was used as the mutagenesis template, and then the entire coding sequence of the channel was sequenced to rule out the presence of errors associated with the mutagenesis (DNA Sequencing Facility, University of Calgary) before transfection into HEK293 (tsA-201) cells for electrophysiological characterization. Study 2 (A480T,P618L, and G755D). Mutagenesis was carried out using

very similar techniques as in Study 1, however human $Ca_v3.2$ (accession NM-001005407) in pCDNA-3.1(Zeo) was used as the mutagenesis template (cloned into vector at NheI and XbaI sites). Once again full-length template and post-mutagenesis sequencing were used. Study 3 (R788C, A876T, G983S, A1059S, E1170K, Q1264H, T1606M, A1705T, T1733A, R1892H, and R2005C). Mutagenesis was performed (human $Ca_v3.2$), for eleven missense mutations, using two different strategies that utilized different templates for a subset of the variants. For four of the mutations (A876T, A1059S, E1170K, and Q1264H), a $\approx$ 900 bp fragment (flanked by BsrGI and AgeI restriction sites) from the $Ca_v3.2$ coding sequence was amplified using PCR and inserted into the pGEM-T-easy vector (Promega) for subsequent mutagenesis. For each variant, the entire insert was sequenced to confirm the presence of the mutation and to check for any PCR-introduced errors. The insert was then re-introduced into the WT $Ca_v3.2$ cDNA and both the inset and flanking regions were re-sequenced to ensure proper ligation. For the remaining seven mutants (R788C, G983S, T1606M, A1705T, T1733A, R1892H, and R2005C), the full-length $Ca_v3.2$ cDNA was used as a mutagenesis template and the entire coding region was sequenced post-mutagenesis to ensure the presence of the mutation and the lack of mutagenesis errors.

2.2.2 Cell Culture and Transient Transfection

Tissue culture and transfection of tsA-201 cells was described by us previously in detail [172]. Briefly, human embryonic kidney (HEK) tsA201 cells were grown to 85% confluence at $37^\circ C$ (5% CO_2) in Dulbecco's modified Eagle's medium (DMEM) (+10% fetal bovine serum, 200 U/mL penicillin, and 0.2 mg/mL streptomycin, Life Technologies, Inc.). Cells were dissociated with trypsin (0.25%)-EDTA before and plated on glass coverslips. Mutant and wild type $Ca_v3.2$ channel α_1 subunits ($4 - 6\mu g$) and green fluorescent protein marker (1 g) DNA were transfected into cells by the calcium phosphate method. In some cases (Study 3), the channel cDNA was co-transfected with a CD8 plasmid to act as a marker. Cells were transferred to $30^\circ C$ 24 hours after transfection, and recordings were conducted 1-2 days later.
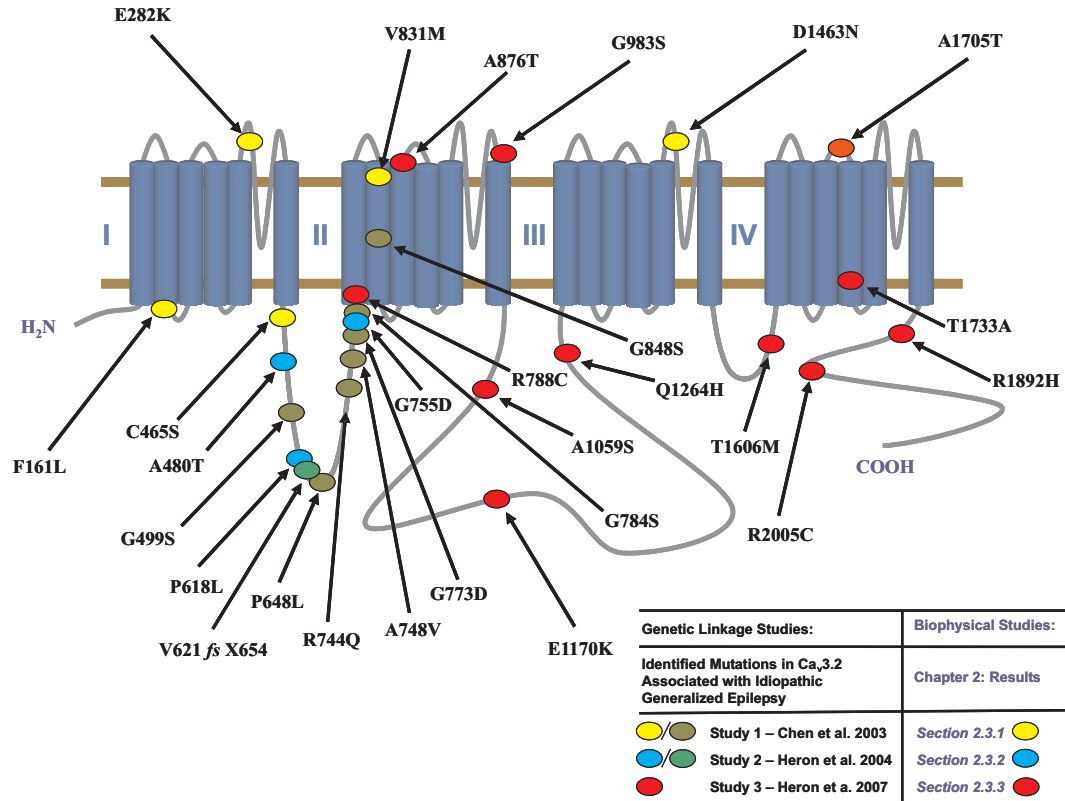
Figure 2.5: An illustration of the α_1 pore-forming subunit of $Ca_v3.2$ T-type calcium channel with its four domains (I through IV) and six transmembrane regions per domain (lipid bilayer shown as two solid brown lines). The location of all twenty-six, biophysically characterized, missense mutations (one nonsense mutation) associated with idiopathic generalized epilepsy are shown. Each amino acid corresponding to an amino acid mutation is color-coded to correspond to the particular genetic linkage study that first identified them. Biophysical characterization in search of functional effects was performed and these results are reported in the following manner: (a) Study 1. Results Section 2.3.1 shows findings on five of the twelve mutations identified by Chen et al. [54] (bright yellow). The remaining seven (dull yellow) were characterized by our group but are not reported on here, see Ref. [259]. (b) Study 2. Results pertaining to the three mutations identified by Heron et al. in 2004 [149] as reported on in Section 2.3.2. (c) Study 3. The most recent (unpublished) research study by Heron and colleagues; biophysical characterization of eleven mutations is presented in Section2.3.3.

2.2.3 Electrophysiology and Data Analysis

Prior to recordings, cells were transferred into an external bath solution. The extracellular solution, as well as intracellular solutions used in each study were slightly modified in each study. Electrophysiological results shown in Sections 2.3.1 and 2.3.2, used a a solution of 5 mM Barium (in mM: 5 $BaCl_2$, 1 $MgCl_2$, 10 HEPES, 40 tetraethylammonium chloride ($TEA - Cl$), 10 $d - glucose$, 88 $CsCl$; pH 7.2 adjusted with $TEA - OH$). Results shown in Section 2.3.3, used a solution of 2 mM Calcium (in mM: 128 $CsCl$, 2 $CaCl_2$, 1.5 $MgCl_2$, 10 $HEPES$, and 25 $d - glucose$; pH was adjusted to 7.4 with $CsOH$). Borosilicate glass pipettes were pulled and polished to 2-4 M resistance and filled with internal solution. For studies in Sections 2.3.1 and 2.3.2 the following intracellular solution was used (in mM) 108 $CsCH_3SO_4$, 4 $MgCl_2$, 9 $EGTA$, 9 $HEPES$, pH 7.2 adjusted with $Cs - OH$. For the third study (Section 2.3.3) a solution containing the following was used (in mM): 135 $CsCl$, 10 $EGTA$, 2 $CaCl_2$, 10 $HEPES$, and 1 $MgCl_2$; pH was adjusted to 7.4 with $CsOH$. Data were acquired at room temperature using a Axopatch 200B or MultiClamp 700B amplifier and pClamp 9.2 software (Axon Instruments), low-pass filtered at 1 kHz, and digitized at 10 kHz. Series resistance was compensated to 80%. Data analysis and off-line leak subtraction was carried out in Clampfit 9.2 (Axon Instruments) and at time used a custom-built software in Matlab (Matworks). All curve fitting was performed using Origin 7.0 (OriginLab) and custom-built Matlab-based analysis software. Current-voltage (IV) plots were fitted using the Boltzmann relations:

$$I = G(V - E_{rev}) \frac{1}{1 + e^{\frac{-(V - V_{0.5a})}{S}}} \tag{2.1}$$

where E_{rev} is the reversal potential, G is the maximum slope conductance, $V_{0.5a}$ is the half-maximal activation potential, and S is the slope factor. Individual inactivation curves were fitted with:

$$I_{normalized} = X + \frac{(1 - X)}{1 + e^{\frac{-z(V_{0.5i} - V)}{25.6}}} \tag{2.2}$$

where $I_{normalized}$ is the fraction of available channels, X is the non-inactivating fraction of current, z is the slope factor, and $V_{0.5i}$ & V are the half-inactivating potential along with the

recorded voltage. Time-constants for inactivation, τ_{inact} or τ_i, were obtained from mono-exponential fits to the raw current data. Time-constants for recovery from inactivation, τ_r, were obtained by mono-exponential fits to the time course of recovery from inactivation. These data were obtained by applying an inactivating conditioning pulse followed by a variable recovery period preceding the test pulse. All averaged data are plotted as mean$\pm$SEM, and numbers in parentheses reflect numbers of cells tested. Unless stated otherwise, statistical analysis was carried out using one way analysis of variance, where $p \leq 0.05$ was considered as significant. In study 3 (Section 2.3.3) t-test analysis with the same statistical significance level was used.

2.3 Results

2.3.1 Study 1. Functional Consequences of Mutations Identified in the Chinese Han Population

Site-directed mutagenesis was used to introduce five of the recently identified CAE-associated missense mutations [54] into the rat $Ca_v3.2$ sequence [228]. As shown in Fig. 2.5 (bright yellow), these mutations are distributed throughout the $Ca_v3.2$ channel protein, including the domain I S2-S3 linker (F161L), the domain I S5-S6 region (E282K), the domain I-II linker (C465S), the domain II S2 segment (V831M), and the domain III S5-S6 region (D1463N), and include two substitutions of negatively charged amino acids. Each of the mutant channels expressed well in HEK cells, had current densities similar to those obtained with the wild type channels (not shown), and produced typical current waveforms expected from T-type calcium channels (Fig. 2.6A). Two of the mutations, F161L and E282K, resulted in statistically significant hyperpolarizing shifts in the half-activation potential of the channel by approximately 10 mV (Fig. 2.6B and C), without affecting the reversal potential. Hence, mutations F161L and E282K, due to a shift in their activation potentials, can open in response to smaller membrane voltage fluctuations and therefore allow for greater Ca^{+2} influx as compared to wild type. In neurons, this behaviour could result in enhanced bursting activity and might facilitate intracellular changes associated with elevated $[Ca^{+2}]_i$ during epochs of intense neuronal activity. The voltage dependence of activation of the remaining mutants did not differ significantly from that

observed with the wild type channel (Fig. 2.6C).

The time course of activation was significantly slowed in the V831M mutant at potentials more positive than -30 mV (Fig. 2.6D), suggesting that this channel might conduct less inward current during brief membrane depolarizations. However, the V831M mutant also exhibited significantly altered inactivation characteristics. At moderate depolarizations (i.e., -20 mV), the time constant for inactivation was significantly slowed in the V831M mutant (Fig. 2.7A), whereas the remaining mutants behaved roughly similar to wild type channels. In addition, the position of the steady-state inactivation curve of the V831M mutant was shifted towards more depolarized potentials by $\approx$10 mV, whereas that of the other mutants did not differ significantly from that of the wild type channel (Fig. 2.7B). This suggests that V831M channels, although slower to activate, are more readily available for opening, and when conducting, remain open for longer durations relative to wild type. The observation that V831M activation was slowed only at depolarized potentials might suggest that in this mutant, one or more of the gating transitions during channel opening become rate limiting at positive voltages, but not at more negative potentials at which activation is generally slower. Recovery from inactivation was not significantly affected by any of the mutations (Fig. 2.7C). Taken together, three of the five mutants examined exhibited statistically significant altered gating behaviour, whereas mutant channels C456S and D1463N were indistinguishable from wild type channels.

2.3.2 Study 2. Functional Consequences of Three IGE Mutations Identified in an Australian Patient Population

Site-directed mutagenesis was used to introduce the three recently identified missense mutations into the cloned human $Ca_v3.2$ cDNA (Fig. 2.5). All of the identified mutations are located within the I-II linker region of the $Ca_v3.2$ voltage-gated calcium channel: A480T and P618L change non-polar residues for uncharged and non-polar residues respectively, while G755D is a change from a non-polar to a negatively charged amino acid. Each of the mutant channels expressed well in HEK tsA-201 cells, exhibited current densities similar to those obtained for the wild type channel, and produced current waveforms typically observed with the cloned T-type calcium channels (Fig. 2.8A). None of the mutants resulted in significant
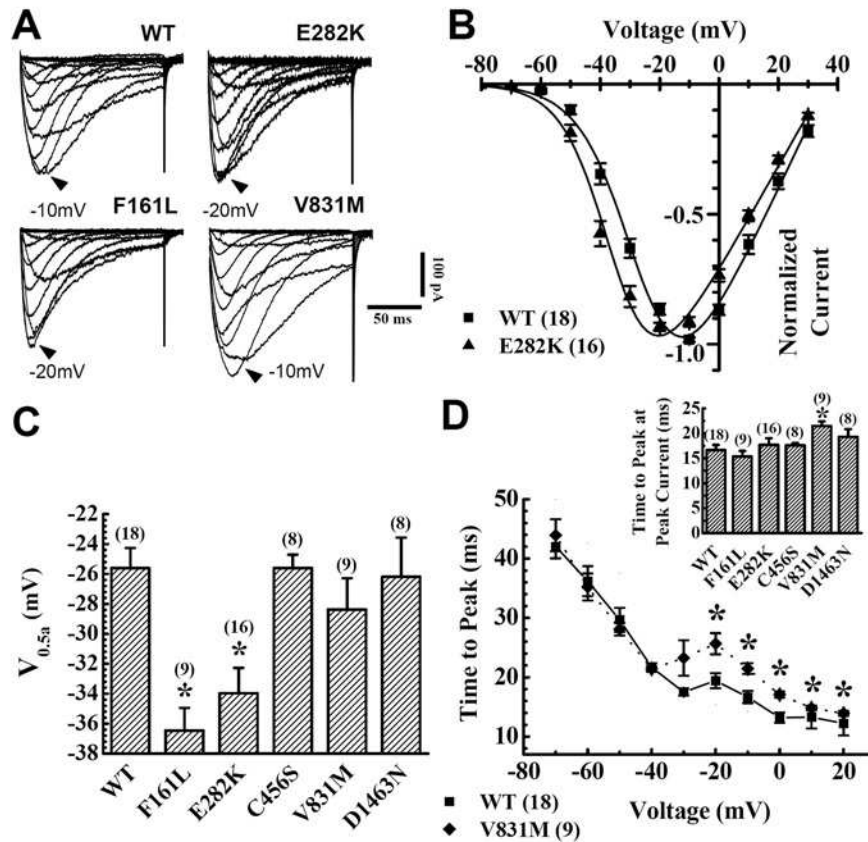
Figure 2.6: **(A)** Families of raw current traces obtained with wild type and mutant $Ca_v3.2$ channels. The currents were elicited by stepping from a holding potential of -110 mV to various test potentials. Note the slowed activation and inactivation kinetics of the V831 mutant. **(B)** Ensemble of whole cell current voltage relations obtained with wild type $Ca_v3.2$ and the E282K mutant. Each individual current voltage relation was normalized to a peak value of 1, and the data points reflect means of the normalized amplitudes. The solid lines are fits via the Boltzmann equation. **(C)** Mean half-activation potentials obtained with the wild type and five different mutant $Ca_v3.2$ channels. The half-activation potentials were determined via Boltzmann fits to individual whole cell current voltage relations. Asterisks denote statistical significance relative to wild type ($p \leq 0.05$, ANOVA). **(D)** Time to peak for wild type and V831M mutant $Ca_v3.2$ channels at various test potentials, asterisks denote statistically significant deviations ($p \leq 0.05$, t-test). Inset: Mean time to peak values obtained for wild type and mutant $Ca_v3.2$ channels at the peak voltage of the I-V relation. V831M shows a statistically significant increase in time to peak ($p \leq 0.05$, ANOVA). Numbers of cells recorded are denoted in parentheses. Adapted from Ref. [172].
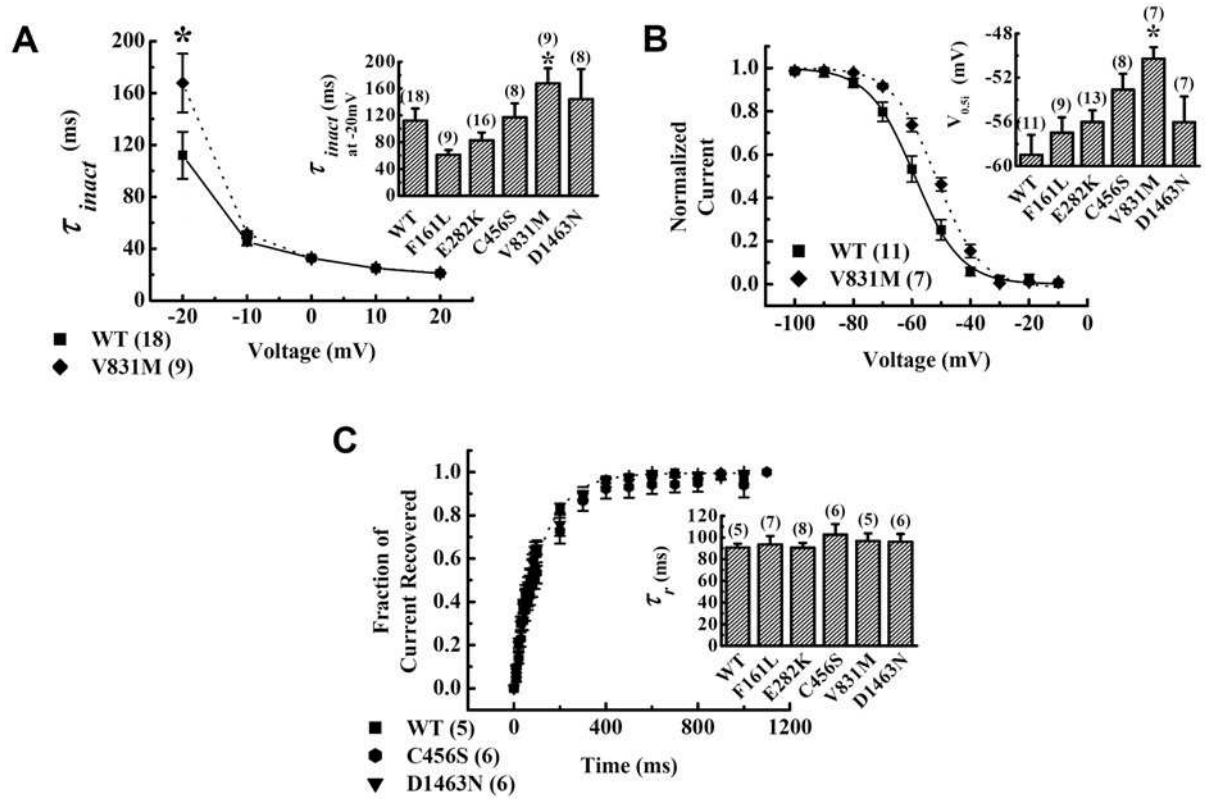
Figure 2.7: **(A)** Time constants of inactivation for wild type and V831M mutant $Ca_v3.2$ channels, obtained from mono-exponential fits to raw current traces at various test potentials. Inset: Mean time constant of inactivation obtained at a test potential of -20 mV for wild type and mutant $Ca_v3.2$ channels. **(B)** Ensemble steady-state inactivation curves obtained with wild type and V831M mutant $Ca_v3.2$ channels. The lines are fits with the Boltzmann relation. Inset: Mean half-inactivation potentials obtained from fits to individual state inactivation curves. The asterisk denotes statistical significance ($p \leq 0.05$, ANOVA). **(C)** Recovery from inactivation for wild type and two of the mutant $Ca_v3.2$ channels, normalized to 1. Inset: Mean time constants for recovery from inactivation for the wild type channels and the $Ca_v3.2$ mutants obtained from mono-exponential fits to the normalized current recovery curve. Adapted from Ref. [172].
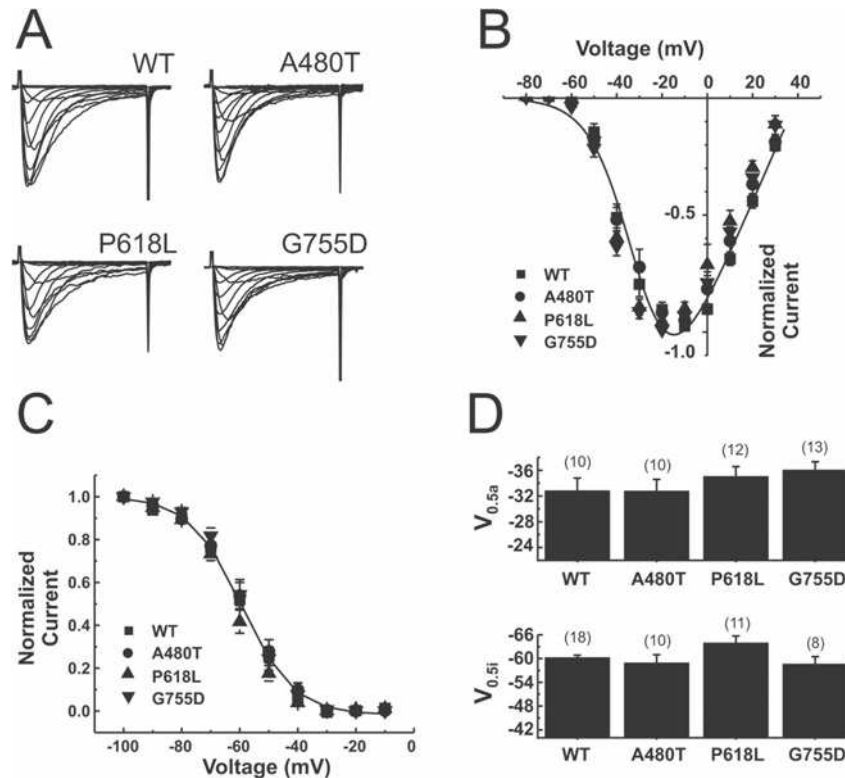
Figure 2.8: **(A)** Families of raw current traces obtained with wild type and mutant $Ca_v3.2$ channels. The currents were elicited by stepping from a holding potential of -110 mV to various test potentials. **(B)** Ensemble of whole cell current-voltage (I-V) relations obtained with wild type and mutant $Ca_v3.2$ channels. Each individual current voltage relation was normalized to a peak value of 1, and the data points reflect means of the normalized amplitudes. The solid line is a fit using the Boltzmann equation to the wild type data. **(C)** Ensemble steady-state inactivation curves obtained with wild type and mutant $Ca_v3.2$ channels. The currents were elicited by inactivating the channel population (-10 mV for 1.5 s) followed by a step to the peak activation current. The line is a fit with the Boltzmann relation to the wild type data. Mean half inactivation potentials are obtained from fits to individual state inactivation curves. **(D)** Mean half-activation and half-inactivation potentials obtained with wild type and mutant channels. The half-activation potentials were determined via Boltzmann fits to individual whole cell current voltage relations. Numbers of cells recorded are denoted in parentheses. Adapted from Ref. [173].
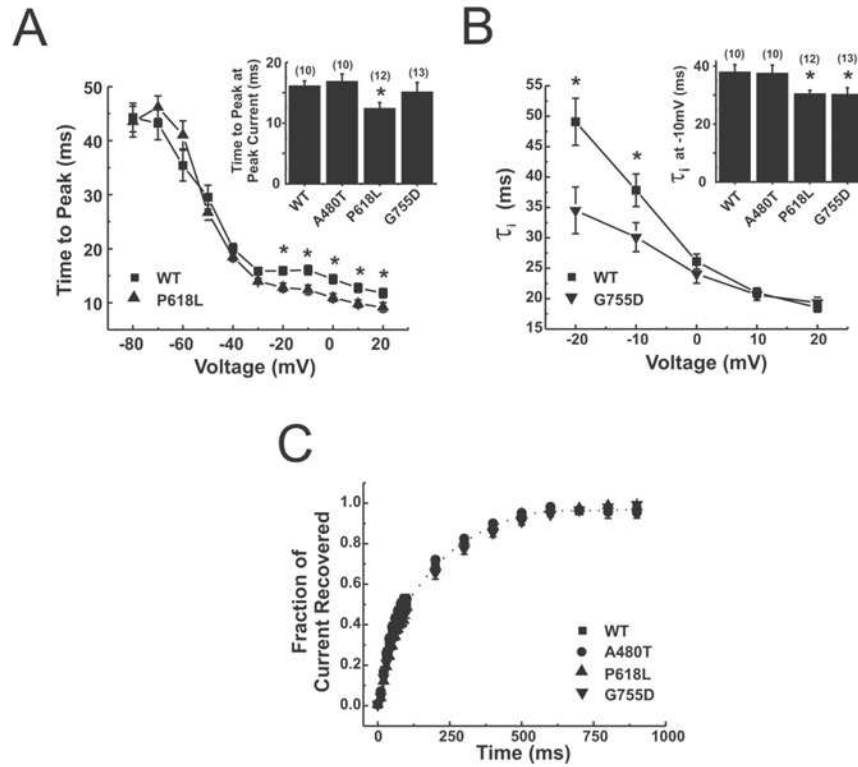
Figure 2.9: **(A)** Time to peak for wild type and P618L mutant Ca_v3.2 channels at various test potentials; asterisks denote statistically significant deviations ($p \leq 0.05$, t-test). Inset: Mean time to peak values obtained for wild type and mutant Ca_v3.2 channels at the peak voltage of the I-V relation. P618L shows a statistically significant decrease in mean time to peak ($p \leq 0.05$, ANOVA). **(B)** Time constants of inactivation for wild type and G755D mutant Ca_v3.2 channels, obtained from mono-exponential fits to raw current traces at various test potentials. Inset: Mean time constant of inactivation obtained at a test potential of -10 mV (peak current) for wild type and mutant Ca_v3.2 channels. P618L and G755D show a statistically significant decrease in inactivation time constants. **(C)** Recovery from inactivation for wild type and mutant Ca_v3.2 channels, normalized to 1 (full current recovered). No statistically significant differences were observed in mean time constants for recovery. Asterisks denote statistical significance relative to wild type ($p \leq 0.05$, ANOVA). Numbers of cells recorded are denoted in parentheses. Adapted from Ref. [173].

differences in the shape or position of the current-voltage (I-V) relation (Fig. 2.8B), or changes in voltage-dependence of steady-state inactivation (Fig. 2.8C), such that neither half-activation nor half-inactivation voltages were affected (Fig. 2.8D). In neurons, one would expect the variant channels to activate and inactivate at similar membrane potentials as compared to the wild type $Ca_v3.2$ channel.

The time course of activation was significantly accelerated in the P618L mutant at potentials more positive than -30 mV (Fig. 2.9A), suggesting that this variant might conduct greater inward current during brief membrane depolarizations. In contrast, both P618L and G755D exhibited significantly altered rates of inactivation. For depolarizations to modest membrane potentials (i.e. -20 mV), the time course of inactivation was significantly accelerated (Fig. 2.9B), whereas that of the A480T mutant was not different from the native channel. This suggests that the P618L mutant is able to both activate and inactivate faster in response to changes in membrane potential, thereby allowing more channels to be available for inward currents in response to varying depolarizations above -20 mV when compared to the native channel. Recovery from inactivation was not significantly affected by any of the mutations (Fig. 2.9C). Taken together, two of the three mutants investigated exhibited relatively small, albeit statistically significant altered channel kinetics, which in a native neuronal environment would likely contribute to altered firing behaviour.

2.3.3   Study 3. Functional Consequences of Eleven Additional IGE Mutations

Nineteen of the amino acid changes identified here have not been reported previously and this reinforces the extent of genetic variation present at this locus. Approximately 25% of the variants identified were also observed in the Han Chinese population [54]. This suggests that the majority of the variants in this gene are present at low frequencies and are population specific, with only relatively common polymorphisms being seen in multiple populations.

Site directed mutagenesis was used to introduce each of the 11 of the novel amino acid changes into the human $Ca_v3.2$ calcium channel cDNA sequence. The mutants were transiently expressed in tsA-201 cells and characterized via whole cell patch clamp. For every channel variant (Table 2.1), the voltage dependences and rates of activation and inactivation,

and the time constant for recovery from inactivation were determined and compared to those of wild type channels. None of the mutants showed changes in the time course of inactivation, but several of the mutants displayed alteration in the other gating characteristics that altered channel function (Figs. 2.10 and 2.11).

2.3.3.1 Mutations Resulting in Altered Channel Function

The variant A876T is seen in one family with IGE, febrile seizures, and temporal lobe epilepsy in which it segregates with affection status and not in controls. This variant affects a conserved amino acid in transmembrane domain II and affects two biophysical parameters of channel activity. First, there is a depolarizing shift in the half-inactivation potential (i.e., the membrane potential at which half of the channels can be activated by a membrane depolarization) of the channel (Fig. 2.10C and D). This results in an increase in the fraction of channels that are available for opening, thus causing a gain of function. Second, the time course of recovery from channel inactivation (Fig. 2.11D) is faster and hence the channels are less likely to accumulate in a non-conducting state during successive membrane depolarizations, in this case this would be consistent with increased channel function.

The variant G983S was observed in a single patient with MAE [2]. The change was inherited from the patient's father, who was unaffected but had a family history of epilepsy. This change alters a highly conserved amino acid in the pore loop of transmembrane domain II and would be expected to significantly alter channel properties. Electrophysiological studies showed that this variant slows the recovery from inactivation (Fig. 2.11D) and shifts the half-inactivation potential towards more negative voltages (Fig. 2.10C). These effects are opposite to those seen with A876T and are therefore consistent with a loss of channel function.

The variant A1059T was seen in three families and one control individual. Susceptibility variants are not unexpected in controls where there are insufficient numbers of susceptibility alleles for the individual to cross the seizure threshold and therefore have epilepsy. This mutation raised, slightly but significantly, the threshold of its activation as evident from a small depolarizing shift in the half-activation potential (i.e., the voltage at which half of the channels

---

[2]Myoclonic-astatic epilepsy (MAE) is a combination of myoclonic seizures and astasia (a decrease or loss of muscular coordination), often resulting in the inability to sit or stand without aid.

are activated, Fig. 2.10B). Moreover, the channel was slower to activate (Fig. 2.11A and B), altogether indicating a slight reduction in channel function.

The variant T1606M was observed in two epilepsy families with GTCS and febrile seizures (see Table 1.2 for classifications) and unclassified epilepsy and was not present in controls. In both families the variant is transmitted from an unaffected parent to the affected children. This variant causes a small, hyperpolarizing, shift in the half-activation potential (Fig. 2B) and would be expected to cause a small gain of function and thus increase in calcium current.

The variant A1705T was seen in two epilepsy families with MAE, febrile seizures, and JAE and one sporadic MAE patient, and was absent in controls. In both families the change co-segregates with the polymorphism R788C, which has been shown to cause small alterations in the recovery from inactivation (Fig. 2.11D). The sporadic patient also carried both changes but DNA was not available from any relatives to allow analysis of the co-segregation of the two changes. When tested alone, the A1705T mutation decreased the time of recovery from inactivation (consistent with a small gain of function), but did not alter any of the other parameters measured (Fig. 2.11D). Although this alteration of kinetics is small, it is possible that the difference would have been larger if the change had been tested with the R788C variant in the same construct, perhaps via some nonlinear interaction.

The variant T1733A was seen in a single epilepsy family with CAE and did not segregate with the epileptic phenotype in the two affected siblings in this family. This variant caused a depolarizing shift in half-inactivation potential (Fig. 2.10C), yet a slowing of recovery from inactivation (Fig. 2.11D), thus perhaps mediating offsetting effects on channel function.

The variant R1892H was seen in a single family with CAE, JAE and GTCS and was not present in controls. The change was transmitted from an unaffected parent to four affected children and was absent in the fifth unaffected child. This variant was slightly faster to activate in response to membrane depolarization, and thus consistent with a gain of function (Fig. 2.11A and B).

The variant R2005C is a polymorphism which was observed in 17.4% of patients and 14.6% of controls. Although the frequency of this polymorphism is increased in the patient population, this increase is not statistically significant in the genetic analysis. The change alters an

amino acid which is conserved in CACNA1H and CACNA1G sequences, suggesting that it is important for channel function. Functional analysis showed that the R2005C variant decreases the time-constant of recovery from inactivation (Fig. 2.11D) leading to a small gain of function.

2.3.3.2 Other Mutations

Two of the variants tested were not found to alter those channel properties tested. Both of these variants are in the intracellular loop between transmembrane domains II and III. The variant E1170K, which alters a highly conserved amino acid, is seen in a single family and not in controls. The change does not segregate with epilepsy in the family and is likely to be present in an unaffected family member or perhaps a larger control population. The variant Q1264H was seen in one family and two other patients and was not present in controls.

2.4 Discussion

2.4.1 Genetic Linkage Study and Mutation Specific Remarks

Biophysical Study 1.

The findings with C456S and D1463N are consistent with a number of reports of calcium channel mutations in various disease states that do not result in detectable effects on channel gating. A lack of effects on channel biophysics does not equate to lack of functional consequences in a neuronal cellular environment. For example, given the cytoplasmic localization of the residue C456, it is conceivable that putative interactions with neuron specific regulatory proteins could result in altered channel function for the C456S mutant. Moreover, it is possible that second messenger modulation could be altered in this channel; residue 456S has been suggested as a possible Casein kinase II (CK2) phosphorylation site [54]. Finally, it is possible that the effects of individual point mutations are only observed in certain of the many splice isoforms of $Ca_v3.2$ calcium channels [51]. In contrast, the results obtained for F161L and the E282K mutants are more easily reconciled with the epileptic phenotype of patients carrying this mutation. A shift in the voltage-dependence of activation to levels that are closer to resting membrane potentials of most neurons would result in increased calcium influx and thus hyperexcitability of neuronal tissue, thus predicting increased spike and wave discharges in cells that predom-
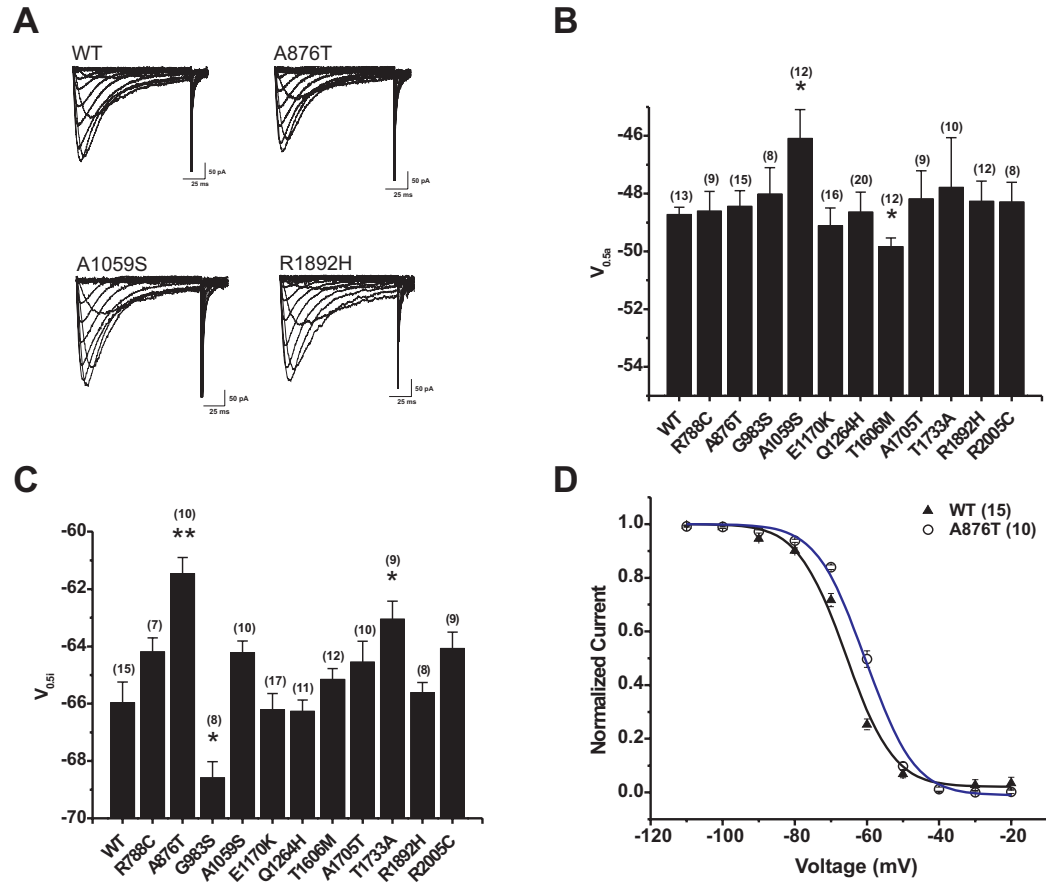
Figure 2.10: **(A)** Families of raw current traces obtained with wild type and mutant $Ca_v3.2$ channels. The currents were elicited by stepping from a holding potential of -110 mV to various test potentials. The mutants featured are those that exhibited segregation with the epileptic phenotype (see Table 2.1). **(B)** Mean half-activation potentials obtained with the wild type and eleven different mutant $Ca_v3.2$ channels. The half-activation potentials were determined via Boltzmann fits to individual whole cell current voltage relations. **(C)** Mean half-inactivation potentials obtained from fits to individual state inactivation curves. **(D)** Steady-state inactivation curves obtained with wild type and A876T, which exhibited the greatest difference, in the depolarizing direction, from mean WT values. Asterisks denote statistical significance relative to wild type (* for $p \leq 0.05$ and ** for $p \leq 0.001$, t-test). Numbers of cells recorded are denoted in parentheses.
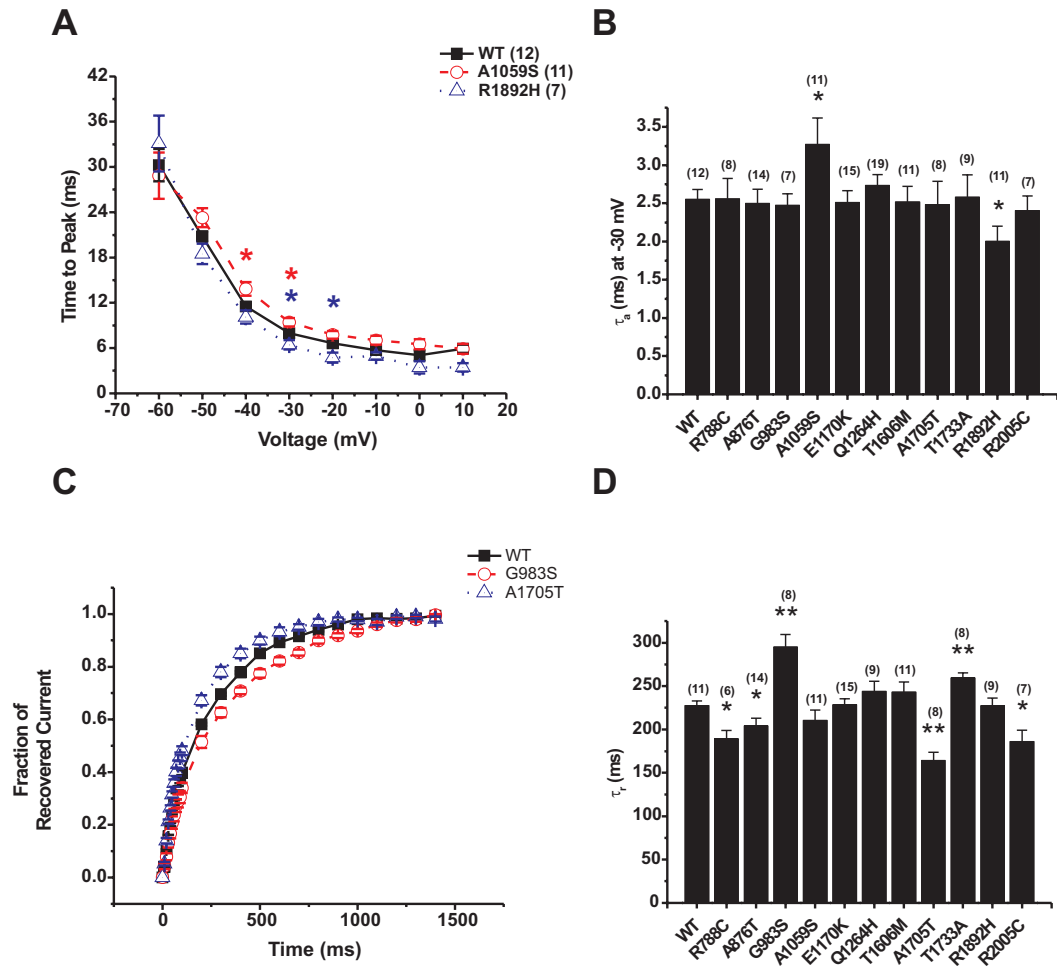
Figure 2.11: **(A)** Time-to-peak for wild type and two of the mutations, A1059S and R1892H, that segregate with the epileptic phenotype. Intriguingly these mutants are amongst the two exhibiting greatest change as manifested by the τ-activation at -30 mV. **(B)** Time constants of activation for wild type and eleven mutant $Ca_v3.2$ channels; these were obtained from mono–exponential fits to raw current traces at various test potentials but are reported for the peak evoked current at -30 mV. No differences were seen for time constants of in-activation (data not shown). **(C)** Recovery from inactivation (fraction of current available) for wild type and two of the mutant $Ca_v3.2$ channels: G983S exhibits slower to recover characteristics, while A1705T recovers more rapidly. **(D)** Mean time constants for recovery from inactivation for the wild type channels and the $Ca_v3.2$ mutants obtained from mono-exponential fits to the normalized current recovery curve (as in C). Asterisks denote statistical significance relative to wild type (* for $p \leq 0.05$ and ** for $p \leq 0.001$, t-test). Numbers of cells recorded are denoted in parentheses.

inantly express the F161L or E282K mutations. Similarly, any slowing of voltage-dependent inactivation and shifts of the half-inactivation potential towards more depolarized potentials such as in the V831M mutant would result in increased availability of the channel for opening, and thus, increased channel activity. It should be noted that I used the rat $Ca_v3.2$ calcium channel as the mutagenesis template, and although this channel is highly homologous with the human channel, subtle differences in homology distributed throughout the channel may result in inter-species differences in the context of channel gating. This notion is supported, in part, by findings that show no specific transmembrane domain is responsible for inactivation channel properties [139]. Overall, the observed biophysical effects for three of the five mutations examined here are consistent with a gain of channel function, which may be relevant to the CAE phenotype.

To date, there have been only limited reports of systematic structure-function studies on cloned T-type calcium channel subtypes. Staes *et al.* [316] implicated the C-terminus of the $Ca_v3.1$ calcium channel in voltage-dependent inactivation, however, based on the current understanding of inactivation of high voltage-activated calcium channels [322], and on mutagenesis studies in $Ca_v3.1$ channels [223], the S6 segments are also likely to contribute to the inactivation process. Interestingly, the only CAE-associated mutation that affected channel inactivation is localized to a region that had not been previously implicated in the inactivation of any type of calcium channel, i.e., the domain II S2 segment. The consequences of mutant channel E282K on voltage-dependent activation are somewhat surprising. Intuitively, one might have expected a substitution of an externally located negatively charged residue for a lysine to electrostatically antagonize voltage sensor movement, thus, inhibiting rather than facilitating activation. These results suggest that the effects of this mutation do not arise from an electrostatic interaction with the voltage-sensor of the channel, but may perhaps be mediated via allosteric coupling to the activation gating machinery.

In summary, these data (Section 2.3.1) constitute the first report of naturally occurring point mutations with functional consequences on the gating behaviour of T-type calcium channels. At least in a subset of mutations reported in children afflicted with CAE, the altered channel gating that arises from the presence of these mutations is qualitatively consistent with the

clinical phenotype. The discovery of these mutations in a subset of individuals but not in a larger number of control subjects suggests that their presence is significant, which is further supported by their functional effects. Their effects in the context of CAE may well be brought about by synergistic interactions with other factors such as other ion channels and intracellular modulators, all of which are capable of a spectrum of activity modes in the epileptic brain.

Biophysical Studies 2 & 3.

In their first study, Heron and colleagues reported four mutations (three missense and one non-sense) [149] associated with IGEs (encompassing a spectrum of generalized seizure types, see Table 1.1, in addition to some patients with febrile seizures), and the functional consequences of the three missense mutations is presented in Section 2.3.2. Although the result of the non-sense mutation was not investigated, expression of this mutant channel results in a premature termination within the I-II linker at residue 654, resulting in the translation of only domain I of $Ca_v3.2$, and thus in all likelihood, a non-functional channel. It is important to point out that transfection of domain I of $Ca_v3.2$ into NG108-15 cells results in a $\approx 50\%$ reduction in native T-type channel amplitude [257]. This suggests the possibility that a similar dominant negative effect might occur in thalamic or cortical neurons. For 2/3 missense mutations a small but significant alteration in rates of activation and inactivation was observed without any steady-state changes. Taken together, the results of this functional study, showing relatively minor biophysical effects on channel function, are once again in-line with a complex inheritance model. Moreover, it is important to note that the mutants discovered in this first study by Heron et al. [149] were obtained by studying a much larger and more diverse epileptic patient population than investigated by Chen et al. [54].

In their second study, Heron and colleagues along with our group investigated 240 patients (largest study to date) and identified twenty novel IGE mutations that result in amino acid changes in the $Ca_v3.2$ channel; of these the biophysical characterization of eleven mutations of interest are presented (see Table 2.1). A key aspect of their genetic findings is the identification of three variants (A876T, A1059S, and R1892H) that segregate with the epileptic phenotype - this was not the case for any of the other previously reported mutations, which suggests that they may be caused by polymorphisms. Upon biophysical characterization of the eleven

mutants, no large biophysical changes were observed, however a $\approx$ 10 mV depolarizing shift in steady-state inactivation curve was observed for A876T, consistent with increased channel availability (from the inactivated state) over a range of membrane potentials (see Fig. 2.10D). Aside from small changes in the rate of activation (Fig. 2.11B, specifically for A1059S and R1892H), the next most significant change was observed for recovery from inactivation where two mutants in particular (G983S and A1705T) showed decreased and increased rates respectively. A connection between loss of function mutations, such as increased rate of recovery from inactivation, and the epileptic phenotype is paradoxical. However, due to complexities inherent to neuronal and network synchrony, both within and in between the key circuits (thalamus and neocortical), it is conceivable that altered channel biophysics can modulate firing behaviour in a manner that ultimately results in pathological synchrony and consequently seizure generation.

Overall, the most intriguing aspect of these findings are that even though biophysical changes were small, they were the greatest in magnitude and frequency for mutants that segregated with the epileptic phenotype. R788C, identified as a polymorphism and found in non-affected individuals, is the only variant that has consistently been identified in more than one linkage study [354, 355]. Therefore, it is tempting to consider R788C as a "true negative" test, suggesting that polymorphisms do occur in patients with IGE but have minimal effects on channel function. However, even for the case of robustly identified variants, that do segregate with the epileptic phenotypes, the biophysical consequences seem to be minimal. This was also the case for the seven mutants from the Chen et al. [54] study that were characterized by our group but were not shown here [259].

2.4.2 Overall Conclusions

I investigated biophysical properties of nineteen missense mutations in the $Ca_v3.2$ T-type calcium channel, as associated with a spectrum of seizure syndromes classified under idiopathic generalized epilepsies. Results from these biophysical measurements (specifically those in Sections 2.3.1 and 2.3.2) are amongst the first characterization of naturally-occurring mutations in T-type channels. Idiopathic generalized epilepsies are widely believed to be caused by genetic

factors and the functional effects of $Ca_v3.2$ mutations reaffirm this notion. The presence of these channels in brain structures such as the thalamus and cortex suggest that altered channel function may play a role in affecting neuronal firing that somehow contributes to pathological (seizure) cellular firing and putative changes at the network level.

As noted in Section 2.4.1, most of the mutants had small or no biophysical effects and none of the segregating mutations were observed more than once across different studies, although they were observed in more than one family. Collectively, these findings support the notion that the CACNA1H gene is an active susceptibility locus associated with the spectrum of IGE seizure disorders. There are precedents for lack of biophysical effects in other calcium channel isoforms as related to other disorders. For example, mutations in the $Ca_v2.1$ P/Q-type calcium channel found in patients with familial hemiplegic migraine do not appear to obviously alter channel function [232]. A recent study on this channel (i.e. $Ca_v2.1$) has identified a novel mutation associated with absence epilepsy that segregates in an autosomal dominant fashion in successive generations, yet, no changes in gating were observed as a result of this mutation. Moreover, several mutations in the $Ca_v1.4$ L-type calcium channel linked to congenital X-linked stationary night blindness do not affect the biophysical properties of expressed channels [229]. Additionally, mutations associated with periodic paralysis mediate only small effects on $Ca_v1.1$ L-type channel inactivation [91].

T-type channels mediate the rebound bursts in thalamic reticular and cortical neurons that are the physiological substrates for SWDs. Therefore, increased T-type channel expression (such as in the GAERS rat) or activity (as seen with gain of function mutations found in humans) can contribute to seizure genesis. Several of the mutations, mainly those reported by Chen et al. [54], are located within the I-II linker and are biophysically silent [172, 259]. However, their functional effects may be caused by changes in trafficking, regulation, alternate splicing, and interaction with other proteins. Indeed, it was recently shown that several of the mutations can enhance surface expression of the channels [355], and also can result in alterations in splicing with unique biophysical properties [389].

Increased T-type calcium channel activity does not necessarily have to result from increased T-type channel expression. For example, alterations in ionic currents that interact with T-type

currents, such as the H-current (I_h), which is mediated by HCN channels can result in absence seizures [210, 267]. This was recently demonstrated in the case of HCN2 (found primarily in the thalamus) deficient mice, which exhibit spontaneous 5 Hz SWDs with absence-like episodes [209]. Similarly, the WAG/Rij rat, which exhibits spontaneous absence-like seizures of neocortical origin [231] has been shown to have reduced levels of HCN1 protein expressed in the cortex; interestingly, mRNA levels for HCN1 were unaffected and protein expression levels did not seem to differ from control animals for the three other HCN genes [324]. Given that cortical, thalamocortical relay, and reticular thalamic neurons express different complements of T-type channel isoforms, all three channel subtypes are potential contributors to the epileptic phenotype, but may do so in a regional- or cell type-specific manner. In this regard, it is interesting to note that in the GAERS rat, intra-thalamic administration of ethosuximide is only effective in reducing seizures by 70% at concentrations well beyond those known to be effective in blocking T-type channels [280]. However, intra-cortical administration of ethosuximide has been shown to be much more effective in halting seizure activity [218], which further supports the notion that T-type mediated SWD generation is not exclusively a thalamic phenomenon. This notion is further supported by the observation that specific knockout of one given channel subtype (i.e., $Ca_v3.1$ which is expressed predominantly in thalamocortical relay neurons) is not universally effective in protecting against all pharmacologically induced generalized seizures. The susceptibility of the KO mice to bicuculline-induced seizures indicates that rebound bursting in thalamocortical relay neurons may not be required for this form of seizure activity and serves as a reminder of the many complex routes to seizure genesis (reviewed in [225, 227]). On the other hand, reticular neurons express $Ca_v3.2$ and $Ca_v3.3$ and it would thus be interesting to explore seizure susceptibility in knockout mice deficient of these channel subtypes. It also remains to be determined whether knockout or downregulation of $Ca_v3.1$ could provide a protective role against absence seizures induced by the putative gain of function in $Ca_v3.2$ such as those found in humans with idiopathic generalized epilepsy.

Genetic association studies have improved greatly in identifying genes and mutations therein involved in disease processes. In the context of idiopathic epilepsies, most of the ion channel defects that have been identified via linkage studies typically account for a small fraction of

patients, with sporadic cases or cases occurring in nuclear families [247]. The majority of families do not exhibit clear inheritance of the gene, which has been suggestive of a polygenic or multifactorial basis to this class of epilepsies. These biophysical data constitute early reports on functional changes attributable to naturally occurring point mutations in T-type calcium channels. These findings suggest that $Ca_v3.2$ T-type channel variants with large biophysical effects, that may be directly causal to an epileptic phenotype, probably represent a rare fraction of the general patient populations affected by this disorder. However, one must consider other factors such as the involvement of other genes. Moreover, environmental factors that may allow a mutation to manifest itself in an individual but not in another (even though both subjects may have the same T-type calcium channel mutation) must be considered.

These results on the functional consequences of $Ca_v3.2$ mutations are best matched with a polygenic complex inheritance model for the etiology of IGEs. Indeed, the emerging picture suggests that idiopathic generalized epilepsy encompasses a spectrum of epilepsies with genetic segregation patterns that are consistent with susceptibility alleles that depart from the pattern of vertical inheritance seen in monogenic autosomal dominant epilepsies. Indeed, all epilepsy-related variants so far described in CACNA1H appear to be susceptibility alleles, which contribute to disease but are not sufficient to cause it on their own. Hence, CACNA1H variants do not segregate with epilepsy in large families. Further characterization of the role of CACNA1H in idiopathic epilepsy can only be achieved by the identification of further variants in patients with a range of epilepsy phenotypes and correlating that with functional properties of the protein. However, it is possible that future genetic linkage studies may identify more calcium channel mutations that clearly segregate, in a Mendelian manner, with an epileptic phenotype and may have associated functional effects.

Chapter 3

High Frequency Oscillations and their Role in Seizure Localization and Seizure Genesis: An *in vitro* and Patient-based Investigation

---

3.1 Introduction: High Frequency Oscillations as Surrogate Markers of Epileptogenicity

3.1.1 Conventional Electroencephalographic Recordings and the $\geq$ 100 Hz Frequency Band

Electroencephalography (EEG) is the primary modality for measuring functional brain activation as a manifestation of neuronal network activity. Recent technologies such as functional MRI are also capable of resolving spatial-temporal changes in brain function, however, EEG remains the best suited technique for fast temporal activity. The main uses of EEG recordings in the context of epilepsy are for detection and diagnosis of seizure activity or epileptiform discharges (typically outpatient uses), and for seizure localization during. The latter is achieved by a combined video-EEG monitoring (VEM) where patients are admitted to hospital and their antiepileptic medications are reduced while their seizures are monitored. EEG as acquired during VEM can be recorded either via scalp electrodes (placed on the head) or via intracranial electrodes (invasive procedure). Use of the latter invasive technique is commonly a prelude to seizure surgery where the identified seizure focus is resected to improve seizure control in patients that are not well controlled by other means such as pharmacotherapy. The seemingly simple task of seizure localization is in fact challenging in a clinical setting due to the heterogeneity of individual patient seizure syndromes (and longstanding history of seizures), and is complicated by epileptiform activity commonly arising from more than one brain location, and/or rapidly spreading to involve other locations [108]. In the case where seizures are aris-

ing from two opposing hemispheres, for example in key structures such as the hippocampus, localization of the primary ictal (i.e. seizure) generator is of critical importance for successful and deficit-free surgery [108]. Moreover, for focal temporal epilepsies, there is evidence suggesting that a patient's quality of life is improved upon receiving seizure surgery as compared with long-term pharmacotherapy [369]. Therefore, there is impetus for improving seizure localization, especially in patients with multi-focal epilepsy with the aim of improving surgical treatment modalities.
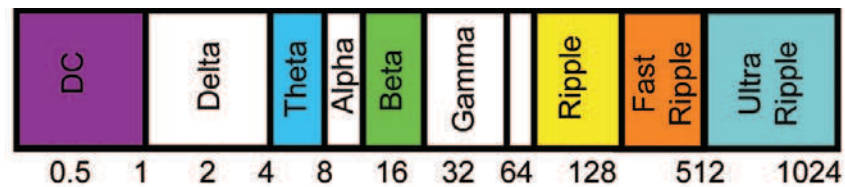
Figure 3.1: A schematic diagram showing the various spectral components of EEG; the spectrum is depicted based on frequencies increasing from DC ($\approx$ 0.5 Hz) towards 1024 Hz. Below 70 Hz corresponds to the "traditional" Berger bands. These lower frequency oscillations are correlates of a diversity of brain states such as theta activity during early sleep stages, alpha activity during eye closure, and gamma activity during cortical binding, which is believed to be indicative of long-range coherent oscillations during sensory processing. Frequencies in the ripple range (100 - 200 Hz) have been observed during both physiological and epileptiform activity. Frequencies above 200 Hz are believed to be generated by networks that are somehow altered or participate in epileptic processes.

Analogous to the electromagnetic spectrum, where different frequency photons have different functional attributes, the spectral components of EEG are also known to represent different states of brain activity with related functional correlates from sleep (theta activity) to epileptic seizures (ripples) [250, 284, 351]. For example, frequencies in the gamma range (40-80 Hz) are believed to be associated with cortical binding that play a role in memory processing, encoding, and recall [284, 351] (see Fig. 3.1). Conventionally, the relevant bandwidth of study in EEG has been limited to DC-70 Hz for two main reasons: (1) the scalp is a dielectric and therefore smooths the potential field resulting in low-pass filtering of signals with conventional EEG's spatial sampling [313], and (2) most clinical centers digitize their EEG recording at a sampling rate close to 200 Hz. This rate of sampling is far below the Nyquist limit for considering oscillations greater than 100 Hz (the practical limit is closer to 50 Hz). With improvements

in analog-to-digital converter technology, alongside improvements in computing speed and file storage, there are more centers using fast-sampling EEG machines (1-10 kHz sampling). Fast sampled EEG exhibits signal characteristics beyond the 70 Hz limit, and thus the relevant bandwidth of EEG has expanded to include frequencies faster than gamma and as fast as 600 Hz in the somatosensory cortex [77, 78].

3.1.2 Attributes of High Frequency Oscillations: A Summary of Animal and Human Studies

High frequency oscillations ($\geq$ 80 Hz, HFOs) can be classified by their "operational" frequency range, and are commonly grouped into ripple (80 - 200 Hz) and fast ripple (FR, $\geq$ 200 Hz) frequency bands [42]. Ripples reflect network activity that includes both physiological and epileptiform activity (reviewed in [276]). Ripples have been recorded in the hippocampus and entorhinal cortex in both normal (behaving rats) [42, 58] and epileptic neuronal networks [42, 118]. Under non-epileptic conditions, ripples may play a role in memory consolidation by transferring information from the hippocampus to the neocortex given that they have been observed in the hippocampus of behaving rodents in the form of sharp waves during spatial exploratory tasks [101], and also hippocampal ripples have been correlated with cortical spindles during slow-wave sleep [300].

Cellular and network mechanisms underlying HFOs are believed to involve both glutamatergic and GABAergic synaptic transmission [215], in addition to gap-junctional coupling [102]. These synchronizing elements allow for dynamic, yet transient, changes in the activity of sub-populations of neurons that operate within larger networks [30]. In addition, there are several studies that point to independent modes of physiological vs. pathological HFO generation in the context of neonatal and adult brain development. Indeed, excitatory GABAergic activity can prime the neonatal brain for HFO-based seizure activity [188].

Ripples and FRs can co-occur under epileptic conditions. They have been observed exclusively at seizure foci in *in vitro* [175, 106, 187] and *in vivo* animal [25, 26, 28, 29] models of epilepsy. In addition, ripples and FRs have been observed in intracranial microelectrode EEG recordings from hippocampal and entorhinal cortices of epileptic patients [24, 25]. Several

human studies suggested that FRs occur predominantly in seizure foci [27, 31, 315]. Increased HFO activity was also correlated with the presence of hippocampal atrophy [314, 315]. Other studies provided further information towards the generators of FRs and their relation to seizure (ictal) genesis. In particular, it was shown that multi-unit synchrony was greater during FR as compared with ripples [31]. In two animal studies involving intrahippocampal injection of kainic acid, spatial contacts that exhibited FRs did so exclusively and in a stable manner over prolonged epochs ranging from days to months [29]. A subsequent study by the same group showed that animals that first exhibited HFOs went on to first develop spontaneous seizures and the time to first seizure was positively correlated with the earlier occurrence of HFO activity [28]. Taken together, these findings suggest that pathological HFOs, and in particular FRs, serve as surrogate markers for the presence of an epileptic condition and may have implications for seizure genesis [28, 276, 338, 340].

In order for HFOs to be demonstrated as surrogate markers of seizure processes more widespread study is necessary. Until recently, it was believed that HFOs (especially ≥ 200 Hz) could only be recorded using custom-built micro depth-electrodes. However, several recent studies have demonstrated their presence in recordings using custom-built macro depth-electrodes [162] and commercially available subdural grid electrodes [5, 4, 253]. Moreover, these studies, in addition to one other using 200 Hz sampling [377], have shown that HFOs are mostly localized to electrode contacts over or in the vicinity of primary ictal onset. Indeed, these findings support earlier observations of HFOs (≤ 150 Hz) localized to channels monitoring sites of primary seizure onset [118, 340, 6]. In addition to their localization, the suggestion exists that HFOs can undergo measurable change over time during the transition to seizure [162, 175, 377].

Previous studies of HFOs have looked at the interictal and ictal period but not the pre-ictal period, which likely represents a fundamental process in seizure initiation [113]. Therefore, I engaged in a prospective study using power spectral analysis to test three hypotheses using both an *in vitro* model of recurrent seizures and recordings from epileptic patients. My specific hypotheses are: (1) HFOs can exhibit temporal changes during the transition to seizure, (2) HFOs localize to specific contacts that correlate with the ictal onset zone (for patients, deter-

mined based on conventional review of video-EEG monitoring data), and (3) HFOs may be detectable using conventional (commercially-available) depth and grid macroelectrodes.

3.2 Experimental Methods I. Induction and Analysis of *in vitro* Seizure-like Events

3.2.1 Brain Slice Recordings

Brain slices and solutions - Seven male Wistar rats (P21-24) were anaesthetized with halothane and decapitated. The brain was quickly dissected and maintained in ice-cold artificial cerebrospinal fluid (ACSF) for 4-5 min. Brain slices were cut according to Rafiq et al [274, 275]. After sectioning, slices were maintained at room temperature in oxygenated ACSF for at least one hour before recording. The ACSF contained (in mM): $NaCl$, 125; KCl, 2.5; NaH_2PO_4, 1.25; $MgSO_4$, 2; $CaCl_2$, 1.5; $NaHCO_3$, 25; $D-glucose$, 10, pH 7.4 when aerated with 95% O_2 and 5% CO_2. Osmolarity was 310±5 mOsm. For electrophysiological recordings, the superfusing ACSF was switched to one containing 5 mM KCl and 0.5 mM $MgSO_4$, to ensure the development of spontaneous epileptiform activity. Twelve out of 14 ($\approx$86%) slices developed interictal events that spontaneously progressed to seizure-like events (SLEs). The observed transition was consistent with previous reports using this model of epilepsy [236, 137]. Given that recurrent seizure-like events are observed in this model, an "episode" is defined as encompassing a single interictal to ictal transition (Fig. 3.2A). For subsequent quantitative analysis, one slice from each of the seven animals that exhibited the aforementioned seizure-like events was used and analyzed; only the first five episodes were used. This was to ensure consistency and viability across seizures from different slices. In total 35 complete recordings (interictal to ictal) were analyzed.

Electrophysiological Recordings - Brain slices were transferred to a superfusion chamber maintained at 35°C (SD 2) (Medical Systems Corp., Model PDMI-2) and superfused with the low Mg^{+2} ACSF at a rate of 4 ml/min. Epileptiform discharges were observed within 10 to 20 min. of perfusion with low Mg^{+2} ACSF (Fig. 3.2A). Extracellular recordings were made using an Axoclamp 2B amplifier (Axon Instruments). Signals were first low-pass filtered (at 625

Hz, hardware 8-pole Bessel filter) and acquired at 2 kHz (Digidata1322A, Axon Instruments) continuously. DC-shifts were subtracted by a moving average filter corresponding to a high-pass frequency of 0.2 Hz. For the purpose of analysis, continuous data for each episode from each slice were segmented into two groups: interictal-to-pre-ictal and ictal. Data were digitally notch filtered at 60, 180, and 300 Hz ($\pm$ 3 Hz) to remove line noise. The recording electrodes were filled with NaCl (150 mM) and placed in the CA1 and/or CA3 cell body layer. For three of the slices (n = 15 episodes), dual simultaneous CA1/CA3 or CA3/CA3 recordings were performed. A stimulating electrode was placed in the mossy fiber region. At approximately one minute after the end of each seizure-like event (between episodes), single evoked field responses were used to monitor tissue viability, while waiting for spontaneous epileptiform discharges (EDs) to reappear. The intensity of stimulation was fixed for each experiment but varied between slices, adjusted to a value that evoked a single field potential in the CA1 layer.

3.2.2 Morlet Wavelet-based Power Spectral Analysis of *in vitro* Field Recordings

Power-frequency analysis of all recordings was performed continuously over time using a local multi-scale Fourier Transform [LMS-FT, [266]]. Its use in analyzing medical imaging (multi-dimensional) MRI signals has been described previously by members of our research group [130, 390]. Here, this algorithm was used to extract power spectral information from one-dimensional electrophysiological signals (voltage vs. time). Use of the LMS-FT allowed for enhanced resolution of power-frequency information over time (in our recordings) and proved to be useful for quantifying spectral changes during interictal, pre-ictal, and ictal epochs; effective frequency resolution was set to 4 Hz. This technique circumvents some of the limitations of the classical Short-Time Fourier Transform (ST-FT) by making use of time windows that scale inversely with the frequency being analyzed [266, 150]. Therefore, lower frequency oscillations were resolved using larger time windows, while the power spectrum of higher frequency oscillations was computed using smaller time windows (Fig. 3.2B, right). Specifically, the ST-FT exhibits no scaling in the frequency axis and hence frequency resolution is traded off for temporal resolution and vice versa (Fig. 3.2B, left). The LMS-FT allows for time-frequency analysis of signals in their most pure form without the need of pre-bandpass filtering

of the data; a practice that can introduce unwanted signal artifacts and consequently inaccurate power spectral information. The LMS-FT shares some similarities with the continuous Wavelet transform in its time-frequency resolution properties. However, a key advantage of this method is its close link to the Fourier domain without the loss of information.

Prior to power-frequency analysis, each of the recordings were decimated from a 2 kHz sampling rate down to 1 kHz by digitally low-pass filtering the data at 800 Hz followed by re-sampling. The LMS-FT was computed in a continuous manner for all episodes (interictal+pre-ictal and ictal recordings). In order to perform quantitative analysis on the power-frequency information obtained using LMS-FT, the computed power amplitudes were summed in the frequency direction using the following frequency bands (in Hz): 0-100 (sub-ripple), 100-200 (ripple), 200-300 (fast ripple1), and 300-400 (fast ripple2). This resulted in four "channels" of continuous power-frequency information, over time, that reflect the amplitude of the power spectrum in each of the four frequency bands. These equally-spaced bands were selected to process all conventional (EEG, $\approx$ 0-100 Hz) low frequency bands together, and to control for cumulative power amplitude in each band for group statistical comparison. Using this analysis, signal components above 400 Hz were approximately twenty times smaller in (power) amplitude relative to lower frequencies. Therefore, we considered the full effective bandwidth of our signal (0-400 Hz) for all subsequent time-frequency analyses.

The time at which interictal, pre-ictal, and ictal discharges occur varied from episode to episode and between different slices. Given that we observed no statistical correlation between the number of discharges leading to seizure and episode number in any of the slices (Pearson's correlation, r = -0.46, $p \geq 0.05$), we elected to use the start of the seizure as a defined relative time point from which to measure all discharges preceding and also during the actual seizure event. This strategy was also employed to allow for subsequent direct statistical group anal-ysis of the power-frequency information in relation to pre-ictal changes that may exist before seizure onset. Therefore, epileptiform discharges were numbered in the negative direction, starting from -1 as the first epileptiform discharge (Fig. 3.2A). Similarly, ictal discharges were numbered in the positive direction starting with zero as the marker for the seizure start time (Fig. 3.2A). All discharges were identified manually by visual inspection of all recordings.
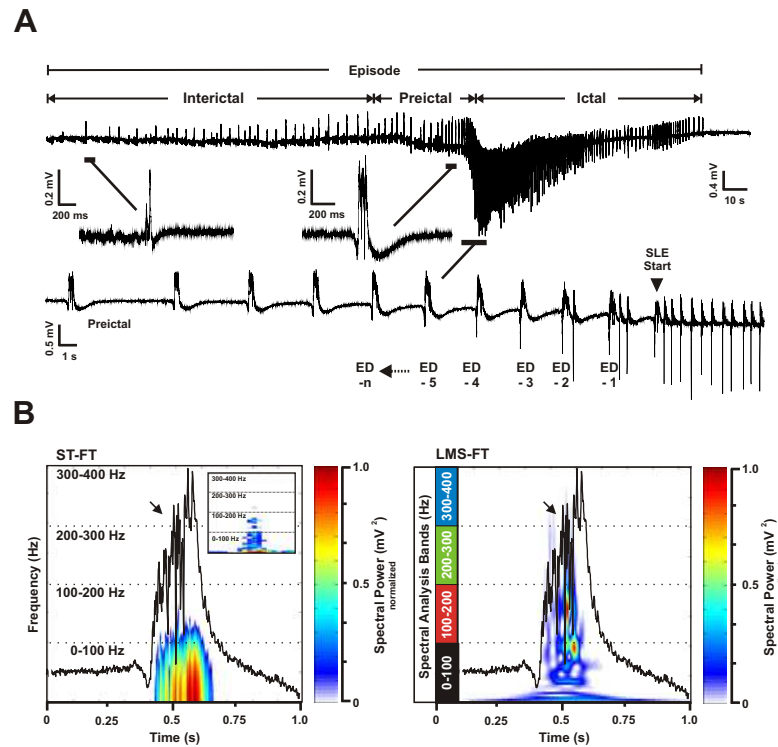
Figure 3.2: Transition to seizure activity and analysis of epileptiform and ictal discharges using power-frequency analysis techniques. **(A)** Extracellular recording from the CA1 layer of a hippocampal slice showing the transition from interictal to pre-ictal and then to ictal activity - this is referred to as a single episode. (insets) Epileptiform discharges (EDs) are numbered backwards starting with -1 as the last pre-ictal discharge. The start of seizure begins with discharge zero (arrow head). **(B)** Power-frequency analysis of a single epileptiform discharge (black overlaid trace) from a different slice. The discharge's power spectrum, in time and frequency (in the range of 0-400 Hz), are shown with power amplitude coded in color, with time and frequency on the x- and y- axes respectively. (left) In order to obtain good time resolution with using the Short-time Fourier Transform (ST-FT), analysis must be performed using small time windows. This compromises the frequency resolution for fast events (arrow head). (inset) This can be can be alleviated by using larger time windows, which sacrifices the temporal resolution. (right) Use of the multi-scale Fourier Transform (LMS-FT) allows for optimal time-frequency resolution by using a window size that varies inversely with the frequency. This provides an improvement in time-frequency resolution of HFOs (arrow head). Analysis parameters were kept fixed for both techniques. The power spectral amplitude is normalized to a maximum of 1 and frequency resolution in the y-axis is 128 points ($\approx$ 4Hz) for both techniques. Adapted from Ref. [175].

The next step in analysis was the precise quantification and statistical comparison of pre-ictal changes in power-frequency information and how these changes evolve from episode to episode. We therefore computed the relative power spectral contribution of each of the computed frequency channels for each discharge using the start of the seizure as a defined reference point. This group statistical comparison was performed for all 35 episodes using a Linear General Model (LGM). A repeated measures ANOVA was used to quantify possible temporal trends across discharges and episodes in relation to each of the four frequency bands. Independent variables used in the ANOVA model were episode number and discharge number. Although we computed the continuous power-frequency information for all recordings and the power spectral make up of each discharge, we restricted the use of the repeated measures ANOVA to the twelve discharges immediately preceding seizure onset that were common to all 35 episodes. In other words, twelve discharges (i.e. EDs) back from the start of seizure was the largest number of discharges common to all recordings. We analyzed all ictal discharges and computed a similar ANOVA matrix for 12 ictal discharges for symmetric investigation of peri-ictal frequency changes in time. All frequency analyses were performed using Matlab (Mathworks Inc.) and statistical comparisons using SPSS (SPSS Inc.). A p-value of $p \leq 0.05$ was considered significant. Mean values are reported as mean $\pm$ SEM (standard error of the mean). Development and data processing were performed on a Linux-based PC. The WestGrid computing facility (University of Calgary) was used for batch data processing.

3.3 Experimental Methods II. Intracranial EEG Recordings and Power-Frequency Analysis

3.3.1 Patient Selection and EEG Recordings

Informed consent was obtained from all patients for this study, which was approved by the University of Calgary Medical Bioethics Committee.

We recruited seven consecutive patients with medically refractory epilepsy who underwent intracranial video EEG monitoring as part of their pre-surgical workup at the University of Calgary Comprehensive Epilepsy Center. Each patient had commercially-available subdural

strip or gride platinum electrodes (4.0 mm diameter, 10 mm spacing) and depth electrodes (6 contacts, 10 mm spacing) implanted according to clinical need using standard protocols in our program (Ad-Tech Medical Instrument Corporation, Racine, WI). Sites for electrode placement were selected based upon clinical history, as well as the following investigations: previous scalp VEM, MRI and single-photon emission computerized tomography scans, and neurophyschological assessment.

During admission for intracranial VEM, each patient's antiepileptic medications were reduced to enhance the probability of seizure occurrence. For each patient, EEG was gathered simultaneously on two EEG machines. The first machine, (the "clinical machine"; Xltek, Oakville, Ontario, Canada) sampled all implanted electrodes at a sampling rate of 500 Hz. The second machine (the "research machine"; SynAmp1, Compumedics Corp., El Paso, Texas, USA) sampled a subset of electrode contacts up to a maximum of thirteen (due to a limited number of available connection inputs) at a sampling rate of 5 kHz (low-passed at 1 kHz). In all cases, the subset of channels selected for recording by the research machine was selected for recording by an epileptologist (Dr. Paolo Federico) based on either the expected seizure onset zone (presence of a structural lesion, previous scalp VEM data, etc) as well as the interictal or ictal data recorded by the clinical EEG machine during the first few days of intracranial VEM. Bipolar recordings were analyzed to avoid reference contamination and to more accurately localize HFOs since they are believed to be locally generated phenomenon. VEM data were recorded continuously by both machines and the clinical EEG was read by the attending epileptologist. The clinical VEM data were used as reference by an expert electroencephalographer (Dr. Paolo Federico) to identify and clip clinical and subclinical EEG events on the research machine. For each seizure, recordings were clipped for 30 minutes preceding seizure onset and 5 minutes after seizure onset (which is longer than the duration of all recorded seizures).

3.3.2 Fourier-based Power-Frequency Analysis of Human EEG

Continuous EEG records obtained via the research EEG machine at a sampling rate of 5 kHz were analyzed using custom analysis software designed in Matlab (Mathworks Corp.). Prior to analysis, pre-processing of the data involved removing linear trends (detrending) and re-

moval of DC baseline shift ($\leq$ 0.5 Hz, Fig.1A). Subsequently, each seizure recording (typically 35 min.) was analyzed using a short-time Fourier transform (STFT) that provided a time-dependent measure of the signal's spectral composition in each channel (Fig. 3.3B). Continuous EEG data were passed to the STFT in "running" windows of 2 s segments with one-half overlap (effective Δt = 1 sec). These were analyzed at STFT level with a temporal resolution of 500 ms with one-half overlap windows; the effective frequency resolution was Δf = 1 Hz. The resulting three-dimensional data (consisting of time vs. frequency vs. power) was then summed in the frequency direction into 5 bands spanning 0-100 (classical EEG), 100-200 (ripple), 200-300 (fast ripple1), 300-400 (fast ripple2), and 400-500 Hz (fast ripple3). This procedure then resulted in a time-dependent measure of spectral composition in five EEG bands. Equidistant bandwidths were selected in order to allow for meaningful statistical comparison across different bands. It should be noted that the bulk of spectral power amplitudes exists in the 0-100 Hz band due to the physical nature of EEG signals whereby there is an inverse correlation between EEG frequency and spectral power. Note that all individuals involved in data analysis were blinded to seizure localization and all other clinical data until analysis was completed for all channels and bands.

Spatial Analysis of HFOs. In order to examine the relation between the presence of HFOs and regions (i.e. channels) of seizure onset, we compared two epochs of EEG for each channel (and each band): immediately pre-ictal and the first few seconds of seizure onset. This technique is similar to that introduced by Jirsch et al. [162]. Specifically, five seconds of power spectral amplitudes was summed preceding EEG seizure onset and compared to those obtained during the first five seconds at (electrographic) seizure onset for each band and channel (Fig. 3.3A). A unitless ratio (relative power ratio, R, Eqn. 3.1) was then derived such that the seizure epoch (for each channel and each band) was normalized to the pre-seizure epoch:

$$R_{(f,c)} = \frac{(\sum_{f'=f}^{f+\Delta f} \sum_{t=0}^{5} P_c(t,f') - \sum_{f'=f}^{f+\Delta f} \sum_{t=-5}^{0} P_c(t,f'))\Delta t \Delta f}{\sum_{f'=f}^{f+\Delta f} \sum_{t=-5}^{0} P_c(t,f')\Delta t \Delta f} \qquad (3.1)$$

where t is time in seconds ($t = 0$ at electrographic onset), f is the lower bound (in Hz, f = {0,100,200,300,400 }) of the range of frequencies in one band, c is channel number (c =
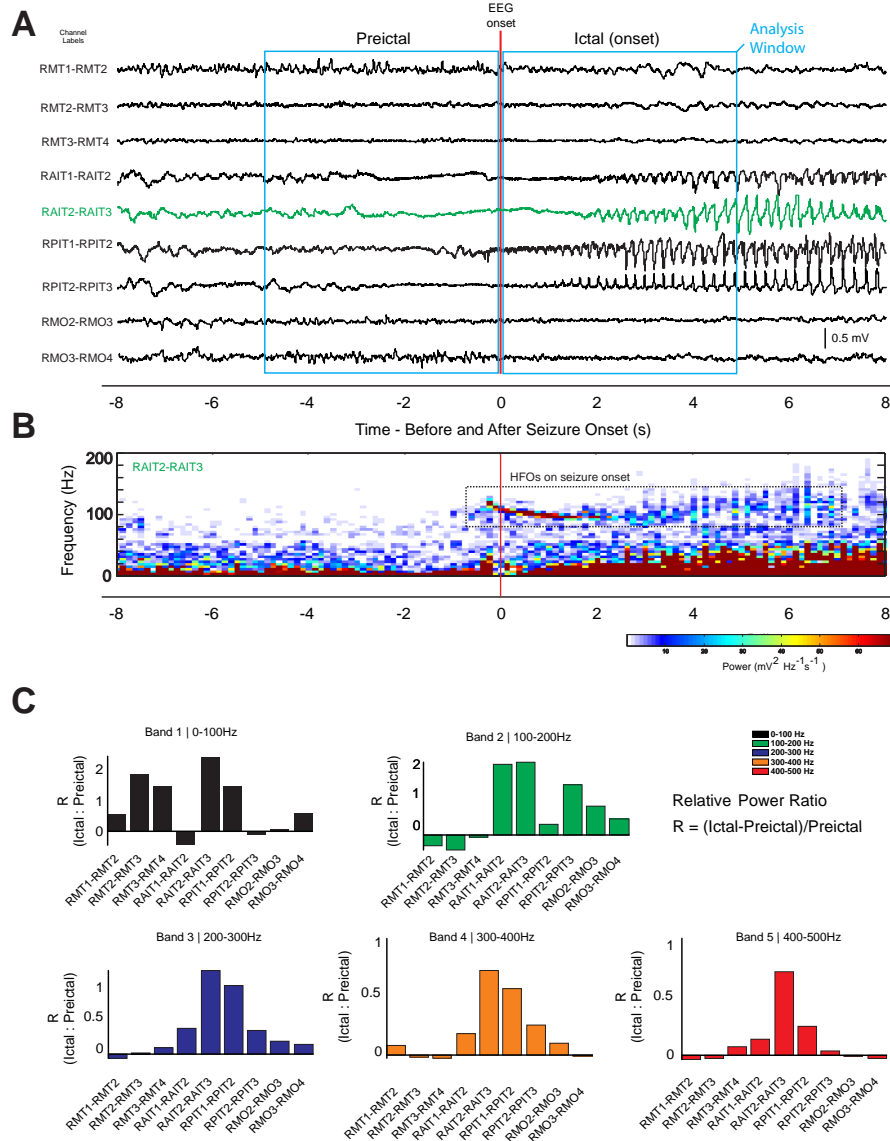
Figure 3.3: HFOs can be recorded using strip electrodes and are recorded with maximal prevalence during the immediate pre-ictal to ictal transition. **(A)** Intracranial EEG recording obtained at 5 kHz in the right amygdala, hippocampus, and occipital lobe in patient 4, who had mild gliosis and was normal on MRI (see Table 3.2). The channel of electrographic onset is highlighted in green. **(B)** Time frequency representation for the primary ictal onset electrode for the seizure shown in A. The appearance of HFOs, with a dominant frequency component at ≈ 120 Hz is clearly visualized by increased power magnitude (bright red colors in highlighted in box). This increase lasts into the seizure but is most intense during the first 5 s as slower spiking activity later predominates. Note that, while the 0-200 Hz bands are shown in this figure, the power analysis was performed from 0-500 Hz in 100 Hz frequency bands (see Methods Section 3.3). **(C)** Spatial (channel) distribution of peri-ictal low frequency and HFO changes for each channel and each frequency band as compared for 5 s of power-amplitude data between ictal and pre-ictal analysis windows (see A).
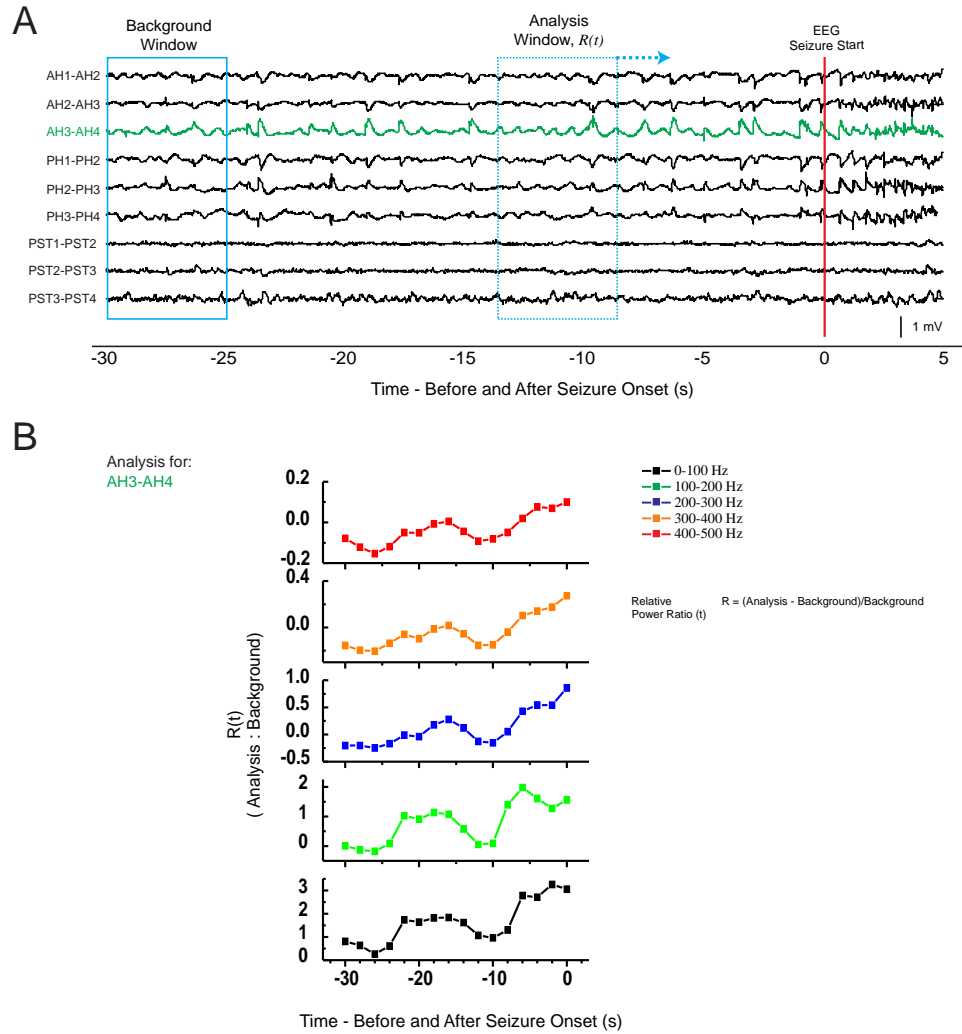
Figure 3.4: Methodology and analysis of temporal trends in HFO power amplitude during the pre-ictal epoch leading up to electrographic seizure onset. **(A)** A 30 s segment of EEG sampled at 5 kHz leading to seizure onset recorded using commercially available macro-depth electrodes placed in the left hippocampal structure in a patient with unilateral temporal epilepsy (patient 1 with hippocampal sclerosis). Continuous (temporal) power spectral analysis was performed (see Methods Section 3.3) and power amplitudes were summed in 5 s moving analysis widows for each channel and band. The continuous power amplitude data were compared to a background analysis window also of 5 s duration (see Methods Section 3.3). This produced a time-dependent R-value [$R_{(f,c)}(t)$]. This process was performed for three independent background EEG windows and averaged. **(B)** Mean time-dependent relative power ratio (R-value) reported in 2 s time-resolution, in each band, for the channel of electrographic onset.

$\{1,...,n\}$), and P is the power (mV^2/Hz). Therefore, the above operation is performed for each band (frequency range, $\Delta f = 100$ Hz) and each channel ($R_{(f,c)}$, see Fig. 3.3C). Use of this normalized ratio was necessary to allow each patient and each seizure to act as their own control and to allow for comparison across patients. Note that positive R-values reflect an increase in power during the ictal epoch compared to the pre-ictal epoch, whereas negative values indicate a relative increase in HFO during the pre-ictal period compared to the ictal period. We did not R-values from different bands (e.g. by subtraction of 0-100 Hz R-values from the other bands). This was based on concerns that R in different bands may not be mutually exclusive at the (causal) level of neuronal populations that are responsible for the generation of the raw waveforms with broadband spectral components.

Seizures that were felt to be originating from the same electrode(s) based on conventional review of the VEM data were grouped together and their R-values were averaged, and reported with SEM values. ANOVA analysis was used to compare summed power amplitudes across bands and t-test for comparing the onset electrode with adjacent or distant contacts.

Temporal Preictal Analysis of HFOs. The change in power spectral amplitude for each band, for each channel, and over time during the immediate pre-ictal epoch was evaluated. Once again a unitless numerical quantifier was required that was independent of patient parameters to allow pooling of data across seizures and patients. The R quantity over time ($R_{(f,c)}(t)$) was computed using a 5 s background epoch and a 5 s analysis epoch (i.e. $\Delta t = 5$ sec) as shown in Fig. 3.4A.

$$R_{(f,c,n)}(t_i) = \frac{(\sum_{f'=f}^{f+\Delta f} \sum_{t=t_i}^{t_i+\Delta t} P_c(t,f') - \sum_{f'=f}^{f+\Delta f} \sum_{t=BKGND_n}^{BKGND_n+\Delta t} P_c(t,f))\Delta t \Delta f}{\sum_{f'=f}^{f+\Delta f} \sum_{t=BKGND_n}^{BKGND_n+\Delta t} P_c(t,f')\Delta t \Delta f} \tag{3.2}$$

$$\bar{R}_{(f,c)}(t_i) = \frac{\sum_{n=1}^{3} R_{(f,c,n)}(t_i)}{3} \tag{3.3}$$

Here i is the interval or analysis window number of Δt duration (see Fig. 3.4A) that is computed continuously for the EEG leading up to electrographic seizure onset. Similar to the spatial analysis, $R_{(f,c,n)}(t)$ is computed once again for the each band, f, spanning the five frequency ranges and also for each channel (c) separately. For each seizure, three background (see *BKGND* in Eqn. 3.2) EEG segments, also of duration Δt, showing no epileptiform dis-

charges were selected by an electroencephalographer (Dr. Paolo Federico). These background segments were typically selected within the epoch 25 - 30 min prior to seizure onset. The calculation of $R_{(f,c,n)}(t_i)$ was performed three times (n = 3) for each channel, each time yield five traces (for each band) in order to avoid any bias towards background window selection. Thus, $\bar{R}_{(f,c)}(t_i)$ is reported as a mean value from the three independent calculations (Equation 3.3 and Fig. 3.4B). Note that equation 3.2 does not take into account the additional windowing overlap procedure that resulted in an effective temporal resolution of 2.5 sec. Subsequent statistical analysis and grouping of multiple seizures based on their site of origin were performed as described in the *spatial analysis* section above.

3.4 Results

3.4.1 Preictal Increases in HFOs in a Low Mg^{+2} Model of in vitro Seizures

	Interictal	Interictal	Ictal	Ictal
Within Category Test	**ANOVA**	**Linear Trend Analysis**	**ANOVA**	**Linear Trend Analysis**
0-100 Hz				
Episodes	p = 0.7	p = 0.9	p = 0.5	p = 0.7
Discharges	p = 0.2	*p = 0.05*	p = 0.5	p = 0.6
100-200 Hz				
Episodes	p = 0.4	p = 0.7	p = 0.3	p = 0.8
Discharges	*p = 0.006*	*p = 0.01*	p = 0.4	p = 0.4
200-300 Hz				
Episodes	p = 0.4	p = 0.9	p = 0.4	p = 0.7
Discharges	*p = 0.004*	*p = 0.01*	p = 0.5	p = 0.2
300-400 Hz				
Episodes	p = 0.5	p = 0.6	p = 0.3	p = 0.8
Discharges	p = 0.2	p = 0.07	p = 0.5	p = 0.3

Table 3.1: Statistical analysis results for epileptiform and ictal discharges in each of the four spectral bands. Repeated measures ANOVA p-values are shown for comparing the power spectral information with respect to differences of means across Discharges or across Episodes. For example, for "Discharges" the p-value represents the probability of accepting the null hypothesis - that there are no differences in the means of neighboring discharge's power spectral amplitude for a particular band when considering all of the discharges. Additional p-values are also cited for compliance with the existence of a linear trend. Significance is considered for $p \leq 0.05$ (italicized values).
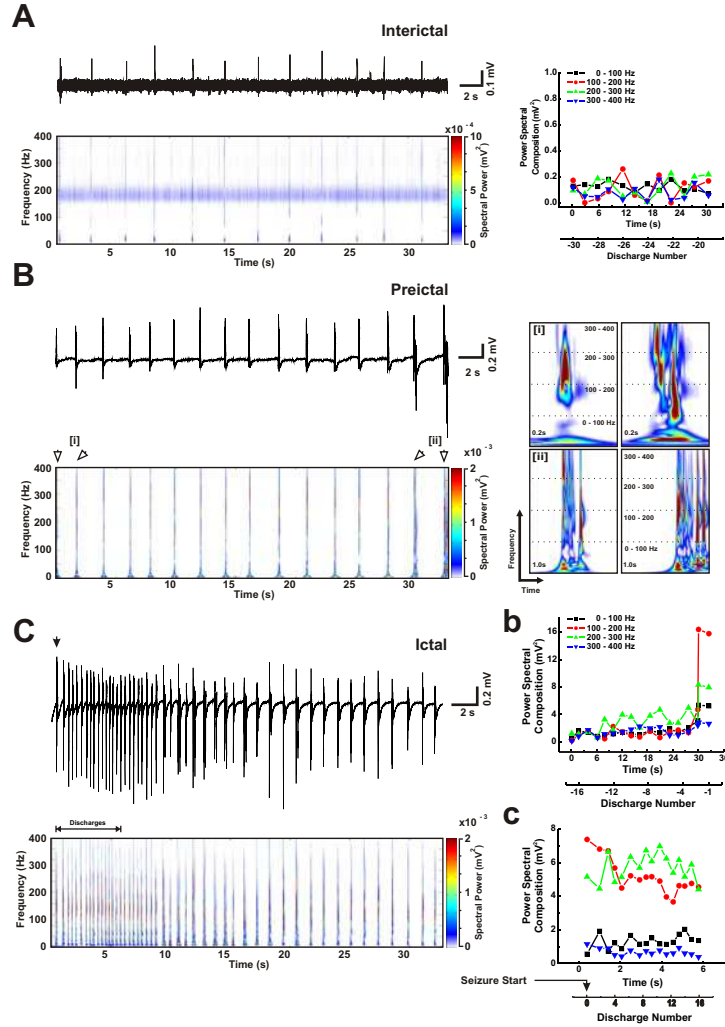
Figure 3.5: Power-frequency analysis over time for interictal, pre-ictal, and ictal activity recorded from the CA1 layer of hippocampal slices. **(A)** (left) Power analysis of interictal activity for an epoch far from seizure onset. Horizontal bands (light blue) on the time-frequency plot correspond to residual power in notch filtered frequencies given the low signal-to-noise. (right) Discharges are typified by small power amplitude values for each frequency band without any observable trends. **(B)** (left) Epileptiform (interictal-to-pre-ictal) activity recorded from a different slice exhibiting 17 discharges before seizure onset. (right insets) Detailed time-frequency morphology of the first two [*i*] and last two [*ii*] epileptiform discharges (marked by hollow arrowheads). **(b)** Power amplitude composition plot for each epileptiform discharge showing an increasing trend for ripple and fast ripple1 (FR1) frequency bands leading up to seizure onset. **(C)** (left) Ictal discharges immediately following the activity in B; seizure onset is marked by a solid arrow head corresponding to discharge number zero. **(c)** Variability is observed in all four frequency bands for ictal discharges. The FR1 (200-300 Hz) band is on average greater in magnitude than the ripple band (100-200 Hz) during the early phase of seizure activity. Power spectral make up of each discharge, in the four frequency bands, was computed by collapsing the summing the continuous power-frequency values in the frequency direction (see methods). Discharge time and number are reported for the power amplitude composition plots (b and c). Absolute power amplitude is color coded. Adapted from Ref. [175].
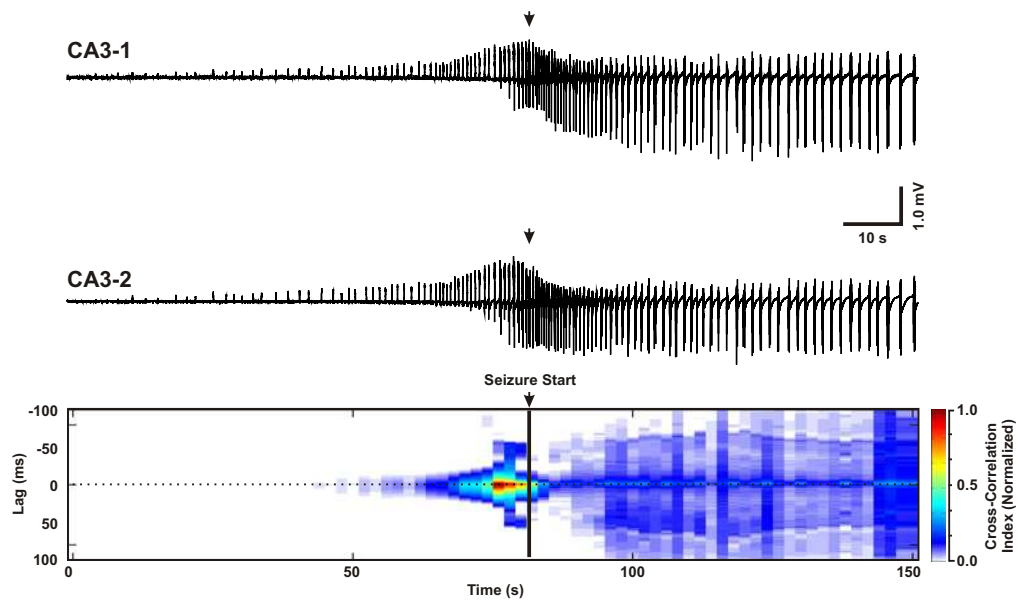
Figure 3.6: Simultaneous dual-extracellular recording and cross-correlation analysis for two neighboring sites in the CA3 cell layer. Cross-correlation was computed in 1s windows with a lag of -100 to +100 ms. A strong correlation value is observed during an epoch lasting ≈25 s corresponding to the pre-ictal period before seizure onset. A strong correlation between the two signals, albeit smaller in relative magnitude, is observed throughout the seizure event (bright region about zero lag). The correlation matrix was normalized to a maximum of 1 in relation to the maximum correlation index for the entire episode. Adapted from Ref. [175].
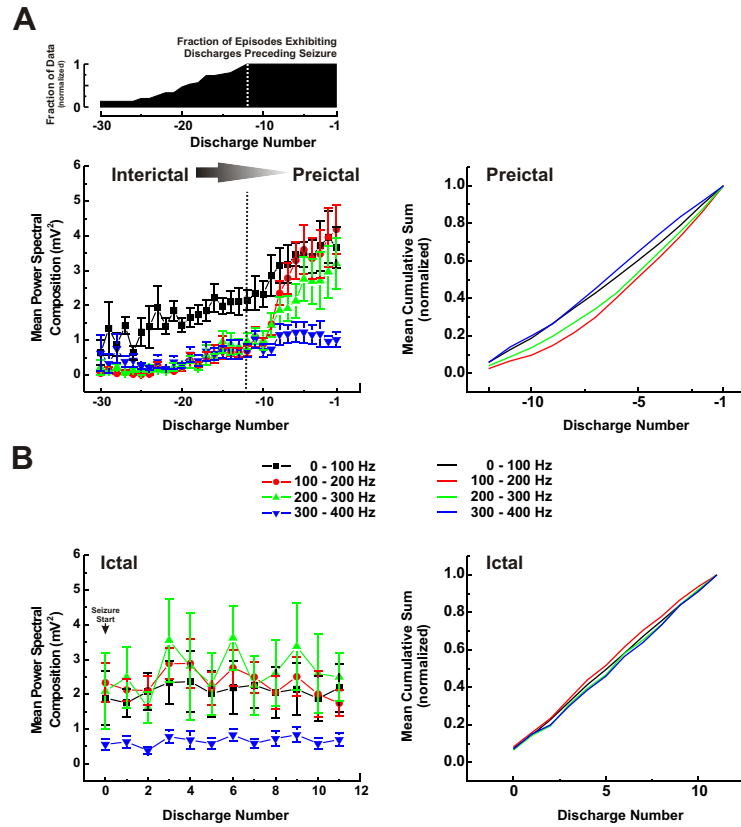
Figure 3.7: Temporal evolution of the mean power spectral amplitude, in each frequency band, for individual discharges during epileptiform (interictal and pre-ictal) and ictal activity. **(A)** (left) Mean power amplitude composition plot for all epileptiform discharges. The 0-100 Hz band increases linearly with discharge number at a rate of change (slope $m = 0.16$) that is smaller in magnitude in relation to the ripple and FR1 bands ($m = 0.36$ and $m = 0.21$ respectively). The ripple (100-200 Hz) and fast ripple1 (200-300 Hz) increase during preictal activity. (inset, top left) The fraction of data, for all episodes ($n = 35$, $n = 7$ slices), that exhibited discharges preceding seizure onset. Linear trends in power spectral amplitude were observed for the 0-100 Hz ($p = 0.05$) and also the ripple and FR1 bands ($p = 0.01$ for both). (right) Normalized mean cumulative sum of the power amplitudes, in each of the four bands. The low frequency (0-100 Hz) and fast ripple2 (300-400 Hz) bands accumulate linearly, whereas the ripple and FR1 bands (100-300 Hz) gain most of their spectral magnitude during the last six discharges preceding the seizure. **(B)** (left) Mean power amplitude composition plot for ictal discharges. Power amplitudes are relatively constant with the greatest values for the FR1 band. (right) Normalized (mean) cumulative sum for each of the spectral bands. All bands seem to gain their power amplitudes together and at an equal rate. When these data were analyzed in relation to changes from one episode to the next no statistically significant (linear) trends were observed for epileptiform or ictal discharges. All values expressed as mean $\pm$ SEM. Adapted from Ref. [175].

Five or more episodes were recorded from each of the seven slices that developed SLEs spontaneously. The mean inter-episode time was 3 min (SD 2). The mean peak amplitude of the stimulus-evoked responses was fairly constant between episodes and after the fifth SLE, was 94 ± 5 % of the control value measured at the start of the low Mg^{+2} perfusion. All pre-seizure discharges were analyzed. In order to assess whether any trends existed in epochs far from the time of transition to seizure, episodes that exhibited greater than 12 EDs (n = 30, 85%) were analyzed. No statistically significant differences or trends in the power spectral amplitude of successive discharges were observed for any of the frequency bands ($p = 0.5$). Figure 3.5A shows such a recording for the first 30 seconds of a 200 second interictal epoch in an episode from one slice. The LMS-FT of discharges far from the pre-ictal epoch consistently had low amplitude power values as visualized by the color map and discharge plot (Fig. 3.5A). Figures 3.5B and C show pre-ictal and ictal discharges taken from a single episode from a different slice. The continuous LMS-FT was computed and values corresponding to the power spectral make up of all EDs are shown in the power spectral composition plot (Fig. 3.5b and c). A gradual increase in the power amplitude of the ripple (100-200 Hz) and FR1 (200-300 Hz) spectral bands was observed for successive discharges leading up to the SLE (Fig. 3.5b). The insets show the detailed time-frequency morphology of the first two [i] and last two [ii] epileptiform discharges (Fig. 3.5B, right). These panels also show the increase in the ripple and FR components of these waveforms just prior to SLE initiation. Analysis of the seizure shows that high frequencies can persist and fluctuate throughout the SLE (Fig. 3.5C). Notably, the contribution of ripple and FR1 bands to the power spectral amplitude of each ictal discharge is consistently larger than that of other bands during seizure onset and remains fairly constant over the observed time course (Fig. 3.5c).

In order to explore temporal interactions between different neighboring recording sites, for slices where dual extracellular recordings were available, "running" cross-correlograms were computed between the two channels over time (CA3/CA3 or CA3/CA1). The cross-correlation was computed in 1s segments of the continuous data and a lag time of -100 to +100 ms was explored. The computed cross-correlation matrix was normalized to the global maximum correlation index between the two signals. This analysis revealed that there was a

strong interaction between CA1/CA3 and local CA3/CA3 recording sites during the pre-ictal epoch (Fig. 3.6). This interaction occurred during the same time period when increasing ripple and FR1 power amplitudes were observed ($\approx$20-30 s.) prior to seizure onset.

We next determined whether the power spectral make up of epileptiform and ictal discharges followed a trend either over the course of a single episode or between episodes. Table 3.1 shows a summary of the repeated measures ANOVA analysis for all 35 episodes as computed for 12 discharges before and after seizure initiation (i.e. peri-ictally). The summed amplitude spectrum for all four bands was not different for discharges across different episodes (Table 3.1). This suggests that no significant changes in the frequency content of pre-ictal and ictal discharges were seen across successive SLEs. However, when the trend across successive discharges was examined during the pre-ictal epoch leading up to each seizure (by collapsing the data across episodes), the amplitude of ripple and FR1 bands were found to be significantly different, on average, from one discharge to the next (ANOVA; $p = 0.006$ and $p = 0.004$, respectively); this was not observed for the low frequency band ($p = 0.2$). Trend analysis showed a linear increase in the power spectral amplitudes corresponding to the low frequency band (0-100 Hz, $p = 0.05$) as well as both ripple and FR1 bands over time ($p = 0.01$ for both). This robust increase, with discharge number, is shown in Figure 3.7A for all 35 pre-seizure recordings. It is intriguing to note that while different episodes exhibited different numbers of EDs, the absolute power amplitude in each band remained in proportion to the mean power at that discharge number. For example, although 75% of the pre-seizure recordings exhibited 15 discharges or less (inset, Fig. 3.7A), discharges close to the pre-ictal period had elevated low frequency power amplitudes (0-100 Hz) in accordance to the trend observed in episodes that had up to 30 EDs (note that SEM values remain fairly constant over the range of discharges).

Analysis of ictal discharges did not show any significant increasing or decreasing trends either across discharges in a single seizure or across seizures in successive episodes (Fig. 3.7B and Table 3.1). However, ripple and FR1 comprised a dominant component of the power spectral amplitude during the initial phase of the seizure but fluctuated over its course (Fig. 3.7B, left). The accumulation of power amplitudes in these bands can also be visualized in an alternative manner (Fig. 3.7B, right).

For pre-ictal activity (Fig. 3.7A, right) the normalized (mean) cumulative sum for each band showed that ripple and FR1 bands gain more of their amplitude during the last few discharges before SLE onset (corresponding to $\approx$20 s pre-ictally). Comparatively, the start of the SLE (Fig. 3.7B, right) was characterized by a comparable increase across all four spectral bands with close superposition of the cumulative power amplitude curves for each band. No statistically significant differences were observed between the power spectral trends computed for recordings obtained from CA1 vs. CA3 pyramidal cell layers ($p \geq 0.9$, t-test).

3.4.2 Temporal and Spatial Attributes of HFOs in the EEG of Patients with Limbic Epilepsy

Patient Characteristics. Seven patients (mean age 35 ± 7 yrs; 4 females) participated in the study and a total of nineteen seizures were recorded with continuous fast-sampling EEG (Table 3.2). Each patient underwent extensive clinical workup in our Comprehensive Epilepsy Program leading to their intracranial monitoring. All patients ultimately underwent surgical resection of the putative seizure focus. The patients studied were diverse and included those with both unilateral and bilateral seizure foci. Specifically, three patients had a clear right-sided focus (Pt. 4, 5, and 7), one had a clear left-sided focus (Pt. 1), two had ictal onset zones in either hemisphere (Pt. 2 and 3), and one had left-sided seizure onset with rapid spread of the right (Pt. 6). All seizures but one (Pt. 6, seizure type 2) originated from the temporal lobe.

Two patients had normal MR scans that showed mild gliosis on pathological examination of resected tissue (Pts. 2 and 4), two others had the same diagnosis with radiological findings (Pts. 5 and 6), two had hippocampal sclerosis (Pts. 1 and 7), and one had a dysembryoplastic neuroepithelial tumor (Pt. 3). Patient 7 exhibited non-specific white matter changes in the right temporal and both frontal lobes. EEG was recorded using either depth macroelectrodes, subdural grids/strip electrodes, or a combination of electrodes. Specific use of electrode types and their locations are summarized in Table 3.2.

Spatial Localization of HFOs. Fast-sampling EEG (at 5 kHz) adequately captured HFOs that were clearly evident on conventional review of the EEG recording (Fig. 3.3A). HFOs were identified in all recordings from each patient, regardless of electrode type (Fig. 3.3A

strip electrode, Fig. 3.4A depth electrode). We used time-frequency analysis to explore two aspects of HFOs: 1) spatial aspects pertaining to the location of HFOs relative to the ictal onset zone (based on conventional review of the EEG) and 2) temporal evolution of HFOs during the transition between interictal/pre-ictal activity to full-blown seizure onset.

Figure 3.3B shows the time frequency representation for the seizure shown in Figure 3.3A. It can be seen that HFOs with a dominant frequency component of $\approx$120 Hz were apparent starting 1 sec prior to seizure onset as well as during the first several seconds of the seizure, after which, slower spiking activity predominates (0 - 40 Hz, Fig 3.3B). In the context of spatial localization, we examined HFO changes in the immediate 5 s pre- and post- electrographic onset time for each channel (Fig 3.3C). It was observed that the greatest increase in ictal HFOs corresponded to the channel of primary electrographic seizure onset, based on conventional review of the EEG.

The spatial distribution of HFO changes for all patients is shown in Figure 3.8A. For all patients, the greatest ictal increase (positive R-value) in HFOs, specifically in the 100-200 Hz band, occurred in the channel where ictal onset occurred based on conventional review of the EEG. In general, HFOs were localized to a single electrode in patients with well defined seizure foci (Pts. 1,2, and 4) and were more widely distributed in cases where multiple contacts were placed over an extended seizure focus (see contacts over lesion in Pt. 3). A similar effect was seen for patient 7, who had a single seizure with onset over two contacts that also showed increased HFOs over the same electrodes.

Pre-ictal elevations in HFO power are shown negative R-values and were also seen in some cases, such as patient 6 (left-sided seizure). Another patient with interesting HFO changes was patient 2 who exhibited independent seizures from the left and right side. This patient's typical clinical seizures were felt to be originating from the left side based on review of the VEM data. The right-sided seizures were of less clinical importance based on prior video monitoring evidence. This individual ultimately received resective surgery to remove the left seizure focus and is now seizure-free. Intriguingly, during right-sided seizure onsets, the contacts that exhibited the greatest ictal change in HFOs for the left sided seizures now showed the greatest pre-ictal (negative R values) increase in HFOs. It should be noted that while increases in all

frequency bands were observed at the seizure focus, the greatest relative increases were seen in the HFOs (100-500 Hz).

Varying numbers of seizures were recorded for the different patients (range 1-4 seizures) which limited statistical analysis on an individual basis (i.e. in-patient analysis). Therefore, statistics were performed only on the pooled results. We obtained mean power amplitude values for each frequency band, for three different channels: the channel of electrographic seizure onset, the immediately adjacent channel, and a distant non-involved channel. We computed t-tests for all permutations across bands for each channel (i.e. origin 0-100 Hz vs origin 100-200 Hz, etc) and between the bands for different contact locations (origin 100-200 Hz vs. distant 100-200 Hz, etc.). Statistically significant differences were observed only for ripple (100-200 Hz, $p \leq 0.05$) and a subset of FR bands (300-400 Hz $p \leq 0.001$; 400-500 Hz $p \leq 0.05$) when the onset channel was compared to a distant one (Fig. 3.8B). In other words, the peri-ictal changes only occurred in the ripple and FR bands predominately at the channel of seizure onset, suggesting that only HFOs and not conventional low-frequencies localize to the region of primary ictal genesis.

Temporal HFO Changes. Since it appeared that HFO power amplitude increases were maximal at the channel of primary ictal onset, we next evaluated the time course of HFO changes for each band in this channel. Using a sliding computation of the *R*-value (see methods Section 3.3), we performed a "running power" calculation of summed power amplitudes for each band and seizure onset channel for 2 s epochs (Fig. 3.4A and 3.4). Temporal analysis was performed for 30 min of EEG recording preceding the electrographic seizure onset and no significant, reliable, or repeatable increases in HFO power amplitude until about 30 s before seizure onset. This observation is consistent with the fact that brain dynamics are stationary on the order of seconds [349], and thus, at present, there are no good non-stationary quantifiers that can be accurate over the course of tens of minutes to hours [242]. All data segments processed were free of artifact; in the case of Pt. 3 the recording associated with one event had to be discarded and is not included in the total seizure count or analysis.

In nearly all patients we observed increases in HFO power amplitude including the low frequency band (0-100 Hz) approximately 5 to 10 s preceding seizure onset (Fig. 3.9A). However,
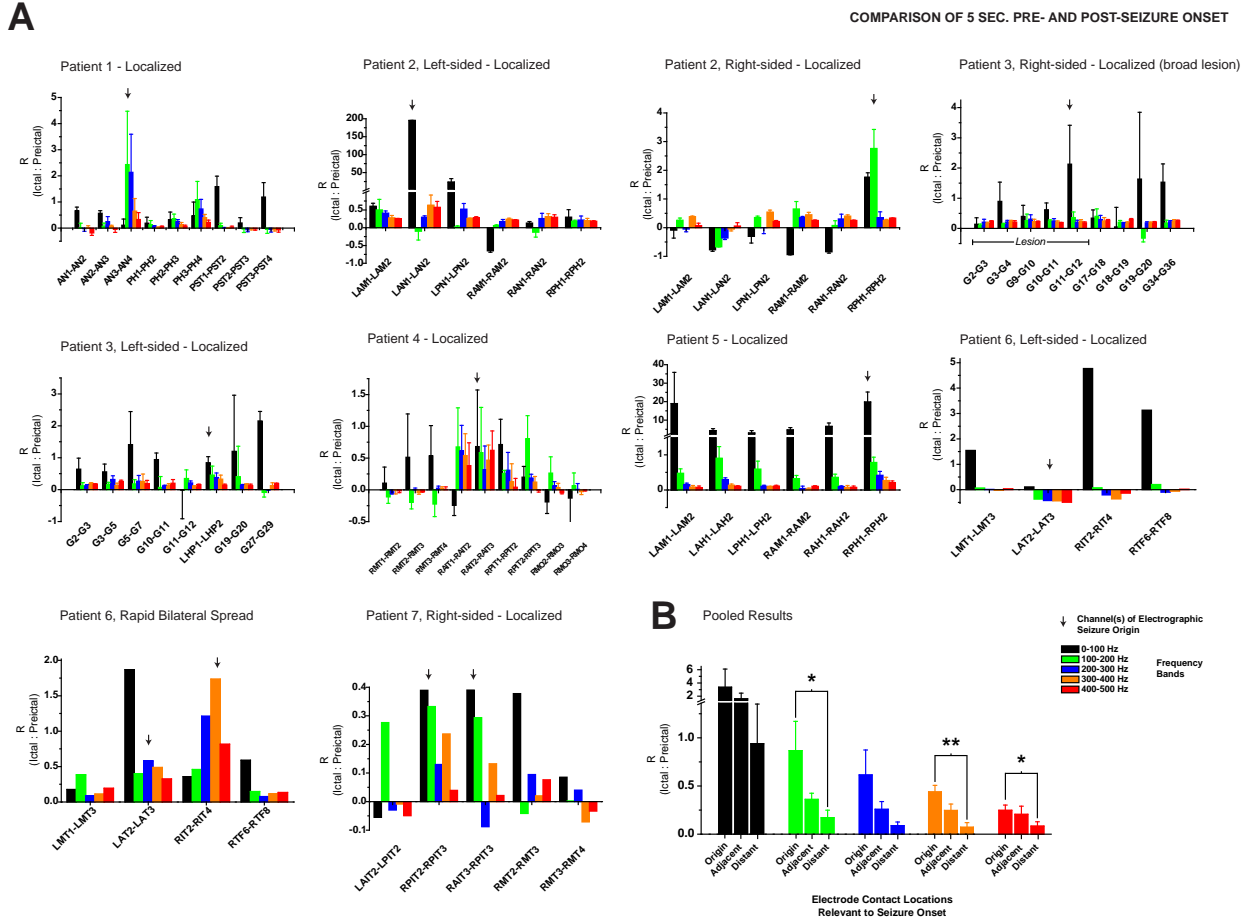
Figure 3.8: Spatial distribution of HFOs in the pre-ictal and early ictal periods for all patients. **(A)** Relative power ratio for each patient for each channel. When more than one seizure focus was recorded in a patient, the seizures were grouped and analyzed separately. The greatest increases in R values were typically observed in the channel of ictal onset (shown by arrows). **(B)** Pooled data for all patients for all seizures. R values were compared using an ANOVA analysis for each channel location across bands, and t-test analysis between permutations of channel locations within each band. Significant differences were seen for HFO power (100-200 and 400-500 Hz, $p \leq 0.05$; 300-400 Hz, $p \leq 0.001$) at the seizure focus compared to a distant channel.

the sharpest increase typically occurred for HFO bands (Fig. 3.9A). Figure 3.9B summarizes the pooled temporal analysis data from all patients and seizures. Statistical analysis was performed at each time point (i.e. -30 to 0 sec, with zero being electrographic seizure onset), within each band, between the three spatial designations (i.e. origin, adjacent, and distant). It can be seen that all HFO bands (100-500 Hz) in the origin and adjacent channels showed pre-ictal increases in power, whereas the power in the 0-100 Hz band increased later (Fig. 3.9B, left and centre column). The time points that achieved statistical significance was for the 100-200 Hz band, only for approximately 8 s prior to seizure onset, and when compared to a distant contact (Fig 3.9B, $p \leq 0.05$). This marked difference can be appreciated by looking at the raw magnitudes of the *R*-values for the distant channel, which are close to an order of magnitude smaller than those computed for the onset and adjacent channels.

3.5   Discussion

3.5.1   Pre-ictal HFO Changes: Findings from an *in vitro* Seizure Model and its Relation to Human Epilepsy

We investigated the temporal dynamics of HFOs *in vitro* and observed distinct changes in ripple and FR activity during the transition (pre-ictal) to seizure onset. We have shown that the spectral composition of epileptiform discharges changes, increasing in a time-dependant manner, leading up to seizure onset. This increasing linear trend in power spectral amplitude was statistically significant for low frequencies (0-100 Hz, $p = 0.05$) as well as for ripple (100-200 Hz) and FR1 (200-300 Hz) frequency bands ($p = 0.01$, n = 35). The pre-ictal period was consistently observed to exhibit strong differences in relation to discharge number, gaining power spectral amplitude towards the time of seizure onset in ripple and FR1 frequency bands ($p = 0.006$ and $p = 0.004$ respectively). No such increase (or decrease) was observed during ictal activity or when pre-seizure and seizure discharges were compared across successive seizure episodes ($p \geq 0.3$). Furthermore, no trends were observed for any of the frequency bands during the early phase of interictal activity ($p \geq 0.5$, n = 30).

The specific association of FRs with abnormal (epileptiform) activity has been explored in
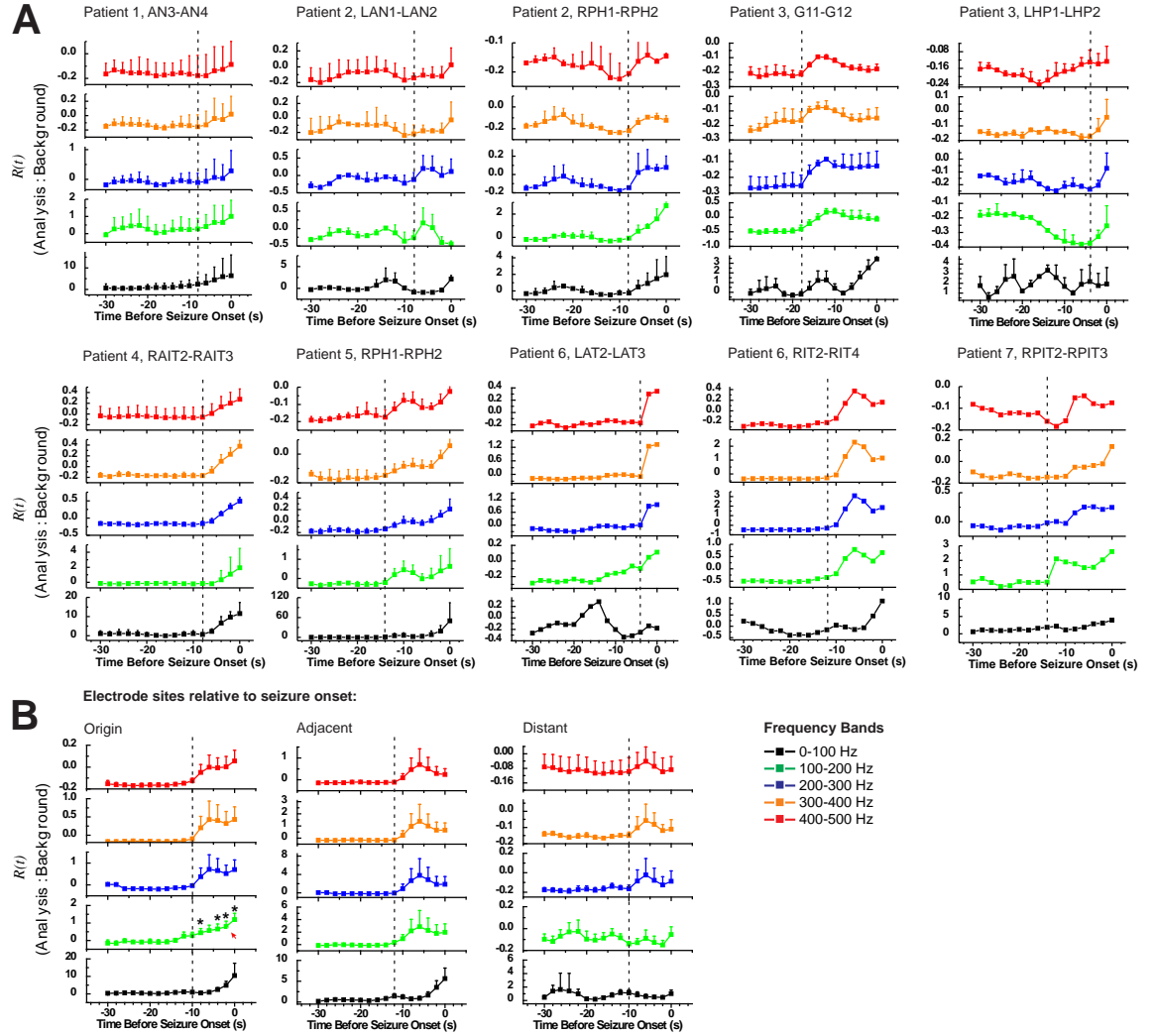
Figure 3.9: Temporal trends in HFO power in the pre-ictal period for all patients. **(A)** The relative power ratio changes over time [$\bar{R}_{(f,c)}(t_i)$] for the ictal onset channels for 30 s leading up to seizure onset (mean $\pm$ SEM). In each case, the power amplitudes for all bands increased just prior to seizure onset (vertical dashed line). However, the HFO bands ($\geq$ 100 Hz) repeatedly exhibited a sharp and consistent increase during that epoch, that often preceded the any low frequency changes (see Pts. 2; 3, grid electrodes G11-G12; 5, for example). **(B)** Pooled data for relative power ratio changes over time (mean $\pm$ SEM) for all patients, for each band, for the three different channels: ictal onset channel, immediately adjacent channel, and a distant uninvolved channel. Significant changes were seen for the 100-200 Hz band for 8 s prior to seizure onset, when compared to a distant contact (see arrow, left panel, asterisk denote $p \leq$ 0.05).

both rodents and humans. Evidence from previous studies suggests that FRs are restricted to areas adjacent to lesioned kainic acid injection sites *in vivo* [25], and occur more frequently ipsilateral to seizure-onset regions in epileptic patients [24, 31, 315]. Specifically, FRs have been found in association with epileptic brain tissue in humans with mesial temporal lobe epilepsy [24], with and without hippocampal atrophy [314], and also in the entorhinal cortex [31]. These findings may reflect the presence of pathologically interconnected clusters of neurons that are active well before the manifestation of spontaneous behavioural seizures [30].

The findings presented here are most consistent with the notion that HFOs occur during interictal activity. Furthermore, it was demonstrated that although low frequency activity (0-100 Hz) increases linearly towards the time of seizure onset, it is the transient and sharp increase in ripple and fast ripples (of 100-300 Hz) that is a characteristic feature of the transition to the ictal state in this model of recurrent seizures (Fig. 3.5b and c). Examination of temporal correlations between different spatial sites (e.g. CA3/CA3 or CA3/CA1) recorded within the slice during epileptic activity revealed strong interactions that take place preictally ($\approx$20 s before seizure onset), which match the time epoch during which increases in HFO activity were observed (Fig. 3.6). This interaction may be interpreted as synchronization processes common to both phenomena. However, it should be noted that cross-correlation analyses identify a relation between signals but do not necessarily provide information about the local timing of that interaction. In other words, these findings suggest that signals are strongly correlated on the order of a lag equal to τ = 10-25 ms (Fig. 3.6). However, we cannot directly relate this to the time-scale in which the cellular elements participating in ripple/fast ripple activity are acting to result in putative neuronal synchronization during the pre-ictal period. Indeed, HFO activity is believed to be a local phenomenon [30], and as such, to properly address the local time-scale of synchronization between individual neurons high impedance multi-site recordings are required (e.g. using silicon-based multi-electrode arrays).

Patient-based studies have described HFOs during interictal activity in the range of 80-500 Hz with the majority of discharges exhibiting oscillations at 100 Hz (ripple) and 250 Hz (FR), and with 90% of FR activity occurring within 186-392 Hz [30, 315]. We have observed HFOs over a similar frequency range except that the power amplitude of frequencies above 400 Hz

were approximately twenty times smaller and did not exhibit detectable temporal trends upon statistical analyses. However, we acknowledge the challenge of relating *in vitro* experimental findings to findings in epileptic patients. Clinically, resection of parahippocampal structures (e.g. entorhinal cortex, subiculum), which are also believed to be involved in FR generation, is correlated with improved seizure control [1, 302]. This implies that neuronal networks involved in HFO generation are both localized to and extend beyond the hippocampus proper.

Two previous *in vitro* studies have observed pre-ictal changes in HFOs. One study used extracellular recordings in areas CA1, CA3, and the dentate gyrus in rat hippocampal slices exposed to either high potassium or 4-aminopyridine [106]. The classical Fourier transform technique was used to analyze EDs for four minutes leading up to a seizure and a gradual rise in low frequency (2-40 Hz) and FR (200-400 Hz) activity was seen in some slices, but variability of this effect was reported as large. Another study used a zero-magnesium model of recurrent seizures and performed extracellular and intracellular voltage and current clamp recordings of CA3 pyramidal cells [187]. Two large spectral bands spanning 50-400 Hz and 400-800 Hz were analyzed using a wavelet technique and quantified using a power-like quantity - "HFO energy". A progressive increase in HFO energy was observed in 400-800 Hz restricted to the immediate transition epoch to seizure onset, although not reported as statistically significant. However, they noted an increasing component with dominant frequencies at 100 and 300 Hz for several discharges preceding seizure onset. Therefore, although reported as not statistically significant, the increasing trends observed in these studies are consistent with the increases we have described. Notably, the aforementioned studies revealed trends in different HFO frequency components prior to seizure onset. We likely obtained statistical significance due to the fact that we used narrower frequency bands for analysis, thereby increasing statistical power. Another factor might be that the previous studies used different chemical manipulations to provoke seizures (i.e. zero Mg^{+2}, high K^+, and 4-aminopyridine versus low Mg^{+2}), in addition to differences in the age of animals (such as younger animals between P9-13).

The mechanisms underlying ripples and FRs are incompletely understood. Under nonepileptic conditions, recordings in the CA1 layer of the hippocampus in behaving and anesthetized rats have implicated dynamic network interactions involving interneurons and pyra-

midal cells as possible causes for ripples [383]. Blockage of excitatory (glutamatergic) and inhibitory ($GABA_A$) synaptic transmission can also modulate HFOs in both normal and epileptic conditions [215, 106]. It has been shown that, in the neocortices of cats, rapid spiking from sub-populations of neuronal networks can cause ripples, which can be associated with seizure initiation [132, 133]. Another study showed that high frequency (200-800 Hz) activity was present in extracellular recordings and that this activity correlated with fast components present in voltage-clamp currents in CA3 neurons, during the transition from interictal to ictal activity, in hippocampal slices exposed to zero magnesium [187]. This suggests that high frequency inputs onto pyramidal neurons contribute to HFO activity in the zero magnesium model of epilepsy. They reported that actual pyramidal cell firing rates never reached such high frequencies as that detected extracellularly or in intracellular voltage clamp recordings. This raises the possibility that anti- and othrodromic axonal firing may also be involved [138].

Synchronization via gap junctions is also implicated in the generation of HFOs in normal and epileptic conditions. Studies using hippocampal slices suggest that inter-neuronal electrical coupling, in the form of axonal connectivity, is required for HFOs [338, 337]. A reduction in spontaneous sharp waves and ripple oscillations in connexin-36 mice has also been reported [214], implicating gap junctions in ripple generation [102]. In addition, halothane and other gap junctional blockers such as carbenoxolone are known to have inhibitory effects on both ripples and FRs [383, 76, 251]. Taken together, these data suggest that both synaptic and non-synaptic mechanisms participate in dynamic alterations in synchronous inputs onto and in between pyramidal neurons in the hippocampus during the transition to ictal activity.

The fact that pyramidal cell firing rates do not reach FR frequencies suggests that temporal and spatially dynamic interactions in epileptic neuronal networks, or interneuronal firing activity per se, are important mechanisms underlying fast oscillations. When recorded extracellularly, these modalities of communication combine to form complex, but analyzable, waveforms. Based on the link between FR oscillations and an underlying epileptic condition, characterization of HFOs may contribute to the understanding of dynamics present in epileptic neuronal networks [207]. Robust detection and visualization of high frequency oscillations may also provide insights towards localization of epileptic foci and aid in the detection of

characteristic electrophysiological changes that precede seizures.

3.5.2 HFOs as Localizing Markers of the Ictal Onset Zone in Patients with Temporal Lobe Epilepsy

In this patient-based study, we tested the feasibility of recording HFOs (ranging from 100-500 Hz) using commercially available depth and subdural grid electrodes coupled with fast EEG sampling at 5 kHz. We further investigated the spatial and temporal nature of HFOs with special consideration given to the time of seizure onset and to the transition from pre-ictal-to-ictal activity. The main findings of this study are three fold. Firstly, this study is the first to demonstrate that HFOs can reliably be recorded using commercially available intracranial depth electrodes (Fig. 3.3). Second, we demonstrated that seizure onset is characterized by focal increases in HFOs that are localized to the ictal onset zone (Fig. 3.8B). Indeed, the more focal electrographic seizures were associated with more localized HFO changes (Fig. 3.8A). Third, we observed that HFO power amplitudes increase in the pre-ictal period (i.e. ≈ 10 seconds prior to seizure onset (Fig. 3.9B).

HFO Recordings with Commercial Electrodes. The finding that HFOs can be recorded using commercially available depth electrodes is in agreement with a recent study by Jirsch et al. [162] who reported similar observations with their in-house macro-depth electrodes. We also show that HFOs ≥ 200 Hz can be recorded using commercially-available subdural grid electrodes. This work also confirms previous observations that HFOs from 100-200 Hz can be recorded using commercially available grid electrodes [4, 5, 253]. Collectively, these data suggest that HFO generators may span larger than previously believed spatial domains. Nonetheless, it is also acknowledged that micro-electrode recordings have specific advantages such as a greater sensitivity towards HFOs due to their finer spatial sampling [27, 31, 58].

Spatial Localization of HFOs. HFO were observed with greatest prominence in the channel of primary ictal onset (Figs. 3.8A and B). Moreover, the number of involved electrode contacts was proportional to the size of the ictal generator; in other words, the larger the ictal generation, the greater the number of contacts showing ≥ 100 Hz activity. For example, patients with focal unilateral seizures (e.g. Pt. 1 and 4) showed a more localized area of HFO

changes compared to those patients with more diffuse brain abnormalities (e.g. Pt. 3 and 7). This observation was confirmed even in the same patient when seizure activity was observed in both hemispheres with a short delay due to rapid spread (Pt. 6). Such a correlation was observed by Jirsch et al. [162] who did not observe significant HFO content in the EEG of patients with poor seizure localization. These findings suggest that HFOs are generated by local, pathologically altered clusters of neurons that operate within larger neuronal networks, and HFOs may play a role or be direct markers of seizure genesis [30]. Furthermore, the localized nature of HFO changes suggests that their presence can be a useful tool in the demarcation of onset zones for tailored surgical resections. Indeed, in this small series of patients, all except patient 6 became seizure-free after resective surgery ($\approx$ 6 month follow-up). This patient was unique in that HFOs were of greatest magnitude in the side opposite to surgical resection (Figure 3.8A). This may therefore suggest that HFO analysis may also be useful in identifying the side of greater seizure-susceptibility in patients with bilateral forms of epilepsy. However, further prospective studies based on long-term surgical outcomes with more patients are needed to properly assess the utility of HFOs in this capacity.

Temporal HFO changes and the Pre-ictal State. We have shown that HFOs undergo measurable and robust increases in the immediate pre-ictal epoch that are specific to the ictal onset zone (Fig. 3.9B). Thus, HFOs can undergo temporal changes in power that signify a pre-ictal alteration in the brain state that may signify the transition between states, such as from interictal to ictal rhythms.

The cellular and network parameters that govern HFO dynamics in the pre-ictal period remain unclear. Nonetheless, it is possible to speculate on some potential mechanisms. Studies of *in vitro* seizure models suggest that seizure precursors may begin locally as a series of rhythmic discharges. As the discharges become more frequent, adjacent or distant projection sites become recruited, increasing the amount of energy and heralding oncoming seizures [106]. Moreover, there exists a precedence for locally enhanced synchrony in the generation of ictal activity that is clearly different when considering distant contacts; even in the case of generalized epilepsies [126]. At the neuronal level there is evidence that HFOs can be caused by alterations in excitatory, inhibitory, and gap-junctional communication (reviewed by Rampp

and Stefan [276]). An important point however is that individual cell firing rates cannot approach the full range of FR activity ($\approx \geq 300$ Hz) in either *in vitro* seizure models [187] or unit recordings in patients [157]. Thus, it has been postulated that field oscillatory rhythms, specifically ripples, arise from population activity from neurons that have variable firing rates and phases [36, 128]. It has also been suggested that formation of ripple, and presumably FR, population activity depends strongly on single cell membrane dynamics that are modulated by inhibitory and excitatory inputs. However, the synchrony of inhibitory cells seems to be a required parameter for the generation of faster field oscillations. Thus, one possible interpretation of HFOs appearing and increasing during the peri-ictal period involves dynamic and rapid changes in local network synchrony as modulated by inhibitory networks, which themselves are believed to be altered in the epileptic brain [67].

The pre-ictal state likely represents a fundamental process in epileptogensis [199]. Understanding how, where, and why this process occurs is of interest for several reasons. At present, HFOs appear to be excellent markers for localizing the ictal onset zone and thereby possess the potential of enhancing the delivery of current treatments such as surgical resection. Another reason to study HFOs is that they can be used, perhaps with other EEG quantifiers, to anticipate seizure onset in the range of tens of seconds. This, in turn, may help guide the location and timing of future therapeutic interventions such as on-demand deep brain stimulation or direct drug delivery devices. Finally, a better understanding of mechanisms underlying the interictal-ictal transition may unmask fundamental mechanisms that may help develop completely novel therapeutic strategies.

Conclusions. We have shown that HFOs can be recorded using commercially available depth and grid electrodes in patients with temporal lobe epilepsy. In addition, the spatial localization of HFOs in particular electrodes correlates with the ictal onset zone and potentially subsequent success of surgical resection. HFOs also undergo robust increases in power in the immediate pre-ictal period in the ictal onset zone. Overall, these findings suggest that HFOs may be markers of neuronal network activity that represent a fundamental precursor to seizure initiation.

Table 3.2: Demographic, imaging, electrophysiological, pathological, and clinical information on the seven patients studied. Square brackets denote the number of seizures recorded. Abbreviations: ant anterior, ATL anterior temporal lobectomy, DNET dysembryoplastic neuroepithelial tumor, F female, inf inferior, LAH left anterior hippocampus, LAM left amygdala, LPH left posterior hippocampus, LIO left inferior occipital, LMTG left middle temporal gyrus, LPF left posterior frontal, LPT left posterior temporal, post posterior, M male, RAH right anterior hippocampus, RAM right amygdala, RMO right mesial occipital, RMTG right middle temporal gyrus, RAM right amygdala, RMF right middle frontal, RPF right posterior frontal, RPH right posterior hippocampus, RPT right posterior temporal, RSO right superior occipital, RSTG right superior temporal gyrus, RTFP right temporal frontal parietal, SAH selective amygdalohippocampectomy, and SF seizure-free. Electrode nomenclature - DE depth electrode, SE strip electrode, GE grid electrode.

Patient	Age	Imaging	Electrodes	Interictal	Ictal	Pathology	Outcome
1	30/M	LA TL resection & HS	DE LAH LPH,LPT LIO	LAH, LPH	[4] LAH, LPH	Hipp. Sclerosis	L SAH, SF
2	28/M	Normal	DE LAM, LAH,LPH, RAH,RPH, RAM	Freqeunt LAP, LPH Less freq. RAH, RPH	[2] LAH [2] RPH	Mild gliosis	L SAH, SF
3	44/F	RMTG DNET	8x8 GE LAM, LAH,LPH, RAM,RAH RPH	freq. LAH, LPH Moderate RPT, RH	[3] RAH, RITG [2] LA	DNET	Lesion SAH SF
4	42/M	Normal	1x4 SE, RAM,RAH, RMTG,RMO, RSO	RAM, RH	[3] RAM, RH	Mild gliosis	R SAH SF
5	36/F	RH atrophy loss of structure	DE LAM, LAH,LPH, RAM,RAH, RPH	Very freq. RAM, RPH, Moderate LAM, LPH	[1] RAM, RH	Mild gliosis	R SAH SF
6	41/F	Prior SAH atrophy	1x8 grid LPF,RPF, RSTG 1x4 SE LAM,LAH, LMTG,RAH, RAM	freq. LAT Less Freq. LIT	[1] LAT [1] RAT, LFT	Mild gliosis	L ATL ongoing seizures
7	28/F	R temporal horn larger than left	1x8 SE LPF,RPF RMF 1x4 SE LAM,LAH, RAM,RAH RMTG	RAM, RH	[1] RAM, RH	HS	R ATL SF

Chapter 4

Prion Protein and its Effects on Neuronal Excitability as Mediated by the NMDA Receptor

4.1 Introduction: The Curious Link between NMDA Receptors and Endogenous Cellular Prion Protein

4.1.1 Preamble

This chapter describes results from a relatively recent set of experiments, carried out over the past 10 months, that have unraveled an interaction between the endogenous Prion protein (PrP) and the NMDA receptor. The experimental findings described (Section 4.3) evolved from a set of preliminary experiments, carried out in hippocampal slices that examined possible differences in endogenous excitability in the hippocampus of WT vs. PrP-null mice. We chose to engage in such a study based on data from a single *in vivo* report [358] that showed differences in seizure threshold between WT and PrP-null neurons. Their findings suggested that PrP ablation results in lower seizure threshold and greater mortality. The purpose of this study was to investigate putative differences in excitability at the synaptic level in order to identify target receptors that may be interacting with PrP. This study began with hippocampal slice recordings where we observed greater basal excitability in PrP-null mice. Experiments expanded to include recordings in neuronal cultures, where we observed increased NMDA receptor activity in the form of altered miniature excitatory postsynaptic currents. A slight decrease in GABAergic activity was also observed. Augmented NMDA receptor activity was observed also for evoked postsynaptic responses resulting in larger than WT inward currents with very prolonged deactivation kinetics; a similar increase in decay time was observed for miniature NMDA currents. As hypothesized, this increased NMDA activity resulted in a lower threshold for seizure-like activity (i.e. hyperexcitability) and was also manifested as increased susceptibility towards NMDA-mediated excitotoxicity. Taken together, these findings are in

support of a protective role for the endogenous PrP protein. Moreover, experimental findings seem to have identified a novel mode of excitotoxic-mediated neuronal death as related to prion proteins.

Given the previously unreported nature of these results and lack an established background literature linking NMDA receptor function with prion proteins, I will initially discuss these proteins separately with NMDA receptors in Section 4.1.2, followed by Prion proteins in Section 4.1.3. Based on the notion that these findings link synaptic activity with endogenous PrP function, I will then discuss the synaptically-relevant prion protein literature in Section 4.1.4 as the final component of the introduction to this chapter.

4.1.2 NMDA Receptors: Form and Function

4.1.2.1 Glutamate Receptors

In the mammalian brain glutamate is the primary molecule for fast excitatory neurotransmission. Glutamate and its receptors (collectively called the GluRs) are widely distributed in the brain and are critical to advanced brain functions such as learning and memory (in particular the NMDA receptor as will be discussed later). During synaptic transmission and/or associated processes, glutamate is released from the presynaptic terminal and can evoke a mixture of postsynaptic responses that are defined by two classes of glutamate receptors. The first grouping are the ionotropic glutamate receptors (iGluRs), which are ligand-gated channels with ion conducting pores that ultimately serve to depolarize the postsynaptic membrane. The second category of glutamate receptors are the metabotropic glutamate receptors or mGluRs. In contrast to the ionotropic glutamate receptors that support an ion conducting pore, the main purpose of mGluRs is to activate G proteins upon glutamate binding, which then go on to activate cascades of modulatory processes targeting other proteins such as K^+ and Ca^+2 channels. Based on the experimental findings linking the PrP^C protein with the NMDA receptor, I will focus exclusively on the ionotropic glutamate receptors and NMDA receptor subtypes for the remainder of the introduction section.

The postsynaptic response mediated by iGluRs can, in principle, be broken down to two components: the first kind of response is rapid (early component) and results in swift depolar-

ization and is also relatively fast to decay. The second type of response is slightly slower to activate (late component) and lasts longer. These two responses are intermixed and are the principal currents underlying excitatory postsynaptic potentials (EPSPs, or EPSCs [Currents when recorded in voltage-clamp]) and can be isolated using selective antagonists. The fast component is composed of AMPA and kainate receptors and are blocked by the antagonist CNQX (6-cyano-7-nitroquinoxaline-2,3-dione). AMPA receptors obtain their name from their potent agonist α-amino-3-hydroxy-5-methyl-4-isoxazole propionic acid (also known as quisqualate) and are built from four closely related subunits: GluR1, GluR2, GluR3, and GluR4, which exhibit approximately 70% homology (Fig. 4.1). A functional AMPA receptor is comprised of four subunits in a multimeric complex typically in a "dimer of dimers". Activation of AMPA receptors results in the influx of Na^+ and K^+ ions; it has been shown that these receptors are also permeable to Mg^{+2} and Ca^{+2} depending on their GluR subunit compositions. The second class of ionotropic glutamate receptors are the Kainate receptors, which obtain their name for a potent agonist effect for kainate. These receptors are categorized based on their affinity for the agonist, where GluR5, GluR6, and GluR7 exhibit lower affinity when compared with the KA1 and KA2 subtypes (Fig. 4.1). They form functional receptors in much the same way as AMPA receptors and NMDA receptors (as will be highlighted later).

Returning to the components of an EPSP, the late component is primarily due to the involvement of NMDA receptors, for it can be blocked by the agonist APV (2-amino-5-phosphonovaleric acid). NMDA receptors activate in response to glutamate and N-methyl-D-aspartate (an analog of glutamate). These receptors exhibit little homology (29%) with the rest of the glutamate receptors (Fig. 4.1). In order for a functional receptor to be assembled, two NR1 subunits are obligatory, which then co-assemble with two NR2 subunits in a heteromeric mix (see following sections for more details). The NR1 subunits contain the glycine binding site; glycine is a required co-factor for NMDA receptor activation. The same region that binds glycine in the NR1 receptors is homologous with the agonist binding site in the NR2 subunits.

4.1.2.2 Molecular Structure of NMDA Receptors

Molecular cloning has identified six types of NMDA receptors. Four of these (in a complex with the obligatory NR1 subunit): NR2A, NR2B, NR2C, and NR2D activate only in response
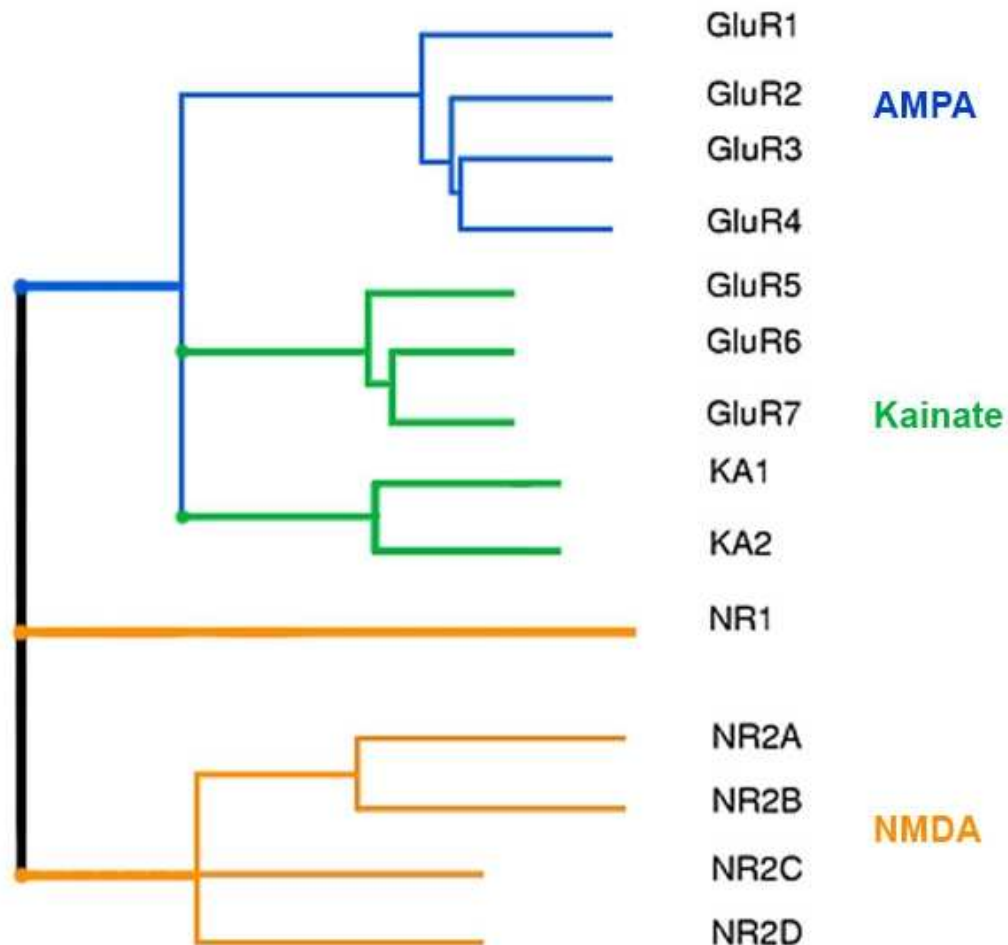
Figure 4.1: A schematic (modified dendrogram) of the members of the ionotropic glutamate receptors. In total, 16 (14 shown) cDNAs have been identified. Note the similarity in homology between the three types of glutamate receptors: AMPA, Kainate, and NMDA. Note that in the case of NMDA, the NR1 subunit is obligatory for the formation of a functional receptor, which comprises a heteromeric assembly of two NR1 subunits and two NR2 subunits. Also note that recently, NR3A and B subunits have also been identified but their activation (in a complex with two NR1 subunits) can occur with glycine (traditionally an inhibitory neurotransmitter) alone in the absence of glutamate or NMDA.

to glutamate or NMDA (Fig. 4.1); it is believed that NR1, NR2A, and NR2B are the pre-dominant subtypes in the CNS. In the case of these isoforms, a functional receptor consists of a heteromeric complex with two of the subtypes being the obligatory NR1 subunit (e.g. 2xNR1/2xNR2A). Recently, two other isoforms of the NMDA family have been identified: NR3A and NR3B. These two subtypes show closer homology to each other than to the NR2s and more so with the NR1 subunit. These subtypes can also co-assemble with other subtypes (e.g. NR1/NR2A/NR3A) but these channels show a five-fold reduction in calcium perme-ability as compared to more common assemblies such as NR1/NR2A. Moreover, NR3s can co-assemble exclusively with NR1s forming functional receptors that result in excitatory ac-tivity in response to glycine binding (traditionally an inhibitory neurotransmitter in the brain). These receptors do not activate in response to glutamate, are not affected by NMDA blockers such as APV, and do not exhibit Mg^{+2} block. Therefore, in the strict sense, as a glutamatergic ligand-gated channel, NR1/NR3 receptors do not seem to be prominent mediators of NMDA receptor currents in synapses.

All iGluR subunits share a common membrane topology at the structural level (see Section 4.2) with variations in sizes of N- or C-termini (e.g. NMDA has a large N-terminus) and also locations of alternate splicing sites. Moreover, as in the case of AMPA receptors, a process known as editing can occur, where a post-transcriptional change in the pre-mRNA can take place to allow for further functional diversity. As for the molecular structure, each subunit consists of three transmembrane domains termed TM1, TM3, and TM4. The region between TM1 and TM3 is referred to as M2 and is a re-entrant hairpin loop that does not cross the plasma membrane. When four subunits are co-assembled as a heteromer the M2 regions of each subunit face inwards to form the ion permeable pore of the receptor. The ligand binding region is located extracellularly on the loop between TM3 and TM4 but in reality the site is manifested in the three dimensional conformation by interactions between parts of the extracellular N-terminus and this loop region. The ligand binding site exclusively binds to glycine for the NR1 subunits and is modified in the NR2s for the binding of glutamate or NMDA (homologous sites). All iGluRs can undergo alternate splicing, which usually takes place in regions of the N- and C-termini but can also occur in a set of residues the vicinity of the ligand binding site.

For example, the NR1 obligatory subunit has eight known functional variants although their functional contribution to the co-assembled receptor remains unclear.
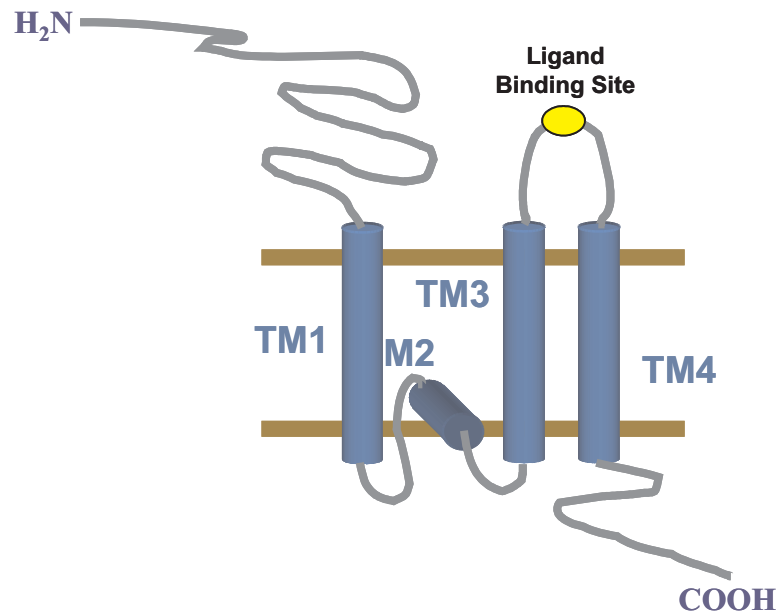
Figure 4.2: Membrane topology of a typical ionotropic glutamate subunit. Each subunit has three transmembrane segments (TM1,TM3, and TM4); the region between TM1 and TM3 is known as M2 and is a re-entrant hair pin structure that forms the ion-permeable pore of the receptor when the multimeric subunits are co-assembled in a complex.

4.1.2.3 Structural Basis of NMDA Function and Physiological Roles

NMDA receptors have a high unitary conductance in comparison to AMPA receptors; 40-50 pS as compared with ≈ 8 pS. NMDA receptors also have the property of being highly permeable to the divalent cation Ca^{+2} in addition to the monovalent cations such as Na^+ and K^+. Another unique property of the NMDA receptor is that it exhibits a voltage-dependent block by Mg^{+2}. Therefore, in the absence of a depolarization and in the presence of extracellular Mg^{+2} the receptor is blocked. Upon membrane depolarization, the Mg^{+2} ion which occupies a region in the pore becomes released by electrostatic repulsion and the channel becomes available for ion permeation. This attribute of the NMDA receptor is believed by some to be indicative of its role as a "molecular co-incidence detector" (i.e. such as an AND logic gate) since receptor activation is timed to when both pre- and postsynaptic cells are excited at the same time.

NMDA Subunit Composition. The functional properties of an NMDA receptor are closely

linked to the subtypes present in the heteromeric complex. In particular, the subtype of NR2 has the greatest influence on the attributes of the synaptic current. Findings from expression systems have investigated diheteromeric combinations of NR1/NR2 and have shown that deactivation rates are fastest for the NR2A, followed by NR2C, which is close to NR2B, and very slow for NR2D [353]. In fact, NR1/NR2D exhibits a very high affinity for glutamate and is typified by very prolonged rates of deactivation as manifested in time-constants as slow as 5 sec. Faster time-constants have been reported for receptors composed of NR1/NR2C and NR1/NR2B (similar in rates), with the fastest rates recorded for NR1/NR2A receptors [240, 75]. In addition to deactivation rates, the single channel conductance and Mg^{+2} block can be modulated by the combination of subunits that make up a functional receptor. The large unitary conductance referred to earlier is a property of receptors containing NR2A and NR2B, whereas smaller conductances ($\approx$ 30 pS) are associated with those containing NR2C and NR2D. We will also make brief mention of pharmacological differences that are subtype specific. As alluded to earlier, APV and its analog AP5 (2-amino-5-phosphonopentanoate) are potent competitive antagonists of the NMDA receptor resulting in efficient block. A compound known as MK-801 (Dizocilpine) is a non-competitive blocker. These blockers act on the receptor without significant differences based on subunit composition, although in the case of MK-801 greater block is observed for NR1/NR2A and NR1/NR2B diheteromeric receptors. Several other blockers also exist that have some capacity to block receptors based on their subunit composition, however, with the exception of Ifenprodil, many of the other blockers are not well characterized. Ifenprodil is highly effective in blocking glutamate or NMDA binding with the NR2B receptor, although a small amount of block is also observed for receptors containing other subtypes (reviewed in [74]); Ifenprodil is by far the best characterized NMDA subtype blocker.

Receptor Assembly. Proper NMDA receptor function relies on appropriate receptor assembly, trafficking, and surface expression. There is some evidence to suggest that NR1 and NR2 receptors play different roles with regards to receptor trafficking. The NR1/NR2x (x denoting a wildcard of NR2 subtypes) can co-assemble before leaving the endoplasmic reticulum (ER), and NR1 in particular is believed to play an important role in ensuring further processing past

the ER. Different splice variants of the NR1 have also been reported to selectively target the assembled receptor to different cellular compartments (e.g. soma) consistent with the obligatory requirement of the NR1 subunit for receptor function since NR2A or B subunits cannot target to the membrane without NR1. However, the converse is true for NR1 alone. The role of the NR2 subunits in trafficking takes place during the final stages of targeting to the membrane (i.e. post-ER) and is believe to involve interactions with several postsynaptic proteins (such as postsynaptic density 95, PSD95).

The NMDA receptor composition, with respect to subtypes of NR2, is expectedly different for cells involved in different pathways and anatomical networks. In addition, as suggested by diversity in the trafficking mechanisms, differential expression also takes place at the level of individual neurons. These alterations occur over a background of developmental changes that result in different NR2 subunits being expressed. The following developmental expression patterns come from experiments performed in rodents using techniques such as in situ hybridization, pharmacology, and kinetic studies of evoked glutamate/NMDA currents. At present thorough NMDA subtype distribution studies using antibodies for assessing protein expression during development are very few in number.

Subtype-specific Developmental Patterns of Expression. During embryonic development NR2B is found in many brain regions as is NR2D, which is believed to be more localized to regions such as the brain stem and diencephalon. It should be noted that NR2D can co-assemble in either a dimer-dimer NR1/NR2D configuration or in a heteromeric complex with NR1 and NR2A or NR2B. Immunoprecipitation studies suggest that most of the NR2D subunits are in complexes with NR1 [105]. NR2D mRNA has also been detected in a subpopulation of CA1 and CA3 hippocampal neurons, although identification of their specific cell type remains undiscerned. NR2D expression is believed to begin diminishing from its peak expression at approximately seven days of life. After birth, at approximately three days of life, NR2A is found in most regions, replacing NR2B in abundance; NR2C also begins to appear in selected brain regions. As would be expected, the switch from NR2B to NR2A manifests as kinetic changes in synaptic EPSCs that have faster kinetics and receptor currents that exhibit lower sensitivity towards Ifenprodil block. However, caution is warranted against generalizations for

subunit expression patterns with development. A layer of complexity is added by the distinction between synaptic and extra-synaptic NMDA receptors. For example, even though a NR2B to NR2A switch can take place at central synapses, extra-synaptic contacts may be spared from this switch; these differences are undoubtedly cell-type specific in nature. In the hippocampus, CA1 pyramidal cells express mRNA for three kinds of subunits NR2A, NR2B, and NR2D ([295] adult humans, and [178, 154] in juvenile rats). The subunit composition of synaptic and extra-synaptic NMDA receptors in adult hippocampal neurons is different: synaptic receptors are composed predominantly of NR2A and also NR2B receptors, whereas extra-synaptic receptors are believed to contain mostly NR2B (Tovar and Westbrook, 1999). NR2D receptors are believed to be exclusively extra-synaptic [237, 74, 74]. The claim that NR1/NR2D (or a multimeric form containing NR2D) receptors are extra-synaptic is supported by the absence of slow kinetic time constants in recorded synaptic responses such as mini-EPSCs in any cell that has previously been shown to exhibit high transcript levels for NR2D. It is appreciated that transcript level may not always correspond to protein levels, however the alternative explanation that is commonly adopted is that recombinant NR2D kinetics are somehow different from the native neuronal form. However, recently a report by Misra et al. [234], using $\approx$ P8 rat cerebellar Purkinje neurons, believed to predominantly express NR1/NR2D at this developmental age, showed that evoked glutamate currents exhibit very slow deactivation kinetics that are consistent with the findings from recombinant NR2D experiments. Their findings have rekindled the debate about the presence of NR2D at central synapses, which still has not been demonstrated. Moreover, immunohistochemical data on NR2D localization is sparse and not well validated. However a recent immunohistochemical study in the adult murine hippocampus observed some overlap between NR2D staining and those of NR1, NR2A, and NR2B (NR2C was not observed) suggesting that some tetrameric assembly may take place in hippocampal pyramidal neurons [334]. The most intense NR2D staining was localized to the oriens layer of CA1, *stratum lucidum* layer of CA3 (areas just superficial to the pyramidal cell layers in CA1 and CA3), and portions of the dentate gyrus cellular layer. Their placement is suggestive, perhaps, of a functional role in the activity of GABAergic interneurons in addition to a subpopulation of pyramidal neurons, which localizes them to both pre- and postsynaptic con-

tacts of pyramidal neurons. Overall, there is no functional evidence that NR2D subunits are targeted to synaptic sites, although the most plausible scenario may be NR2D placement in heterotetrameric assemblies with other NR2s. However the formation of heterotetrameric NMDA complex remains to be demonstrated in vivo. The presence of NR2D during early pre- and postnatal development in combination with its high affinity for NMDA, has been suggested by some, to be indicative of a role in synapse formation [234] and/or regulation of burst-mode firing [344] although these claims require experimental validation.

NMDA Receptors and Synaptic Plasticity. The most commonly known role of NMDA receptors is their involvement in synaptic plasticity. In particular, for their role in long-term potentiation (LTP). LTP is believed to mostly reflect a strengthening of the postsynaptic response, caused by a brief period of hyperexcitability that releases large amounts of glutamate such as during brief tetanic stimulation. The effects of the ensuing potentiation can last over a period of min. to hrs (*in vitro*) and up to days in some experiments (*in vivo*). The potentiating mechanisms underlying LTP are believed to be the dominant model of activity-dependent synaptic plasticity. LTP is best characterized and understood in the hippocampus.

It was realized quickly that strengthening of postsynaptic responses must involve some sort of postsynaptic modifications such as positive receptor modulation via intracellular protein or signalling pathways, or increased receptor density. However it was unclear if the shear depolarizing strength of the initial conditioning stimulus (i.e. brief tetanic stimulation) was responsible or whether other factors were at play. It was shown that application of APV during tetanic stimulation blocked the induction of LTP; therefore, both strong depolarization and the action of the NMDA receptors are required. Moreover, mice lacking NMDA receptors in CA1 neurons had impaired LTP and could not perform well in spatial memory tasks [343]. The ensuing calcium influx due to NMDA receptor activation triggers several cell signalling pathways that ultimately result in post- and presynaptic modifications that serve to potentiate the response; these alterations have an early and late component of manifestation; for late component LTP several conditioning stimuli are required. Examples of early changes include alterations in probability of transmitter release, whereas late changes can result in changes such as postsynaptic AMPA receptor insertion and even formation of new synapses [167]. Indeed,

many elegant studies have looked at the NMDA dependence of LTP induction but cannot be comprehensively reviewed here (for a review see [167]).

A synaptic depotentiation process also exists that results in the opposite effects of LTP; this process is known as long-term depression or LTD that also has an NMDA-dependent component. In contrast to brief tetanic stimulation, as is used in the induction of LTP, establishing LTD requires low frequency stimulation (e.g. 1 Hz for 15 min). Successful and repeatable induction of LTD depends on the parameters used for the conditioning stimulus and more importantly on the age of the animal. In juvenile animals ($\approx P12 \leq P21$) a low frequency protocol is effective and the mechanism of LTD is believed to depend on the activity of NMDA receptors. In older animals, the conditioning protocol has to be modified to include paired-pulses; in this case AMPA receptors in addition to mGluRs are believed to be responsible for the synaptic depotentiation - we will return to this point later.

It is believed that different subtypes of NMDA may be differentially associated with facilitating LTP and/or LTD induction. In particular, it was recently shown by Liu and colleagues that LTP is mediated by NR2A subunits whereas LTD is mediated by NR2B [200]. Given that NR2B subunits are maximally expressed in neonatal animals, the involvement of NR2B in LTD was attributed towards explaining the difficulty of establishing LTD in older animals using the same protocols that seem to work effectively in younger animals. However, the findings of Liu and colleagues have come under significant scrutiny as other groups have not been able to replicate their work [241]. Moreover, a recent *in vivo* study found that a clear distinction between the roles of these subunits (NR2A in LTP and NR2B in LTD) are not mutually exclusive. Nonetheless, it is clear that both NR2A and NR2B are key mediators of alterations in synaptic plasticity with perhaps a greater NR2B contribution in LTD.

NMDA Receptors and Excitotoxicity. The term excitotoxicity refers to excessive activation of excitatory neurotransmitter receptors that ultimately lead to neuronal cell death. The specific cell death caused by the amino acid glutamate is the key factor in neuronal death in many diseases and disorders. In particular, excessive accumulation of intracellular calcium, resulting in alteration of cellular calcium homeostasis, is the prime causal process that leads to excitotoxic cell death. The NMDA receptor has been implicated as the main glutamatergic

receptor due to its high permeability to calcium. AMPA and kainate receptors are not believed to be major players in glutamate-mediated excitotoxicity due to their rapid desensitization and low calcium permeability. However, permeability to calcium is highly dependent on receptor subunit composition and thus there may be instances where these receptor channels are involved in excitotoxicity.

Excessive excitatory transmitter release, such as during a state of continuous clinical convulsive seizure activity (referred to as *status epilepticus*), can result in overactivation of NMDA receptors. This results in excessive calcium influx into neurons and such hyper-release of transmitter can also overload some of the regulatory processes that clear glutamate (via uptake and breakdown) from the synapse, further contributing to prolonged NMDA receptor activation. In a related scenario, brain ischemia causes elevated glutamate levels in the extracellular space due to altered function of glutamate transporter activity [34]. Elevated or prolonged glutamate (both at the synapse and extracellular space) results in hyper-activation of both synaptic and extrasynaptic receptors. Specifically, calcium influx via the NMDA ionotropic glutamate receptor (with much smaller contributions from AMPA and kainate receptors) has been implicated as the primary cause of calcium-mediated excitotoxicity. Moreover, the sustained depolarization caused by excessive NMDA receptor activity can contribute to the activation of voltage-gated calcium channels that further contribute to an increased calcium influx; although the NMDA contribution remains a key mediator of cell death [361]. Abnormally elevated intracellular calcium levels trigger intracellular cascades including activation of calcium-dependent enzymes, such as phosphatases (e.g. calcineurin), proteases (calpains), and lipases that ultimately result in cell death. Another key toxicity pathway involves the action of increased intracellular calcium on mitochondrial calcium loading, which results in depolarization of the mitochondria that is know to be a parallel indicator of cell death by disrupting ATP synthesis pathways (i.e. electron transport chain). Dysfunction of the electron transport chain results in the production of reactive oxygen species (free radicals). In addition to the formation of hydrogen peroxide another toxic species, peroxynitrite, is formed by the combination of a molecular oxygen radical and nitric oxide. Nitric oxide (NO) production is part of this pathway where NMDA receptors activate neuronal nitric oxide synthase (nNOS). The presence of NO may be a requirement for

mitochondrial depolarization [361]. The importance of nNOS is supported by a key study that showed interruption of PSD-95, the mediator protein between nNOS and the NMDA receptor, leads to attenuated NMDA-mediated neuronal death [292]. In addition, mitochondrial calcium uptake can promote the release of pro-apoptotic factors such as cytochrome c and subsequent activation of caspases [361, 375].

It should be noted that the precise role of NMDA receptors, in particular, in the context of synaptic vs. extra-synaptic receptors is not well understood. There are two competing hypotheses on the mechanisms of NMDA-mediated excitotoxicity [375]: (1) source specificity, and (2) calcium load. The first maintains that calcium entry through one source (e.g. extra-synaptic NR2B containing receptors) over another (e.g. NR2A containing receptors) facilitates particular excitotoxic pathways. In this hypothesis, the NR2A receptors participate mainly in plasticity-related physiological functions (as do NR2Bs [121, 241]), but that the primary source of excitotoxic calcium entry is mediated by NR2B containing receptors. However, experimental evidence for a clear dissociation between the roles of NR2A and NR2B is lacking. For example, in expression systems, NR1/NR2A transfected cells exhibit greater excitotoxic cell death as compared with those transfected with NR1/NR2B. Whereas, in cultured cortical neurons, it is only the extra-synaptic NMDA receptors (presumably of NR1/NR2B composition) that are mediators of excitotoxic cell death [293]. Intriguingly, *in vivo* nNOS expression is maximal in neurons selectively expressing NR2D (believed to be extra-synaptic) such as in the cerebral cortex and a subpopulation of hippocampal neurons [240, 334, 361]. Nonetheless, some degree of caution is warranted when interpreting the results of NMDA-mediated excitotoxicity in the context of synaptic vs. extra-synaptic receptors since it is experimentally challenging to separate these components (even *in vitro*), and it is often the case that both NR2A and NR2B receptors participate in tandem [332]. The second hypothesis (calcium load), suggests that it is the elevated concentration of intracellular calcium (regardless of source) that is responsible for triggering excitotoxicity. From the discussion of NMDA-mediated cell death, it is clear that many of the same intracellular pro-apoptotic pathways would be triggered by an intracellular increase in calcium concentration. However, it should be noted that equivalent calcium entry via pathways such as voltage-gated calcium channels are not or are significantly

less associated with neuronal cell death. Most probably, attributes of both hypotheses are in play during the course of glutamate-mediated excitotoxic neuronal death.

4.1.3 Physiology and Pathophysiology of Prion Proteins

4.1.3.1 A Brief History of Prion Protein Discovery

The path leading to the discovery of Prion proteins (PrP) would have been made easier through the now commonly used molecular biological techniques. However, at the time of their discovery such methodologies were not well established, which lead to years of controversy and disbelief about their existence and mode of transmission. We now know that prion proteins represent yet another change to the dogma of molecular biology where a proteinaceous agent (lacking nucleic acid) exhibits transmissible (infectious) properties. The first documented reference to prion proteins comes from the work of Carleton Gajdusek in the 1950s, where he was studying a fatal neurodegenerative disease in Fore tribes of New Guinea called Kuru [13, 125]. The Kuru was known to be transmissible amongst members of the tribe and believed to be associated with their cannibalistic rituals. The Kuru was at the time believed to be a slow-acting virus, however several investigators had begun to make a connection between Kuru and other protracted neurological diseases such as scrapie (in sheep), and Creutzfeldt-Jakob disease (CJD, in humans). Subsequent work by Gajdusek showed that Kuru could be transmitted to animals, similar to scrapie and CJD, thereby linking these neurodegenerative disorders [13]. However, the nature of the transmissible entity remained elusive. Work continued to be carried on this topic by a small number of groups around the world and progress was slow due to the prolonged incubation time (years) required for the manifestation of the disease; it was later shown that in hamsters $\approx$ 150 days was sufficient thereby aiding scientific studies. Studies showed that the infectious agent displayed unique properties such as resistance to compounds that normally damage nucleic acids. Moreover, analysis of brain homogenates consistently showed the presence of an unknown glycoprotein [13]. The suggestion that the infectious agent was "proteinaceous particle lacking nucleic acid", was put forth by Stanley Prusiner in 1982 [271, 13].

4.1.3.2 Molecular Structure, Expression of PrP variants, and Infectivity of Altered PrP Forms

Many of the puzzling attributes of the cellular prion protein (PrP^C) became better understood with the finding that the prion protein was actually encoded by an endogenous gene in the uninfected CNS. The prion protein gene contains 253 codons and is located entirely within a single exon [13]. This gene is ubiquitously expressed in many different tissues and organs with maximal expression in the central nervous system. It was discovered that the infectious form of the protein, denoted PrP^{Sc} (Sc for scrapie), represented a misfolded version of the endogenous protein where a portion of the α-helical and coil structures are refolded into β-sheets (PrP^C 40% α very little β; PrP^{Sc} 30% α 45% β) [272]. This conformational change of the endogenous PrP^C protein is accompanied by a wide spectrum of pathophysiological changes that defined the disease state. Unlike PrP^C, the PrP^{Sc} form is not soluble in denaturing agents and is only partially digested by proteases that are capable of fully digesting the native form. This attribute of PrP^{Sc} facilitates the formation of PrP-rich plaques that are observed in histological examination of the affected neural tissues. Although a large body of evidence supports the notion of a misfolded prion protein as the infectious agent, many prion researchers still caution that it is within the realm of possibility that the infection can be due to some small ligand bound to the PrP^{Sc}; this cautionary statement is most probably triggered by the unusual nature of a proteinaceous infectious agent. Before we discuss further the nature of PrP^{Sc} and its role in neurodegeneration, we will explore the complex biosynthesis, trafficking, and degradation pathways of the endogenous prion protein and its several bioactive molecular species.

There are four topologically distinct bioactive forms of PrP and it is postulated that each form mediates a specific physiological function that is also carried forward to the disease state, albeit in altered form, where it contributes to or can even hinder the pathophysiology of PrP (Fig. 4.3). Translated PrP amino acid sequence (polypeptide chain, visualized with ribosomal complex, entering the endoplasmic reticulm) results in a cytosolic form of prion protein ^{Cy}PrP. This cytosolic form can arise by two pathways: either via an aborted translocation to the endoplasmic reticulum (ER), or retrotranslocation from the ER without further process-

ing (purple, Fig. 4.3). The most abundant cellular form of prion protein is referred to as the secretory form of ^{Sec}PrP (blue, Fig. 4.3). This form is fully translocated into the ER lumen where it undergoes a C-terminal cleaving of a hydrophobic domain and the addition of a gly-cosylphosphatidylinositol (GPI) anchor. It is then translocated from the ER to the Golgi where it undergoes further modifications such as alterations to the glycans and the GPI-anchor; this process dramatically increases the diversity of molecular species for PrP. It is estimated that upwards of 80% of PrP in cells is in ^{Sec}PrP form and it is either secreted into the extracellular space [143, 13] or (mostly) expressed on the membrane surface; for this reason it is called cellular prion protein PrP^C. The second most studied form of prion protein is the transmembrane form called ^{Ctm}PrP (red, Fig. 4.3), where a highly conserved and hydrophobic region of PrP is transmembrane to the ER lumen. ^{Ctm}PrP is C-terminally GPI-anchored with its N-terminus residing in the cytosol. Another, less well understood, form of prion protein is also transmembrane across the ER. This ^{Ntm}PrP form of PrP is oriented in the opposite direction of ^{Ctm}PrP, with the C-terminus now being cytosolic (brown, Fig. 4.3). It also does not undergo any detectable alterations in ER, such as the addition of a GPI-anchor. The transmembrane region corresponds to the same region in the ^{Ctm}PrP, mainly the central hydrophobic domain within the prion protein.

As pointed to earlier, there are two primary modes of acquiring the infection PrP^{Sc} form. The first is via direct transmission of the infectious protein, commonly via ingestion of the affected nervous tissue. The second mode of acquiring the prion disease state involves mutations in the PrP gene that result in misfolding of the endogenous PrP^C to PrP^{Sc}. This mode of transmission is suggestive of a mechanism underlying the familial form of neurodegenerative diseases such as CJD [272]. There are also well documented cases of sporadic prion disease, which as believed to be caused by de novo mutations in the prion gene [13, 272]. Therefore the current framework of infectivity requires that the host organism acquire PrP^{Sc}, either exogenously or by a spontaneous conversion from PrP^C, thereby triggering a cascade of pathophysiological processes that result in the conversion of more and more PrP^C to the scrapie form; the spectrum of disorders associated with this disease process are collectively known as the transmissible spongiform encephalopathies (TSEs). During the relatively long incubation
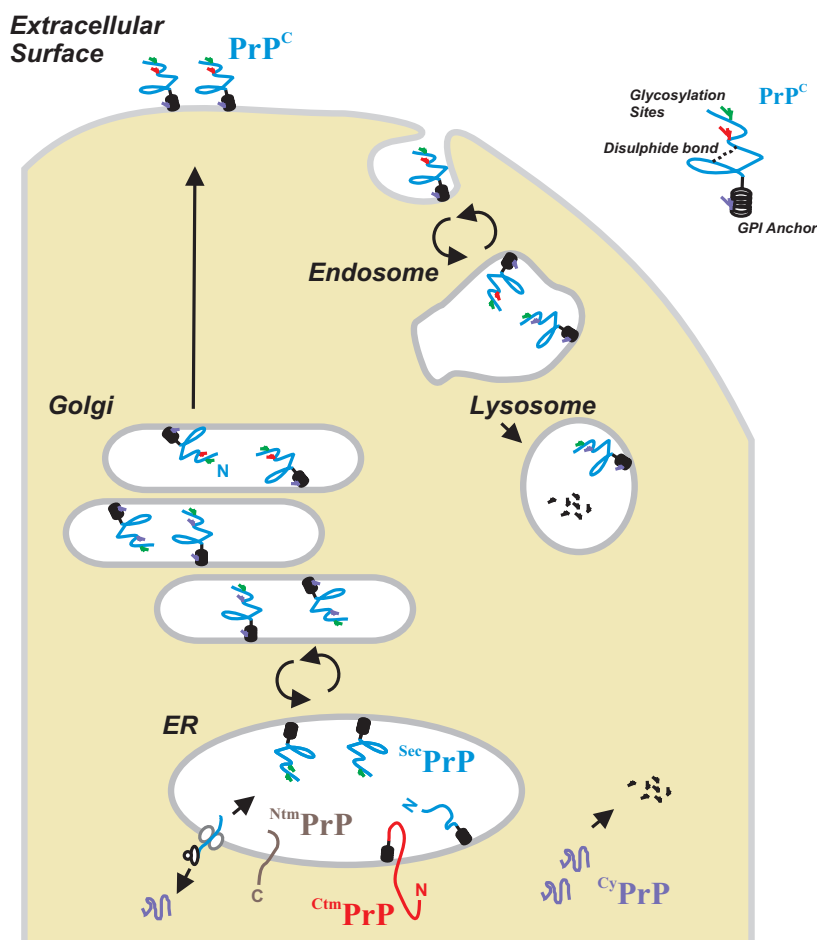
Figure 4.3: Synthesis, post-translational modification, trafficking, and degradation of native prion protein. The products of PrP biosynthesis result in multiple molecular forms, each with different putative functional roles in physiology and pathophysiology. There are four distinct forms: (1) ^{Cy}PrP (purple) cytosolic PrP formed either via aborted translocation to the ER or retrograde translocation from the ER. (2) ^{Sec}PrP (blue) Secretory PrP is the most common form of PrP, which undergoes ER translocation and post-translational modification in the ER (addition of glycosylphosphatidylinositol (GPI) anchor) with subsequent processing in the Golgi prior to trafficking to the membrane. Given that this is the most common and abundant form of PrP it is referred to as cellular prion protein PrP^C. Cell surface PrP^C undergoes degradation via endocytosis and trafficking into the endosomal-lysosomal pathway. (3) The second most well studied form of prion protein is the transmembrane form, ^{Ctm}PrP (red), where it spans the ER membrane at a highly conserved central hydrophobic region with the C-terminus anchored in the ER. The level of ^{Ctm}PrP correlates with the level of neurodegeneration in prion-associated diseases. (4) Another transmembrane form is the ^{Ntm}PrP (brown) which does not undergo GPI-anchor addition, glycosylation, or further processing. The physiological significance of ^{Ntm}PrP remains unclear. (inset, top right-hand corner) Anatomy of PrP^C showing the large coiled N-terminus with a single disulphide bond, in addition to two main glycosylation sites and the GPI-anchor. This figure was adapted from the work of Chakrabarti and Hegde on PrP synthesis and trafficking as described in Chapter in 18 of Ref. [13].

period of prion disease, the PrP^{Sc} form of the protein begins to accumulate in affected tissues, forming deposits in the brain that result in cellular and network dysfunction. Neuronal death is a large component of TSEs, reaching culmination at the late-stages of the disease [13]. These mentioned forms of disease acquisition, transmission, and progression are validated by three key experimentally verified observations: (1) PrP-null mice are immune to infection, (2) the course of the disease tracks the accumulation rate and amount of PrP^{Sc}, and (3) in the case of inherited diseases caused by PrP mutations, accumulation of PrP^{Sc} was readily observed and transmissible to other host animals. It should be noted that in patients affected with CJD, there have been some cases where PrP^{Sc} accumulation has not been observed. This fact is consistent with the experimental observation that certain PrP mutants lead to neurodegeneration but do not result in the accumulation of PrP^{Sc} [13]. Another interesting attribute of prion diseases is that the PrP^{Sc} is in itself not sufficient for neurodegeneration unless the endogenous PrP^{C} is present. This notion is supported by grafting experiments where brain grafts from PrP-WT mice were transplanted into PrP-null mice. Upon incubation with PrP^{Sc}, only the grafted tissue (from WT mouse) began to accumulate PrP^{Sc} while surrounding cells did not show any sign of infection even in the presence of high concentrations of PrP^{Sc} [144].

In addition to the PrP^{Sc} form, several studies have shown a link between the ^{Ctm}PrP form of prion protein and neurodegeneration. Analysis of both naturally occurring and artificial mutations in PrP, have implicated the transmembrane hydrophobic region of ^{Ctm}PrP as critical to regulating the amount of ^{Ctm}PrP produced. This is significant due to the fact that the amount of ^{Ctm}PrP synthesized correlates with susceptibility for neurodegeneration; this was experimentally validated in infected animals but also via transfection experiments in PrP-null mice. In the most severe case, a 10-20% fraction of expression (i.e. ^{Ctm}PrP : all PrP forms) resulted in neurodegeneration within the first two months of life. To further exemplify the role of ^{Ctm}PrP in the disease state, even a 2-5% fraction of expression resulted in neurodegeneration after 18 months of life [13, 144].

The role of the other two PrP forms in neurodegenerative processes remains unclear. In the case of ^{Ntm}PrP there are no identified links to the disease state and investigators have as of yet to propose a putative mechanism for its involvement. In contrast, greater attention has

recently been focused on the cytosolic form (^{Cy}PrP) of prion protein. As alluded to earlier, the ^{Cy}PrP form of PrP may be generated due to abnormalities in its signal sequence, which interferes with its proper translocation to the ER. This idea is supported by the observation that ^{Cy}PrP levels are dramatically decreased if the translocation signal sequence of PrP is replaced with another more efficient signal sequence from another protein. The consequence of decreased ^{Cy}PrP is a decrease in PrP^{Sc} aggregates, and thus a putative protective effect against neurodegeneration. However, there have been reports of increased pathogenicity in cases where ^{Cy}PrP concentration has been made to be excessively high [13]. Thus, at present, it would be correct to state that the true functional roles of ^{Cy}PrP and ^{Ctm}PrP in physiological function and disease conditions remain to be fully investigated.

Several key observations support the hypothesis that the role of PrP in TSEs extends beyond the transmissibility of PrP^{Sc} and that the other bioactive forms of PrP interact in a complex manner to bring about and modulate the disease state. The finding that PrP^{Sc} does not accumulate or alter surrounding normal tissue in a host animal suggests that although it is central to disease transmission, it is neither sufficient or necessary to cause the full-blown neurodegeneration observed in the TSEs. In other words, the presence of PrP^{Sc} is not in itself inherently neurotoxic or sufficient to trigger neuronal death. This is further supported by the observation that neurodegeneration can take place in the absence of PrP^{Sc} accumulation. These findings, together with the positive disease progression correlated with ^{Ctm}PrP strongly suggest that neuronal death in the disease state involves a complex interplay between the different bioactive forms of PrP, in addition to modulation of their synthesis, trafficking, and degradation.

4.1.4 Prion Protein Function

Realization that the prion disease was linked to a misfolded endogenous protein led to greater understanding of the pathophysiology of PrP and its relation to neurodegeneration. However, the number of studies that focus on the role of PrP^{Sc} in the disease state far out number those focused on understanding and describing the normal functional role of PrP^{C} [32]. Indeed, after fifteen years of research very little is understood about how this remarkable and diverse protein species functions within the overall dynamics governing neuronal activity. We will now discuss

the regional localization of PrP in the brain, its cellular localization, and functional properties relevant to synaptic structures and direct effects on transmission.

4.1.4.1 PrP Localization

As mentioned previously, PrP is expressed in almost every cell type and has been found in many species including: most vertebrates, many mammals, many avian species, and even in some amphibians [32]. Immunohistological studies in rodents have shown that native PrP (i.e. PrP^C) can exhibit strong expression patterns in brain structures such as the hippocampus (most intense) and ventral striatum. Intense staining is also observed in the entorhinal cortex and neocortex, with prevalent staining in layer 1 following the contour of the cortical surface [244]. Some of these staining patterns have also been confirmed in human tissues for structures such as the hippocampus and striatum [287]. At the cellular level, strong immunostaining is commonly observed in neuropiles and has been shown to co-localize with presynaptic proteins such as synaptophysin [119]. These observations in addition to a single functional study have prompted some investigators to imply that PrP is expressed predominantly on the presynaptic side. A study by Herms and colleagues utilized wild-type, PrP-null, and two forms of transgenic mice (Tg20 and Tg35) to show functional evidence for presynaptic localization of PrP [146]. Tg35 mice express PrP^C in all neurons, while Tg20 mice express PrP^C in all neurons except cerebellar Purkinje cells. Using brief hydrogen peroxide application, they showed that the frequency of spontaneous inhibitory postsynaptic currents (IPSCs) was still altered for Purkinje cells in Tg20 mice; in addition, high concentrations of PrP were found in synaptosomes. Their findings are the only functional study attempting to discern a difference between pre- vs. postsynaptically localized PrP. However, these findings must be interpreted with some caution since electron microscope studies using gold labeling [119], in conjunction with immunohistochemical findings [244, 287] have not been able to convincingly demonstrate a pre- vs. postsynaptic localization. Moreover, the immunohistochemical studies show strong staining in the *stratum oriens* and *stratum moleculare* regions of the hippocampus, that clearly are full of both presynaptic and postsynaptic contacts [244].

4.1.4.2 PrP Copper Binding

Although the precise physiological role of PrP remains unknown, cloning and subsequent molecular biological experiments have determined that the cellular prion protein possesses four highly conserved octarepeat (eight amino acids repeated) sequences that have been shown to bind four copper ions [272, 352]. Copper is released into the synaptic cleft during neurotransmitter vesicle release and at the synaptic level, copper concentration has been related to the presence of PrP^C. Synaptosomes isolated from PrP-null mice exhibit a $\approx 50\%$ decrease in copper concentration [146]. It was at first concluded that this decrease was too great to be solely due to less bound copper (to PrP), and that PrP might participate in copper metabolism. However, it was demonstrated that copper, at physiological concentrations, is not affected in the form of uptake by prion protein [352]. Moreover, the total copper content in brain lysates did not differ between WT and PrP-null mice. The precise role of PrP in relation to copper remains unclear, however the most likely hypothesis suggest that PrP^C participates in some form of copper buffering and restoration of copper back to the presynaptic terminals (e.g. during endocytosis). Another role involving PrP and its ability to bind copper involves protection against oxidation. In most cells superoxide dismutase (SOD) catalyzes the breakdown of the superoxide radical to water and hydrogen peroxide and copper is a key cofactor for this enzyme's function. Indeed, neuronal cultures from PrP-null mice were more sensitive to oxidative stress and cell death [352]. More studies are required to better define the role of the endogenous prion protein and its relation to cellular copper homeostasis and potential protective effects against oxidative insults.

4.1.4.3 PrP and the Synapse: Novel Roles in Plasticity and Excitability

As we have mentioned previously, the precise physiological role of the endogenous PrP^C remains unknown and much of the previous studies have focussed on the involvement of the PrP^{Sc} form and in some disease context. Nonetheless, there are several studies that suggest a link between PrP and synaptic transmission and/or plasticity. It is important to note at the start that this sub-field (arguably the most important) of prion protein research is controversial due to different findings having been reported by different research groups [272]. However, differences can be due to experimental conditions and variability between the animal models used.

Indeed, much of the research into the physiological roles of PrP utilize knockout (KO) animals and there are five different KO variants [364]. Three of these variants (Nagasaki, Rcm0, and Zürich II) exhibit gene deletion that spans slightly beyond the exon coding region for PrP. Consequently, these mice exhibit attributes such as severe ataxia and cerebellar cell loss [364]. The two other KO mice, Zürich I and Edinburgh are limited to the proper exon coding region, with the latter being the most commonly used KO mice. This KO mouse strain exhibits normal reproduction, development, and behaviour [38], but does show alterations in sleep rhythms. Specifically, the Zürich I mice show greater sleep architecture fragmentation and increases in the frequency of short waking episodes [335]. The Zürich I KO mouse [38] is used in this study and unless mentioned otherwise, the word "PrP-null" or "KO mouse" will be used to refer to this mouse.

Due to the controversy surrounding the role of PrP in synaptic transmission we will review the literature relevant to plasticity in somewhat of a chronological order. I will focus on studies that assess the induction and level of LTP, in addition to those that investigate the role of PrP in hyperexcitable seizure models.

Network-level Alterations. The first report assaying hippocampal network function was published by Collinge et al. who investigated the functional role of PrP in synaptic transmission and compared WT with PrP-null mice [64]. Extracellular CA1 hippocampal field recordings (afferent stimulation) in PrP-null mice showed an altered field response with the presence of additional population spikes; this was greater than the typical singlet observed in this well established synaptic pathway. Intracellular sharp recordings showed the presence of multiple spikes (more than WT) with a lack of a hyperpolarizing IPSP (inhibitory postsynaptic potential). When examined in isolation in KO mice, evoked IPSPs exhibited smaller amplitudes and slower rise and decay times; the decreased amplitude was persistent over a large range of membrane holding potentials. These findings are consistent with impairment of $GABA_A$ (specifically fast GABAergic) activity. Induction of LTP was examined and was found to be impaired in PrP-null mice (regardless of $GABA_A$ block or not). The typical time course of LTP changes was not different between WT and KO mice. The authors also suggested that there were no differences in pharmacologically isolated NMDA currents, although no data

were shown. Nonetheless, they attributed their diminished LTP findings to lower GABAergic activity that somehow abnormally enhanced NMDA receptor function, and that this abnormal NMDA activation is causal to poor LTP induction. Overall, the study by Collinge et al. supports postsynaptic alterations in PrP-null mice [64]. These effects on LTP were confirmed by Manson and colleagues, using the Edinburgh KO mouse [219]. They showed that in addition to decreased LTP, the time course of recovery to baseline synaptic activity was faster in the KO mice; this is more consistent with a short-term change in plasticity. Conversely, the effects of PrP KO on synaptic transmission were brought into question by Lledo and colleagues, who failed to find any alteration of inhibitory or excitatory synaptic transmission, and also found no differences in LTP induction [204]. Experimental differences between this and the original study by Collinge et al. [64] included age of animals ($\approx$ 3 vs. 8 months old) and temperature (35°C vs. room temperature); temperature is known to affect LTP induction [372].

Several other studies have investigated synaptic plasticity in the hippocampus. The purpose of these studies has been to attempt to resolve the controversy surrounding the initial studies. Carleton and colleagues examined plasticity in CA1 hippocampal neurons using WT (i.e. $PrP^{+/+}$), two strains of PrP KO (Zürich I and Nagasaki), and transgene mice created on $PrP^{+/+}$ and $PrP^{-/-}$ backgrounds [45]. In the case of PrP transgenic mice on a $PrP^{+/+}$ background, the PrP expression was approximately 8-fold greater than WT. Intriguingly, synaptic strength was observed to increase in a dose-dependent manner with expression of PrP regardless of the strain or background. A dependence on age was observed however with maximal effect observed in younger animals (6 months) and no effect for older animals (10-14 months). Presynaptic probability of transmitter release was assessed by monitoring paired-pulse facilitation and was found to be not different amongst any of the animal types, suggesting a postsynaptic mechanism for the observed potentiating effects of PrP expression. Unfortunately, a subsequent study by Curtis and colleagues further complicated interpretation of previous results [79]. The authors compared both the Zürich I and Edinburgh KO mice to WT and each other at several different ages and found no differences in hippocampal synaptic transmission (*in vitro* and *in vivo*), specifically LTP induction, although some deterioration was observed in mice older than $\approx$ 8 months. The authors postulated that, in part, the observed differences

between earlier studies and theirs could be a result of alterations in oxidative stress (based on PrP copper buffering), that may be tolerated differently by the mice strains and/or during tissue preparation [79]. Paired-pulse facilitation was again not found to be altered. In yet another study, spatial and non-spatial learning was examined in adult ($\approx$ 5 month old) PrP-null mice and deficits were observed in spatial learning, which could be rescued in the transgenic animal expressing PrP in $PrP^{-/-}$ background [71]. The authors also investigated *in vivo* induction of LTP in the dentate gyrus and found it to be impaired, along with paired pulse facilitation, in the KO animal. The topic of LTP induction was revisited by Maglio et al. [213] who examined LTP induction in the dentate gyrus in 3-4 month old animals, comparing WT with Zürich I KO mice. Using a gradually increasing (in frequency) conditioning pulse, these authors reported a lower threshold for the generation of LTP in KO mice; this is consistent with a hyperexcitable state. Moreover, KO animals exhibited lower sensitivity towards NMDA blockers (both APV and MK-801). In situ hybridization was used to show greater transcript levels for NR2A and NR2B in KO mice, once again suggesting an augmented glutamatergic synaptic transmission in KO mice. Similar observations (i.e. lower threshold for LTP and increased NR2A/NR2B transcript levels) were also reproduced in a later study by the same group [212]. Interestingly, a study examining the effect of PrP^{Sc} disease-related processes on glutamatergic neurotransmission reported decreased MK-801 binding in the hippocampus suggesting alteration of NMDA receptor activity of unknown origin [93]. This observation, together with a report that MK-801 can protect against glutamate-mediated excitotoxicity in PrP^{Sc} infected neuronal cultures [245], suggests a direct involvement of NMDA receptors in the pathophysiology of PrP.

Cellular-level Alterations. Intracellular recordings in adult PrP KO CA1 hippocampal neurons have shown a dramatic reduction (near loss) of the slow after-hyperpolarizing current (AHP, a Ca^{+2} activated K^{+} current) [62], which is known to modulate the pattern of neuronal firing by altering spike frequency adaptation. In this case, loss of the AHP would be consistent with hyperexcitability. The loss of the slow AHP component was also recently investigated using a conditional KO of PrP, at 10 weeks of life, in order to assess the possible influence of secondary effects of the embryonic KO of PrP on the observed effects. The loss of AHP currents was also confirmed in this conditional KO mouse suggesting that the observed effects are

due to loss of a differentiated cellular function and not a developmental effect of the KO [216]. The authors speculate that the observed effects may have a link to the newly reported signal transduction role for PrP, perhaps via tyrosine kinase Fyn [243], that modulates the activity of Ca^{+2}-dependent K^+ currents.

A structural study of the hippocampus in PrP KO mice showed aberrant mossy fiber connections, referred to as Mossy fiber sprouting, a condition commonly observed in epileptic neural networks in rodent kindling studies and in some patients with TLE [63, 270]. Intriguingly the authors did not detect any differences between WT and KO field responses evoked *via* perforant path stimulation; this was attributed to some compensatory changes that may have taken place to counteract the pro-seizure effects of mossy fiber sprouting. The cause and mechanism for the observed sprouting remain unclear. However, a series of recent findings utilizing recombinant PrP show an interaction of PrP with NCAM (neuronal cell adhesion molecule), facilitating its localization to lipid rafts where it interacts with Fyn kinase, thereby facilitating neurite outgrowth, synapse formation, and possibly development of neuronal polarity [297, 290, 166]; some of these functional effects are akin to the role of a neuronal growth factor. Interestingly however, in experiments where neuronal cultures were incubated (1-2 days) with recombinant PrP, effects such as neurite outgrowth, increased synaptic contacts, and polarity determination were not dependent on the neuronal substrate used for experimentation (i.e. WT or KO PrP neurons) [166]. A similar lack of dependency on substrate was observed in the context of neurite outgrowth and cell survival when neurons were plated onto a PrP-Fc coated (PrP in fusion with Fc portion of human IgG) vs.Fc-coated surface [53]. These observations suggest that the neurite growth-related properties of PrP are restricted to the secreted form and do not depend strongly on the presence or absence of the (GPI-anchored) membrane form. Development of neuronal polarity has not been linked, as of yet, to the described NCAM-mediated pathway.

Experimental findings such as altered AHP and $GABA_A$ currents [216, 62, 64], mossy fiber sprouting [63], and lower sensitivity to NMDA blockers [93] are all consistent with the notion that PrP-null mice exhibit a susceptibility towards hyperexcitability. For example, this would imply that threshold to seizure-like activity would also be lower in PrP-null mice. This hypothesis was examined and reported to be valid by comparing several *in vivo* models of

pharmacologically-induced seizures [358]. Walz et al. reported that in response to a single injection of pentylenetetrazol (PTZ, $GABA_A$ antagonist) KO mice exhibited 91% mortality due to seizures as compared with 33% in WT mice. Similar observations were reported for kainic acid (KA) induced seizures and KO animals once again exhibited a greater seizure occurrence and increased seizure-related mortality. In a very recent study by Rangel et al., the consequences of kainic acid induced seizures in the hippocampus of WT vs. PrP-null mice were examined using a combined *in vitro*/*in vivo* approach [278]. PrP-null mice were confirmed to be more sensitive to KA-induced seizures both *in vivo* and *in vitro*. In addition, greater excitotoxic-related neuronal death occurred in PrP-null mice and cultures. These observations were also duplicated with RNA interference experiments targeted against PrP in WT mice. RT-PCR analysis showed elevated basal levels of GluR6 and 7 in PrP-null mice, while all other AMPA/Kainate iGluR subunits were unaffected; it is believed that GluR6 in particular is involved in KA-mediated seizure threshold. Intriguingly, application of MK-801 reduced KA-induced cell death by up to 40%, suggesting that the susceptibility of PrP-null mice to excitotoxicity is also mediated by NMDA receptor activation.

4.2 Experimental Methods

4.2.1 Brain Slices

Adult male and female WT (C57BL/6J) and PrP-null (Zürich I [38]) mice between P30-P45 were used for all slice experiments. These mice were obtained from a specific set of six breeding pairs composed of $PrP^{+/-}$ male/female animals. Genotyping was performed by gel electrophoresis of PCR products obtained from genomic DNA obtained from tail samples from animals older than three weeks of life. Primers and PCR parameters were similar to those used by Büeler [38]. Comparisons were made between electrophysiological recordings obtained from offspring pups from the original breeding pairs or from offspring obtained from WTxWT or KOxKO crosses. The results were indistinguishable (n >20 in each case). Similarly, the experimentalists were blinded to the genotype of the mice for greater than half of the electrophysiological experiments (n >30 for each genotype) and became un-blinded when no

differences were identified that suggested a experimenter-dependent segregation of results.

For brain slices, mice were were anaesthetized with halothane and quickly decapitated. The brain was dissected and maintained in ice-cold artificial cerebrospinal fluid (ACSF) for approximately 1 min. Horizontal hippocampal slices (250 μm) were obtained at an angle of $\approx$ 12° in the fronto-occipital direction (Vibratome 1000, Vibratome Inc.) while submerged in ice-cool oxygenated ACSF. The slices were immediately transferred to a holding chamber where cool oxygenated ACSF was gradually warmed to $\approx$ 32°C at the end of the sectioning and maintained at that temperature for 2-5 hours for subsequent electrophysiological recordings. All were allowed a minimum of 1 hour of recovery prior to experimentation. Tissue samples used for all biochemical and/or protein biochemistry experiments consisted of the isolated whole intact hippocampus (from each hemisphere) as quickly dissected on an ice-cold surface with regular perfusion of cold oxygenated ACSF.

4.2.2 Neuronal Primary Culture and Transfection

Dissociated hippocampal neurons were prepared as previously described [61]. Briefly, hippocampal neurons and glia were isolated by dissection from (P0-P1) WT or Prp-null mouse pups. The tissue was cut into smaller pieces and was set for 30 min. of digestion at 37°C in a papain solution (20U/ml, Worthington; 50uM EDTA and calcium chloride/L-cystenine (150mM/100mM)) which was prepared in cell plating media (Basal Medium Eagle (BME, Invitrogen), 0.3% glucose, 5% fetal bovine serum (FBS, Hyclone), 0.5 mM L-glutamine (Sigma), 10 mM HEPES-NaOH pH 7.35, 2% B27 (Invitrogen), 15 mM Na-Pyruvate (Invitrogen), 100 μg/ml penicillin-streptomycin (Invitrogen)). After digestion the hippocampal tissue was washed three times in plating media and triturated into a single cell suspension by passing the digested tissue repeatedly through two 1 ml glass pipettes, heat shrunk to 1/2 and 1/3 the original diameter tip. This procedure was performed gently until all tissue was dissociated. The tissue suspension was then seeded at high density ($\approx 5x10^5 \ cells/cm^2$) onto glass coverslips pre-treated with poly-D-lysine (PDL; 70kDa, 10μg/ml, Sigma), followed by laminin (1μg/ml, Sigma) for 3 hours, in 24 well plates. Cultures were used for electrophysiological recordings between 10 and 16 days post-plating, and were maintained in a humidified atmosphere of 5% carbon

dioxide 95% air at 37°C. Cells were fed once a week by replacing approximately 1/3 of total media volume in each well. Electroporation was used to introduce exogenous plasmid (either cDNA or siRNA) constructs into the cells; this was performed post-trituration while cells were in suspension and before plating. EYFP (3-5 μg) was used as the transfection marker. The electroporation protocol consisted of the following: voltage 100 V, square pulse duration 100 ms, 1 pulse, and using a 4 mm cuvette (X-Cell, Bio-Rad Systems). Note: All data obtained from neuronal culture-based experiments were repeated/measured from at least three separate culture rounds. This includes: electrophysiology, immunostaining, ELISA, transfections, and *in vitro* excitotoxicity experiments.

4.2.3 Molecular Biology

Constructs. mPrp cDNA (Cat. No. MMM1013-64097), a full length cDNA (accession BC006703) was was cloned into mammalian expression vector pCMV-SPORT6 (Open Biosystems). For siRNA experiments, we used mouse retroviral short hairpin RNA (shRNAmir) individual clones spanning different regions of mPrp cDNA, (Clone ID RMM1766-98468689, RMM1766-96744825 and RMM1766-9336256) cloned in pSHAG-MAGIC2 (Open Biosystems). All three siRNA constructs were transfected into neurons for siRNA experiments. In order to achieve maximum purity, plasmids were prepared using the endonuclease-free maxiprep kit according to the manufacturers instructions (Qiagen Ltd., UK). Clone identities were confirmed by restriction endonuclease digestion/agarose gel analysis, and/or nucleotide sequencing by standard methods.

RNA Isolation. Total RNA from wild type or mPrP-null mice using adult brain and/or hippocampus was isolated using Trizol according to the manufacturer instruction (Invitrogen). Total RNA was also isolated from wild type or mPrP-null new born mice hippocampus. The quality of RNA was analyzed by agarose gel electrophoresis and ethidium bromide staining by standard methods.

NR2 Subunits: Reverse Transcription Polymerase Chain Reaction Synthetic oigodeoxynucleotides based upon various N2R sequences (i.e. for NR2A, 2B, 2C, and 2D) in GenBank were synthesized and used to characterize NMDA2R subtype expression hippocampal tissue isolated

Primer No.	Protein	Primer Sequence
1	γ-actin-F	ACT GGC ATT GTC ATG GAC TCT GGT GAC GGG
2	γ-actin-R	GCA GTG GTG GTA AAG CTG TAG CCC CGT TCA
3	NR2A-3'F	CAG GAG ACA GGC AAC CCA GCT ACT CGT
4	NR2A-3'-R	GCT CCT CTT GCT GTC CTC CAG ACC TTG
5	NR2A5'-R	GCA ACT GTA GAT GCC CCT GCT GAT GGA GA
6	NR2A5'-F	CAT CTT TGC CAC CAC AGG CTA TGG AAT TGC
7	NR2B-3'-F	TGC AAG AAG GCT GGC AAC CTG TAT GAC ATC
8	NR2B-3'-R	GGT CAC TGA GGA CTT GTT GGC AAA GGA GCT
9	NR2B-5'-F	CAA AAA GAC TCT GGT TGG AAA CGC CAG GTG GAC
10	NR2B-5'-R	ACA CCC ATG AAG CAA TGT CGG AAC TGC CA
11	NR2C-3'-F	GGG ACA GTG GGG TGC TAG AAG AGG TCA GCA
12	NR2C-3'-R	CAA AGA AGA AGG CAG AGG AGT CAA AGC TTG TC
13	NR2C-5'-F	CCA GGG AGG CTT TCT ACA GGC ATC TGC T
14	NR2C-5'-R	GAA GGT GTG GTT GCT CTG TCT ACG GCA GG
15	NR2D-3'-F	TAG CTG GGA CTA CCT GCC CCC GCG
16	NR2D-3'-R	CGA GGG CCC GGT GAG CCT GCG
17	NR2D-5'-F	CAA TGA GGA GCG GTC AGA GAT CGT GGA C
18	NR2D-5'-R	AGG ATT CTC CAC TGG CAC GGA GTT GTT GAA C
19	mPrP1-F	CTC GAG CCG CCA TGG CGA ACC TTG GCT AC
20	mPrP1-R	CCG CGG TCA TCC CAC GAT CAG GAA GAT GAG GAA G
21	mPrP2-F	CAA GGA GGG GGT ACC CAT AAT CAG TGG AAC AAG C
22	mPrP2-R	CCA CCA AGG CCC CCC ACT ACT GCC CC

Table 4.1: A listing of the oligodeoxynucleotide sequences used for RT-PCR experiments to assess mRNA expression for various NR2 subunits. Two sets of primers were selected for each subtype targeting either 3' or 5' end of the mRNA. F and R refer to forward and reverse primers respectively.

from WT and PrP-null mice. We performed RT-PCR on hippocampal samples from both young (P0-P1) and adult (P30-P45) mice. For each receptor subtype two different regions of mRNA sequence were selected: a region in the 5' half and another close to the 3' end region. Additionally one primer set was designed for amplification of housekeeping gene, γ-actin. PCR primers based upon various mPrP cDNA regions were also designed for PrP gene. These were used for RT-PCR analysis in order confirm the presence of mPrP RNA in WT hippocampi, and its absence in hippocampi obtained from PrP-null; these results matched genomic sequencing results.

Reverse Transcription. Approximately 5 μg total RNA was used per each reverse tran-

scription reaction using superscript III and oligo-dT- primers. After the first strand synthesis RNA was digested by treatment with RNAse H. The single stranded cDNA was stored at -20°C till use in PCR with appropriate oligonucleotide pairs and Taq polymerase (Invitrogen). After amplification for 25, 30 and 40 cycles, the products were analyzed by agarose gel electrophoresis. These experiments were performed in a blinded manner and performed on tissues obtained from two or more independent pairs of WT and PrP-null animals.

4.2.4 Electrophysiology and Imaging

Electrophysiology. All slice and cultured cell recordings utilized a standard extracellular solution, ACSF, containing the following (in mM): $NaCl$, 125; KCl, 5; NaH_2PO_4, 1.25; $MgSO_4$, 2; $CaCl_2$, 1.5; $NaHCO_3$, 25; $D-glucose$, 10, pH $\approx$ 7.4 when bubbled with with 95% O_2 and 5% CO_2. Osmolarity was 310±5 mOsm. For recording seizure-like events, in a model of spontaneous recurrent seizures, the superfusing ACSF was switched to one containing no $MgSO_4$ (zero-magnesium model). All field recordings were performed in the CA1 layer of the hippocampus. Evoked (orthodromic) field responses were delivered using a bipolar stimulating electrode placed in the Scheffer collaterals. Extracellular potentials were recorded using a patch pipette filled with 150 mM NaCl.

Successful electrophysiological recordings were made from neuronal cultures between DIV (days *in vitro*) 10 to 16. Recordings were made in the whole-cell configuration of the patch-clamp technique in both voltage- and current-clamp modes. Miniature postsynaptic currents (mPSCs) were recorded in voltage-clamp mode from putative pyramidal neurons using either Axopatch 200B or Multiclamp 700B amplifiers (Molecular Devices). For recording excitatory (i.e. AMPA/Kainate and NMDA) mEPSCs a holding potential of -60 mV was used to obtain maximal responses. Inhibitory $GABA_A$ mIPSCs were recorded at a holding potential of +10 mV. Current-clamp recordings were made in I-Fast mode with cells hyperpolarized to -70 mV. The intracellular solution for voltage-clamp experiments contained the following (in mM): 100 Cs-gluconate, 1.7 CsCl, 10 ethylene glycol bis(2-aminoethyl ether)-N,N,N'N'-tetraacetic acid (EGTA), 5 $MgCl_2$, 40 4-(2-hydroxyethyl)-1-piperazineethanesulfonic acid (HEPES), and adjusted to pH 7.3 with CsOH. The intracellular solution for current-clamp experiments con-

tained the following (in mM): 100 K-gluconate, 1.7 KCl, 0.6 EGTA, 5 $MgCl_2$, 40 HEPES, and adjusted to pH 7.25 with KOH. Both internal solutions were supplemented with (in mM): 2 Tris-ATP, 0.5 Na-GTP, and 5 phosphocreatine. The standard extracellular bath solution was ACSF. The following agonists and antagonists were used for isolating specific synaptic currents: for recording AMPA/Kainate EPSCs we used 0.5 μM TTX (Alomone), 100 μM Picrotoxin (Sigma) in standard 2 mM Mg^{+2}. For isolating NMDA EPSCs or whole-cell currents we used 15 μM CNQX (6-Cyano-7-nitroquinoxaline-2,3-dione disodium salt) and 20 μM Glycine, which were added to a zero-magnesium ACSF in the presence of TTX and Picrotoxin. Ifenprodil (3 μM) was used in experiments were selective block of NR2B subunit function was required. Miniature GABAergic IPSCs were recorded in ACSF with 2 mM Mg^{+2} in the presence of CNQX and TTX. Current-clamp recordings were performed in standard ACSF in the absence of any drugs. All experiments were performed at $32 \pm 1°C$ with perfusion rates near 1-2 ml/min. Patch electrodes had a tip resistances ranging from 5 to 8 $M\Omega$ when filled with internal solution. The resistance to ground of the whole-cell seal was 2-8 $G\Omega$ before breakthrough. For voltage-clamp experiments only cells with series resistances less than ≈ 40 $M\Omega$ and leak currents less than ≈ 100 pA were considered in the analysis. For current-clamp recordings only neurons with input resistances less than ≈ 250 $M\Omega$ and resting membrane potentials more hyperpolarized than -50mV were considered for analysis. For NMDA puff experiments a second micromanipulator with a patch pipette was brought in the vicinity of the cell soma; position and distance were kept as constant as possible using video guidance with designated markings on the viewing monitor for cell center in relation to the puff electrode placement. NMDA was applied at a concentration of 100 μM (made in external solution) and a pressure of 8 psi; the electrode tip diameters were similar to those used for the whole-cell patch experiments. The three puff durations used (50, 100, and 500 ms) were computer controlled for timing and initiation using a DigiData 1322A (Molecular Devices); the transistor-transistor logic (TTL) pulse was also digitized by the DigiData, allowing for the determination of the puff; on time relative to the recorded NMDA currents. Electrophysiological data was acquired in PClamp 9.2 using a DigiData 1322A. For voltage-clamp recording an 8-pole low-pass filter with $f_c = 2$ kHz was used with a $f_s = 10$ kHz sampling rate; current clamp recordings used an

f_c = 10 kHz in conjunction with a f_s = 50 kHz sampling rate. Recordings of spontaneous excitatory miniatures were analyzed using MiniAnalysis (Synaptosoft Inc). All recordings were processed using an in-house software package developed in Matlab (Mathworks Inc.) by the author. Statistical analyses were performed using SigmaStat (SPSS Inc). Statistical analysis, unless stated otherwise, was performed using t-test for comparing two groups, and one-way analysis of variance (ANOVA) for comparison of multiple groups vs. control using the Bonferroni variant. Mean values for miniature postsynaptic current parameters was computed as a mean of means. Specifically, a mean value (e.g. mEPSC amplitude) was computed for all events recorded in a cell and then averaged (e.g. mean of means mEPSC amplitude) for subsequent comparison between WT and PrP-null animals. Raw values were used for calculating cumulative probability. In instances where the total number of events was different between WT and KO conditions (e.g. 450 mEPSCs in WT and 700 in KO), we used SPSS to randomly sample 450 events from the 700, and these were used for subsequent analysis. This was done in order not to bias calculation of cumulative ensemble-type statistics. Cumulative probability plots were compared and significant differences were established for $p \le 0.05$, using the Kolmogorov-Smirnov test. Statistical significance was reported for quantities with $p \le 0.05$ (single asterisk), and $p \le 0.001$ (double asterisks). All other analysis and plotting was performed using PClamp 9.2 and/or Origin 7.5 (OriginLab).

Immunofluorescence Microscopy of Neuronal Cultures. All imaging was performed on an upright Axioskop 2 FS (Carl Zeiss, Germany) microscope with IR-DIC and fluorescence capability. Images were visualized through water-immersion objectives: either Achroplan 40x 0.8 NA or Achroplan 63x 0.95 NA. Epifluorescence was visualized through dichroic mirrors with the following excitation—emission (wavelength in nm) filter properties: 450-490—515-565 (green channel), 500-520—535-565 (yellow channel), and 530-585—Long-pass 615 nm (red channel). Imaging was typically performed using unmounted coverslips in phosphate-buffered saline (PBS). Images were acquired using a CCD camera with on-chip signal integration (Watec 120N) and sampled by a high-resolution video capture card.

Cells were grown on glass coverslips and were briefly rinsed with PBS and fixed for 15 min with 4% paraformaldehyde (PFA) at room temperature. Coverslips were rinsed three times with

PBS and after blocking nonspecific binding with blocking buffer (3% bovine serum albumin in PBS). They were incubated overnight at 4°C with the primary antibody in blocking buffer. Pre and postsynaptic contacts were visualized by co-staining with anti-Synapsin-I (Chemicon, 1:1000) conjugated with Alexa Fluor 568 goat anti-rabbit IgG (Invitrogen, 1:1000), and Anti-NR1 (Synaptic Systems, 1:500) conjugated with Alexa Fluor 488 goat anti-mouse IgG (Invitrogen, 1:1000). NR2D subunit distribution was detected using a polyclonal antibody raised against a peptide mapping to the N-terminus of the NR2D subunit - anti-NR2D (Santa Cruz, R-20 1:300) conjugated with either Alexa Fluor 488 donkey anti-goat IgG, or Alexa Fluor 568 donkey anti-goat IgG; both secondary antibodies were used at 1:1000 dilution. Post-secondary staining, the coverslips were subjected to three washing cycles with PBS and then stored in PBS containing a drop of Vectashield anti-fade reagent (Vector Laboratories). All immunostaining of neuronal cultures was repeated on a minimum of two independent culture rounds for NR1 and greater than three for NR2D.

4.2.5   Immunoblotting

Fresh brain tissue was removed and the hippocampal region was quickly dissected under a microscope and used as a sample. Neonatal samples were collected from P0-P1 pups, whereas adult samples were obtained from P30-P45 mice. The tissue was homogenized by gently jouncing thirty times in a glass tissue homogenizer in cold lysis buffer (100mM NaCl, 10mM Tris.Cl pH 8.0 0.5% Triton X-100, a cocktail of protease inhibitor). After incubating on ice for 1 hour the supernatant was collected. The homogenate was centrifuged at 10,000 x g for 20 min at 4°C and supernatant was collected. Protein concentrations were determined by comparison with a known concentration of bovine serum albumin using a kit (BioRad). 20 - 30 μg of protein was load per lane onto a 10% SDS polyacrylamide gel and run under constant voltage. Proteins were transferred electrophoretically at constant voltage from polyacrylamide gels to nitrocellulose in 20 mM Tris, 150 mM glycine, and 20% methanol. Membrane was dried and briefly rinsed with PBS and then incubated in blocking buffer (5% milk in PBS containing 0.5% Tween-20) overnight at 4°C. Membrane was briefly rinsed with PBST and incubated with suitably diluted primary antibody (Anti-NR2D 1:200, Santa Cruz) in PBS containing 1% milk and

0.5% Tween-20. After 2 hours at room temperature, the membrane was washed three times in the PBS containing 0.5% tween-for 30 min. Membrane was incubated for 1 hour in HRP conjugated second antibody (1:10000) and antigen was detected using enhanced chemiluminescent horseradish peroxidase substrate (ECL, Amersham Biosciences). Immunoreactive bands were visualized following exposure of the membranes to Hyperfilm MP (Amersham Biosciences). These experiments were performed in a blinded manner and using tissues obtained from three independent pairs of WT and PrP-null animals.

4.2.6 ELISA Assays

Hippocampal neurons (DIV 14) were fixed in 4% PFA followed by 2 x 5 min. washes with PBS. Half of the cells were permeabilized with 0.1% Triton-X100 for 5 min. followed by a 30 min. incubation in blocking solution (PBS+3% BSA). Expression of NR2D was measured using extracellular antibody (Ab, 1:200, also see Section 4.2.4) and an HRP-conjugated donkey anti-goat (1:1000, Antibody Jackson Immunoresearch). SuperSignal ELISA femto maximum sensitivity substrate (Pierce) was added and the luminescence was measured with a Victor 2 luminometer (Perkin Elmer) as described previously [7]. The ratio between signals obtained from non-permeabilized neurons (i.e., surface expression) and permeabilized (i.e., total expression) was then calculated from 12 coverslips (6 permeabilized, 6 non-permeabilized) with WT, and 10 coverslips with PrP-null neurons.

4.2.7 Excitotoxicity Assays

Primary hippocampal cultures between DIV 16-18 were used in NMDA excitotoxicity assays. Coverslips with plated WT or PrP-null cells were transferred to a new 24-well dish with fresh medium. Cells were exposed to vehicle (control) or NMDA for at varying concentrations (in mM: 0.3, 0.6, 1.0) for 20 min. Coverslips were then transferred back to their originating wells and allowed to recover for 24 hours post-exposure. Cells were then exposed to Trypan blue dye (0.4% stock diluted 1:100) for 1 min. Coverslips were washed in 3 x PBS and fixed with 4% PFA. These coverslips were then stained with a TUNEL (Terminal transferase dUTP nick end labeling) cell death detection kit (Chemicon) and the number of TUNEL-positive

cells counted for each NMDA concentration. Imaging was performed in PBS for Trypan blue stained cells and on mounted coverslips for TUNEL stained cells. For each imaging session, ten randomly selected fields were imaged using conventional light microscopy. Within each field, the total number of cells was visualized by either DIC (for Trypan blue) or via counter staining with methyl green (for TUNEL). The number of Trypan blue and TUNEL cells were counted during independent imaging sessions. The number of postiviely stained cells (either Trypan or TUNEL) is reported as a fraction of the total number of cells taken as an average over the imaged fields. All *in vitro* excitotoxicity experiments were repeated using at least two independent culture rounds.

4.3   Results

4.3.1   PrP-null Mice Exhibit Greater Basal and Seizure-like Excitability

Hippocampal synaptic physiology was examined in WT and PrP-null mice. Using a stimulating electrode placed in the Scheffer collaterals, synaptic responses were recorded in the CA1 layer of horizontal hippocampal slices in normal ACSF. Paired-pulse (Δ t = 60 ms) stimulation was used in order to assess paired-pulse facilitation (PPF). In WT slices, the synaptic responses observed were typical of hippocampal slice physiology with waveforms exhibiting a robust presynaptic volley, a sharp downward deflecting population spike, and upward deflecting field EPSP (fEPSP). These were observed for each pulse (P1 and P2) along with paired-pulse facilitation as evident by an augmented population spike amplitude in P2 relative to P1 (top, Fig. 4.4A). Paired pulses evoked in slices from PrP-null mice exhibited similar waveform properties such as PPF but also showed a key difference in the number of overriding population spikes on the fEPSP. This observation is suggestive of a basal increase in excitability that is present under normal extracellular ionic conditions. The cellular correlate of these additional spikes is relatively synchronous ensemble neuronal firing (such as 2-3 spikes) in response to the field stimulus. We also examined the minimum stimulus threshold required to evoke a single population spike and observed that in PrP-null slices this value is reduced, which is consistent with elevated basal hyperexcitability (top left, Fig. 4.4B). In addition, the stimulus intensity required

to reach maximal threshold, where the peak population spike amplitude attains a plateau, was significantly lower for PrP-null slices (top right, Fig. 4.4B). This is consistent with the notion that greater basal excitability results in less potential for subsequent enhancement of synaptic potentials. Quantitative analysis of the number of population spikes within each pulse (P1 & P2) revealed that PrP-null slices consistently displayed more than a single population spike under normal (ACSF) recording conditions (bottom right, Fig. 4.4B). Robust PPF was observed in slices from both WT and PrP-null mice, however, the extent of facilitation was not different between these two groups (bottom left, Fig. 4.4B).
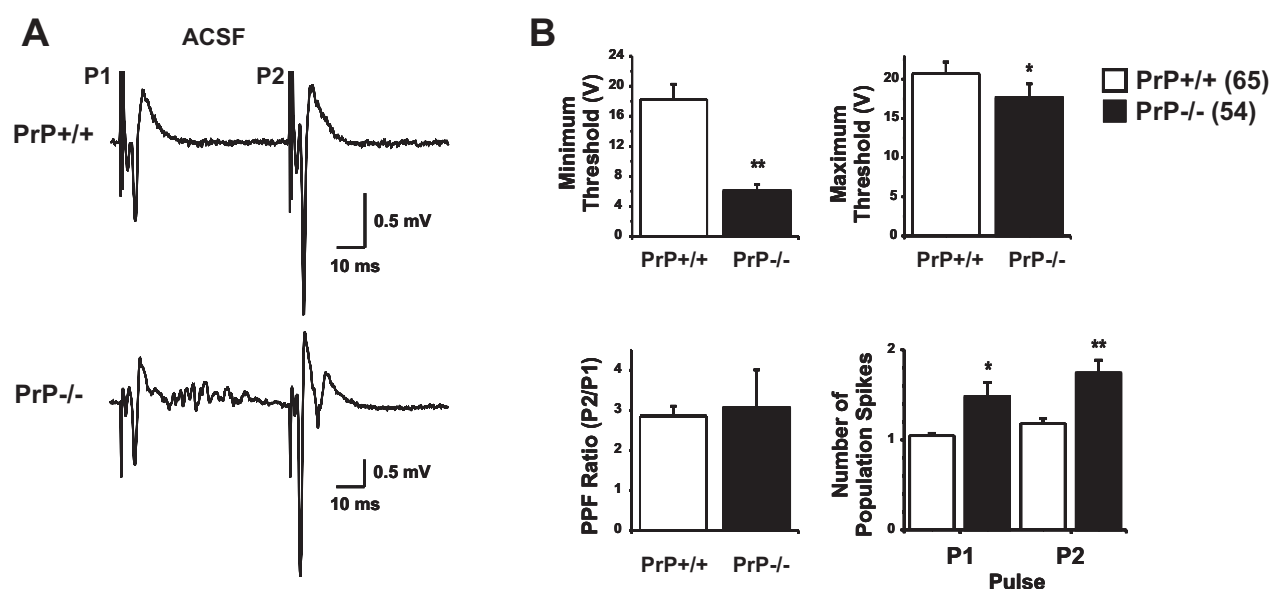
Figure 4.4: Field potentials recorded in the CA1 layer of hippocampal slices perfused in ACSF. **(A)** Paired-pulses evoked by stimulation of the Scheffer collaterals and recorded in the CA1 layer of horizontal hippocampal slices from P30-P45 mice. In standard ACSF, both WT and PrP-null slices exhibit paired-pulse facilitation. Note that the PrP-null slices show the presence of several population spikes superimposed on the field EPSP. **(B)** (clockwise) Stimulation threshold to evoke a single minimum amplitude population spike was significantly lower in PrP-null slices. Similarly, PrP-null mice reached max stimulation threshold; this was measured as the potential where the first population spike amplitude reached a plateau. The number of population spikes within each pulse (P1 & P2) were calculated and found to be increased for PrP-null slices. Slices from KO mice often exhibited more than a single population spike. Paired-pulse facilitation (PPF) was also examined by taking the ratio of the first (maximal) population spike amplitude (P2:P1). Both WT and PrP-null slices exhibited PPF, however this increase was not different amongst them. Numbers in parentheses indicate number of slices.

Given that PrP-null mice have been shown to exhibit greater sensitivity to *in vivo* pharmacologically-

induced seizures, and the observation that PrP-null slices exhibit a greater basal level of excitability, we proceeded to investigate differences in hippocampal synaptic physiology under a hyperexcitable state. Brain slices were initially recorded from in normal ACSF where field responses were acquired and observed to be stable. This was assessed by a relatively constant population spike amplitude. Slices were then exposed to an external solution containing zero Mg^{+2} (ZM-ACSF) and over a period of minutes to tens of minutes, a state of hyperexcitability was achieved. ZM-ACSF promotes the development of spontaneous recurrent seizure-like events (SLEs) [275]. Although we recorded from upwards of 70 slices (separately for WT and PrP-null mice), we analyzed only slices that went on to exhibit SLEs ($\approx 70\%$ of slices). The fact that some of the slices did not exhibit spontaneous SLEs has been observed previously [174], and is believed to be caused by factors such as lack of preserved network circuitry during slicing [94]. Approximately 5 min. after perfusion with ZM-ACSF, evoked synaptic responses were assessed using the paired-pulse stimulus (Fig. 4.5A). Both WT and PrP-null mice exhibited hyperexcitability in response to ZM-ACSF perfusion and exhibited a marked increase in the number of population spikes. Moreover, the ability to induce PPF was less under this hyperexcitable state. This observation is expected given that PPF is inversely proportional to the probability of presynaptic transmitter release, which is augmented as a result of the induced hyperexcitability. Furthermore, the first evoked response (P1) is more likely to trigger a larger synaptic response. In ZM-ACSF, the number of population spikes in response to each pulse was increased, but this increase was greater for slices from PrP-null mice (top left, Fig. 4.5B). As alluded to earlier, in a majority of slices, prolonged perfusion with ZM-ACSF results in the appearance of spontaneous epileptiform discharges that culminate with the occurrence of SLEs (see Fig. 4.6A). The time to the appearance of the first epileptiform discharge, upon initiating ZM-ACSF perfusion, was quantified and found to be significantly shortened for PrP-null slices. (top right, Fig. 4.5B). This supports the idea that an increased level of basal excitability for PrP-null slices is also maintained during a hyperexcitable state. Similarly, for slices that exhibited SLEs, the time to their first appearance was noted to be shorter, by several min. in slices obtained from PrP-null mice (bottom left, Fig. 4.5B). However, once SLEs were observed, their duration did not seem to be affected by the genotype of the animal (bottom right, Fig. 4.5B). In

order to characterize possible differences between spontaneous epileptiform discharges in WT and PrP-null slices, we used a Fourier-based analysis (similar to that in Section 3.2.2). Briefly, the cumulative power spectral amplitude for each discharge was computed for five frequency bands (0-500 Hz, 100 Hz for each bandwidth). This was performed for 500 randomly selected discharges each from SLEs in WT (n = 18) and PrP-null (n = 21) slices. Discharges recorded in PrP-null mice consistently showed a greater composition of higher frequency oscillations in two power spectral bands (100-200 and 200-300 Hz). The presence of high frequency oscillations within epileptiform discharges (specifically $\geq$ 200 Hz) has been associated with the existence and degree of an underlying epileptic condition (see Section 3.1.2). Taken together, these findings indicate that spontaneous seizure-like activity in PrP-null slices is more severe, which is consistent with the increased hyperexcitability in response to removal of extracellular magnesium.

4.3.2 Alterations in Excitatory and Inhibitory Synaptic Currents in PrP-null Mice

Based on our findings in brain slices, we investigated glutamatergic and GABAergic spontaneous synaptic currents, which are key factors in shaping synaptic responses in the hippocampus. In addition, evoked NMDA receptor currents were examined to further elucidate the possible involvement of specific glutamatergic receptor subtypes in bringing about greater excitability in PrP-null neurons. These experiments were performed in primary hippocampal neuronal/glial co-culture (DIV 12-16) allowing for examination of isolated synaptic currents. Although perhaps more physiological in a slice setting, these currents are more difficult to separate due a greater number of interacting experimental variables (e.g. glutamate spillover resulting in synaptic cross-talk). Moreover, the culture setting allows for easier access to the cells and the ability to perform experimental manipulations involving techniques such as transient transfection.

AMPA-mediated miniature excitatory postsynaptic currents (mEPSCs) were recorded in primary cultured neurons from WT and PrP-null mice. These were performed in the presence of TTX, picrotoxin, and standard 2 mM Mg^{+2} ACSF. mEPSCs were analyzed for waveform attributes such as: frequency, amplitude, rise time, and decay time (Fig. 4.7A). The mean
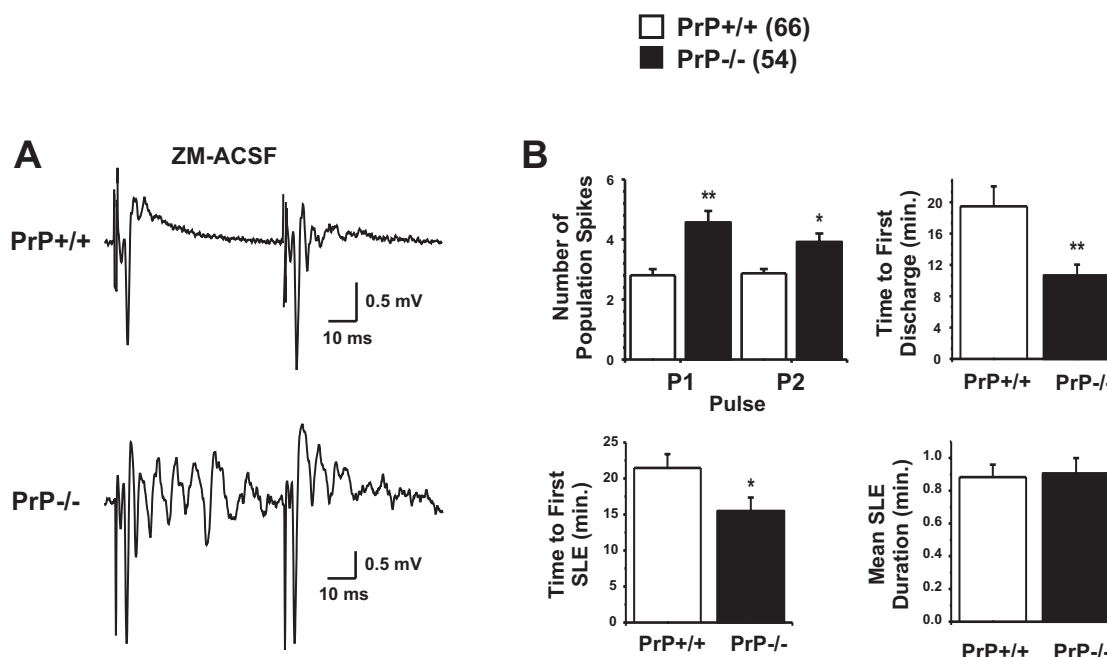
Figure 4.5: Field potentials recorded in the CA1 layer of hippocampal slices perfused in zero–magnesium ACSF (ZM-ACSF) resulting in a hyperexcitable state. **(A)** Paired-pulses evoked in zero magnesium using the same stimulation protocol as in Fig. 4.4. In ZM-ACSF solutions, both WT and PrP-null slices are hyperexcitable as seen by the presence of several population spikes overriding the field EPSP for both pulse 1 and 2. Upon perfusion with ZM-ACSF for several min., spontaneous seizure-like events (SLEs) are observed that begin with the appearance of epileptiform discharges that increase in frequency and then terminate (see Fig. 4.6). In some slices, SLEs can reoccur every few min. after their first appearance. The evoked responses were recorded prior to the appearance of any SLEs but approximately 5 min. after start of ZM-ACSF perfusion. **(B)** (clockwise) The hyperexcitability brought on by ZM-ACSF is clearly visible by the increase in the number of population spikes in P1 and P2; PrP-null slices exhibited a greater number of populations spikes within each pulse. The time required to bring about the first epileptiform discharge upon starting ZM-ACSF was significantly shorter for PrP-null slices. In addition, the time to the start of the first full-blown SLE was also shortened. Once observed, the duration of the seizure-like event did not differ between WT and PrP-null slices. Numbers in parentheses indicate number of slices.
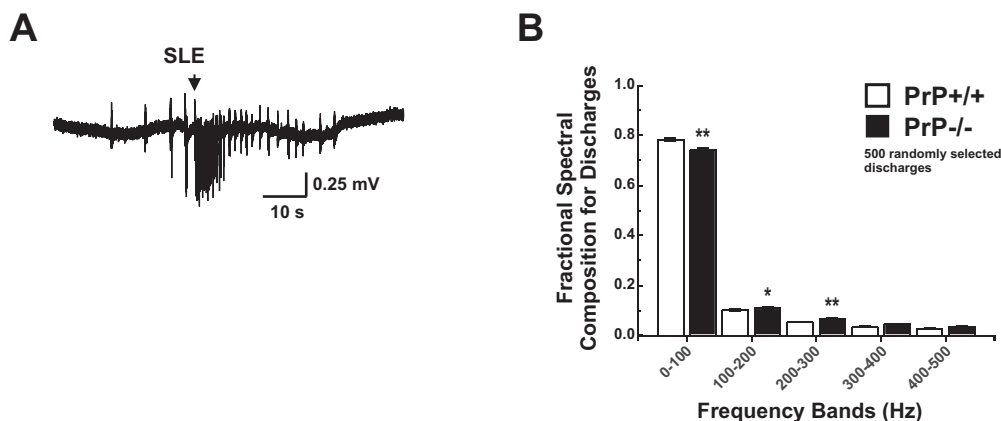
Figure 4.6: Waveforms and analysis of discharges in zero magnesium-induced seizure-like events. **(A)** A recording of a typical SLE from a WT slice. After several min. of perfusion in ZM-ACSF (ranging from 4 min. for PrP-null to 20 min. in WT slices) spontaneous epileptiform discharges appear, increase in frequency to the point of a full-blown SLE, which is typically characterized by a flip in the polarity of the waveform and a rapid succession of population spikes (arrow). The SLE terminates and recordings return to a quiescent baseline from which other SLEs can arise every few min. **(B)** Bandwidth-limited Fourier transform analysis of 500 randomly selected discharges from either WT or PrP-null slices during SLE activity showing that PrP-null mice exhibit faster frequency components in their discharges with greater 100-200 Hz and 200- 300 Hz signal components.

AMPA-mediated mEPSC amplitude was found to be slightly, but significantly, increased in PrP-null neurons without any apparent alterations in other waveform parameters. These observations are consistent with a fractional increase in AMPA-mediated synaptic currents. The recorded currents were successfully blocked by CNQX, an AMPA/Kainate receptor antagonist (data not shown). We next examined the effect of PrP on long-term depression (LTD) in the *in vitro* hippocampal slice and observed that for adult mice (P30-45); there appeared to be no differences in the efficacy of LTD induction or recovery to baseline synaptic responses (Fig. 4.7B). Miniature inhibitory postsynaptic currents (mIPSCs) were also recorded in WT and PrP-null cultured neurons in the presence of TTX, CNQX, and standard 2 mM Mg^{+2} ACSF. Miniature IPSCs were analyzed and found to display increased rise time and decay time in PrP-null neurons (Fig. 4.8). Other parameters were seemingly unchanged. mIPSCs were successfully blocked by picrotoxin, confirming that the currents recorded were generated by $GABA_A$ receptor activity (data not shown).

NMDA-mediated mEPSCs were recorded in WT and PrP-null neurons in the presence of
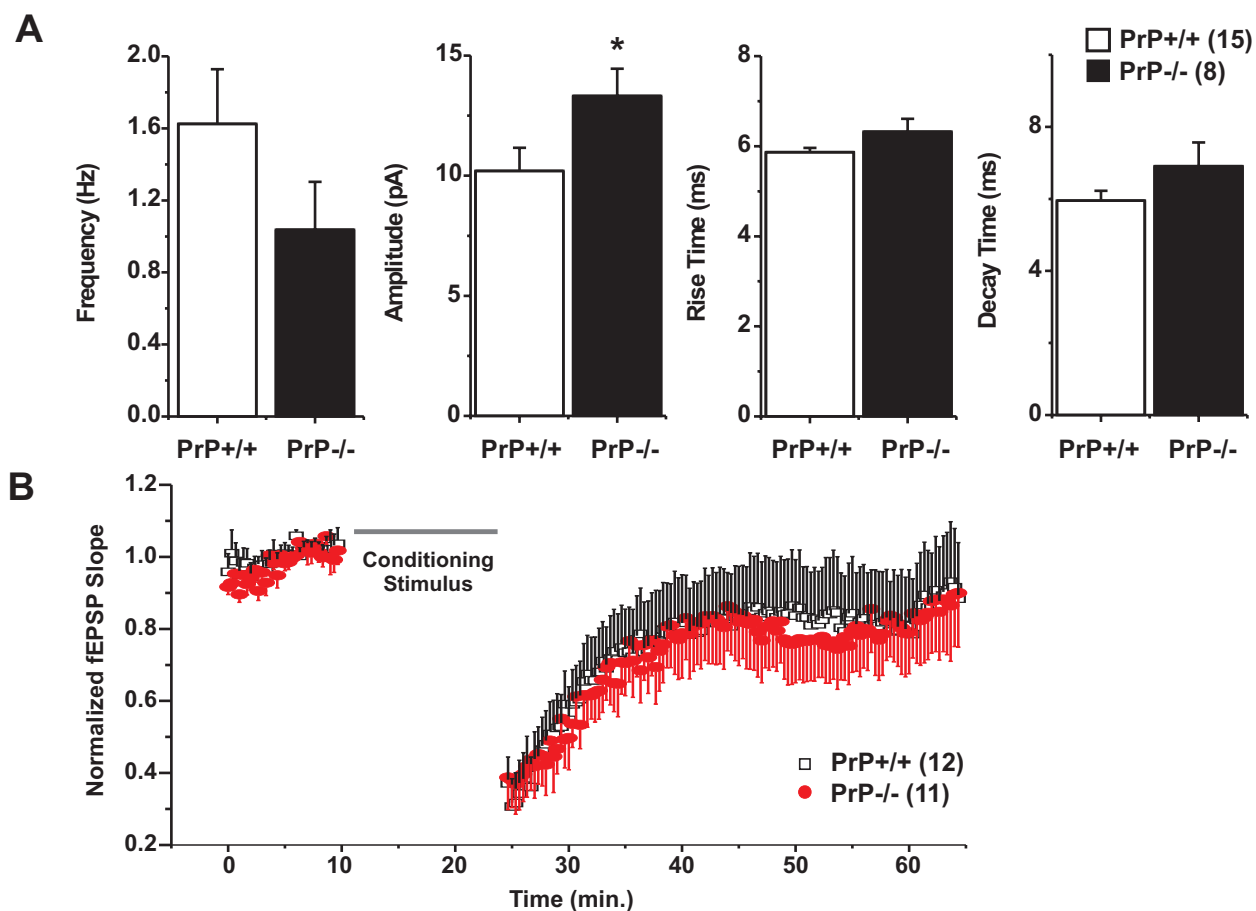
Figure 4.7: Alterations in AMPA receptor-mediated glutamatergic synaptic transmission. **(A)** Miniature EPSCs were recorded in cultured pyramidal neurons (DIV 12-16) from WT and PrP-null mice. Analysis of mEPSCs revealed an increase in the mean amplitude of spontaneous postsynaptic potentials ($p \leq 0.05$) without alterations in any of the other waveform parameters. Number of cells recorded in parentheses. **(B)** LTD in the CA1 region of hippocampal slices from adult (P30-P45) WT and PrP-null mice. The conditioning pulse was paired-pulses ($\Delta t = 60$ ms) delivered at 1 Hz for 15 min at the Scheffer collateral. Analysis of field EPSP slope revealed no statistically significant differences in the extent of induced LTD or the time course of its recovery to baseline. Numbers in parentheses indicate number of cells.
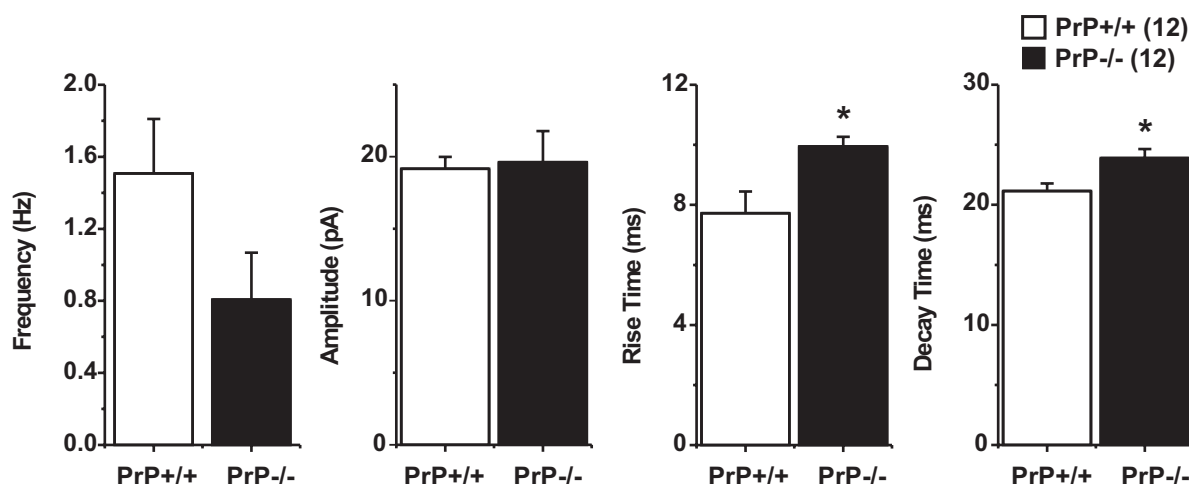
Figure 4.8: Alterations in *GABA~A~* receptor-mediated synaptic transmission. Miniature IPSCs were recorded in WT and PrP-null pyramidal neurons in culture. Analysis of mIPSC waveforms revealed slightly prolonged rise and decay times ($p \leq 0.05$). Number of cells recorded in parentheses.

TTX, picrotoxin, CNQX, glycine and ZM-ACSF (see methods Section 4.2.4). Visual inspection of raw current traces revealed the presence of large amplitude mEPSCs in PrP-null neurons [range $\approx$ 10-200 pA] when compared with WT [range $\approx$ 10-100 pA] (Fig. 4.9A). In addition, prolonged decay of NMDA-mediated mEPSCs were observed in PrP-null neurons. mEPSCs were analyzed for waveform characteristics. Cumulative probability curves were computed for all waveform parameters and displayed for amplitude and decay time (Fig. 4.9B); these curves are computed based on histogram distributions (Fig. 4.9C), showing significantly larger and prolonged currents for PrP-null neuons. Note that in the case of mEPSC amplitudes, the shape of the distribution is largely unaltered, whereas the distribution is shifted to larger amplitudes. This fact is visualized also from cumulative probability curves that look similar in shape but are shifted in relation to each other (Fig. 4.9B, Kolmogorov-Smirnov test $p \leq 0.05$). These differences were also evident from the mean values for mEPSC amplitude and decay time (Fig. 4.9D).

In order to determine evoked NMDA current kinetics we recorded whole-cell currents in response to transient (puff) application of NMDA (100 μM in external solution). Currents were evoked using three different puff durations (50, 100, and 500 ms). NMDA receptor cur-
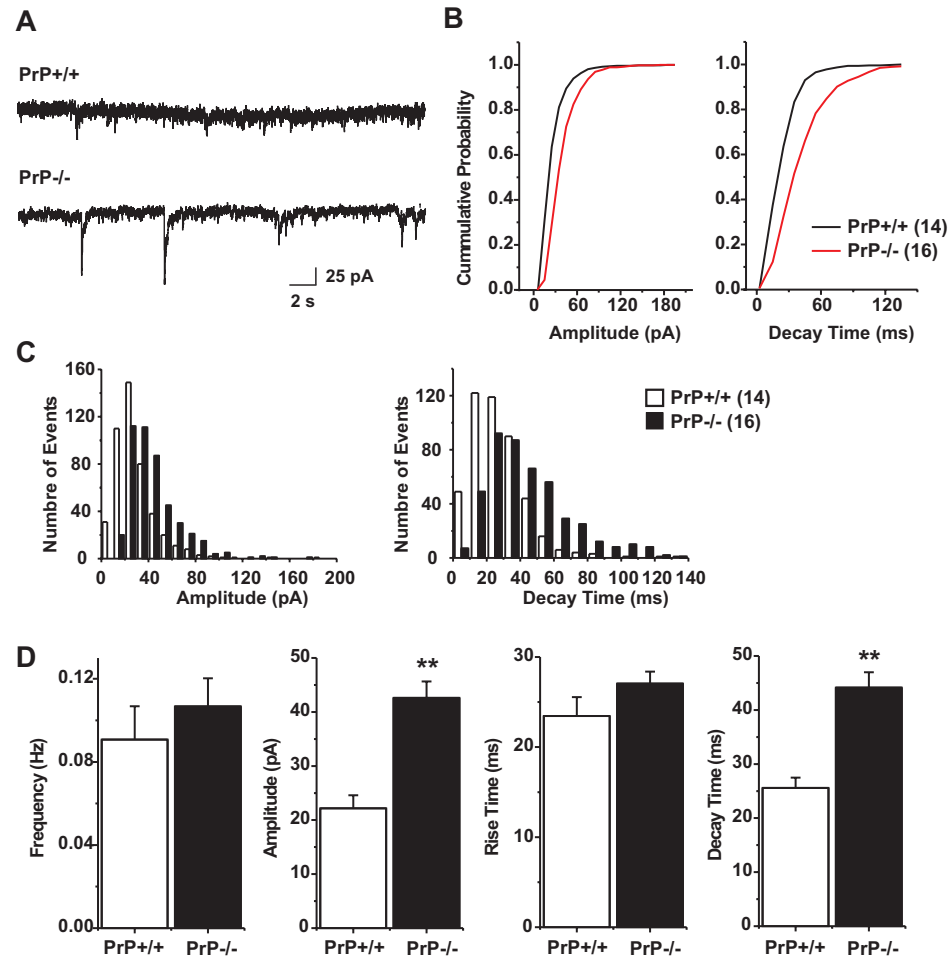
Figure 4.9: Alterations in NMDA receptor-mediated glutamatergic synaptic transmission recorded in the presence of TTX, CNQX, picrotoxin, and glycine. **(A)** Current traces recorded from a WT and PrP-null hippocampal neuron in culture (DIV 12). Larger amplitude mEPSCs, showing prolonged decay times are visible in PrP-null neurons. **(B)** Cumulative probabilities, obtained from a normalized cumulative sum, from mEPSC amplitude and decay time distributions in **(C)**. A clear rightward shift is observed in both distributions for amplitude and decay time. **(D)** Mean values for several EPSC waveform parameters showing an increase EPSC amplitude and prolonged decay time ($p \leq 0.001$). Numbers in parentheses indicate number of cells.

rents were recorded in the presence of TTX, picrotoxin, CNQX, and glycine for both WT and PrP-null neuronal cultures. The evoked currents were dramatically different between WT and PrP-null neurons, with the latter exhibiting very prolonged deactivation kinetics (Fig. 4.10A). This effect is easily appreciated by visual inspection of normalized (to peak amplitude) currents for each puff duration. The peak evoked current in response to NMDA application was compared and found to be greatly increased for PrP-null mice in response to a 50 ms application (Fig. 4.10B). Subsequently increasing durations of NMDA application did not markedly affect the magnitude of the evoked current in PrP-null neurons but exhibited an increase for WT neurons consistent with a dose-response relation (Fig. 4.10B). This observation suggests that postsynaptic receptor affinity for NMDA is somehow increased in the absence of native prion protein. Given vast differences in NMDA deactivation kinetics between WT and PrP-null neurons, we quantified the time required to reach the half-max of peak amplitude, as measured starting from the peak. For all durations of NMDA application, PrP-null currents exhibited a greater degree of prolonged deactivation, beyond the linear increase observed for WT neurons (Fig. 4.10C). Note that exponential (single and double termed) fitting was attempted but not used due to inability to adequately fit the responses.

Given that NR1/NR2A and NR1/NR2B are the most common compositions of NMDA receptors, and that the presence of NR2B subunits result in slower deactivation kinetics as compared with NR2A, we examined the contribution of NR2B receptor subunits to the observed prolonged deactivation in PrP-null neurons. Currents were examined for the most dramatic case, the 500 ms application of NMDA, and recorded first in the presence of control solutions (TTX, picrotoxin, CNQX, glycine) and then evoked again with the addition of bath-applied Ifenprodil (predominantly a NR2B antagonist, [74]). Evoked currents were slightly reduced relative to baseline but exhibited further prolonged deactivation kinetics that was insensitive to Ifenprodil block (Fig. 4.11A). These findings suggest that the highly prolonged deactivation rates observed in PrP-null mice are not mostly dependent on the involvement of native NR2B subunits.

These findings show that NMDA receptor function is enhanced in the absence of prion protein. However, knockout animals may exhibit other genetic abnormalities and/or developmen-
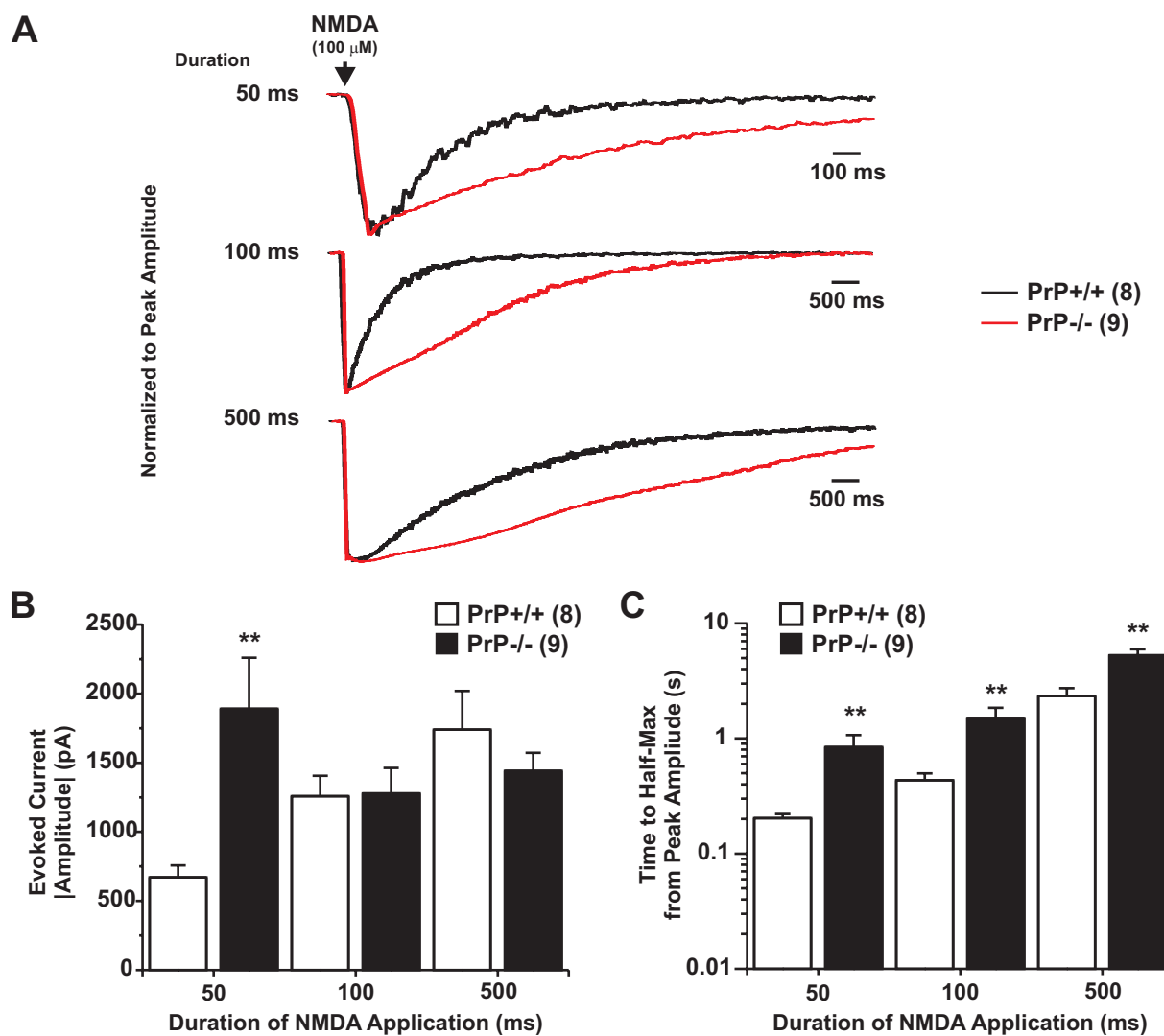
Figure 4.10: Evoked whole-cell NMDA currents in WT and PrP-null neurons in culture. **(A)** Sample NMDA-evoked whole-cell currents as a result of brief NMDA puffs (delivered at 50, 100, or 500 ms durations) at 100 μM (see Section 4.2.4). NMDA postsynaptic currents were recorded at a holding potential of -60 mV in the presence of TTX, picrotoxin, CNQX, and glycine. Current peak amplitudes have been normalized in order to compare prolonged de-activation kinetics observed for PrP-null neurons for each puff duration. **(B)** Evoked current amplitudes, for different puff durations of NMDA, for WT and PrP-null neurons. A large current is observed in PrP-null neurons even for a 50 ms puff of NMDA, which remains relatively unchanged for increasing puff durations ($p \leq 0.001$). **(C)** Deactivation kinetics were measured by noting the time to reach half-max amplitude (from peak current). For each duration of NMDA application tested, PrP-null neurons exhibit prolonged deactivation kinetics ($p \leq$ 0.001). Numbers in parentheses indicate number of cells.

tal alterations that could be the cause of the observed effects. In order to control for such factors and to further explore a causal link between PrP and NMDA receptor function, we engaged in transient transfection and RNAi experiments involving prion protein. PrP-null cultures were transfected prior to plating with either (murine) mPrP cDNA or three RNAi constructs targeting mPrP RNA species (along with YFP marker). Responses to a 500 ms application of NMDA was examined in untransfected (in the same dish) and/or control YFP transfected neurons and compared with PrP transfected cells. The transient expression of PrP was able to rescue the WT phenotype by accelerating deactivation rates (Fig. 4.11B). When WT neurons were transfected with RNAi constructs, NMDA currents exhibited prolonged deactivation that was reminiscent of observations in PrP-null neurons (Fig. 4.11C).

4.3.3   Expression and Trafficking of the NR2D NMDA Subunit in PrP-null Mice

The prolonged deactivation kinetics observed in evoked whole-cell NMDA currents in PrP-null mice is highly reminiscent of kinetics observed in transient transfection experiments of NR1/NR2D receptors in expression systems [353]. In order to assess putative involvement of NR2D subunits, we engaged in a series of experiments to assess mRNA transcript levels, protein expression levels, and possible differential targeting to the membrane. These experiments were performed for neonatal and adult (WT and PrP-null) mice in order to match the developmental stages of neuronal culture and brain slice electrophysiological data. Transcript levels for NR2D, as assayed by RT-PCR, were found to be similar between WT and PrP-null neurons. No appreciable differences were observed for other NR2 subunits when comparing WT vs. PrP-null transcript levels (Fig. 4.12A). Although neonatal NR2C transcript levels were not examined, it is expected that they would not be different due to the fact that this particular subunit is mostly expressed in the cerebellum during neonatal development and therefore would not be properly assayed in primary cultures from isolated hippocampi. Protein expression levels for NR2D were also assayed using Western blot analysis for both neonatal and adult tissue samples and were found to be comparable between WT and PrP-null neurons.

We next examined NR2D expression patterns in cultured ($\geq$ DIV 12) neurons. The NR2D antibody used recognizes an extracellular (N-terminus) epitope allowing for visualization in
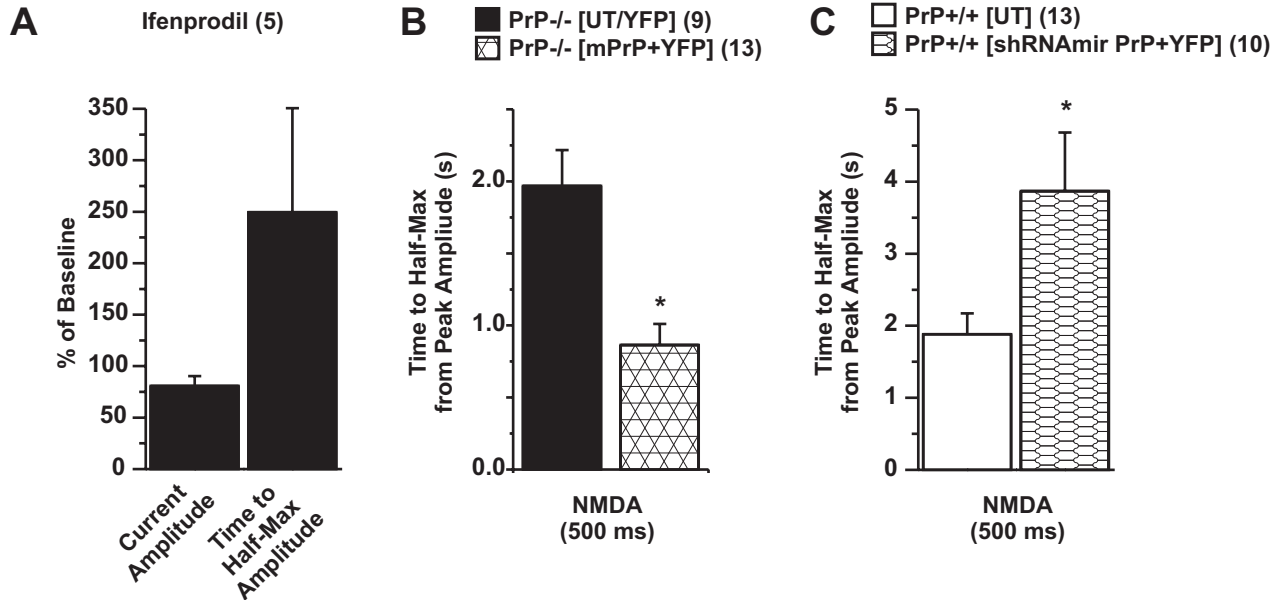
Figure 4.11: NR2B pharmacology along with rescue and knockdown experiments involving PrP and NMDA receptor deactivation kinetics. **(A)** Whole-cell current amplitudes were recorded in response to a 500 ms puff of NMDA and compared in relation to control values (100%) in the same cell before and after application of Ifenprodil. Overall, a small decrease in amplitude was observed, whereas deactivation kinetics became more prolonged. **(B)** Time to half-max amplitude was measured in PrP-null neurons that were either untransfected (UT) in the same dish, or were expressing YFP alone; there was no difference between these two groups and the data were pooled ($p \geq 0.7$). These control recordings were compared with those obtained from PrP-null mice transfected with mPrP and YFP. The expression of PrP resulted in faster (restored) deactivation kinetics ($p \leq 0.05$). **(C)** Time to half-max amplitude was measured in WT neurons that were either untransfected (UT, in the same dish), or transfected with three short hairpin siRNA constructs (shRNAmir) with YFP. Expression of the siRNA plasmid in WT neurons resulted in prolonged deactivation kinetics reminiscent of KO neurons ($p \leq 0.05$). Numbers in parentheses indicate number of cells.
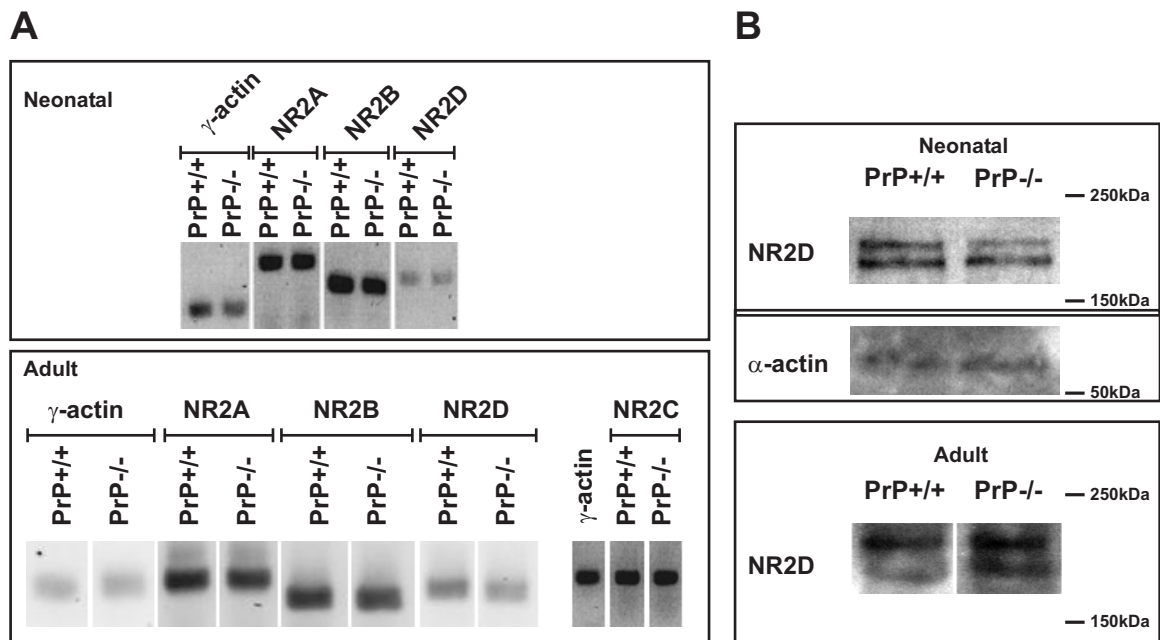
Figure 4.12: RT-PCR and Western blot analysis of NMDA receptor subtypes during neonatal and adult stages of development. **(A)** (top) RT-PCR analysis of transcript levels for ND2A, NR2B, and NR2D showing the presence of mRNA species for these NMDA receptor subtypes at a neonatal stage of development. (bottom) RT-PCR analysis of NMDA receptor subtypes showing transcript levels for all subtypes present in adult (P30-P45) animals. No appreciable differences were observed between WT and PrP-null mice. **(B)** Western blot analysis of the NR2D subunit in both neonatal and adult mice showing no apparent differences between WT and PrP-null NR2D expression. Experimental results were reproduced for tissues obtained from neonatal and adult mice using at least two independent pairs of WT and PrP-null animals. Note: RT-PCR experiments were performed by Dr. Jawed Hamid. Western blot experiments were performed by Dr. Shahid Hameed.
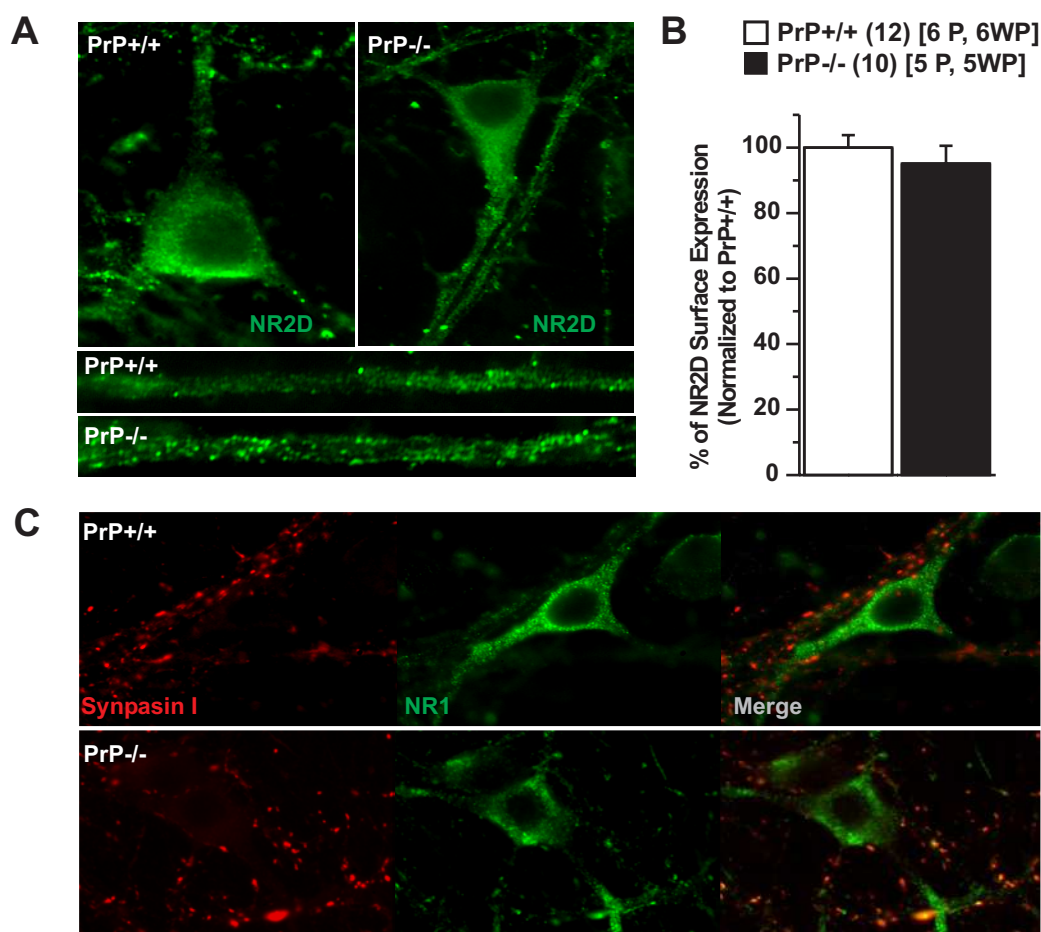
Figure 4.13: Expression patterns of NR2 subunits. **(A)** Visualization of NR2D expression patterns in adult WT and PrP-null neurons showing antibody reactivity both in the soma and processes. A punctate pattern of receptor distribution is visualized along dendritic processes. The depth of field is ≈ 1 μm. **(B)** Surface expression of NR2D, relative to total cellular protein content was quantified using ELISA (extracellular NR2D Ab) and shown as normalized to values obtained for WT neurons. No significant differences were observed in the quantity of NR2D expressed in the membrane vs. total protein between WT and PrP-null neurons. P and WP refer to permeabilization vs. without permeabilization respectively; number of neuronal culture samples are indicated in parentheses. **(C)** NR1 and synapsin-I (presynaptic marker) protein expression patterns were visualized in WT and PrP-null neurons and were observed not to be different. For each imaging condition, upwards of 30 cells were randomly imaged in at least two independent culture rounds. Note: ELISA experiments were performed by Dr. Christophe Altier and immunostaining was performed by Dr. Shaid Hameed and the author.

non-permeabilized cells. No significant differences in the pattern of NR2D subunit expression were observed between WT and PrP-null neurons (Fig. 4.13A). Expression of NR2D was measured using the extracellular Ab in permeabilized vs. non-permeabilized cells (DIV 14). Membrane expression was quantified through luminometrycally for each genotype and compared with the total cell protein expression. No differences were observed between WT and PrP-null cultures for the quantity of NR2D in the membrane vs. total protein (Fig. 4.13B). In addition, the distribution of synapsin I and NMDA receptors, as putative markers of pre- and postsynaptic contacts, was used to examine the possibility of gross morphological synaptic alterations. However, after imaging many representative neuronal fields no appreciable differences were observed (Fig. 4.13C).

4.3.4 Elevated NMDA-mediated Cell Death in PrP-null Mice

The observation of increased NMDA activity in PrP-null mice both at the level of spontaneous and evoked synaptic currents, suggests that these mice may be more susceptible to glutamate/NMDA-mediated excitotoxicity. We examined this prospect in mature hippocampal cultures transiently (20 min.) exposed to NMDA at varying concentrations and allowed to recover (24 h). Cell death was evaluated using two markers: Trypan blue and TUNEL (Fig. 4.14A). Trypan blue is a dye that becomes incorporated into cells with compromised cell membranes, and therefore can be considered as a late marker of neuronal death as compared with TUNEL. TUNEL staining is a technique used to detect DNA fragmentation and was used to assay the fraction of TUNEL+ cells due to NMDA exposure in WT and PrP-null cultures. It was observed that PrP-null neurons exhibited a greater degree of cellular DNA damage, consistent with cell death, for increasing concentrations of NMDA (0, 0.3, 0.6, 1.0 mM); this increase exhibits a dose-response relation (Fig. 4.14B). In fact, increased cell death was observed for PrP-null neurons using Trypan blue staining (Fig. 4.14C). This increase was evident for the control condition and remained relatively constant until NMDA was increased from 0.6 mM to 1.0 mM. The fraction of dead cells was relatively constant in WT neurons despite increasing concentrations of NMDA. We believe that this may be artifactual - Trypan blue (relative to TUNEL) is perhaps a less specific but more sensitive marker. It will also stain all dead cells
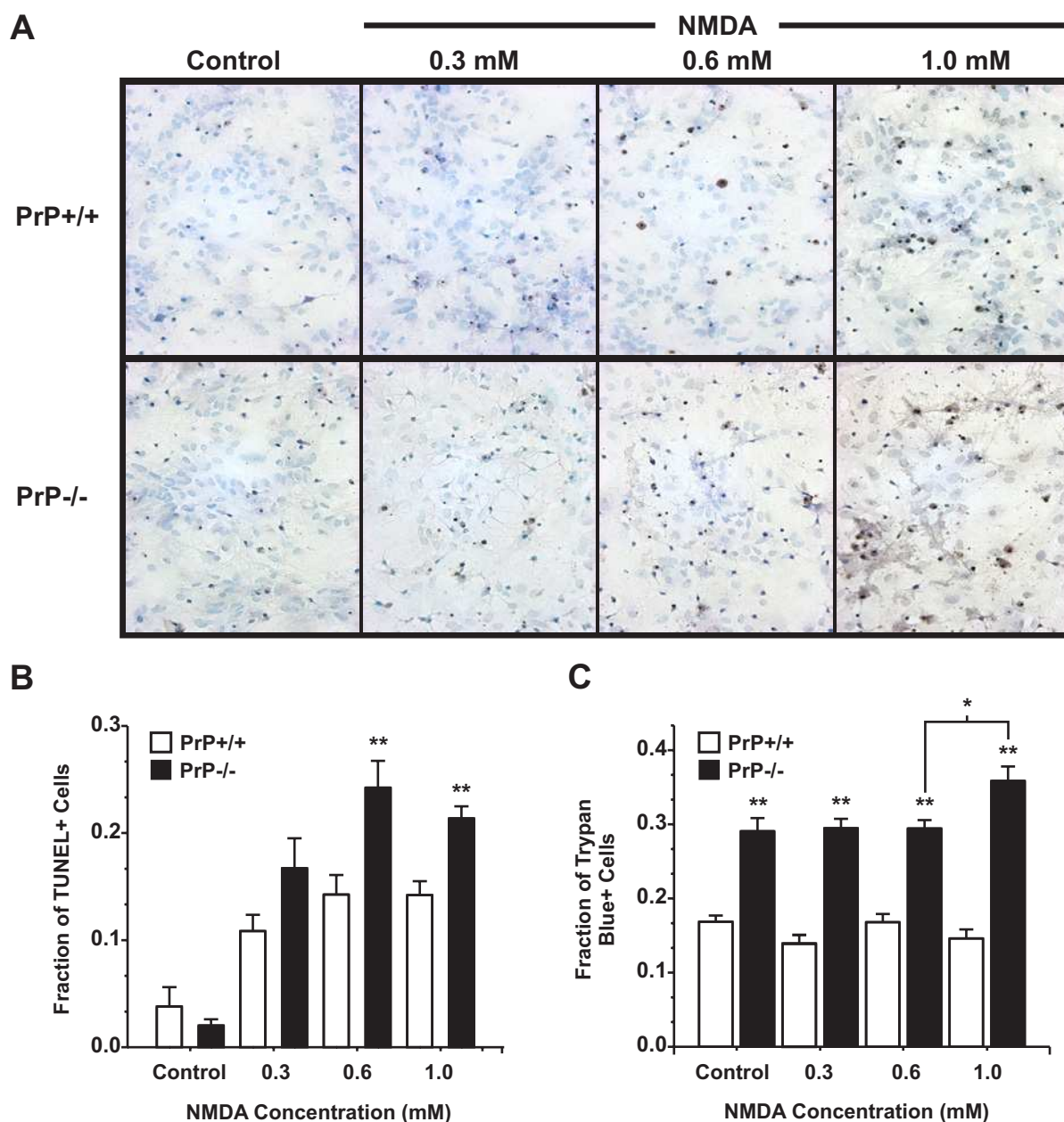
Figure 4.14: Differential effects of NMDA excitotoxicity on WT and PrP-null neuronal cultures. **(A)** Light microscope images of neuronal cultures after 20 min. of exposure to NMDA and 24 hrs recovery. Cells were exposed to Trypan blue, fixed, and then TUNEL stained. Trypan blue positive cells are visualized as deep blue-stained cells; TUNEL positive cells as dark brown. Methyl green was used as the counter stain visible as light blue/green colored cells. **(B)** Survival of cells was assessed by TUNEL staining showing that PrP-null cells are more susceptible to NMDA-mediated excitotoxicity. **(C)** Cell survival was also assessed by counting Trypan blue stained cells showing an elevated degree of death in PrP-null neurons, with the effects of NMDA being most significant between 0.6 and 1.0 mM. $*$ $p \leq 0.05$, $**$ $p \leq 0.001$. Note: The TUNEL staining was performed by Dr. Shigeki Tsutsui.

that may have been present during the early days of recovery post-plating. This may explain why the fraction of Trypan blue positive cells does not change dramatically until an order of magnitude greater NMDA concentration is used to induce toxicity. Nonetheless, a consistently greater fraction of dead cells was observed for PrP-null vs. WT neurons.

4.4 Discussion

4.4.1 Overall Findings

Ever since its discovery as an endogenous protein, the physiological functions of PrP have remained unclear. Their ubiquitous expression across many tissue types, with particularly high expression in nervous tissue, has pointed to a functional role in neuronal and/or glial elements. The disease state associated with prion proteins affects the central nervous system and alters cellular function, via a misfolded variant of the prion protein. It is this misfolded form that ultimately results in cellular death via apoptotic pathways [272]. The fact that prion proteins are found in several forms within neurons suggests that PrP is a complex protein with the potential of interacting with a multitude of other proteins within the cells. Perhaps the most powerful evidence for this comes from the observed cellular stress, in the presence of the misfolded protein, that ultimately results in cell death. Prion protein has been localized to synaptic contacts, even though its precise localization to pre and/or postsynaptic membranes are still being fully explored. This localization has suggested that PrP may play an important role in synaptic physiology. Indeed, observations suggesting that PrP-null mice exhibit changes in synaptic plasticity have contributed to this notion. As might be expected for a complex protein such as PrP, its physiological effects are equally diverse and probably extend beyond one particular aspect of synaptic function. PrP-null mice display phenotypes at the level of excitatory and inhibitory neurotransmission, altered ion channel function, altered gross structural changes relevant to neurite growth and axonal sprouting , impaired spatial learning, and increased susceptibility towards cell death [64, 213, 63, 62, 71, 56, 53, 21].

Our results add to the diversity of synaptic effects of prion protein by identifying a novel target - the NMDA receptor. Our findings show that absence of prion protein results in markedly

enhanced receptor function. This effect is observed both in spontaneous and evoked whole-cell NMDA currents. The enhanced activity appears to be of postsynaptic origin and is also conserved throughout development as it was observed in both primary cultures (neonatal) and brain slices (adult). Furthermore, the observed effect on NMDA receptor currents in PrP-null mice does not seem to arise from a diffuse developmental effect due to long-term absence of PrP. This is supported by the fact that WT neurons could be made to exhibit receptor activation kinetics observed in PrP-null neurons via RNAi experiments. Similarly, PrP-null neurons could be rescued by transient transfection of PrP cDNA. The enhanced NMDA activity was also recorded in the form of hyperexcitable synaptic activity in the CA1 layer of hippocampal slices. PrP-null mice displayed a basal reduction of threshold towards excitability and were more susceptible to seizure-like activity in an NMDA-based *in vitro* seizure model. NMDA receptor currents were altered in two principle ways: receptor affinity for NMDA (and by extension glutamate) was greatly enhanced as suggested by large amplitude currents in response to brief NMDA application. Also, both miniature and evoked whole-cell currents displayed very prolonged deactivation kinetics.

These results suggest that the observed increase in NMDA receptor currents in PrP-null mice can cause the hyperexcitability observed in CA3/CA1 synaptic responses. Moreover, this increase manifests a greater susceptibility towards NMDA-mediated excitotoxic cell death. This latter finding provides a novel link between the well established role of NMDA receptors in excitotoxicity and a possible mechanism for cellular death associated with the prion protein disease state. These experimental results are in support of the notion that prion protein serves a physiological neuroprotective role.

4.4.2 Functional Relevance of Experimental Findings

We observed greater basal excitability in CA3/CA1 hippocampal synapses in PrP-null mice as manifested by the presence of multiple population spikes and lower thresholds for evoking synaptic responses. These findings are consistent with early reports suggesting that these mice can exhibit greater excitability in the hippocampus [358, 64, 62, 216]. In addition, several reports suggest that PrP-null mice exhibit a lower threshold for LTP induction [213, 212].

However, the generation of LTP in WT vs. PrP-null mice is somewhat controversial with some reports showing either no changed or diminished LTP in PrP-null mice [204, 64, 147, 79]. The precise cause of these differences remains unresolved but could be due to experimental conditions and also inter-strain differences between KO animals and their method of generation [364].

Our findings showing no differences in paired-pulse facilitation are consistent with previous reports [45, 79] and suggest that loss of PrP does not necessarily result in presynaptic factors governing neurotransmitter release, as assayed by this technique. However, this does not preclude a functional presynaptic role for PrP given its localization to presynaptic, as well as, postsynaptic membranes [244, 119, 146, 287]. Also, consistent with increased seizure severity and mortality in several *in vivo* models of epilepsy [358], we observed that PrP-null mice show increased susceptibility towards *in vitro* zero-magnesium induced seizure-like activity. Although patients with CJD can experience seizures, this is not a common finding [370]. Therefore, the clinical link between loss of PrP and altered seizure threshold is tenuous. Thus, these results must be interpreted with some caution, perhaps, better placed in the context of altered excitability. Nonetheless, altered seizure threshold in the zero-magnesium model served as an indication of altered glutamatergic transmission, in particular involving NMDA receptors.

PrP-null mice were more susceptible to kainate induced seizures *in vivo* and have recently been shown to exhibit greater excitotoxicity in response to kainic acid [358, 278]. Our observations concerning AMPA/kainate mEPSCs showed slightly increased quantal amplitudes, which could be caused by increased presynaptic quantal size, increased postsynaptic receptor function, and/or increased receptor expression. This change may also be due to alteration of receptor subunits or modifications thereof (e.g. alternate splicing). This latter alteration is known to modulate unitary AMPA conductances [140, 278]. Consistent with changes in subunit composition for AMPA-mediated excitotoxicity, the study by Rangel et al. suggests that GluR6 and GluR7 expression are elevated [278]. In the context of our observations, it is conceivable that evoked AMPA currents may also be augmented. Taken together, our findings are in agreement with increased AMPA-mediated excitotoxicity, although this notion requires further experimental validation. In adult animals, AMPA/kainate as well as mGluR receptor function

is believed to play a role in LTD induction (reviewed in [171]). However, we observed no differences in LTD between WT and PrP-null mice in the CA1 layer of hippocampal slices. It is challenging to interpret this finding, however, it does evoke caution when translating changes at the level of isolated spontaneous synaptic currents to synaptic transmission at the level of intact hippocampal circuits. In addition to alterations in AMPA/kainate activity in PrP-null mice, we observed slight modifications of $GABA_A$-mediated IPSCs in the form of prolonged rise and decay times. Although these changes are quite small, they are consistent with earlier findings showing similar effects for synaptically evoked $GABA_A$ currents [64].

Our main finding is that NMDA receptor currents are enhanced in the absence of PrP expression. NMDA currents exhibit greater amplitude during basal miniature activity and in response to brief NMDA application. In addition, NMDA current decay times were greatly slowed. The prolonged decay of NMDA receptor currents in PrP-null mice is most consistent with a change in deactivation kinetics and not receptor desensitization [353, 164].

The observed increase in postsynaptic NMDA currents can be caused by several factors, and in the context of our experimental findings, it is entirely possible that either one or several of these may be responsible for the observed effects. These include: modification of synaptic architecture in a way that would facilitate potentiation, allosteric modulation of the receptor resulting in a conformational change for either the ligand or cofactor binding sites, modulation via pathways involving the action of phosphatases and/or kinases, increased receptor expression and/or targeting to synaptic contacts, and finally, possible alterations in NMDA receptor subunit composition.

Protein-protein Interactions. The fact that PrP^C, in its most common form, is extracellular and GPI-anchored to the membrane has prompted some investigators to speculate that it may play a role in synapse formation and/or modulation of synaptic contacts [64]. Recent studies have shown that PrP aids in the localization of NCAM to lipid rafts where it can participate in Fyn tyrosine kinase signalling that ultimately promotes neurite outgrowth [166, 290, 297]. However, the membrane bound form of PrP does not seem to be necessary in this interaction given that NCAM-mediated neurite growth occurs with equal robustness for PrP-null neurons [290]. Nonetheless, PrP has been shown to be secreted by neurons into the extracellular en-

vironment [143, 13]. Thus, the pro-neurite growth effects that seem to depend on this form of PrP are perhaps altered in PrP-null mice resulting in altered NCAM-mediated signalling that somehow could affect NMDA receptor function. NCAM has been shown to be important in accumulating spectrin at postsynaptic densities that ultimately leads to the recruitment of receptors such as the NMDA [328]. Another possible explanation for our findings, although highly speculative, may be that PrP serves as a form of synaptic adhesion molecule that may have a presynaptic partner. Thus, via a pre- and/or postsynaptic interaction, membrane anchored PrP can somehow cluster NMDA receptors under physiological conditions. If such a mechanism were in place, in PrP-null neurons this interaction would be lost and NMDA receptors would take on a different synaptic distribution. Our immunostaining experiments which visualized the obligatory NR1 subunit and synapsin-I suggest that gross synaptic remodeling does not take place. However, these observations do not exclude more subtle changes at the ultrastructural level, which may result in large effects on synaptic transmission.

Alternatively, PrP may act directly on the NMDA receptor via an extracellular protein-protein interaction (e.g. with large NMDA receptor N-terminus) and result in its allosteric modulation. Such a modulation can affect the glutamate and/or glycine binding sites. In the absence of PrP function (i.e. PrP-null mice), this modulation (presumably inhibitory in the WT animal) would be abolished resulting in enhanced NMDA receptor function. Our ability to easily rescue the effect in PrP-null neurons, and bring it about in WT neurons via RNAi, could be viewed as supportive evidence for a direct interaction between PrP and NMDA. However this effect may not be mutually exclusive or be limited to these two proteins (i.e. PrP and NMDA) and could involve other partners. A recent study may provide additional support towards an interaction hypothesis. Solforosi and colleagues recently showed that *in vivo* focal hippocampal injection of PrP-specific antibodies results in cross-liking of native PrP^C resulting in extensive hippocampal neuronal loss [308]. Coincidentally, NCAM was cross-linked as a control experiment for a GPI-anchored protein and did not result in neuronal loss. Antibody-mediated cross-linking in PrP-null mice was also ineffective in causing cell death, suggesting that cell-surface expressed PrP is the key mediator of the neuronal loss. However, the authors note that the neuronal death probably did not result due to blocking of a direct interaction

between PrP and some other molecule. This was suggested by the observation that monovalent Fab fragments of the same death-inducing antibody did not result in neuronal loss. Indeed, the authors suggested that the cross-liked PrP, perhaps by interacting with another molecule, can initiate apoptotic cell death cascades. Another protein interaction relevant to NMDA receptor function involves ephrins, which are a class of receptor tyrosine kinases that are GPI-anchored to the membrane and are present at both pre and postsynaptic membranes. Ephrins can interact trans-synaptically to modulate hippocampal synaptic plasticity [80]. Moreover, postsynaptic ephrins (EphB) have been shown to directly interact with NMDA receptors both extracellularly and intracellularly to modulate CA3 and CA1 hippocampal plasticity. Mice lacking EphB2 have normal AMPA currents but exhibit diminished LTP, which is reminiscent of findings in PrP-null mice [80, 64].

At present, there are no direct molecular links between PrP and NMDA receptors. However, findings such as those described for NCAM and ephrins open a realm of possibilities where PrP in its physiological role, can either directly modulate NMDA receptors (via an extracellular, possibly allosteric interaction) and/or interact with another protein species, such as a phosphatase (or kinase), to alter NMDA receptor function.

Modulation of NMDA Receptors via Phosphatases and/or Kinases. NMDA receptor function is tightly controlled by a balance between protein tyrosine phosphatases (PTPs) and protein tyrosine kinases (PTKs) [80, 360, 198]. There is precedent for enhanced NMDA receptor currents by tyrosine kinase-dependent mechanisms. Src and Fyn tyrosine kinase, of the Src family of kinases (SFKs), are known modulators of NMDA receptor function. Specifically, using peptide activators, the activity of protein tyrosine kinases (PTKs) has been shown to increase synaptic NMDA receptor currents [288]. In particular, studies have identified NR2 subunits (mainly NR2B) as main targets of phosphorylation. The precise manner by which NMDA receptor phosphorylation results in increased currents remains unknown, but due to the large number of tyrosine residues in the c-termini of NR2 receptors many potential targets exist. In addition, the phosphorylating action of PTKs may be on other proteins that are in a complex with NMDA receptors, such as PSD93 [288]. Another potential effect of PTKs could affect receptor trafficking to and from the plasma membrane. Indeed, during tetanic

stimulation, the pool of NMDA receptors is decreased due to presumed increased membrane insertion [288]. Thus, it may be that membrane vs. total protein levels are unchanged during low levels of activity but become altered during epochs of intense activity (such as hyperexcitability or seizure-like activity). Inhibitors of SFKs activity have been shown to diminish NMDA-receptor dependent potentiation that is a key component for LTP in CA1 hippocampal neurons. Furthermore, in relation to excitotoxicity, SFK inhibitors suppress NMDA-mediated cell death *in vitro* [141]. If the enhanced NMDA receptor currents in PrP-null mice are mediated by the action of PTKs, it would imply that this becomes the case in the absence of PrP. Thus, the presence of PrP may somehow act to inhibit the action of PTKs (or subtypes thereof such as src kinase). Alternatively, PrP can interact with PTPs to maintain some basal level of phosphatase activity. In keeping with this concept, early studies have shown that NMDA receptor function is reduced by the action of PTPs [198, 360]. Specifically, block of calcineurin activity (a calcium/calmodulin-dependent phosphatase) results in prolonged NMDA receptor activation [198]. Most notably, there exists a link between calcineurin and prion protein associated neurodegeneration. The transgenic mouse Tg(PG14) expresses a PrP homolog that is associated with human prion disease. These mice show accumulation of a protein that forms aggregates and is resistant to proteases, which closely tracks the pathophysiology of human prion-associated diseases. These mice ultimately develop neurodegeneration that culminates in a severe ataxia and apototic cell death. Very recent work by Biasini and colleagues has shown that a 50% reduction of calcineurin takes place in the cerebellum of pre-symptomatic Tg(PG14) mice [16]. This reduction occurs well before there are any histological signs of neuronal death, which strongly suggests that a decrease in calcineurin function precedes neurodegeneration in a causative manner. The fact that calcineurin is a cytoplasmic protein and that most of the cellular PrP resides on the extracellular surface may indicate the presence of an intermediate signalling protein. Alternatively, calcineurin may interact with one of the intracellular prion protein species to bring about the reported effects. Taken together, these studies along with findings obtained from this study, suggest that there may be a role for native PrP in directly or indirectly regulating the extent of NMDA receptor function (perhaps via calcineurin). When this influence is removed, such as in PrP-null mice, it can result in overactive

NMDA receptor function that mediates excitotoxicity.

Changes in NMDA Receptor Subunit Composition. Another hypothesis that may explain our findings involves a possible alteration in the subunit composition of functional NMDA receptors. Our observation of prolonged deactivation kinetics in evoked currents is highly resemblant of isolated currents from NR1/NR2D containing NMDA receptors [353, 240]. In fact, the mean deactivation rate in expression systems (τ = 4.8 s for 300 ms [100 μM] NMDA application) [240] was very close to what we observed in PrP-null primary neurons ($\tau_{(0.5\ Max\ Amp)}$ = 5.3 s for 500 ms [100 μM] NMDA application). Thus, our observations can also be interpreted to involve NR2D. This NMDA receptor subunit was believed to be exclusively a prenatal/neonatal NR2 subunit based on early reports that its expression dramatically decreased after approximately day seven of life [254, 240]. However, recent evidence suggests that NR2D is well expressed into adulthood [334]. Our findings support this notion given that we detect both mRNA and protein species for NR2D in neonatal and adult isolated hippocampi. Hippocampal localization of NR2D is also well known [240] and is similar to that of prion proteins [201, 287]. While it is accepted that glutamatergic NMDA-dependent synaptic transmission is mostly facilitated by NR1/NR2A or NR1/NR2B, or NR1/NR2A/NR2B heteromeric NMDA receptors, the role of NR2D has to-date been classified as non-synaptic [75]. The notion that NR2D receptors may be non-synaptic comes from the discrepancy between their presence in pre- and postsynaptic membranes but lack of prolonged synaptic currents in neurons known to express them. If our findings in PrP-null mice are due to an NR2D functional effect, it would represent a condition where NR2D can be localized to the synapse give that we observed prolonged kinetics for both miniature and evoked NMDA currents. Our results also suggest that transcription, expression, and membrane localization of NR2D are not altered between WT and PrP-null neurons. Specifically, using RT-PCR, western blot, and ELISA analysis we showed evidence that there are no appreciable differences between WT and PrP-null neurons of transcription, expression, and membrane targeting of NR2D subunits. Immunostaining also did not reveal dramatic differences in receptor clustering along neuronal processes. However, our experiments cannot exclude the possibility that the absence of PrP somehow uncovers or augments NR2D function without affecting the expression-related parameters. For example, by

recruiting more functional receptors to synaptic membranes. One such alteration could involve a shift in abundance from triheteromeric NMDA receptors (e.g. NR1/NR2B/NR2D) to the diheteromeric form (e.g. NR1/NR2D). Indeed, it is speculated that triheteromeric receptors would not exhibit the prolonged deactivation kinetics observed for the diheteromeric form [74]. NMDA receptors containing NR2B subunits also exhibit slow deactivation kinetics but these can be 3 fold faster than NR2D. Using a relatively selective antagonist for NR2B we were able to show that the involvement of these subunits is seemingly minimal. This is also supported by our RT-PCR data. In our experiments we also observed larger than WT evoked NMDA currents in response to brief (50 ms) NMDA application; this observation could support greater involvement of NR2D subunits given that their IC_{50} for glutamate is the lowest amongst all NMDA subunits [74]. However, it should be noted that in transgenic mice over-expressing NR2D, NMDA evoked receptor currents exhibit prolonged deactivation kinetics but also showed a decrease of approximately 20-30% in peak current amplitude [254]. Therefore, we cannot exclude the possibility that other NMDA subunits are affected in the PrP-null mice in a manner consistent with our findings.

NMDA-mediated Excitotoxicity. Regardless of the precise mechanism by which abolishment of endogenous PrP results in enhanced NMDA receptor currents, our findings show that these mice would exhibit greater susceptibility towards excitotoxic neuronal death. The fact that PrP-null mice or primary cultures are more susceptible to NMDA excitotoxicity (and for glutamate by inference) has been alluded to in the literature without identification of the mode by which it can occur. Specifically, previous studies have shown: reduced MK-801 sensitivity in PrP-null mice [213, 93], enhanced neuronal survival by MK-801 block in *PrP^Sc* infected cultures [245] and in cultures treated with a PrP infectious fragment [33]. In addition, recently MK-801 block reduced cell death in a kainate model of induced neurotoxicity [278]. The role of glutamate-dependent neuronal death involving NMDA receptors is well established in other fields such as ischemic stroke [10]. Intriguingly, in a very recent study involving patients and both *in vitro* and *in vivo* animal models, Mitsios and colleagues have shown that endogenous PrP up-regulated in response to acute ischemic stroke, thereby linking the long-suggested protective role of endogenous PrP to clinical observations [235]. Specifically they demonstrated

that: endogenous PrP expression is elevated in plasma samples obtained from patients during the acute phase of ischemic stroke. Also, increased levels of PrP are detectable in surviving neurons localized to the peri-infract region; this latter finding was shown in animal models both in this and another study [363]. Taken together, all of these findings support the notion that loss of PrP function, either via gene KO or misfolding to the PrP^{Sc} form, equate to removal of a neuroprotective role served by this complex and diverse protein.

Concluding Remarks. Collectively, our results demonstrate a novel link between prion protein and the NMDA receptor, and furthermore support the notion that PrP serves as a protective agent against excitotoxic neuronal death. This implies that the cellular dysfunction and neurodegeneration, which are hallmarks of the prion disease state, may in part be facilitated by excessive calcium entry via NMDA receptors. Further research is required to elucidate the precise mechanisms by which PrP affects NMDA receptor function. Nonetheless, identification of this interaction between PrP and the NMDA receptor offers a novel target for protective therapies for prion-associated neurological diseases. A recent study in rodents has shown that a PrP^{Sc} infected animal can be made to improve from both neurodegeneration and synaptic dysfunction by targeted removal of the endogenous PrP gene at nine days post-infection [217]. Our observations of dramatic alterations in NMDA receptor activity suggest that PrP exhibits properties that qualify it as a modulator of NMDA receptor function under physiological conditions. Thus, our results, along with those from previous studies describing a variety of cellular roles for PrP, strongly advocate for further research into the entire spectrum of physiological functions for this diverse and intriguing protein.

Chapter 5

General Discussion: Overall Remarks & Future Directions

The overarching theme in this dissertation has been neuronal excitability as studied through the prism of hyperexcitability and epileptiform seizure activity. The mandate of this chapter is to make some suggested links between the three topics studied in this dissertation - mainly T-type channels, High Frequency Oscillations (HFOs), and prion protein. On the surface, these topics are each independent but if one considers the broad topic of neuronal excitability and hyperexcitable states associated with seizure activity, it is realized that these topics share mechanisms that are each inter-related and insightful towards each topic. I will briefly discuss how altered neuronal and network dynamics, under hyperexcitable conditions such as epileptiform activity, can facilitate the interaction of cellular parameters that may not otherwise directly affect one another. I will also propose some experiments dealing with each of the topics described in the previous chapters.

5.1 The Complexities of Investigating Neurophysiology in the Brain

The brain is tremendously complex not only due to the number of neuronal, glial, and vascular elements but also due to the number of parameters and interactions between these "subsystems". Indeed, it is difficult to capture all of the aspects that govern brain function in a final chapter of any document, but a more precise description would also state that many of these parameters, the so-called state-variables which govern the dynamics of the brain, are functions of one another (in a mathematical sense). In other words, even it were presently possible to consider all of the individual components and their individual functions within a neuron (e.g. genes to proteins with associated functions), it would take considerably more effort to work out their inter-relations. However, at the same time, a small perturbation in a key parameter can have dramatic consequences for the overall system. For example, a small alteration in the ratio of alpha helices and beta sheets, as reflected in a misfolded version of an endogenous

protein goes on to wreak havoc in many host species. Such an observation is not surprising given factors such as the ubiquitous nature of a particular protein, or perhaps its interaction with other proteins that are themselves ubiquitous can be at play. Alternatively, different cellular states of activity (brought on by either the environment or internally triggered) may affect many downstream processes via cell signaling cascades. Nonetheless, there is a key message that can be learned from biological systems in stress or affected by a disease condition. That is, when a system is operating in extreme ranges of its dynamic range, it often exhibits simpler dynamics and occupies a state where multiple previously un-interacting variables begin to interact. Borrowing again from the physical sciences, a simple analogy here would be the parameters governing the dynamics of gas molecules, which are more complex, say at room temperature, but become much simpler and predictable at high temperatures and low pressures (i.e. the ideal gas law). In keeping with the notion that some system parameters only interact or become relevant for particular, typically more extreme, overall system states, I will discuss possible inter-relations between our observations concerning T-type channel function, high frequency oscillations, and prion proteins. Indeed, a framework that allows for conceptualization and analysis of complex systems with many interacting variables is nonlinear dynamical systems theory (see Section 1.2.2).

No research project is ever truly completed, as each answer raises new questions. This of course also applies to my doctoral research. Some of the potential avenues for future research are given below for each chapter.

5.2   T-type Channels, Bursting, and Links to HFOs

Seizures represent a state of close-to-maximal neuronal network excitability whose effects are manifested across many elements governing neuronal function. During seizure activity many cellular processes are augmented and also suppressed, these include: the activity of ion channels, receptors involved in neurotransmission, cytoskeletal elements involved in short-term/long-term changes in dendrite spine morphology, activity of kinases and phosphatases, cell metabolism, and gene transcription. Indeed, it is during such hyperexcitable states where many system parameters interact under rapid dynamics. Some of these interac-

tions may not normally occur during "normal" function. Perhaps a good example would be a hyperexcitability-mediated activation of a particular or subgroup of protein kinases that have many diverse downstream targets (e.g. src family of kinases). Alternatively, the occurrence of a hyperexcitable state, such as via a single seizure episode, can trigger an alteration or unmasking of function of a native protein. I will describe such a change involving T-type channels and its putative effects on hippocampal high frequency oscillations (HFOs).

Previously, I have alluded to the fact that T-type channels participate in physiological (sleep) and pathological (SWDs) neuronal firing. Specifically, in the thalamus and possibly the neocortex, T-type channel activity facilitates rebound bursting. Although T-type channels are robustly expressed in the hippocampus, their functional role had not been identified in the form of rebound bursting; they are believed to participate in dendritic calcium currents. However, a very recent study investigating alterations in CA1 cell firing in response to a single episode of status epilepticus has shown that T-type channels are responsible in converting normal, regular, CA1 cell firing to bursting [380]. This *de novo* bursting mechanism is facilitated by an alteration in distal dendritic T-type currents that interplay with somatic backpropagating spikes to generate epileptiform bursting activity. The precise mechanism for this alteration is unknown but it is speculated that it involves increases in $Ca_v3.2$ expression (including alternate splice variants) and/or channel modulation [389]. This finding has important implications for HFOs that are most robustly generated in the hippocampus in the presence of an underlying epileptic condition. Indeed, much evidence supports the notion that interictal (epileptiform) discharges are generated by clusters of bursting neurons. Therefore, the involvement of T-type channels as contributors to HFO generation offers new avenues for further research. As introduced in section 3.1.2, HFOs are an ensemble phenomenon generated by rapid changes in neuronal synchrony. Therefore, their mode of generation can involve a spectrum of cellular mechanisms. With regards to our findings concerning prion proteins, in addition to increased NMDA currents, seizure-like events in PrP-null mice exhibit greater HFOs. Moreover, NMDA receptors are particularly involved in hippocampal HFO generation [258]. Therefore, modulation of NMDA receptor function via endogenous prion protein may also have a role in seizure-related processes.

5.2.1   Future Directions: Elucidating the Role of $Ca_v3.2$ Mutations in Seizure Genesis

Mutations in $Ca_v3.2$ Channels Associated with IGEs. In the study of $Ca_v3.2$ mutations associated with IGEs I observed minimal alterations in channel gating. However, as confirmed by other studies, biophysically silent mutations do not equate to a lack of functional consequences. Experimental evidence suggests that mutations can affect channel membrane expression and can also be involved in affecting alternate splicing of the native CACNA1H gene. Furthermore, it is evident that different T-type channel isoforms are preferentially expressed in different cells types in the thalamus and neocortex, which most likely correlates with different firing properties of these neurons. The following future experiments may serve to enhance our understanding of $Ca_v3.2$ mutations and the putative functional consequences in relevance to seizures.

Transient transfection of channel variants into a neuronal background - perhaps primary cortical cultures and/or dissociated thalamocortical neurons, in order to assess possible biophysical changes in a neuronal background. The channel constructs could also be tagged with a fluorophore and the overexpressed mutant, when compared with WT, can be used to examine differential targeting. This may perhaps be very interesting for mutations in the I-II linker that have been show to alter membrane channel expression, which may have different effects in a neuronal background.

Knock-in experiments for mutants that show the greatest functional effects. It would be ideal if this could be done in a temporal (e.g. neonatal) and tissue specific (thalamus and/or neocortex) manner. The knockin animals would then be examined using slice and *in vivo* electrophysiology and perhaps imaging to search for possible changes in function and channel trafficking.

In the case of mutations in the C-terminus of the channel, it would be interesting to search for potential intracellular targets (i.e. involved in cell signalling) that may be affected or that can bind to the channel as a result of the altered amino acid sequence.

It would be ideal if one could explore the precise functional consequences of each Ca_v3 isoform on neuronal activity in the neocortex, thalamus, and hippocampus. With the prospect of future selective T-type channel blockers, a great many number of electrophysiological ex-

periments can be performed to provide a better understanding of this topic. In this context, the effect of different T-type isoforms could be investigated in relation to neuronal bursting and possibly HFO generation.

It is also clear that larger and more diverse patient population studies are required to further identify potential families that exhibit T-type channel mutations that clearly segregate with the epileptic phenotype. One can speculate that it would be such mutations that offer the greatest probability of finding a causative relation between channel variants and an underlying epileptic phenotype.

5.2.2 Future Directions: Preictal Changes in HFOs and their Dissociation with Seizure Type

Our study of HFOs both *in vitro* and in patients with epilepsy suggest that they are localized to the seizure onset zone and seem to be surrogate markers of epileptogenicity in seizure generating brain regions. Moreover, HFOs exhibit temporal changes during the immediate preictal epoch that seem to be indicative of rapid changes in synchrony that culminate in the ictal event. One aim for this research was to ultimately utilize HFOs to improve seizure localization in patients with difficult to characterize epilepsy, thereby guiding treatment. A second aim was to better characterize pre-seizure changes. There is a body of evidence that suggest that there exists a "preictal state" - a state of brain activity in the immediate time leading up to seizure when the affected neuronal network is in the process of making a transition to the seizure state. Alterations in network synchrony are in their most dynamic form during this state and it is not entirely clear whether the transition to seizure is a gradual process or a sudden transition between the two states. Nonetheless, the preictal state represents an intermediate state and due to this it represents a point in system dynamics when it is most venerable to perturbation. Therefore, better definition of the preictal state may allow for the use of transient treatment modalities such as electrical deep brain stimulation and/or focal pharmacological delivery.

Our study of HFOs in patients with epilepsy needs to be expanded to include more patients. It also needs to include analysis of all EEG contacts, which is significant computational undertaking. Our findings seem to suggest that HFOs are present in more contacts in relation to the

size of the affected region generating epileptiform activity. This topic needs to be expanded on by analyzing data for more patients with large (e.g. 128 electrode) grid implantations. HFOs have mainly been studied in temporal lobe epilepsy. It is of critical importance to examine HFO dynamics for other seizure types, specifically the more difficult to treat forms such as neocortical epilepsy. This is of great importance if HFOs, as surrogate markers of epilepto-genicity, are to have implications for clinical practice. HFOs are poorly understood in pediatric patient populations. Analysis of EEG obtained in children undergoing seizure monitoring is required to assess their utility in localizing seizures in this patient population.

5.3   Prion Proteins as an Important Endogenous Synaptic Protein

Our results show a novel link between PrP and NMDA receptor function. In the absence of PrP, NMDA receptor currents are greatly augmented. Specifically, NMDA receptor affinity for ligand is enhanced and activated receptor channels show very prolonged deactivation ki-netics; together these changes support greater calcium entry upon receptor activation. The precise mechanism for this alteration is unknown, however it may include: a change involv-ing allosteric modulation of the NMDA receptor or its ligand or cofactor binding sites, altered regulation by kinases and/or phosphatases, and also possibly changes in the composition of NMDA receptor subunits. The augmented receptor currents result in greater excitotoxicity in PrP-null mice. Given that in the disease state, much of the endogenous PrP is converted to the PrP-Sc form, which is believed to be misfolded and insoluble - it would be reasonable to consider the infected animal or human, in some capacity, as either a complete or partial knockout. Therefore, NMDA-mediated excitotoxic cell death may be an additional cause for neurodegeneration.

5.3.1   Future Directions

In order to further test the involvement of PrP in altering the functional composition of NMDA receptors (e.g. increased functional NR1/NR2D), RNAi experiments can be carried out tar-geting NR2A, NR2B, and NR2D in order to evaluate which of these can abolish prolonged receptor deactivation in PrP-null mice. If NR2D is involved, the RNAi experiment should

rescue, to some level, the WT phenotype.

The src family of tyrosine kinases may be affected or triggered in the absence of PrP resulting in augmented NMDA function. Experiments can be performed with both src kinase inhibitors and activators to assess the role of these proteins in bringing about the observed NMDA receptor kinetics.

At present, I do not believe that the glycine binding site is affected by the lack of PrP, however it is possible that glycine affinity is altered, thus resulting in potentiated NMDA currents. Experiments can be performed in WT neurons with even greater glycine concentrations to test how NMDA receptor currents may be affected.

Current clamp and calcium imaging experiments can be performed in neuronal cultures in order to assess the effect of augmented NMDA currents on neuronal and network excitability. Indeed, at present my experimental findings do now show a direct alteration of NMDA currents at the level of slice recordings, although the zero-magnesium data are highly suggestive. It would be useful to directly address this issue with whole-cell voltage clamp recordings using QX-314 in the patch pipette while recording evoked (via Scheffer collaterals) potentials at different holding potentials that selectively allow for AMPA/kainate vs. NMDA currents. In addition, the AMPA-to-NMDA ratio can be computed for the currents in both slice and neuronal culture recordings in order to directly control for slice-to-slice and culture-to-culture variations in cell responses.

It would be very interesting to perform calcium imaging, perhaps in the isolated hippocampus, using patch clamp and two-photon experimental modalities. Two-photon imaging can also be used to visualize calcium dynamics in spines (both *in vitro* and *in vivo*) to further assess the functional consequences of PrP removal on synaptic NMDA currents. The increased amplitude and prolonged deactivation kinetics need to be validated *in vivo*.

In the context of our excitotoxicity experiments, it would be important to show that the extensive cell death can be reduced by application of APV or MK-801. Moreover, in light of the recent findings suggesting the participation of AMPA receptors, it would be intriguing to also isolate possible contributions of AMPA receptor activation as possibly triggered during NMDA-mediated cell death. Neuronal loss in the context of apoptosis can also be examined

with more specific markers in addition to the TUNEL staining (e.g. caspase-3 staining). Also, the response to NMDA should be assayed *in vivo* and perhaps in hippocampal slice cultures. For *in vivo* experiments, NMDA would be focally injected in one hippocampus (vehicle in the other) and neuronal loss assessed by staining techniques.

Historically, the study of seizures and epileptic patients have been an avenue for the exploration of normal brain function. The described studies in this dissertation concerning three separate parameters affecting neuronal excitability and seizures aim to follow through a similar path, where the knowledge gained can be applied to advance physiological understanding.

Appendix A

Ethics Approval for EEG Study

FACULTY OF MEDICINE | UNIVERSITY OF CALGARY

November 7, 2006

Dr. P. Federico
Department of Clinical Neurosciences
FMC
Calgary, Alberta

OFFICE OF MEDICAL BIOETHICS
Room 93, Heritage Medical Research Bldg
3330 Hospital Drive NW
Calgary, AB, Canada T2N 4N1
Telephone: (403) 220-7990
Fax: (403) 283-8524
Email: omb@ucalgary.ca

Dear Dr. Federico:

Re: Detection and Analysis of High Frequency Components in Epileptiform EEG

      Sub Study: Multimodal Analysis of the Pre-ictal State

      Grant ID: 18252

Your request to modify the above-named research protocol and the related informed consent form has been reviewed and approved.

I am pleased to advise you that it is permissible for you to use the revised protocol including the revised adult consent form, Version 1.0 dated August 2006, based on the information contained in your correspondence of August 3, 2006.

A progress report concerning this study is required annually, from the date of the original approval 2005-03-03. The report should contain information concerning:

(i)   the number of subjects recruited;
(ii)   a description of any protocol modification;
(iii) any unusual and/or severe complications, adverse events or unanticipated problems involving risks to subjects or others, withdrawal of subjects from the research, or complaints about the research;
(iv)   a summary of any recent literature, finding, or other relevant information, especially information about risks associated with the research;
(v)   a copy of the current informed consent form;
(vi)   the expected date of termination of this project;

Thank you for the attention which I know you will bring to these matters.

Yours sincerely,

Glenys Godlovitch (BA(Hons) LLB, PhD.
Chair, Conjoint Health Research Ethics Board
GG/eb

c.c.   Adult Research Committee

Figure A.1: Ethics approval for patient-based EEG study.

Appendix B

Journal Copyright Approvals

Copyright Permission Policy

ASBMB Journals
Journal of Biological Chemistry
Molecular and Cellular Proteomics
Journal of Lipid Research
Biochemistry and Molecular Biology Education
ASBMB Today

ASBMB does not charge for and grants use without requiring your copyright permission request for:

- Original authors wanting to reproduce portions of their own work; or to republish their material in not-for-profit formats or venues.
- Students wanting to reproduce or republish their work for educational purposes.
- Students using other authors' material for their theses.
- Reproduction or republication of abstracts only.
- Photocopying up to 5 copies for personal use.
- Non-profit educational institutions making multiple photocopies of articles for classroom use; all such reproduction must utilize institutionally owned equipment for this purpose.

Use of copyrighted material requires proper citation.

For all other uses, contact Copyright Clearance Center.

Figure B.1: Copyright approval from *Journal of Biological Chemistry*.

Houman Khosravani, PhD
Hotchkiss Brain Institute,
Faculty of Medicine,
University of Calgary
3330 Hospital Drive NW
Calgary, Alberta, Canada
houman@ucalgary.ca
Fax. 403-547-4172

Monday April 2, 2007

Farah Alladin, Production Editor
Annals of Neurology,
John Wiley & Sons
111 River Street
Hoboken, NJ 07030 USA
Fax. 201-748-6052

Re: Permission to use figures

Dear Ms. Alladin,

Greetings and I hope that you are doing well. I am not certain if you are the correct person at *Annals of Neurology* to ask regarding my question. I have just completed my PhD and would like to use figures from my previous manuscript (*Khosravani H, Bladen C, Parker DB, Snutch TP, McRory JE, Zamponi GW. Effects of Cav3.2 channel mutations linked to idiopathic generalized epilepsy. Ann Neurol. 2005 May;57(5):745-9*) in the thesis. How do I go about obtaining permission to use the figures in my thesis? Do I need permission from *Annals of Neurology?*

Thank you in advance,
Houman Khosravani.

PERMISSION GRANTED
BY: _____ 4/5/07
Global Rights Dept., John Wiley & Sons, Inc.

NOTE: No rights are granted to use content that appears in the work with credit to another source

Figure B.2: Copyright approval from *Annals of Neurology*.

Penny Ripka

From:	Houman Khosravani [houman@ucalgary.ca]
Sent:	Saturday, March 31, 2007 12:59 AM
To:	Penny Ripka
Cc:	Houman Khosravani
Subject:	permission to use figures in PhD thesis

Dear Ms. Ripka,

Greetings and I hope that you are doing well. I am not certain if you are the correct person at *Physiological Reviews* to ask regarding my question. I have just completed my PhD and would like to use figures from my previous manuscript (Khosravani H, Zamponi GW. Voltage-gated calcium channels and idiopathic generalized epilepsies. Physiol Rev. 2006 Jul;86(3):941-66) in the thesis. How do I go about obtaining permission to use the figures in my thesis? Do I need permission from *Physiological Reviews*? Figures 1-6

Thank you in advance,
Houman.

```
--
Houman Khosravani, PhD
Department of Physiology & Biophysics and
Department of Clinical Neurosciences,
University of Calgary
172HMRB, 3330 Hospital Dr. NW
Calgary, Alberta, Canada
T2N 4N1
Tel. 403.835.0870
Fax. 403.547.4172
Email. houman@ucalgary.ca
```

APPROVED
By PRipka at 8:28 am, Apr 02, 2007

THE AMERICAN PHYSIOLOGICAL SOCIETY
9650 Rockville Pike, Bethesda, MD 20814-3991

Permission is granted for use of the material specified above provided the publication is credited as the source, including the words "used with permission."

Margaret Reich

Publications Manager & Executive Editor

Figure B.3: Copyright approval from *Physiological Reviews*.

Epilepsia

Published on behalf of the International League Against Epilepsy (ILAE)

Edited by:
Philip A. Schwartzkroin, PhD, and Simon D. Shorvon, MA MD FRCP

Print ISSN: 0013-9580
Online ISSN: 1528-1167
Frequency: Monthly
Current Volume: 48 / 2007
ISI Journal Citation Reports® Ranking: 2005: 23/148 (Clinical Neurology)
Impact Factor: 3.227

Permissions and Copyright Information

Reprinting

Requests for permission to reprint material from this journal should be addressed to:

Journals Rights & Permissions Controller
Blackwell Publishing
9600 Garsington Road
Oxford OX4 2DQ
UK
Email: JournalsRights@oxon.blackwellpublishing.com

Please be sure to include the following information:

- The title, author(s) and page extent of the article you wish to republish, or, in the case where you do not wish to reproduce the whole article, details of which section(s), with a word count where relevant.
- The journal title, volume/issue number and year of publication in which the article appeared, and the page numbers of the article.
- The title, editor(s)/author(s), price, print run, publication date and publisher of the publication in which you wish to reprint the Journal material.
- If the material is being edited or amended in any way, a copy of the final material as it will appear in your publication.
- Contact details for yourself, including a postal address.

If you wish to include your own article (or an amended version of it) in a volume of which you are the editor or co-editor, prior permission is not required, but the usual acknowledgements should be made.

Figure B.4: Copyright approval from *Epilepsia*.

Bibliography

[1] A. Abosch, N. Bernasconi, W. Boling, M. Jones-Gotman, N. Poulin, F. Dubeau, F. Andermann, and A. Olivier. Factors predictive of suboptimal seizure control following selective amygdalohippocampectomy. *J Neurosurg*, 97(5):1142–51, 2002.

[2] M. E. Adams, R. A. Myers, J. S. Imperial, and B. M. Olivera. Toxityping rat brain calcium channels with omega-toxins from spider and cone snail venoms. *Biochemistry*, 32(47):12566–70, 1993.

[3] Commission on Classification Against and Terminology of the International League. Proposal for revised classification of epilepsies and epileptic syndromes. epilepsy. *Epilepsia*, 30(4):389–99, 1989.

[4] T. Akiyama, H. Otsubo, A. Ochi, E. Z. Galicia, S. K. Weiss, E. J. Donner, J. T. Rutka, and 3rd Snead, O. C. Topographic movie of ictal high-frequency oscillations on the brain surface using subdural eeg in neocortical epilepsy. *Epilepsia*, 47(11):1953–7, 2006.

[5] T. Akiyama, H. Otsubo, A. Ochi, T. Ishiguro, G. Kadokura, R. Ramachandrannair, S. K. Weiss, J. T. Rutka, and 3rd Carter Snead, O. Focal cortical high-frequency oscillations trigger epileptic spasms: confirmation by digital video subdural eeg. *Clin Neurophysiol*, 116(12):2819–25, 2005.

[6] P. J. Allen, D. R. Fish, and S. J. Smith. Very high-frequency rhythmic activity during seeg suppression in frontal lobe epilepsy. *Electroencephalogr Clin Neurophysiol*, 82(2):155–9, 1992.

[7] C. Altier, H. Khosravani, R.M. Evans, S. Hameed, J.B. Peloquin, B.A. Vartian, L. Chen, A.M. Beedle, S.S. Ferguson, A. Mezghrani, S.J. Dubel, E. Bourinet, J.E. McRory, and G.W. Zamponi. Orl1 receptor-mediated internalization of n-type calcium channels. *Nat Neurosci*, 9(1):31–40, 2006.

[8] F. Andermann and S. F. Berkovic. Idiopathic generalized epilepsy with generalized and other seizures in adolescence. *Epilepsia*, 42(3):317–20, 2001.

[9] J. Arikkath and K. P. Campbell. Auxiliary subunits: essential components of the voltage-gated calcium channel complex. *Curr Opin Neurobiol*, 13(3):298–307, 2003.

[10] M. Arundine and M. Tymianski. Molecular mechanisms of glutamate-dependent neurodegeneration in ischemia and traumatic brain injury. *Cell Mol Life Sci*, 61(6):657–668, 2004.

[11] H. Bading, D. D. Ginty, and M. E. Greenberg. Regulation of gene expression in hippocampal neurons by distinct calcium signaling pathways. *Science*, 260(5105):181–6, 1993.

[12] S. Baulac, G. Huberfeld, I. Gourfinkel-An, G. Mitropoulou, A. Beranger, J. F. Prud'homme, M. Baulac, A. Brice, R. Bruzzone, and E. LeGuern. First genetic evidence of *gaba_A* receptor dysfunction in epilepsy: a mutation in the gamma2-subunit gene. *Nat Genet*, 28(1):46–8, 2001.

[13] A.J. Bean. *Protein trafficking in neurons*. Academic Press, 2007.

[14] S. F. Berkovic. *in Epilepsy : a comprehensive textbook by Engel J Jr., Pedley T.A.* Lippincott-Williams & Wilkins, Philadelphia, 1998.

[15] C. Bernard, R. Cossart, J.C. Hirsch, M. Esclapez, and Y. Ben-Ari. What is gabaergic inhibition? how is it modified in epilepsy? *Epilepsia*, 41 Suppl 6:S90–5, 2000.

[16] E. Biasini, T. Massignan, L. Fioriti, V. Rossi, S. Dossena, M. Salmona, G. Forloni, V. Bonetto, and R. Chiesa. Analysis of the cerebellar proteome in a transgenic mouse model of inherited prion disease reveals preclinical alteration of calcineurin activity. *Proteomics*, 6(9):2823–2834, 2006.

[17] D. Bichet, V. Cornet, S. Geib, E. Carlier, S. Volsen, T. Hoshi, Y. Mori, and M. De Waard. The i-ii loop of the ca^{2+} channel alpha1 subunit contains an endoplasmic reticulum retention signal antagonized by the beta subunit. *Neuron*, 25(1):177–90, 2000.

[18] 3rd Black, J. L. The voltage-gated calcium channel gamma subunits: a review of the literature. *J Bioenerg Biomembr*, 35(6):649–60, 2003.

[19] H. Blumenfeld. The thalamus and seizures. *Arch Neurol*, 59(1):135–7, 2002.

[20] H. Blumenfeld. Cellular and network mechanisms of spike-wave seizures. *Epilepsia*, 46 Suppl 9:21–33, 2005.

[21] Y. Bounhar, Y. Zhang, C.G. Goodyer, and A. LeBlanc. Prion protein protects human neurons against bax-mediated apoptosis. *J Biol Chem*, 276(42):39145–39149, 2001.

[22] E. Bourinet, T. W. Soong, K. Sutton, S. Slaymaker, E. Mathews, A. Monteil, G. W. Zamponi, J. Nargeot, and T. P. Snutch. Splicing of alpha 1a subunit gene generates phenotypic variants of p- and q-type calcium channels. *Nat Neurosci*, 2(5):407–15, 1999.

[23] E. Bourinet, S. C. Stotz, R. L. Spaetgens, G. Dayanithi, J. Lemos, J. Nargeot, and G. W. Zamponi. Interaction of snx482 with domains iii and iv inhibits activation gating of alpha(1e) (ca(v)2.3) calcium channels. *Biophys J*, 81(1):79–88, 2001.

[24] A. Bragin, Jr. Engel, J., C. L. Wilson, I. Fried, and G. Buzsaki. High-frequency oscillations in human brain. *Hippocampus*, 9(2):137–42, 1999.

[25] A. Bragin, Jr. Engel, J., C. L. Wilson, I. Fried, and G. W. Mathern. Hippocampal and entorhinal cortex high-frequency oscillations (100-500 hz) in human epileptic brain and in kainic acid–treated rats with chronic seizures. *Epilepsia*, 40(2):127–37, 1999.

[26] A. Bragin, Jr. Engel, J., C. L. Wilson, E. Vizentin, and G. W. Mathern. Electrophysiologic analysis of a chronic seizure model after unilateral hippocampal ka injection. *Epilepsia*, 40(9):1210–21, 1999.

[27] A. Bragin, I. Mody, C. L. Wilson, and Jr. Engel, J. Local generation of fast ripples in epileptic brain. *J Neurosci*, 22(5):2012–21, 2002.

[28] A. Bragin, C. L. Wilson, J. Almajano, I. Mody, and Jr. Engel, J. High-frequency oscillations after status epilepticus: Epileptogenesis and seizure genesis. *Epilepsia*, 45(9):1017–23, 2004.

[29] A. Bragin, C. L. Wilson, and J. Engel. Spatial stability over time of brain areas generating fast ripples in the epileptic rat. *Epilepsia*, 44(9):1233–7, 2003.

[30] A. Bragin, C. L. Wilson, and Jr. Engel, J. Chronic epileptogenesis requires development of a network of pathologically interconnected neuron clusters: a hypothesis. *Epilepsia*, 41 Suppl 6:S144–52, 2000.

[31] A. Bragin, C. L. Wilson, R. J. Staba, M. Reddick, I. Fried, and Jr. Engel, J. Interictal high-frequency oscillations (80-500 hz) in the human epileptic brain: entorhinal cortex. *Ann Neurol*, 52(4):407–15, 2002.

[32] D.R. Brown. Prion and prejudice: normal protein and the synapse. *Trends Neurosci*, 24(2):85–90, 2001.

[33] D.R. Brown, J.W. Herms, B. Schmidt, and H.A. Kretzschmar. Prp and beta-amyloid fragments activate different neurotoxic mechanisms in cultured mouse cells. *Eur J Neurosci*, 9(6):1162–1169, 1997.

[34] D.R. Brown and C.M. Mohn. Astrocytic glutamate uptake and prion protein expression. *Glia*, 25(3):282–292, 1999.

[35] D. L. Browne, S. T. Gancher, J. G. Nutt, E. R. Brunt, E. A. Smith, P. Kramer, and M. Litt. Episodic ataxia/myokymia syndrome is associated with point mutations in the human potassium channel gene, kcna1. *Nat Genet*, 8(2):136–40, 1994.

[36] N. Brunel and X. J. Wang. What determines the frequency of fast network oscillations with irregular neural discharges? i. synaptic dynamics and excitation-inhibition balance. *J Neurophysiol*, 90(1):415–30, 2003.

[37] T. Budde, F. Sieg, K. H. Braunewell, E. D. Gundelfinger, and H. C. Pape. ca^{2+}-induced ca^{2+} release supports the relay mode of activity in thalamocortical cells. *Neuron*, 26(2):483–92, 2000.

[38] H. Bueler, M. Fischer, Y. Lang, H. Bluethmann, H.P. Lipp, S.J. DeArmond, S.B. Prusiner, M. Aguet, and C. Weissmann. Normal development and behaviour of mice

lacking the neuronal cell-surface prp protein. *Nature*, 356(6370):577–582, 1992.

[39] D. E. Burgess, O. Crawford, B. P. Delisle, and J. Satin. Mechanism of inactivation gating of human t-type (low-voltage activated) calcium channels. *Biophys J*, 82(4):1894–906, 2002.

[40] S. P. Burke, M. E. Adams, and C. P. Taylor. Inhibition of endogenous glutamate release from hippocampal tissue by ca^{2+} channel toxins. *Eur J Pharmacol*, 238(2-3):383–6, 1993.

[41] G. Buzsaki. Memory consolidation during sleep: a neurophysiological perspective. *J Sleep Res*, 7 Suppl 1:17–23, 1998.

[42] G. Buzsaki, Z. Horvath, R. Urioste, J. Hetke, and K. Wise. High-frequency network oscillation in the hippocampus. *Science*, 256(5059):1025–7, 1992.

[43] S. J. Caddick, C. Wang, C. F. Fletcher, N. A. Jenkins, N. G. Copeland, and D. A. Hosford. Excitatory but not inhibitory synaptic transmission is reduced in lethargic (cacnb4(lh)) and tottering (cacna1atg) mouse thalami. *J Neurophysiol*, 81(5):2066–74, 1999.

[44] C. Canti, M. Nieto-Rostro, I. Foucault, F. Heblich, J. Wratten, M. W. Richards, J. Hendrich, L. Douglas, K. M. Page, A. Davies, and A. C. Dolphin. The metal-ion-dependent adhesion site in the von willebrand factor-a domain of alpha2delta subunits is key to trafficking voltage-gated ca^{2+} channels. *Proc Natl Acad Sci U S A*, 102(32):11230–5, 2005.

[45] A. Carleton, P. Tremblay, J.D. Vincent, and P.M. Lledo. Dose-dependent, prion protein (prp)-mediated facilitation of excitatory synaptic transmission in the mouse hippocampus. *Pflugers Arch*, 442(2):223–229, 2001.

[46] W. A. Catterall. Structure and function of voltage-gated sodium and calcium channels. *Curr Opin Neurobiol*, 1(1):5–13, 1991.

[47] W. A. Catterall. Structure and modulation of na+ and ca^{2+} channels. *Ann N Y Acad Sci*, 707:1–19, 1993.

[48] W. A. Catterall. Structure and regulation of voltage-gated ca^{2+} channels. *Annu Rev Cell Dev Biol*, 16:521–55, 2000.

[49] W. A. Catterall, E. Perez-Reyes, T. P. Snutch, and J. Striessnig. International union of pharmacology. xlviii. nomenclature and structure-function relationships of voltage-gated calcium channels. *Pharmacol Rev*, 57(4):411–25, 2005.

[50] C. Charlier, N. A. Singh, S. G. Ryan, T. B. Lewis, B. E. Reus, R. J. Leach, and M. Leppert. A pore mutation in a novel kqt-like potassium channel gene in an idiopathic epilepsy family. *Nat Genet*, 18(1):53–5, 1998.

[51] J. Chemin, A. Monteil, E. Perez-Reyes, E. Bourinet, J. Nargeot, and P. Lory. Specific contribution of human t-type calcium channel isotypes (alpha(1g), alpha(1h) and alpha(1i)) to neuronal excitability. *J Physiol*, 540(Pt 1):3–14, 2002.

[52] L. Chen, D. M. Chetkovich, R. S. Petralia, N. T. Sweeney, Y. Kawasaki, R. J. Wenthold, D. S. Bredt, and R. A. Nicoll. Stargazin regulates synaptic targeting of ampa receptors by two distinct mechanisms. *Nature*, 408(6815):936–43, 2000.

[53] S. Chen, A. Mange, L. Dong, S. Lehmann, and M. Schachner. Prion protein as trans-interacting partner for neurons is involved in neurite outgrowth and neuronal survival. *Mol Cell Neurosci*, 22(2):227–233, 2003.

[54] Y. Chen, J. Lu, H. Pan, Y. Zhang, H. Wu, K. Xu, X. Liu, Y. Jiang, X. Bao, Z. Yao, K. Ding, W. H. Lo, B. Qiang, P. Chan, Y. Shen, and X. Wu. Association between genetic variation of cacna1h and childhood absence epilepsy. *Ann Neurol*, 54(2):239–43, 2003.

[55] Y. H. Chen, M. H. Li, Y. Zhang, L. L. He, Y. Yamada, A. Fitzmaurice, Y. Shen, H. Zhang, L. Tong, and J. Yang. Structural basis of the alpha1-beta subunit interaction of voltage-gated ca^{2+} channels. *Nature*, 429(6992):675–80, 2004.

[56] L.B. Chiarini, A.R. Freitas, S.M. Zanata, R.R. Brentani, V.R. Martins, and R. Linden. Cellular prion protein transduces neuroprotective signals. *EMBO J*, 21(13):3317–3326, 2002.

[57] A. J. Chien, X. Zhao, R. E. Shirokov, T. S. Puri, C. F. Chang, D. Sun, E. Rios, and M. M. Hosey. Roles of a membrane-localized beta subunit in the formation and targeting of functional l-type ca^{2+} channels. *J Biol Chem*, 270(50):30036–44, 1995.

[58] J. J. Chrobak and G. Buzsaki. Selective activation of deep layer (v-vi) retrohippocampal cortical neurons during hippocampal sharp waves in the behaving rat. *J Neurosci*, 14(10):6160–70, 1994.

[59] R. S. Chuang, H. Jaffe, L. Cribbs, E. Perez-Reyes, and K. J. Swartz. Inhibition of t-type voltage-gated calcium channels by a new scorpion toxin. *Nat Neurosci*, 1(8):668–74, 1998.

[60] L. Claes, J. Del-Favero, B. Ceulemans, L. Lagae, C. Van Broeckhoven, and P. De Jonghe. De novo mutations in the sodium-channel gene scn1a cause severe myoclonic epilepsy of infancy. *Am J Hum Genet*, 68(6):1327–32, 2001.

[61] M. A. Colicos, B. E. Collins, M. J. Sailor, and Y. Goda. Remodeling of synaptic actin induced by photoconductive stimulation. *Cell*, 107(5):605–16, 2001.

[62] S.B. Colling, J. Collinge, and J.G. Jefferys. Hippocampal slices from prion protein null mice: disrupted ca(2+)-activated k+ currents. *Neurosci Lett*, 209(1):49–52, 1996.

[63] S.B. Colling, M. Khana, J. Collinge, and J.G. Jefferys. Mossy fibre reorganization in the hippocampus of prion protein null mice. *Brain Res*, 755(1):28–35, 1997.

[64] J. Collinge, M.A. Whittington, K.C. Sidle, C.J. Smith, M.S. Palmer, A.R. Clarke, and J.G. Jefferys. Prion protein is necessary for normal synaptic function. *Nature*, 370(6487):295–297, 1994.

[65] D. Contreras, A. Destexhe, and M. Steriade. Intracellular and computational characterization of the intracortical inhibitory control of synchronized thalamic inputs in vivo. *J*

Neurophysiol, 78(1):335–50, 1997.

[66] D. Contreras and M. Steriade. Spindle oscillation in cats: the role of corticothalamic feedback in a thalamically generated rhythm. *J Physiol*, 490 (Pt 1):159–79, 1996.

[67] R. Cossart, C. Bernard, and Y. Ben-Ari. Multiple facets of gabaergic neurons and synapses: multiple fates of gaba signalling in epilepsies. *Trends Neurosci*, 28(2):108–15, 2005.

[68] P. Cossette, L. Liu, K. Brisebois, H. Dong, A. Lortie, M. Vanasse, J. M. Saint-Hilaire, L. Carmant, A. Verner, W. Y. Lu, Y. T. Wang, and G. A. Rouleau. Mutation of gabra1 in an autosomal dominant form of juvenile myoclonic epilepsy. *Nat Genet*, 31(2):184–9, 2002.

[69] D. A. Coulter, J. R. Huguenard, and D. A. Prince. Calcium currents in rat thalamocortical relay neurones: kinetic properties of the transient, low-threshold current. *J Physiol*, 414:587–604, 1989.

[70] P.J. Craig, R.E. Beattie, E.A. Folly, M.D. Banerjee, M.B. Reeves, J.V. Priestley, S.L. Carney, E. Sher, E. Perez-Reyes, and S.G. Volsen. Distribution of the voltage-dependent calcium channel alpha1g subunit mrna and protein throughout the mature rat brain. *Eur J Neurosci*, 11(8):2949–2964, 1999.

[71] J.R. Criado, M. Sanchez-Alavez, B. Conti, J.L. Giacchino, D.N. Wills, S.J. Henriksen, R. Race, J.C. Manson, B. Chesebro, and M.B. Oldstone. Mice devoid of prion protein have cognitive deficits that are rescued by reconstitution of prp in neurons. *Neurobiol Dis*, 19(1-2):255–265, 2005.

[72] L. L. Cribbs, J. H. Lee, J. Yang, J. Satin, Y. Zhang, A. Daud, J. Barclay, M. P. Williamson, M. Fox, M. Rees, and E. Perez-Reyes. Cloning and characterization of alpha1h from human heart, a member of the t-type ca^{2+} channel gene family. *Circ Res*, 83(1):103–9, 1998.

[73] V. Crunelli, S. Lightowler, and C. E. Pollard. A t-type ca^{2+} current underlies low-threshold ca^{2+} potentials in cells of the cat and rat lateral geniculate nucleus. *J Physiol*,

413:543–61, 1989.

[74] S. Cull-Candy, S. Brickley, and M. Farrant. Nmda receptor subunits: diversity, development and disease. *Curr Opin Neurobiol*, 11(3):327–35, 2001.

[75] S.G. Cull-Candy and D.N. Leszkiewicz. Role of distinct nmda receptor subtypes at central synapses. *Sci STKE*, 255(255):re16, 2004.

[76] M.O. Cunningham, D.M. Halliday, C.H. Davies, R.D. Traub, T.E. Buhl Tl, and M.A. Whittington. Coexistence of gamma and high-frequency oscillations in rat medial entorhinal cortex in vitro. *J Physiol*, 559(Pt 2):347–53, 2004.

[77] G. Curio. Linking 600-hz "spikelike" eeg/meg wavelets ("sigma-bursts") to cellular substrates: concepts and caveats. *J Clin Neurophysiol*, 17(4):377–96, 2000.

[78] G. Curio, B. M. Mackert, M. Burghoff, R. Koetitz, K. Abraham-Fuchs, and W. Harer. Localization of evoked neuromagnetic 600 hz activity in the cerebral somatosensory system. *Electroencephalogr Clin Neurophysiol*, 91(6):483–7, 1994.

[79] J. Curtis, M. Errington, T. Bliss, K. Voss, and N. MacLeod. Age-dependent loss of ptp and ltp in the hippocampus of prp-null mice. *Neurobiol Dis*, 13(1):55–62, 2003.

[80] M.B. Dalva, A.C. McClelland, and M.S. Kayser. Cell adhesion molecules: signalling functions at the synapse. *Nat Rev Neurosci*, 8(3):206–220, 2007.

[81] K.S. De Jongh, C. Warner, and W A. Catterall. Subunits of purified calcium channels. alpha 2 and delta are encoded by the same gene. *J Biol Chem*, 265(25):14738–41, 1990.

[82] E. de la Pena and E. Geijo-Barrientos. Laminar localization, morphology, and physiological properties of pyramidal neurons that have the low-threshold calcium current in the guinea-pig medial frontal cortex. *J Neurosci*, 16(17):5301–11, 1996.

[83] E. de la Pena and E. Geijo-Barrientos. Participation of low-threshold calcium spikes in excitatory synaptic transmission in guinea pig medial frontal cortex. *Eur J Neurosci*, 12(5):1679–86, 2000.

[84] M. De Waard, J. Hering, N. Weiss, and A. Feltz. How do g proteins directly control neuronal ca^{2+} channel function? *Trends Pharmacol Sci*, 26(8):427–36, 2005.

[85] K. Dedek, B. Kunath, C. Kananura, U. Reuner, T. J. Jentsch, and O. K. Steinlein. Myokymia and neonatal epilepsy caused by a mutation in the voltage sensor of the kcnq2 k+ channel. *Proc Natl Acad Sci U S A*, 98(21):12272–7, 2001.

[86] C. Denier, A. Ducros, A. Durr, B. Eymard, B. Chassande, and E. Tournier-Lasserve. Missense cacna1a mutation causing episodic ataxia type 2. *Arch Neurol*, 58(2):292–5, 2001.

[87] A. Destexhe, D. Contreras, M. Steriade, T. J. Sejnowski, and J. R. Huguenard. In vivo, in vitro, and computational analysis of dendritic calcium currents in thalamic reticular neurons. *J Neurosci*, 16(1):169–85, 1996.

[88] A. Destexhe, M. Neubig, D. Ulrich, and J. Huguenard. Dendritic low-threshold calcium currents in thalamic relay cells. *J Neurosci*, 18(10):3574–88, 1998.

[89] A. Destexhe and T. J. Sejnowski. The initiation of bursts in thalamic neurons and the cortical control of thalamic sensitivity. *Philos Trans R Soc Lond B Biol Sci*, 357(1428):1649–57, 2002.

[90] A. Destexhe and T. J. Sejnowski. Interactions between membrane conductances underlying thalamocortical slow-wave oscillations. *Physiol Rev*, 83(4):1401–53, 2003.

[91] M.R. Dias da Silva, J.M. Cerutti, C.H. Tengan, G.K. Furuzawa, T.C. Vieira, A.A. Gabbai, and R.M. Maciel. Mutations linked to familial hypokalaemic periodic paralysis in the calcium channel alpha1 subunit gene (cav1.1) are not associated with thyrotoxic hypokalaemic periodic paralysis. *Clin Endocrinol (Oxf)*, 56(3):367–75, 2002.

[92] L. M. Dibbens, H. J. Feng, M. C. Richards, L. A. Harkin, B. L. Hodgson, D. Scott, M. Jenkins, S. Petrou, G. R. Sutherland, I. E. Scheffer, S. F. Berkovic, R. L. Macdonald, and J. C. Mulley. Gabrd encoding a protein for extra- or peri-synaptic gabaa receptors is a susceptibility locus for generalized epilepsies. *Hum Mol Genet*, 13(13):1315–9, 2004.

[93] M. Diez, S.J. DeArmond, D. Groth, S.B. Prusiner, and T. Hokfelt. Decreased mk-801 binding in discrete hippocampal regions of prion-infected mice. *Neurobiol Dis*, 8(4):692–699, 2001.

[94] R. Dingledine. *Brain slices*. Plenum Press, 1984.

[95] R.E. Dolmetsch, U. Pajvani, K. Fife, J.M. Spotts, and M.E. Greenberg. Signaling to the nucleus by an l-type calcium channel-calmodulin complex through the map kinase pathway. *Science*, 294(5541):333–339, 2001.

[96] A. C. Dolphin. Beta subunits of voltage-gated calcium channels. *J Bioenerg Biomembr*, 35(6):599–620, 2003.

[97] A. C. Dolphin. G protein modulation of voltage-gated calcium channels. *Pharmacol Rev*, 55(4):607–27, 2003.

[98] A. C. Dolphin, C. N. Wyatt, J. Richards, R. E. Beattie, P. Craig, J. H. Lee, L. L. Cribbs, S. G. Volsen, and E. Perez-Reyes. The effect of alpha2-delta and other accessory subunits on expression and properties of the calcium channel alpha1g. *J Physiol*, 519 Pt 1:35–45, 1999.

[99] P. A. Doroshenko, A. Woppmann, G. Miljanich, and G. J. Augustine. Pharmacologically distinct presynaptic calcium channels in cerebellar excitatory and inhibitory synapses. *Neuropharmacology*, 36(6):865–72, 1997.

[100] D. A. Doyle, J. Morais Cabral, R. A. Pfuetzner, A. Kuo, J. M. Gulbis, S. L. Cohen, B. T. Chait, and R. MacKinnon. The structure of the potassium channel: molecular basis of k+ conduction and selectivity. *Science*, 280(5360):69–77, 1998.

[101] A. Draguhn, R. D. Traub, A. Bibbig, and D. Schmitz. Ripple (approximately 200-hz) oscillations in temporal structures. *J Clin Neurophysiol*, 17(4):361–76, 2000.

[102] A. Draguhn, R. D. Traub, D. Schmitz, and J. G. Jefferys. Electrical coupling underlies high-frequency oscillations in the hippocampus in vitro. *Nature*, 394(6689):189–92, 1998.

[103] S. J. Dubel, C. Altier, S. Chaumont, P. Lory, E. Bourinet, and J. Nargeot. Plasma membrane expression of t-type calcium channel alpha(1) subunits is modulated by high voltage-activated auxiliary subunits. *J Biol Chem*, 279(28):29263–9, 2004.

[104] S. J. Dubel, T. V. Starr, J. Hell, M. K. Ahlijanian, J. J. Enyeart, W. A. Catterall, and T. P. Snutch. Molecular cloning of the alpha-1 subunit of an omega-conotoxin-sensitive calcium channel. *Proc Natl Acad Sci U S A*, 89(11):5058–62, 1992.

[105] A.W. Dunah, J. Luo, Y.H. Wang, R.P. Yasuda, and B.B. Wolfe. Subunit composition of n-methyl-d-aspartate receptors in the central nervous system that contain the nr2d subunit. *Mol Pharmacol*, 53(3):429–437, 1998.

[106] V. I. Dzhala and K. J. Staley. Transition from interictal to ictal activity in limbic networks in vitro. *J Neurosci*, 23(21):7873–80, 2003.

[107] P. T. Ellinor, J. Yang, W. A. Sather, J. F. Zhang, and R. W. Tsien. ca^{2+} channel selectivity at a single locus for high-affinity ca^{2+} interactions. *Neuron*, 15(5):1121–32, 1995.

[108] Jerome Engel, Timothy A. Pedley, and Jean Aicardi. *Epilepsy: a comprehensive textbook*. Lippincott-Williams & Wilkins, Philadelphia, 1998.

[109] Jr. Engel, J. A proposed diagnostic scheme for people with epileptic seizures and with epilepsy: report of the ilae task force on classification and terminology. *Epilepsia*, 42(6):796–803, 2001.

[110] A. Erisir, S.C. Van Horn, M.E. Bickford, and S.M. Sherman. Immunocytochemistry and distribution of parabrachial terminals in the lateral geniculate nucleus of the cat: a comparison with corticogeniculate terminals. *J Comp Neurol*, 377(4):535–49, 1997.

[111] A. Erisir, S.C. Van Horn, and S.M. Sherman. Relative numbers of cortical and brainstem inputs to the lateral geniculate nucleus. *Proc Natl Acad Sci U S A*, 94(4):1517–20, 1997.

[112] A. Escayg, B. T. MacDonald, M. H. Meisler, S. Baulac, G. Huberfeld, I. An-Gourfinkel, A. Brice, E. LeGuern, B. Moulard, D. Chaigne, C. Buresi, and A. Malafosse. Mutations

of scn1a, encoding a neuronal sodium channel, in two families with gefs+2. *Nat Genet*, 24(4):343–5, 2000.

[113] Paolo Federico, David F Abbott, Regula S Briellmann, A Simon Harvey, and Graeme D Jackson. Functional MRI of the pre-ictal state. *Brain*, 128(Pt 8):1811–7, 2005.

[114] Z. P. Feng, M. I. Arnot, C. J. Doering, and G. W. Zamponi. Calcium channel beta subunits differentially regulate the inhibition of n-type channels by individual gbeta isoforms. *J Biol Chem*, 276(48):45051–8, 2001.

[115] Z. P. Feng, C. J. Doering, R. J. Winkfein, A. M. Beedle, J. D. Spafford, and G. W. Zamponi. Determinants of inhibition of transiently expressed voltage-gated calcium channels by omega-conotoxins gvia and mviia. *J Biol Chem*, 278(22):20171–8, 2003.

[116] Z. P. Feng, J. Hamid, C. Doering, S. E. Jarvis, G. M. Bosey, E. Bourinet, T. P. Snutch, and G. W. Zamponi. Amino acid residues outside of the pore region contribute to n-type calcium channel permeation. *J Biol Chem*, 276(8):5726–30, 2001.

[117] R. D. Fields, P. R. Lee, and J. E. Cohen. Temporal integration of intracellular ca^{2+} signaling networks in regulating gene expression by action potentials. *Cell Calcium*, 37(5):433–42, 2005.

[118] R. S. Fisher, W. R. Webber, R. P. Lesser, S. Arroyo, and S. Uematsu. High-frequency eeg activity at the start of seizures. *J Clin Neurophysiol*, 9(3):441–8, 1992.

[119] J.G. Fournier, F. Escaig-Haye, and V. Grigoriev. Ultrastructural localization of prion proteins: physiological and pathological implications. *Microsc Res Tech*, 50(1):76–88, 2000.

[120] A. P. Fox, M. C. Nowycky, and R. W. Tsien. Kinetic and pharmacological properties distinguishing three types of calcium currents in chick sensory neurones. *J Physiol*, 394:149–72, 1987.

[121] C.J. Fox, K.I. Russell, Y.T. Wang, and B.R. Christie. Contribution of nr2a and nr2b

nmda subunits to bidirectional synaptic plasticity in the hippocampus in vivo. *Hippocampus*, 16(11):907–915, 2006.

[122] P. Fuentealba and M. Steriade. The reticular nucleus revisited: intrinsic and network properties of a thalamic pacemaker. *Prog Neurobiol*, 75(2):125–41, 2005.

[123] P. Fuentealba, I. Timofeev, M. Bazhenov, T. J. Sejnowski, and M. Steriade. Membrane bistability in thalamic reticular neurons during spindle oscillations. *J Neurophysiol*, 93(1):294–304, 2005.

[124] P. Fuentealba, I. Timofeev, and M. Steriade. Prolonged hyperpolarizing potentials precede spindle oscillations in the thalamic reticular nucleus. *Proc Natl Acad Sci U S A*, 101(26):9816–21, 2004.

[125] D.C. Gajdusek and V. Zigas. Degenerative disease of the central nervous system in new guinea; the endemic occurrence of kuru in the native population. *N Engl J Med*, 257(20):974–978, 1957.

[126] L. Garcia-Dominguez, R. A. Wennberg, W. Gaetz, D. Cheyne, O. C. Snead, and J. L. Perez-Velazquez. Enhanced synchrony in epileptiform activity? local versus distant phase synchronization in generalized seizures. *J Neurosci*, 25(35):8077–84, 2005.

[127] M. Gardiner. Genetics of idiopathic generalized epilepsies. *Epilepsia*, 46 Suppl 9:15–20, 2005.

[128] C. Geisler, N. Brunel, and X. J. Wang. Contributions of intrinsic membrane dynamics to fast network oscillations with irregular neuronal discharges. *J Neurophysiol*, 94(6):4344–61, 2005.

[129] J. C. Gomora, A. N. Daud, M. Weiergraber, and E. Perez-Reyes. Block of cloned human t-type calcium channels by succinimide antiepileptic drugs. *Mol Pharmacol*, 60(5):1121–32, 2001.

[130] B. G. Goodyear, H. Zhu, R. A. Brown, and J. R. Mitchell. Removal of phase artifacts from fmri data using a stockwell transform filter improves brain activity detection. *Magn*

Reson Med, 51(1):16–21, 2004.

[131] D. Greenbaum, C. Colangelo, K. Williams, and M. Gerstein. Comparing protein abundance and mrna expression levels on a genomic scale. *Genome Biol*, 4(9):117, 2003.

[132] F. Grenier, I. Timofeev, and M. Steriade. Focal synchronization of ripples (80-200 hz) in neocortex and their neuronal correlates. *J Neurophysiol*, 86(4):1884–98, 2001.

[133] F. Grenier, I. Timofeev, and M. Steriade. Neocortical very fast oscillations (ripples, 80-200 hz) during seizures: intracellular correlates. *J Neurophysiol*, 89(2):841–52, 2003.

[134] Alan Guberman, J. Bruni, and Alan Guberman. *Essentials of clinical epilepsy*. Butterworth-Heinemann, Boston, 2nd edition, 1999.

[135] W. Guido, S. M. Lu, and S. M. Sherman. Relative contributions of burst and tonic responses to the receptive field properties of lateral geniculate neurons in the cat. *J Neurophysiol*, 68(6):2199–211, 1992.

[136] W. Guido and T. Weyand. Burst responses in thalamic relay cells of the awake behaving cat. *J Neurophysiol*, 74(4):1782–6, 1995.

[137] R. Gutierrez, V. Armand, S. Schuchmann, and U. Heinemann. Epileptiform activity induced by low mg2+ in cultured rat hippocampal slices. *Brain Res*, 815(2):294–303, 1999.

[138] M. J. Gutnick and D. A. Prince. Thalamocortical relay neurons: antidromic invasion of spikes from a cortical epileptogenic focus. *Science*, 176(33):424–6, 1972.

[139] J. Hamid, J.B. Peloquin, A. Monteil, and G.W. Zamponi. Determinants of the differential gating properties of cav3.1 and cav3.3 t-type channels: a role of domain iv? *Neuroscience*, 143(3):717–728, 2006.

[140] M.S. Hammond, C. Sims, K. Parameshwaran, V. Suppiramaniam, M. Schachner, and A. Dityatev. Neural cell adhesion molecule-associated polysialic acid inhibits nr2b-containing n-methyl-d-aspartate receptors and prevents glutamate-induced cell death. *J Biol Chem*, 281(46):34859–34869, 2006.

[141] R. Hashimoto, K. Fujimaki, M.R. Jeong, L. Christ, and D.M. Chuang. Lithium-induced inhibition of src tyrosine kinase in rat cerebral cortical neurons: a role in neuroprotection against n-methyl-d-aspartate receptor-mediated excitotoxicity. *FEBS Lett*, 538(1-3):145–148, 2003.

[142] K. Haug, M. Warnstedt, A. K. Alekov, T. Sander, A. Ramirez, B. Poser, S. Maljevic, S. Hebeisen, C. Kubisch, J. Rebstock, S. Horvath, K. Hallmann, J. S. Dullinger, B. Rau, F. Haverkamp, S. Beyenburg, H. Schulz, D. Janz, B. Giese, G. Muller-Newen, P. Propping, C. E. Elger, C. Fahlke, H. Lerche, and A. Heils. Mutations in clcn2 encoding a voltage-gated chloride channel are associated with idiopathic generalized epilepsies. *Nat Genet*, 33(4):527–32, 2003.

[143] B. Hay, S.B. Prusiner, and V.R. Lingappa. Evidence for a secretory form of the cellular prion protein. *Biochemistry*, 26(25):8110–8115, 1987.

[144] R.S. Hegde and N.S. Rane. Prion protein trafficking and the development of neurodegeneration. *Trends Neurosci*, 26(7):337–339, 2003.

[145] S. T. Herman. Epilepsy after brain insult: targeting epileptogenesis. *Neurology*, 59(9 Suppl 5):S21–6, 2002.

[146] J. Herms, T. Tings, S. Gall, A. Madlung, A. Giese, H. Siebert, P. Schurmann, O. Windl, N. Brose, and H. Kretzschmar. Evidence of presynaptic location and function of the prion protein. *J Neurosci*, 19(20):8866–8875, 1999.

[147] J.W. Herms, H.A. Kretzchmar, S. Titz, and B.U. Keller. Patch-clamp analysis of synaptic transmission to cerebellar purkinje cells of prion protein knockout mice. *Eur J Neurosci*, 7(12):2508–2512, 1995.

[148] S. E. Heron, K. M. Crossland, E. Andermann, H. A. Phillips, A. J. Hall, A. Bleasel, M. Shevell, S. Mercho, M. H. Seni, M. C. Guiot, J. C. Mulley, S. F. Berkovic, and I. E. Scheffer. Sodium-channel defects in benign familial neonatal-infantile seizures. *Lancet*, 360(9336):851–2, 2002.

[149] S. E. Heron, H. A. Phillips, J. C. Mulley, A. Mazarib, M. Y. Neufeld, S. F. Berkovic, and I. E. Scheffer. Genetic variation of cacna1h in idiopathic generalized epilepsy. *Ann Neurol*, 55(4):595–6, 2004.

[150] P. Hilfiker and M. Egli. Detection and evolution of rhythmic components in ictal eeg using short segment spectra and discriminant analysis. *Electroencephalogr Clin Neurophysiol*, 82(4):255–65, 1992.

[151] S. Hirose, A. Mitsudome, M. Okada, and S. Kaneko. Genetics of idiopathic epilepsies. *Epilepsia*, 46 Suppl 1:38–43, 2005.

[152] M. Hobom, S. Dai, E. Marais, L. Lacinova, F. Hofmann, and N. Klugbauer. Neuronal distribution and functional characterization of the calcium channel alpha2delta-2 subunit. *Eur J Neurosci*, 12(4):1217–26, 2000.

[153] M. D. Holmes, M. Brown, and D. M. Tucker. Are "generalized" seizures truly generalized? evidence of localized mesial frontal and frontopolar discharges in absence. *Epilepsia*, 45(12):1568–79, 2004.

[154] S. Hrabetova, P. Serrano, N. Blace, H.W. Tse, D.A. Skifter, D.E. Jane, D.T. Monaghan, and T.C. Sacktor. Distinct nmda receptor subpopulations contribute to long-term potentiation and long-term depression induction. *J Neurosci*, 20(12):RC81, 2000.

[155] S. W. Hughes, D. W. Cope, K. L. Blethyn, and V. Crunelli. Cellular mechanisms of the slow (¡1 hz) oscillation in thalamocortical neurons in vitro. *Neuron*, 33(6):947–58, 2002.

[156] J. R. Huguenard and D. A. Prince. A novel t-type current underlies prolonged ca(2+)-dependent burst firing in gabaergic neurons of rat thalamic reticular nucleus. *J Neurosci*, 12(10):3804–17, 1992.

[157] M. Isokawa-Akesson, C. L. Wilson, and T. L. Babb. Diversity in periodic pattern of firing in human hippocampal neurons. *Exp Neurol*, 98(1):137–51, 1987.

[158] P. Isope and T.H. Murphy. Low threshold calcium currents in rat cerebellar purkinje cell dendritic spines are mediated by t-type calcium channels. *J Physiol*, 562(Pt 1):257–269, 2005.

[159] E.M. Izhikevich. *Dynamical systems in neuroscience*. MIT Press, 2007.

[160] P. Jallon and P. Latour. Epidemiology of idiopathic generalized epilepsies. *Epilepsia*, 46 Suppl 9:10–4, 2005.

[161] Y. Jiang, A. Lee, J. Chen, V. Ruta, M. Cadene, B. T. Chait, and R. MacKinnon. X-ray structure of a voltage-dependent k+ channel. *Nature*, 423(6935):33–41, 2003.

[162] J. D. Jirsch, E. Urrestarazu, P. LeVan, A. Olivier, F. Dubeau, and J. Gotman. High-frequency oscillations during human focal seizures. *Brain*, 129(Pt 6):1593–608, 2006.

[163] P. M. Joksovic, D. A. Bayliss, and S. M. Todorovic. Different kinetic properties of two t-type ca^{2+} currents of reticular thalamic neurons and their modulation by enflurane. *J Physiol*, 566:125–42, 2005.

[164] M.V. Jones and G.L. Westbrook. The impact of receptor desensitization on fast synaptic transmission. *Trends Neurosci*, 19(3):96–101, 1996.

[165] Jung, N.P. Staff, and N. Spruston. Action potential bursting in subicular pyramidal neurons is driven by a calcium tail current. *J Neurosci*, 21(10):3312–3321, 2001.

[166] J. Kanaani, S.B. Prusiner, J. Diacovo, S. Baekkeskov, and G. Legname. Recombinant prion protein induces rapid polarization and development of synapses in embryonic rat hippocampal neurons in vitro. *J Neurochem*, 95(5):1373–1386, 2005.

[167] E. R. Kandel, J. H. Schwartz, and T. M. Jessell. *Principles of neuroscience*. McGraw-Hill, 2000.

[168] H. Karst, M. Joels, and W.J. Wadman. Low-threshold calcium current in dendrites of the adult rat hippocampus. *Neurosci Lett*, 164(1-2):154–158, 1993.

[169] M. Kase, S. Kakimoto, S. Sakuma, T. Houtani, H. Ohishi, T. Ueyama, and T. Sugimoto. Distribution of neurons expressing alpha 1g subunit mrna of t-type voltage-dependent calcium channel in adult rat central nervous system. *Neurosci Lett*, 268(2):77–80, 1999.

[170] E. T. Kavalali, M. Zhuo, H. Bito, and R. W. Tsien. Dendritic ca^{2+} channels characterized by recordings from isolated hippocampal dendritic segments. *Neuron*, 18(4):651–63, 1997.

[171] N. Kemp and Z.I. Bashir. Long-term depression: a cascade of induction and expression mechanisms. *Prog Neurobiol*, 65(4):339–365, 2001.

[172] H. Khosravani, C. Altier, B. Simms, K. S. Hamming, T. P. Snutch, J. Mezeyova, J. E. McRory, and G. W. Zamponi. Gating effects of mutations in the cav3.2 t-type calcium channel associated with childhood absence epilepsy. *J Biol Chem*, 279(11):9681–4, 2004.

[173] H. Khosravani, C. Bladen, D. B. Parker, T. P. Snutch, J. E. McRory, and G. W. Zamponi. Effects of ca(v)3.2 channel mutations linked to idiopathic generalized epilepsy. *Ann Neurol*, 57(5):745–9, 2005.

[174] H. Khosravani, P. L. Carlen, and J. L. Velazquez. The control of seizure-like activity in the rat hippocampal slice. *Biophys J*, 84(1):687–95, 2003.

[175] H. Khosravani, C. R. Pinnegar, J. R. Mitchell, B. L. Bardakjian, P. Federico, and P. L. Carlen. Increased high-frequency oscillations precede in vitro low-mg seizures. *Epilepsia*, 46(8):1188–97, 2005.

[176] H. Khosravani and G.W. Zamponi. Voltage-gated calcium channels and idiopathic generalized epilepsies. *Physiol Rev*, 86(3):941–66, 2006.

[177] D. Kim, I. Song, S. Keum, T. Lee, M. J. Jeong, S. S. Kim, M. W. McEnery, and H. S. Shin. Lack of the burst firing of thalamocortical relay neurons and resistance to absence seizures in mice lacking alpha(1g) t-type ca(2+) channels. *Neuron*, 31(1):35–45, 2001.

[178] E.D. Kirson, C. Schirra, A. Konnerth, and Y. Yaari. Early postnatal switch in magnesium sensitivity of nmda receptors in rat ca1 pyramidal cells. *J Physiol*, 521 Pt 1:99–111, 1999.

[179] U. Klockner, J. H. Lee, L. L. Cribbs, A. Daud, J. Hescheler, A. Pereverzev, E. Perez-Reyes, and T. Schneider. Comparison of the ca2 + currents induced by expression of three cloned alpha1 subunits, alpha1g, alpha1h and alpha1i, of low-voltage-activated t-type ca2 + channels. *Eur J Neurosci*, 11(12):4171–8, 1999.

[180] N. Klugbauer, L. Lacinova, E. Marais, M. Hobom, and F. Hofmann. Molecular diversity of the calcium channel alpha2delta subunit. *J Neurosci*, 19(2):684–91, 1999.

[181] N. Klugbauer, E. Marais, and F. Hofmann. Calcium channel alpha2delta subunits: differential expression, function, and drug binding. *J Bioenerg Biomembr*, 35(6):639–47, 2003.

[182] C. Koch. *Biophysics of Computation. Information Processing in Single Neurons*. Oxford University Press, 1999.

[183] A. Koschak, D. Reimer, D. Walter, J. C. Hoda, T. Heinzle, M. Grabner, and J. Striessnig. Cav1.4alpha1 subunits can form slowly inactivating dihydropyridine-sensitive l-type ca^{2+} channels lacking ca^{2+}-dependent inactivation. *J Neurosci*, 23(14):6041–9, 2003.

[184] J. B. Kuzmiski, W. Barr, G. W. Zamponi, and B. A. MacVicar. Topiramate inhibits the initiation of plateau potentials in ca1 neurons by depressing r-type calcium channels. *Epilepsia*, 46(4):481–9, 2005.

[185] R. C. Lambert, Y. Maulet, J. Mouton, R. Beattie, S. Volsen, M. De Waard, and A. Feltz. T-type ca^{2+} current properties are not modified by ca^{2+} channel beta subunit depletion in nodosus ganglion neurons. *J Neurosci*, 17(17):6621–8, 1997.

[186] M. E. Larkum and J. J. Zhu. Signaling of layer 1 and whisker-evoked ca^{2+} and na+ action potentials in distal and terminal dendrites of rat neocortical pyramidal neurons in vitro and in vivo. *J Neurosci*, 22(16):6991–7005, 2002.

[187] B. Lasztoczi, K. Antal, L. Nyikos, Z. Emri, and J. Kardos. High-frequency synaptic input contributes to seizure initiation in the low-[mg2+] model of epilepsy. *Eur J Neurosci*, 19(5):1361–72, 2004.

[188] M. Le Van Quyen, I. Khalilov, and Y. Ben-Ari. The dark side of high-frequency oscillations in the developing brain. *Trends Neurosci*, 29(7):419–27, 2006.

[189] A. Lee, S. T. Wong, D. Gallagher, B. Li, D. R. Storm, T. Scheuer, and W. A. Catterall. ca^{2+} calmodulin binds to and modulates p/q-type calcium channels. *Nature*, 399(6732):155–9, 1999.

[190] J. Lee, D. Kim, and H. S. Shin. Lack of delta waves and sleep disturbances during non-rapid eye movement sleep in mice lacking alpha1g-subunit of t-type calcium channels. *Proc Natl Acad Sci U S A*, 101(52):18195–9, 2004.

[191] J. H. Lee, A. N. Daud, L. L. Cribbs, A. E. Lacerda, A. Pereverzev, U. Klockner, T. Schneider, and E. Perez-Reyes. Cloning and expression of a novel member of the low voltage-activated t-type calcium channel family. *J Neurosci*, 19(6):1912–21, 1999.

[192] J. H. Lee, J. C. Gomora, L. L. Cribbs, and E. Perez-Reyes. Nickel block of three cloned t-type calcium channels: low concentrations selectively block alpha1h. *Biophys J*, 77(6):3034–42, 1999.

[193] A.G. Leenders, A.M. van den Maagdenberg, F.H. Lopes da Silva, Z.H. Sheng, P.C. Molenaar, and W.E. Ghijsen. Neurotransmitter release from tottering mice nerve terminals with reduced expression of mutated p- and q-type ca^{2+}-channels. *Eur J Neurosci*, 15(1):13–8, 2002.

[194] M. Leonardi and T. B. Ustun. The global burden of epilepsy. *Epilepsia*, 43 Suppl 6:21–5, 2002.

[195] N. Leresche, H. R. Parri, G. Erdemli, A. Guyon, J. P. Turner, S. R. Williams, E. Asprodini, and V. Crunelli. On the action of the anti-absence drug ethosuximide in the rat and cat thalamus. *J Neurosci*, 18(13):4842–53, 1998.

[196] V. Leuranguer, E. Bourinet, P. Lory, and J. Nargeot. Antisense depletion of beta-subunits fails to affect t-type calcium channels properties in a neuroblastoma cell line. *Neuropharmacology*, 37(6):701–8, 1998.

[197] H. Liang, C. D. DeMaria, M. G. Erickson, M. X. Mori, B. A. Alseikhan, and D. T. Yue. Unified mechanisms of ca^{2+} regulation across the ca^{2+} channel family. *Neuron*, 39(6):951–60, 2003.

[198] D.N. Lieberman and I. Mody. Regulation of nmda channel function by endogenous ca(2+)-dependent phosphatase. *Nature*, 369(6477):235–239, 1994.

[199] B. Litt and K. Lehnertz. Seizure prediction and the preseizure period. *Curr Opin Neurol*, 15(2):173–7, 2002.

[200] L. Liu, T.P. Wong, M.F. Pozza, K. Lingenhoehl, Y. Wang, M. Sheng, Y.P. Auberson, and Y.T. Wang. Role of nmda receptor subtypes in governing the direction of hippocampal synaptic plasticity. *Science*, 304(5673):1021–1024, 2004.

[201] T. Liu, T. Zwingman, R. Li, T. Pan, B.S. Wong, R.B. Petersen, P. Gambetti, K. Herrup, and M.S. Sy. Differential expression of cellular prion protein in mouse brain as detected with multiple anti-prp monoclonal antibodies. *Brain Res*, 896(1-2):118–129, 2001.

[202] X. B. Liu, C. N. Honda, and E. G. Jones. Distribution of four types of synapse on physiologically identified relay neurons in the ventral posterior thalamic nucleus of the cat. *J Comp Neurol*, 352(1):69–91, 1995.

[203] X. B. Liu and E. G. Jones. Predominance of corticothalamic synaptic inputs to thalamic reticular nucleus neurons in the rat. *J Comp Neurol*, 414(1):67–79, 1999.

[204] P.M. Lledo, P. Tremblay, S.J. DeArmond, S.B. Prusiner, and R.A. Nicoll. Mice deficient for prion protein exhibit normal neuronal excitability and synaptic transmission in the hippocampus. *Proc Natl Acad Sci*, 93(6):2403–2407, 1996.

[205] R. Llinas and H. Jahnsen. Electrophysiology of mammalian thalamic neurones in vitro. *Nature*, 297(5865):406–8, 1982.

[206] S. B. Long, E. B. Campbell, and R. Mackinnon. Voltage sensor of kv1.2: structural basis of electromechanical coupling. *Science*, 309(5736):903–8, 2005.

[207] F. Lopes da Silva, W. Blanes, S. N. Kalitzin, J. Parra, P. Suffczynski, and D. N. Velis. Epilepsies as dynamical diseases of brain systems: basic models of the transition between normal and epileptic activity. *Epilepsia*, 44 Suppl 12:72–83, 2003.

[208] F.H. Lopes da Silva, W. Blanes, S.N. Kalitzin, J. Parra, P. Suffczynski, and D.N. Velis. Dynamical diseases of brain systems: different routes to epileptic seizures. *IEEE Trans Biomed Eng*, 50(5):540–8, 2003.

[209] A. Ludwig, T. Budde, J. Stieber, S. Moosmang, C. Wahl, K. Holthoff, A. Langebartels, C. Wotjak, T. Munsch, X. Zong, S. Feil, R. Feil, M. Lancel, K. R. Chien, A. Konnerth, H. C. Pape, M. Biel, and F. Hofmann. Absence epilepsy and sinus dysrhythmia in mice lacking the pacemaker channel hcn2. *Embo J*, 22(2):216–24, 2003.

[210] A. Luthi and D. A. McCormick. H-current: properties of a neuronal and network pacemaker. *Neuron*, 21(1):9–12, 1998.

[211] J. C. Magee and D. Johnston. Characterization of single voltage-gated na+ and ca^{2+} channels in apical dendrites of rat ca1 pyramidal neurons. *J Physiol*, 487 (Pt 1):67–90, 1995.

[212] L.E. Maglio, V.R. Martins, I. Izquierdo, and O.A. Ramirez. Role of cellular prion protein on ltp expression in aged mice. *Brain Res*, 1097(1):11–18, 2006.

[213] L.E. Maglio, M.F. Perez, V.R. Martins, R.R. Brentani, and O.A. Ramirez. Hippocampal synaptic plasticity in mice devoid of cellular prion protein. *Brain Res Mol Brain Res*, 131(1-2):58–64, 2004.

[214] N. Maier, M. Guldenagel, G. Sohl, H. Siegmund, K. Willecke, and A. Draguhn. Reduction of high-frequency network oscillations (ripples) and pathological network discharges in hippocampal slices from connexin 36-deficient mice. *J Physiol*, 541(Pt 2):521–8, 2002.

[215] N. Maier, V. Nimmrich, and A. Draguhn. Cellular and network mechanisms underlying spontaneous sharp wave-ripple complexes in mouse hippocampal slices. *J Physiol*, 550(Pt 3):873–87, 2003.

[216] G.R. Mallucci, S. Ratte, E.A. Asante, J. Linehan, I. Gowland, J.G. Jefferys, and J. Collinge. Post-natal knockout of prion protein alters hippocampal ca1 properties, but does not result in neurodegeneration. *EMBO J*, 21(3):202–210, 2002.

[217] G.R. Mallucci, M.D. White, M. Farmer, A. Dickinson, H. Khatun, A.D. Powell, S. Brandner, J.G. Jefferys, and J. Collinge. Targeting cellular prion protein reverses early cognitive deficits and neurophysiological dysfunction in prion-infected mice. *Neuron*, 53(3):325–335, 2007.

[218] J. P. Manning, D. A. Richards, N. Leresche, V. Crunelli, and N. G. Bowery. Cortical-area specific block of genetically determined absence seizures by ethosuximide. *Neuroscience*, 123(1):5–9, 2004.

[219] J.C. Manson, J. Hope, A.R. Clarke, A. Johnston, C. Black, and N. MacLeod. Prp gene dosage and long term potentiation. *Neurodegeneration*, 4(1):113–114, 1995.

[220] C. Marini, M. A. King, J. S. Archer, M. R. Newton, and S. F. Berkovic. Idiopathic generalized epilepsy of adult onset: clinical syndromes and genetics. *J Neurol Neurosurg Psychiatry*, 74:192–96, 2005.

[221] H. Markram and B. Sakmann. Calcium transients in dendrites of neocortical neurons evoked by single subthreshold excitatory postsynaptic potentials via low-voltage-activated calcium channels. *Proc Natl Acad Sci U S A*, 91(11):5207–11, 1994.

[222] H. Markram, M. Toledo-Rodriguez, Y. Wang, A. Gupta, G. Silberberg, and C. Wu. Interneurons of the neocortical inhibitory system. *Nat Rev Neurosci*, 5(10):793–807, 2004.

[223] R. Marksteiner, P. Schurr, S. Berjukow, E. Margreiter, E. Perez-Reyes, and S. Hering. Inactivation determinants in segment iiis6 of ca(v)3.1. *J Physiol*, 537(Pt 1):27–34, 2001.

[224] R. L. Martin, J. H. Lee, L. L. Cribbs, E. Perez-Reyes, and D. A. Hanck. Mibefradil block of cloned t-type calcium channels. *J Pharmacol Exp Ther*, 295(1):302–8, 2000.

[225] D. A. McCormick and D. Contreras. On the cellular and network bases of epileptic seizures. *Annu Rev Physiol*, 63:815–46, 2001.

[226] B.E. McKay, J.E. McRory, M.L. Molineux, J. Hamid, T.P. Snutch, G.W. Zamponi, and R.W. Turner. Ca(v)3 t-type calcium channel isoforms differentially distribute to somatic and dendritic compartments in rat central neurons. *Eur J Neurosci*, 24(9):2581–2594, 2006.

[227] J. O. McNamara. Emerging insights into the genesis of epilepsy. *Nature*, 399(6738 Suppl):A15–22, 1999.

[228] J. E. McRory, C. M. Santi, K. S. Hamming, J. Mezeyova, K. G. Sutton, D. L. Baillie, A. Stea, and T. P. Snutch. Molecular and functional characterization of a family of rat brain t-type calcium channels. *J Biol Chem*, 276(6):3999–4011, 2001.

[229] John E McRory, Jawed Hamid, Clinton J Doering, Esperanza Garcia, Robin Parker, Kevin Hamming, Lina Chen, Michael Hildebrand, Aaron M Beedle, Laura Feldcamp, Gerald W Zamponi, and Terrance P Snutch. The cacna1f gene encodes an l-type calcium channel with unique biophysical properties and tissue distribution. *J Neurosci*, 24(7):1707–1718, Feb 2004.

[230] H. Meeren, G. van Luijtelaar, F. Lopes da Silva, and A. Coenen. Evolving concepts on the pathophysiology of absence seizures: the cortical focus theory. *Arch Neurol*, 62(3):371–6, 2005.

[231] H.K. Meeren, J.P. Pijn, E.L. Van Luijtelaar, A.M. Coenen, and F.H. Lopes da Silva. Cortical focus drives widespread corticothalamic networks during spontaneous absence seizures in rats. *J Neurosci*, 22(4):1480–95, 2002.

[232] K. Melliti, M. Grabner, and G. R. Seabrook. The familial hemiplegic migraine mutation r192q reduces g-protein-mediated inhibition of p/q-type (ca(v)2.1) calcium channels expressed in human embryonic kidney cells. *J Physiol*, 546(Pt 2):337–47, 2003.

[233] A. Mikami, K. Imoto, T. Tanabe, T. Niidome, Y. Mori, H. Takeshima, S. Narumiya, and S. Numa. Primary structure and functional expression of the cardiac dihydropyridine-sensitive calcium channel. *Nature*, 340(6230):230–3, 1989.

[234] C. Misra, S.G. Brickley, D.J. Wyllie, and S.G. Cull-Candy. Slow deactivation kinetics of nmda receptors containing nr1 and nr2d subunits in rat cerebellar purkinje cells. *J Physiol*, 525 Pt 2:299–305, 2000.

[235] N. Mitsios, M. Saka, J. Krupinski, R. Pennucci, C. Sanfeliu, M. Miguel Turu, J. Gaffney, P. Kumar, S. Kumar, M. Sullivan, and M. Slevin. Cellular prion protein is increased in the plasma and peri-infarcted brain tissue after acute stroke. *J Neurosci Res*, 85(3):602–611, 2007.

[236] I. Mody, J. D. Lambert, and U. Heinemann. Low extracellular magnesium induces epileptiform activity and spreading depression in rat hippocampal slices. *J Neurophysiol*, 57(3):869–88, 1987.

[237] A. Momiyama, D. Feldmeyer, and S.G. Cull-Candy. Identification of a native low-conductance nmda channel with reduced sensitivity to mg2+ in rat central neurones. *J Physiol*, 494 (Pt 2):479–492, 1996.

[238] A. Monteil, J. Chemin, E. Bourinet, G. Mennessier, P. Lory, and J. Nargeot. Molecular and functional properties of the human alpha(1g) subunit that forms t-type calcium channels. *J Biol Chem*, 275(9):6090–100, 2000.

[239] A. Monteil, J. Chemin, V. Leuranguer, C. Altier, G. Mennessier, E. Bourinet, P. Lory, and J. Nargeot. Specific properties of t-type calcium channels generated by the human alpha 1i subunit. *J Biol Chem*, 275(22):16530–5, 2000.

[240] H. Monyer, N. Burnashev, D.J. Laurie, B. Sakmann, and P.H. Seeburg. Developmental and regional expression in the rat brain and functional properties of four nmda receptors. *Neuron*, 12(3):529–540, 1994.

[241] W. Morishita, W. Lu, G.B. Smith, R.A. Nicoll, M.F. Bear, and R.C. Malenka. Activation

of nr2b-containing nmda receptors is not required for nmda receptor-dependent long-term depression. *Neuropharmacology*, 52(1):71–76, 2007.

[242] F. Mormann, R. G. Andrzejak, C. E. Elger, and K. Lehnertz. Seizure prediction: the long and winding road. *Brain*, 130(Pt 2):314–33, 2007.

[243] S. Mouillet-Richard, M. Ermonval, C. Chebassier, J.L. Laplanche, S. Lehmann, J.M. Launay, and O. Kellermann. Signal transduction through prion protein. *Science*, 289(5486):1925–1928, 2000.

[244] K.L. Moya, N. Sales, R. Hassig, C. Creminon, J. Grassi, and L. Di Giamberardino. Immunolocalization of the cellular prion protein in normal brain. *Microsc Res Tech*, 50(1):58–65, 2000.

[245] W.E. Muller, H. Ushijima, H.C. Schroder, J.M. Forrest, W.F. Schatton, P.G. Rytik, and M. Heffner-Lauc. Cytoprotective effect of nmda receptor antagonists on prion protein (prionsc)-induced toxicity in rat cortical cell cultures. *Eur J Pharmacol*, 246(3):261–267, 1993.

[246] J. C. Mulley, I. E. Scheffer, L. A. Harkin, S. F. Berkovic, and L. M. Dibbens. Susceptibility genes for complex epilepsy. *Hum Mol Genet*, 14 Spec No. 2:R243–9, 2005.

[247] J. C. Mulley, I. E. Scheffer, S. Petrou, and S. F. Berkovic. Channelopathies as a genetic cause of epilepsy. *Curr Opin Neurol*, 16(2):171–6, 2003.

[248] J. Murbartian, J. M. Arias, J. H. Lee, J. C. Gomora, and E. Perez-Reyes. Alternative splicing of the rat ca(v)3.3 t-type calcium channel gene produces variants with distinct functional properties(1). *FEBS Lett*, 528(1-3):272–8, 2002.

[249] R. Newcomb, B. Szoke, A. Palma, G. Wang, X. Chen, W. Hopkins, R. Cong, J. Miller, L. Urge, K. Tarczy-Hornoch, J. A. Loo, D. J. Dooley, L. Nadasdi, R. W. Tsien, J. Lemos, and G. Miljanich. Selective peptide antagonist of the class e calcium channel from the venom of the tarantula hysterocrates gigas. *Biochemistry*, 37(44):15353–62, 1998.

[250] E. Niedermeyer and F. Lopes Da Silva. *Electroencephalography: Basic Principles, Clinical Applications, and Related Fields*. Lippincott Williams & Wilkins, 5 edition, 2004.

[251] V. Nimmrich, N. Maier, D. Schmitz, and A. Draguhn. Induced sharp wave-ripple complexes in the absence of synaptic inhibition in mouse hippocampal slices. *J Physiol*, 563(Pt 3):663–70, 2005.

[252] N. Niwa, K. Yasui, T. Opthof, H. Takemura, A. Shimizu, M. Horiba, J. K. Lee, H. Honjo, K. Kamiya, and I. Kodama. Cav3.2 subunit underlies the functional t-type ca^{2+} channel in murine hearts during the embryonic period. *Am J Physiol Heart Circ Physiol*, 286(6):H2257–63, 2004.

[253] A. Ochi, H. Otsubo, E. J. Donner, I. Elliott, R. Iwata, T. Funaki, Y. Akizuki, T. Akiyama, K. Imai, J. T. Rutka, and O. C. Snead. Dynamic changes of ictal high-frequency oscillations in neocortical epilepsy: using multiple band frequency analysis. *Epilepsia*, 48(2):286–296, 2007.

[254] S. Okabe, C. Collin, J.M. Auerbach, N. Meiri, J. Bengzon, M.B. Kennedy, M. Segal, and R.D. McKay. Hippocampal synaptic plasticity in mice overexpressing an embryonic subunit of the nmda receptor. *J Neurosci*, 18(11):4177–4188, 1998.

[255] B. M. Olivera, J. M. McIntosh, L. J. Cruz, F. A. Luque, and W. R. Gray. Purification and sequence of a presynaptic peptide toxin from conus geographus venom. *Biochemistry*, 23(22):5087–90, 1984.

[256] Y. Opatowsky, O. Chomsky-Hecht, M. G. Kang, K. P. Campbell, and J. A. Hirsch. The voltage-dependent calcium channel beta subunit contains two stable interacting domains. *J Biol Chem*, 278(52):52323–32, 2003.

[257] K. M. Page, F. Heblich, A. Davies, A. J. Butcher, J. Leroy, F. Bertaso, W. S. Pratt, and A. C. Dolphin. Dominant-negative calcium channel suppression by truncated constructs involves a kinase implicated in the unfolded protein response. *J Neurosci*, 24(23):5400–9, 2004.

[258] C. Papatheodoropoulos. Nmda receptor-dependent high-frequency network oscillations (100-300 hz) in rat hippocampal slices. *Neurosci Lett*, 414(3):197–202, 2007.

[259] J. Peloquin, H. Khosravani, W. Barr, C. Bladen, R. Evans, J. Mezeyova, D. Parker, T. P. Snutch, J. E. McRory, and G. W. Zamponi. Functional analysis of $ca_v3.2$ t-type calcium channel mutations linked to childhood absence epilepsy. *Epilepsia*, 47(3):655–658, 2006.

[260] E. Perez-Reyes. Molecular characterization of a novel family of low voltage-activated, t-type, calcium channels. *J Bioenerg Biomembr*, 30(4):313–8, 1998.

[261] E. Perez-Reyes. Molecular physiology of low-voltage-activated t-type calcium channels. *Physiol Rev*, 83(1):117–61, 2003.

[262] B. Z. Peterson, C. D. DeMaria, J. P. Adelman, and D. T. Yue. Calmodulin is the ca^{2+} sensor for ca^{2+}-dependent inactivation of l-type calcium channels. *Neuron*, 22(3):549–58, 1999.

[263] D. Pietrobon. Calcium channels and channelopathies of the central nervous system. *Mol Neurobiol*, 25(1):31–50, 2002.

[264] D. Pinault. Cellular interactions in the rat somatosensory thalamocortical system during normal and epileptic 5-9 hz oscillations. *J Physiol*, 552(Pt 3):881–905, 2003.

[265] D. Pinault, N. Leresche, S. Charpier, J. M. Deniau, C. Marescaux, M. Vergnes, and V. Crunelli. Intracellular recordings in thalamic neurones during spontaneous spike and wave discharges in rats with absence epilepsy. *J Physiol*, 509 (Pt 2):449–56, 1998.

[266] R.C. Pinnegar and L. Mansinha. The s-transform with windows of arbitrary and varying shape. *Geophysics*, 68(1):381–385, 2003.

[267] N. P. Poolos. The h-channel: a potential channelopathy in epilepsy? *Epilepsy Behav*, 7(1):51–6, 2005.

[268] B. Potier, P. Dutar, and Y. Lamour. Different effects of omega-conotoxin gvia at excitatory and inhibitory synapses in rat ca1 hippocampal neurons. *Brain Res*, 616(1-2):236–41, 1993.

[269] M. Pragnell, M. De Waard, Y. Mori, T. Tanabe, T. P. Snutch, and K. P. Campbell. Calcium channel beta-subunit binds to a conserved motif in the i-ii cytoplasmic linker of the alpha 1-subunit. *Nature*, 368(6466):67–70, 1994.

[270] E.A. Proper, A.B. Oestreicher, G.H. Jansen, C.W. Veelen, P.C. van Rijen, W.H. Gispen, and P.N. de Graan. Immunohistochemical characterization of mossy fibre sprouting in the hippocampus of patients with pharmaco-resistant temporal lobe epilepsy. *Brain*, 123 (Pt 1):19–30, 2000.

[271] S.B. Prusiner. Novel proteinaceous infectious particles cause scrapie. *Science*, 216(4542):136–144, 1982.

[272] S.B. Prusiner, M.R. Scott, S.J. DeArmond, and F.E. Cohen. Prion protein biology. *Cell*, 93(3):337–348, 1998.

[273] N. Qin, D. Platano, R. Olcese, J. L. Costantin, E. Stefani, and L. Birnbaumer. Unique regulatory properties of the type 2a ca^{2+} channel beta subunit caused by palmitoylation. *Proc Natl Acad Sci U S A*, 95(8):4690–5, 1998.

[274] A. Rafiq, R. J. DeLorenzo, and D. A. Coulter. Generation and propagation of epileptiform discharges in a combined entorhinal cortex/hippocampal slice. *J Neurophysiol*, 70(5):1962–74, 1993.

[275] A. Rafiq, Y. F. Zhang, R. J. DeLorenzo, and D. A. Coulter. Long-duration self-sustained epileptiform activity in the hippocampal-parahippocampal slice: a model of status epilepticus. *J Neurophysiol*, 74(5):2028–42, 1995.

[276] S. Rampp and H. Stefan. Fast activity as a surrogate marker of epileptic network function? *Clin Neurophysiol*, 117(10):2111–7, 2006.

[277] A. Randall and R. W. Tsien. Pharmacological dissection of multiple types of ca^{2+} channel currents in rat cerebellar granule neurons. *J Neurosci*, 15(4):2995–3012, 1995.

[278] A. Rangel, F. Burgaya, R. Gavin, E. Soriano, A. Aguzzi, and J.A. Del Rio. Enhanced susceptibility of prnp-deficient mice to kainate-induced seizures, neuronal apoptosis, and death: Role of ampa/kainate receptors. *J Neurosci Res*, [Epub ahead of print], 2007.

[279] I. J. Reynolds, J. A. Wagner, S. H. Snyder, S. A. Thayer, B. M. Olivera, and R. J. Miller. Brain voltage-sensitive calcium channel subtypes differentiated by omega-conotoxin fraction gvia. *Proc Natl Acad Sci U S A*, 83(22):8804–7, 1986.

[280] D. A. Richards, J. P. Manning, D. Barnes, L. Rombola, N. G. Bowery, S. Caccia, N. Leresche, and V. Crunelli. Targeting thalamic nuclei is not sufficient for the full anti-absence action of ethosuximide in a rat model of absence epilepsy. *Epilepsy Res*, 54(2-3):97–107, 2003.

[281] M. W. Richards, A. J. Butcher, and A. C. Dolphin. ca^{2+} channel beta-subunits: structural insights aid our understanding. *Trends Pharmacol Sci*, 25(12):626–32, 2004.

[282] T. A. Richter, M. Kolaj, and L. P. Renaud. Low voltage-activated ca^{2+} channels are coupled to ca^{2+}-induced ca^{2+} release in rat thalamic midline neurons. *J Neurosci*, 25(36):8267–71, 2005.

[283] E. Rodin and O. Ancheta. Cerebral electrical fields during petit mal absences. *Electroencephalogr Clin Neurophysiol*, 66(6):457–66, 1987.

[284] E. Rodriguez, N. George, J. P. Lachaux, J. Martinerie, B. Renault, and F. J. Varela. Perception's shadow: long-distance synchronization of human brain activity. *Nature*, 397(6718):430–3, 1999.

[285] C. R. Rose and A. Konnerth. Stores not just for storage. intracellular calcium release and synaptic plasticity. *Neuron*, 31(4):519–22, 2001.

[286] M. Rousset, T. Cens, S. Restituito, C. Barrere, 3rd Black, J. L., M. W. McEnery, and P. Charnet. Functional roles of gamma2, gamma3 and gamma4, three new ca^{2+} channel

subunits, in p/q-type ca^{2+} channel expressed in xenopus oocytes. *J Physiol*, 532(Pt 3):583–93, 2001.

[287] N. Sales, K. Rodolfo, R. Hassig, B. Faucheux, L. Di Giamberardino, and K.L. Moya. Cellular prion protein localization in rodent and primate brain. *Eur J Neurosci*, 10(7):2464–2471, 1998.

[288] M.W. Salter and L.V. Kalia. Src kinases: a hub for nmda receptor regulation. *Nat Rev Neurosci*, 5(4):317–328, 2004.

[289] T. Sander, H. Schulz, K. Saar, E. Gennaro, M.C. Riggio, A. Bianchi, F. Zara, D. Luna, C. Bulteau, A. Kaminska, D. Ville, C. Cieuta, F. Picard, J.F. Prud'homme, L. Bate, A. Sundquist, R.M. Gardiner, G.A. Janssen, G.J. de Haan, D.G. Kasteleijn-Nolst-Trenite, A. Bader, D. Lindhout, O. Riess, T.F. Wienker, D. Janz, and A. Reis. Genome search for susceptibility loci of common idiopathic generalised epilepsies. *Hum Mol Genet*, 9(10):1465–72, 2000.

[290] A. Santuccione, V. Sytnyk, I. Leshchyns'ka, and M. Schachner. Prion protein recruits its neuronal receptor ncam to lipid rafts to activate p59fyn and to enhance neurite outgrowth. *J Cell Biol*, 169(2):341–354, 2005.

[291] W. A. Sather and E. W. McCleskey. Permeation and selectivity in calcium channels. *Annu Rev Physiol*, 65:133–59, 2003.

[292] R. Sattler, Z. Xiong, W.Y. Lu, M. Hafner, J.F. MacDonald, and M. Tymianski. Specific coupling of nmda receptor activation to nitric oxide neurotoxicity by psd-95 protein. *Science*, 284(5421):1845–1848, 1999.

[293] R. Sattler, Z. Xiong, W.Y. Lu, J.F. MacDonald, and M. Tymianski. Distinct roles of synaptic and extrasynaptic nmda receptors in excitotoxicity. *J Neurosci*, 20(1):22–33, 2000.

[294] I. E. Scheffer and S. F. Berkovic. The genetics of human epilepsy. *Trends Pharmacol Sci*, 24(8):428–33, 2003.

[295] C.R. Scherzer, G.B. Landwehrmeyer, J.A. Kerner, T.J. Counihan, C.M. Kosinski, D.G. Standaert, L.P. Daggett, G. Velicelebi, J.B. Penney, and A.B. Young. Expression of n-methyl-d-aspartate receptor subunit mrnas in the human brain: hippocampus and cortex. *J Comp Neurol*, 390(1):75–90, 1998.

[296] J. Schiller, Y. Schiller, G. Stuart, and B. Sakmann. Calcium action potentials restricted to distal apical dendrites of rat neocortical pyramidal neurons. *J Physiol*, 505 (Pt 3):605–16, 1997.

[297] G. Schmitt-Ulms, G. Legname, M.A. Baldwin, H.L. Ball, N. Bradon, P.J. Bosque, K.L. Crossin, G.M. Edelman, S.J. DeArmond, F.E. Cohen, and S.B. Prusiner. Binding of neural cell adhesion molecules (n-cams) to the cellular prion protein. *J Mol Biol*, 314(5):1209–1225, 2001.

[298] M. Seagar and M. Takahashi. Interactions between presynaptic calcium channels and proteins implicated in synaptic vesicle trafficking and exocytosis. *J Bioenerg Biomembr*, 30(4):347–56, 1998.

[299] S. M. Sherman. Interneurons and triadic circuitry of the thalamus. *Trends Neurosci*, 27(11):670–5, 2004.

[300] A. G. Siapas and M. A. Wilson. Coordinated interactions between hippocampal ripples and cortical spindles during slow-wave sleep. *Neuron*, 21(5):1123–8, 1998.

[301] S. S. Sidach and I. M. Mintz. Kurtoxin, a gating modifier of neuronal high- and low-threshold ca channels. *J Neurosci*, 22(6):2023–34, 2002.

[302] A. M. Siegel, H. G. Wieser, W. Wichmann, and G. M. Yasargil. Relationships between mr-imaged total amount of tissue removed, resection scores of specific mediobasal limbic subcompartments and clinical outcome following selective amygdalohippocampectomy. *Epilepsy Res*, 6(1):56–65, 1990.

[303] G.J. Sills. The mechanisms of action of gabapentin and pregabalin. *Curr Opin Pharmacol*, 6(1):108–13, 2006.

[304] N. A. Singh, C. Charlier, D. Stauffer, B. R. DuPont, R. J. Leach, R. Melis, G. M. Ronen, I. Bjerre, T. Quattlebaum, J. V. Murphy, M. L. McHarg, D. Gagnon, T. O. Rosales, A. Peiffer, V. E. Anderson, and M. Leppert. A novel potassium channel gene, kcnq2, is mutated in an inherited epilepsy of newborns. *Nat Genet*, 18(1):25–9, 1998.

[305] S. J. Slaght, N. Leresche, J. M. Deniau, V. Crunelli, and S. Charpier. Activity of thalamic reticular neurons during spontaneous genetically determined spike and wave discharges. *J Neurosci*, 22(6):2323–34, 2002.

[306] T. P. Snutch, J. Peloquin, E. Mathews, and J. E. McRory. *Molecular properties of voltage-gated calcium channels. In: Voltage-gated calcium channels*. Landes Bioscience/Eurekah.com ; Kluwer Academic/Plenum Publishers, Georgetown, Tex. New York, N.Y., 2005.

[307] V. S. Sohal and J. R. Huguenard. Inhibitory interconnections control burst pattern and emergent network synchrony in reticular thalamus. *J Neurosci*, 23(26):8978–88, 2003.

[308] L. Solforosi, J.R. Criado, D.B. McGavern, S. Wirz, M. Sanchez-Alavez, S. Sugama, L.A. DeGiorgio, B.T. Volpe, E. Wiseman, G. Abalos, E. Masliah, D. Gilden, M.B. Oldstone, B. Conti, and R.A. Williamson. Cross-linking cellular prion protein triggers neuronal apoptosis in vivo. *Science*, 303(5663):1514–1516, 2004.

[309] I. Song, D. Kim, S. Choi, M. Sun, Y. Kim, and H. S. Shin. Role of the alpha1g t-type calcium channel in spontaneous absence seizures in mutant mice. *J Neurosci*, 24(22):5249–57, 2004.

[310] T. W. Soong, A. Stea, C. D. Hodson, S. J. Dubel, S. R. Vincent, and T. P. Snutch. Structure and functional expression of a member of the low voltage-activated calcium channel family. *Science*, 260(5111):1133–6, 1993.

[311] J. D. Spafford, J. Van Minnen, P. Larsen, A. B. Smit, N. I. Syed, and G. W. Zamponi. Uncoupling of calcium channel alpha1 and beta subunits in developing neurons. *J Biol Chem*, 279(39):41157–67, 2004.

[312] J. D. Spafford and G. W. Zamponi. Functional interactions between presynaptic calcium channels and the neurotransmitter release machinery. *Curr Opin Neurobiol*, 13(3):308–14, 2003.

[313] R. Srinivasan, P.L. Nunez, D.M. Tucker, R.B. Silberstein, and P.J. Cadusch. Spatial sampling and filtering of eeg with spline laplacians to estimate cortical potentials. *Brain Topogr*, 8(4):355–66, 1996.

[314] R. J. Staba, C. L. Wilson, A. Bragin, I. Fried, and Jr. Engel, J. Quantitative analysis of high-frequency oscillations (80-500 hz) recorded in human epileptic hippocampus and entorhinal cortex. *J Neurophysiol*, 88(4):1743–52, 2002.

[315] R. J. Staba, C. L. Wilson, A. Bragin, D. Jhung, I. Fried, and Jr. Engel, J. High-frequency oscillations recorded in human medial temporal lobe during sleep. *Ann Neurol*, 56(1):108–15, 2004.

[316] M. Staes, K. Talavera, N. Klugbauer, J. Prenen, L. Lacinova, G. Droogmans, F. Hofmann, and B. Nilius. The amino side of the c-terminus determines fast inactivation of the t-type calcium channel alpha1g. *J Physiol*, 530(Pt 1):35–45, 2001.

[317] M. Steriade. To burst, or rather, not to burst. *Nat Neurosci*, 4(7):671, 2001.

[318] M. Steriade. Sleep, epilepsy and thalamic reticular inhibitory neurons. *Trends Neurosci*, 28(6):317–24, 2005.

[319] M. Steriade and D. Contreras. Relations between cortical and thalamic cellular events during transition from sleep patterns to paroxysmal activity. *J Neurosci*, 15(1 Pt 2):623–42, 1995.

[320] M. Steriade and D. Contreras. Spike-wave complexes and fast components of cortically generated seizures. i. role of neocortex and thalamus. *J Neurophysiol*, 80(3):1439–55, 1998.

[321] Mircea Steriade. *Neuronal substrates of sleep and epilepsy*. Cambridge University Press, Cambridge; New York, 2003.

[322] S. C. Stotz, S. E. Jarvis, and G. W. Zamponi. Functional roles of cytoplasmic loops and pore lining transmembrane helices in the voltage-dependent inactivation of hva calcium channels. *J Physiol*, 554(Pt 2):263–73, 2004.

[323] S. C. Stotz and G. W. Zamponi. Identification of inactivation determinants in the domain iis6 region of high voltage-activated calcium channels. *J Biol Chem*, 276(35):33001–10, 2001.

[324] U. Strauss, M. H. Kole, A. U. Brauer, J. Pahnke, R. Bajorat, A. Rolfs, R. Nitsch, and R. A. Deisz. An impaired neocortical ih is associated with enhanced excitability and absence epilepsy. *Eur J Neurosci*, 19(11):3048–58, 2004.

[325] H. Su, D. Sochivko, A. Becker, J. Chen, Y. Jiang, Y. Yaari, and H. Beck. Upregulation of a t-type ca^{2+} channel causes a long-lasting modification of neuronal firing mode after status epilepticus. *J Neurosci*, 22(9):3645–55, 2002.

[326] T. Sugawara, Y. Tsurubuchi, K. L. Agarwala, M. Ito, G. Fukuma, E. Mazaki-Miyazaki, H. Nagafuji, M. Noda, K. Imoto, K. Wada, A. Mitsudome, S. Kaneko, M. Montal, K. Nagata, S. Hirose, and K. Yamakawa. A missense mutation of the na+ channel alpha ii subunit gene na(v)1.2 in a patient with febrile and afebrile seizures causes channel dysfunction. *Proc Natl Acad Sci U S A*, 98(11):6384–9, 2001.

[327] K. G. Sutton, J. E. McRory, H. Guthrie, T. H. Murphy, and T. P. Snutch. P/q-type calcium channels mediate the activity-dependent feedback of syntaxin-1a. *Nature*, 401(6755):800–4, 1999.

[328] V. Sytnyk, I. Leshchyns'ka, A.G. Nikonenko, and M. Schachner. Ncam promotes assembly and activity-dependent remodeling of the postsynaptic signaling complex. *J Cell Biol*, 174(7):1071–1085, 2006.

[329] S. X. Takahashi, J. Miriyala, and H. M. Colecraft. Membrane-associated guanylate kinase-like properties of beta-subunits required for modulation of voltage-dependent ca^{2+} channels. *Proc Natl Acad Sci U S A*, 101(18):7193–8, 2004.

[330] E. M. Talley, G. Solorzano, A. Depaulis, E. Perez-Reyes, and D. A. Bayliss. Low-voltage-activated calcium channel subunit expression in a genetic model of absence epilepsy in the rat. *Brain Res Mol Brain Res*, 75(1):159–65, 2000.

[331] E.M. Talley, L.L. Cribbs, J.H. Lee, A. Daud, E. Perez-Reyes, and D.A. Bayliss. Differential distribution of three members of a gene family encoding low voltage-activated (t-type) calcium channels. *J Neurosci*, 19(6):1895–1911, 1999.

[332] C.G. Thomas, A.J. Miller, and G.L. Westbrook. Synaptic and extrasynaptic nmda receptor nr2 subunits in cultured hippocampal neurons. *J Neurophysiol*, 95(3):1727–1734, 2006.

[333] E. Thomas and T. Grisar. Increased synchrony with increase of a low-threshold calcium conductance in a model thalamic network: a phase-shift mechanism. *Neural Comput*, 12(7):1553–71, 2000.

[334] C.L. Thompson, D.L. Drewery, H.D. Atkins, F.A. Stephenson, and P.L. Chazot. Immunohistochemical localization of n-methyl-d-aspartate receptor subunits in the adult murine hippocampal formation: evidence for a unique role of the nr2d subunit. *Brain Res Mol Brain Res*, 102(1-2):55–61, 2002.

[335] I. Tobler, T. Deboer, and M. Fischer. Sleep and sleep regulation in normal and prion protein-deficient mice. *J Neurosci*, 17(5):1869–1879, 1997.

[336] W. J. Tomlinson, A. Stea, E. Bourinet, P. Charnet, J. Nargeot, and T. P. Snutch. Functional properties of a neuronal class c l-type calcium channel. *Neuropharmacology*, 32(11):1117–26, 1993.

[337] R. D. Traub, A. Bibbig, F. E. LeBeau, E. H. Buhl, and M. A. Whittington. Cellular mechanisms of neuronal population oscillations in the hippocampus in vitro. *Annu Rev Neurosci*, 27:247–78, 2004.

[338] R. D. Traub, A. Draguhn, M. A. Whittington, T. Baldeweg, A. Bibbig, E. H. Buhl, and D. Schmitz. Axonal gap junctions between principal neurons: a novel source of network oscillations, and perhaps epileptogenesis. *Rev Neurosci*, 13(1):1–30, 2002.

[339] R. D. Traub, D. Schmitz, J. G. Jefferys, and A. Draguhn. High-frequency population oscillations are predicted to occur in hippocampal pyramidal neuronal networks interconnected by axoaxonal gap junctions. *Neuroscience*, 92(2):407–26, 1999.

[340] R. D. Traub, M. A. Whittington, E. H. Buhl, F. E. LeBeau, A. Bibbig, S. Boyd, H. Cross, and T. Baldeweg. A possible role for gap junctions in generation of very fast eeg oscillations preceding the onset of, and perhaps initiating, seizures. *Epilepsia*, 42(2):153–70, 2001.

[341] Roger D. Traub, John G. R. Jefferys, and Miles A. Whittington. *Fast oscillations in cortical circuits*. Computational neuroscience. MIT Press, Cambridge, Mass., 1999.

[342] E. Tsakiridou, L. Bertollini, M. de Curtis, G. Avanzini, and H. C. Pape. Selective increase in t-type calcium conductance of reticular thalamic neurons in a rat model of absence epilepsy. *J Neurosci*, 15(4):3110–7, 1995.

[343] J.Z. Tsien, P.T. Huerta, and S. Tonegawa. The essential role of hippocampal ca1 nmda receptor-dependent synaptic plasticity in spatial memory. *Cell*, 87(7):1327–1338, 1996.

[344] J.E. Turman, O.K. Lee, and S.H. Chandler. Differential nr2a and nr2b expression between trigeminal neurons during early postnatal development. *Synapse*, 44(2):76–85, 2002.

[345] J. Turnbull, H. Lohi, J. A. Kearney, G. A. Rouleau, A. V. Delgado-Escueta, M. H. Meisler, P. Cossette, and B. A. Minassian. Sacred disease secrets revealed: the genetics of human epilepsy. *Hum Mol Genet*, 14(17):2491–500, 2005.

[346] D. Ulrich and J. R. Huguenard. $gaba_A$-receptor-mediated rebound burst firing and burst shunting in thalamus. *J Neurophysiol*, 78(3):1748–51, 1997.

[347] L. Vadlamudi, I. E. Scheffer, and S. F. Berkovic. Genetics of temporal lobe epilepsy. *J Neurol Neurosurg Psychiatry*, 74(10):1359–61, 2003.

[348] R. Vajna, U. Klockner, A. Pereverzev, M. Weiergraber, X. Chen, G. Miljanich, N. Klugbauer, J. Hescheler, E. Perez-Reyes, and T. Schneider. Functional coupling between

'r-type' ca^{2+} channels and insulin secretion in the insulinoma cell line ins-1. *Eur J Biochem*, 268(4):1066–75, 2001.

[349] M J van der Heyden, D N Velis, B P Hoekstra, J P Pijn, W van Emde Boas, C W van Veelen, P C van Rijen, F H Lopes da Silva, and J DeGoede. Non-linear analysis of intracranial human EEG in temporal lobe epilepsy. *Clin Neurophysiol*, 110(10):1726–40, 1999.

[350] F. Van Petegem, K. A. Clark, F. C. Chatelain, and Jr. Minor, D. L. Structure of a complex between a voltage-gated calcium channel beta-subunit and an alpha-subunit domain. *Nature*, 429(6992):671–5, 2004.

[351] F. Varela, J. P. Lachaux, E. Rodriguez, and J. Martinerie. The brainweb: phase synchronization and large-scale integration. *Nat Rev Neurosci*, 2(4):229–39, 2001.

[352] N. Vassallo and J. Herms. Cellular prion protein function in copper homeostasis and redox signalling at the synapse. *J Neurochem*, 86(3):538–544, 2003.

[353] S. Vicini, J.F. Wang, J.H. Li, W.J. Zhu, Y.H. Wang, J.H. Luo, B.B. Wolfe, and D.R. Grayson. Functional and pharmacological differences between recombinant n-methyl-d-aspartate receptors. *J Neurophysiol*, 79(2):555–566, 1998.

[354] I. Vitko, Y. Chen, J. M. Arias, Y. Shen, X. R. Wu, and E. Perez-Reyes. Functional characterization and neuronal modeling of the effects of childhood absence epilepsy variants of cacna1h, a t-type calcium channel. *J Neurosci*, 25(19):4844–55, 2005.

[355] Iuliia Vitko, Isabelle Bidaud, Juan Manuel Arias, Alexandre Mezghrani, Philippe Lory, and Edward Perez-Reyes. The i-ii loop controls plasma membrane expression and gating of ca(v)3.2 t-type ca2+ channels: a paradigm for childhood absence epilepsy mutations. *J Neurosci*, 27(2):322–330, Jan 2007.

[356] R. H. Wallace, C. Marini, S. Petrou, L. A. Harkin, D. N. Bowser, R. G. Panchal, D. A. Williams, G. R. Sutherland, J. C. Mulley, I. E. Scheffer, and S. F. Berkovic. Mutant *gaba*$_A$ receptor gamma2-subunit in childhood absence epilepsy and febrile seizures. *Nat Genet*, 28(1):49–52, 2001.

[357] R. H. Wallace, D. W. Wang, R. Singh, I. E. Scheffer, Jr. George, A. L., H. A. Phillips, K. Saar, A. Reis, E. W. Johnson, G. R. Sutherland, S. F. Berkovic, and J. C. Mulley. Febrile seizures and generalized epilepsy associated with a mutation in the na+-channel beta1 subunit gene scn1b. *Nat Genet*, 19(4):366–70, 1998.

[358] R. Walz, O.B. Amaral, I.C. Rockenbach, R. Roesler, I. Izquierdo, E.A. Cavalheiro, V.R. Martins, and R.R. Brentani. Increased sensitivity to seizures in mice lacking cellular prion protein. *Epilepsia*, 40(12):1679–1682, 1999.

[359] G. Wang, G. Dayanithi, R. Newcomb, and J. R. Lemos. An r-type ca(2+) current in neurohypophysial terminals preferentially regulates oxytocin secretion. *J Neurosci*, 19(21):9235–41, 1999.

[360] Y.T. Wang and M.W. Salter. Regulation of nmda receptors by tyrosine kinases and phosphatases. *Nature*, 369(6477):233–235, 1994.

[361] E.A. Waxman and D.R. Lynch. N-methyl-d-aspartate receptor subtypes: multiple roles in excitotoxicity and neurological disease. *Neuroscientist*, 11(1):37–49, 2005.

[362] J. P. Weick, R. D. Groth, A. L. Isaksen, and P. G. Mermelstein. Interactions with pdz proteins are required for l-type calcium channels to activate camp response element-binding protein-dependent gene expression. *J Neurosci*, 23(8):3446–56, 2003.

[363] J. Weise, O. Crome, R. Sandau, W. Schulz-Schaeffer, M. Bahr, and I. Zerr. Upregulation of cellular prion protein (prpc) after focal cerebral ischemia and influence of lesion severity. *Neurosci Lett*, 372(1-2):146–150, 2004.

[364] C. Weissmann and E. Flechsig. Prp knock-out and prp transgenic mice in prion research. *Br Med Bull*, 66:43–60, 2003.

[365] P. J. Welsby, H. Wang, J. T. Wolfe, R. J. Colbran, M. L. Johnson, and P. Q. Barrett. A mechanism for the direct regulation of t-type calcium channels by ca^{2+}/calmodulin-dependent kinase ii. *J Neurosci*, 23(31):10116–21, 2003.

[366] R. E. Westenbroek, J. W. Hell, C. Warner, S. J. Dubel, T. P. Snutch, and W. A. Catterall. Biochemical properties and subcellular distribution of an n-type calcium channel alpha 1 subunit. *Neuron*, 9(6):1099–115, 1992.

[367] R. E. Westenbroek, T. Sakurai, E. M. Elliott, J. W. Hell, T. V. Starr, T. P. Snutch, and W. A. Catterall. Immunochemical identification and subcellular distribution of the alpha 1a subunits of brain calcium channels. *J Neurosci*, 15(10):6403–18, 1995.

[368] D. B. Wheeler, A. Randall, and R. W. Tsien. Changes in action potential duration alter reliance of excitatory synaptic transmission on multiple types of ca^{2+} channels in rat hippocampus. *J Neurosci*, 16(7):2226–37, 1996.

[369] S. Wiebe, W.T. Blume, J.P. Girvin, and M. Eliasziw. A randomized, controlled trial of surgery for temporal-lobe epilepsy. *N Engl J Med*, 345(5):311–8, 2001.

[370] H.G. Wieser, K. Schindler, and D. Zumsteg. Eeg in creutzfeldt-jakob disease. *Clin Neurophysiol*, 117(5):935–951, 2006.

[371] M. C. Wiest and M. A. Nicolelis. Behavioral detection of tactile stimuli during 7-12 hz cortical oscillations in awake rats. *Nat Neurosci*, 6(9):913–4, 2003.

[372] J.H. Williams, Y.G. Li, A. Nayak, M.L. Errington, K.P. Murphy, and T.V. Bliss. The suppression of long-term potentiation in rat hippocampus by inhibitors of nitric oxide synthase is temperature and age dependent. *Neuron*, 11(5):877–884, 1993.

[373] M. E. Williams, D. H. Feldman, A. F. McCue, R. Brenner, G. Velicelebi, S. B. Ellis, and M. M. Harpold. Structure and functional expression of alpha 1, alpha 2, and beta subunits of a novel human neuronal calcium channel subtype. *Neuron*, 8(1):71–84, 1992.

[374] M. E. Williams, L. M. Marubio, C. R. Deal, M. Hans, P. F. Brust, L. H. Philipson, R. J. Miller, E. C. Johnson, M. M. Harpold, and S. B. Ellis. Structure and functional characterization of neuronal alpha 1e calcium channel subtypes. *J Biol Chem*, 269(35):22347–57, 1994.

[375] M. Wittmann, C. P. Bengtson, and H. Bading. *In The Pharmacology of Cerebral Ischemia*. Medpharm Scientific Publishers, 2004.

[376] J. T. Wolfe, H. Wang, J. Howard, J. C. Garrison, and P. Q. Barrett. T-type calcium channel regulation by specific g-protein betagamma subunits. *Nature*, 424(6945):209–13, 2003.

[377] G. A. Worrell, L. Parish, S. D. Cranstoun, R. Jonas, G. Baltuch, and B. Litt. High-frequency oscillations and seizure generation in neocortical epilepsy. *Brain*, 127(Pt 7):1496–506, 2004.

[378] X. S. Wu, H. D. Edwards, and W. A. Sather. Side chain orientation in the selectivity filter of a voltage-gated ca^{2+} channel. *J Biol Chem*, 275(41):31778–85, 2000.

[379] W. Xu and D. Lipscombe. Neuronal ca(v)1.3alpha(1) l-type channels activate at relatively hyperpolarized membrane potentials and are incompletely inhibited by dihydropyridines. *J Neurosci*, 21(16):5944–5951, Aug 2001.

[380] Y. Yaari, C. Yue, and H. Su. Recruitment of Apical Dendritic T-Type Ca2+ Channels by Backpropagating Spikes Underlies de novo Intrinsic Bursting in Hippocampal Epileptogenesis. *J Physiol*, EPub ahead of print., 2007.

[381] J. Yang, P. T. Ellinor, W. A. Sather, J. F. Zhang, and R. W. Tsien. Molecular determinants of ca^{2+} selectivity and ion permeation in l-type ca^{2+} channels. *Nature*, 366(6451):158–61, 1993.

[382] T. Yasuda, L. Chen, W. Barr, J. E. McRory, R. J. Lewis, D. J. Adams, and G. W. Zamponi. Auxiliary subunit regulation of high-voltage activated calcium channels expressed in mammalian cells. *Eur J Neurosci*, 20(1):1–13, 2004.

[383] A. Ylinen, A. Bragin, Z. Nadasdy, G. Jando, I. Szabo, A. Sik, and G. Buzsaki. Sharp wave-associated high-frequency oscillation (200 hz) in the intact hippocampus: network and intracellular mechanisms. *J Neurosci*, 15(1 Pt 1):30–46, 1995.

[384] C. T. Yokoyama, R. E. Westenbroek, J. W. Hell, T. W. Soong, T. P. Snutch, and W. A. Catterall. Biochemical properties and subcellular distribution of the neuronal class e calcium channel alpha 1 subunit. *J Neurosci*, 15(10):6419–32, 1995.

[385] H. Yoshinaga, Y. Ohtsuka, K. Tamai, I. Tamura, M. Ito, I. Ohmori, and E. Oka. Eeg in childhood absence epilepsy. *Seizure*, 13(5):296–302, 2004.

[386] R. Yuste, M. J. Gutnick, D. Saar, K. R. Delaney, and D. W. Tank. ca^{2+} accumulations in dendrites of neocortical pyramidal neurons: an apical band and evidence for two functional compartments. *Neuron*, 13(1):23–43, 1994.

[387] G. W. Zamponi. Determinants of g protein inhibition of presynaptic calcium channels. *Cell Biochem Biophys*, 34(1):79–94, 2001.

[388] J. F. Zhang, A. D. Randall, P. T. Ellinor, W. A. Horne, W. A. Sather, T. Tanabe, T. L. Schwarz, and R. W. Tsien. Distinctive pharmacology and kinetics of cloned neuronal ca^{2+} channels and their possible counterparts in mammalian cns neurons. *Neuropharmacology*, 32(11):1075–88, 1993.

[389] X. Zhong, J. R. Liu, J. W. Kyle, D. A. Hanck, and W. S. Agnew. A profile of alternative rna splicing and transcript variation of cacna1h, a human t-channel gene candidate for idiopathic generalized epilepsies. *Hum Mol Genet*, 15(9):1497–512, 2006.

[390] H. Zhu, B. G. Goodyear, M. L. Lauzon, R. A. Brown, G. S. Mayer, A. G. Law, L. Mansinha, and J. R. Mitchell. A new local multiscale fourier analysis for medical imaging. *Med Phys*, 30(6):1134–41, 2003.

[391] S. M. Zuberi, L. H. Eunson, A. Spauschus, R. De Silva, J. Tolmie, N. W. Wood, R. C. McWilliam, J. P. Stephenson, D. M. Kullmann, and M. G. Hanna. A novel mutation in the human voltage-gated potassium channel gene (kv1.1) associates with episodic ataxia type 1 and sometimes with partial epilepsy. *Brain*, 122 (Pt 5):817–25, 1999.

[392] R. D. Zuhlke, G. S. Pitt, K. Deisseroth, R. W. Tsien, and H. Reuter. Calmodulin supports both inactivation and facilitation of l-type calcium channels. *Nature*, 399(6732):159–62, 1999.